

Wilkinson Microwave Anisotropy Probe (*WMAP*):  
Nine-Year Explanatory Supplement<sup>1</sup>

The *WMAP* Science Working Group

December 19, 2012

<sup>1</sup>Version 5.0

---

## Preface

This document is a concise description of the delivered data sets for the nine years of scientific operation of the Wilkinson Microwave Anisotropy Probe (*WMAP*). It is intended as an overview of the delivered sky temperature and polarization maps and other data sets and as a description of the specific quantities contained in the *WMAP* time-ordered data. This document also describes the basic architecture and *modus operandi* of the instrument and spacecraft. Detailed descriptions of the spacecraft, instrument and data reduction methods have been described in publications that are referenced throughout this document and in particular at the beginning of Chapter 1.

This document is the cumulative effort of the following people: M. R. Greason, M. Limon, E. Wollack, C. Barnes, R. Bean, C. L. Bennett, O. Doré, J. Dunkley, B. Gold, M. Halpern, R. S. Hill, G. Hinshaw, N. Jarosik, A. Kogut, E. Komatsu, W. Landsman, D. Larson, S. S. Meyer, M. R. Nolta, N. Odegard, L. Page, H. V. Peiris, K. M. Smith, D. N. Spergel, G. S. Tucker, L. Verde, J. L. Weiland, and E. L. Wright. The high quality graphics in this document were created by B. Griswold and S. Bensusen.

Last revised: December 19, 2012

This document is to be referenced as:

*Wilkinson Microwave Anisotropy Probe (WMAP): Nine-Year Explanatory Supplement*, editor M. R. Greason, M. Limon, E. Wollack, et al., (Greenbelt, MD: NASA/GSFC)

Available in electronic form at <http://lambda.gsfc.nasa.gov/>

Previous versions of this document were referred to as:

*Wilkinson Microwave Anisotropy Probe (WMAP): Explanatory Supplement*, editor M. Limon, et al., (Greenbelt, MD: NASA/GSFC)

*Wilkinson Microwave Anisotropy Probe (WMAP): Three-Year Explanatory Supplement*, editor M. Limon, et al., (Greenbelt, MD: NASA/GSFC)

*Wilkinson Microwave Anisotropy Probe (WMAP): Five-Year Explanatory Supplement*, editor M. Limon, et al., (Greenbelt, MD: NASA/GSFC)

and

*Wilkinson Microwave Anisotropy Probe (WMAP): Seven-Year Explanatory Supplement*, editor M. Limon, et al., (Greenbelt, MD: NASA/GSFC)

# Contents

<b>1</b>	<b>Mission Explanatory Supplement</b>	<b>1</b>
1.1	The Observatory . . . . .	2
1.2	The Instrument . . . . .	3
1.2.1	The Optics . . . . .	3
1.2.2	The Radiometers . . . . .	3
1.2.3	The HEMT Amplifiers . . . . .	6
1.2.3.1	WMAP Amplifier Build, Qualification and Testing . . . . .	6
1.2.3.2	Ionizing Radiation Testing . . . . .	7
1.2.3.3	Amplifier Life Testing . . . . .	7
1.2.3.4	Safe Operating Bias and Power Levels . . . . .	8
1.3	The Journey . . . . .	11
1.3.1	Time Line . . . . .	11
1.3.2	Launch . . . . .	12
1.3.3	Deployment and Instrument Power On . . . . .	12
1.3.4	Observatory Checkout . . . . .	14
1.3.5	Phasing Loops . . . . .	14
1.3.6	Earth IR and Outgassing . . . . .	16
1.3.7	Lunar Fly-by . . . . .	17
1.3.8	Mid-course Correction . . . . .	17
1.3.9	Observing Mode . . . . .	17
1.3.10	Station Keeping . . . . .	17
1.3.11	Pointing . . . . .	18
1.3.11.1	Pointing Correction . . . . .	18
1.3.12	End of Mission . . . . .	20
1.4	The Thermal Environment . . . . .	20
1.4.1	Temperature Monitor Architecture . . . . .	31
1.4.2	Temperature Monitor Performances . . . . .	33
1.4.3	Sun Driven Yearly Temperature Changes . . . . .	35
1.4.4	Aging of Thermal Control Surfaces . . . . .	35
1.4.5	Operationally Induced Disturbances . . . . .	37
1.4.6	Radiometric Baselines Discontinuities . . . . .	38
1.5	The Radiation Environment . . . . .	41

---

1.5.1	Plasma Environment . . . . .	41
1.5.2	Spacecraft Charge Control . . . . .	42
1.5.3	Solar Flares: Charged Particle Heating . . . . .	43
1.6	Battery Capacity Loss . . . . .	45
1.7	Telemetry . . . . .	46
<b>2</b>	<b>Data Products</b>	<b>49</b>
2.1	Derived CMB Products . . . . .	50
2.1.1	Combined TT Power Spectra . . . . .	51
2.1.2	TE, TB, EE, and BB Power Spectra . . . . .	53
2.1.3	Cosmological Parameter Table . . . . .	56
2.1.4	Likelihood Code . . . . .	69
2.1.5	Predicted Sunyaev-Zeldovich Power Spectrum . . . . .	70
2.2	Sky Maps . . . . .	71
2.2.1	Coadded Nine Year Sky Maps . . . . .	74
2.2.2	Full Resolution Individual Year Sky Maps . . . . .	75
2.2.3	Reduced Resolution Sky Maps . . . . .	76
2.2.4	Loss Imbalance Templates . . . . .	77
2.3	Derived Foreground Products . . . . .	79
2.3.1	Internal Linear Combination (ILC) Map . . . . .	80
2.3.2	Point Source Catalog . . . . .	81
2.3.3	Point Source Variability Table . . . . .	82
2.3.4	Foregrounds Derived from Maximum Entropy Method . . . . .	83
2.3.5	Foregrounds Derived from an MCMC Method . . . . .	84
2.3.6	Foregrounds Templates . . . . .	86
2.3.7	Smoothed Single Year K1 and Ka1 Sky Maps . . . . .	87
2.4	Ancillary Data . . . . .	88
2.4.1	Masks . . . . .	89
2.4.2	Beam Transfer Functions . . . . .	90
2.4.3	Beam Maps . . . . .	91
2.4.4	Beam Radial Profiles . . . . .	93
2.4.5	Far-Sidelobe Maps . . . . .	94
2.4.6	Bandpass Frequency Response . . . . .	95
2.5	Time-Ordered Data . . . . .	96
2.5.1	Calibrated Time-Ordered Data . . . . .	97
2.5.2	Uncalibrated Time-Ordered Data . . . . .	98
2.5.3	Optimal Time-Domain Filters . . . . .	99
<b>3</b>	<b>Time Ordered Data (TOD)</b>	<b>100</b>
3.1	The Meta Data Table . . . . .	101
3.2	The Science Data Table . . . . .	103
3.3	The Analog Instrument Housekeeping (AIHK) Data Table . . . . .	107
3.4	The Digital Instrument Housekeeping (DIHK) Data Table . . . . .	108

3.5	The Line-Of-Sight (LOS) Table . . . . .	108
3.6	Headers . . . . .	108
<b>4</b>	<b>Telemetry Data</b>	<b>110</b>
<b>5</b>	<b>Software</b>	<b>111</b>
5.1	FITS Readers . . . . .	111
5.1.1	FITS_READ_MAP . . . . .	111
5.1.2	READ_COMBINED_MAP . . . . .	112
5.1.3	FITS_READ_TOD . . . . .	113
5.2	Time-Ordered Data Access . . . . .	114
5.2.1	Interpolate_Quaternions . . . . .	114
5.2.2	Pckt2Mnemonic() . . . . .	115
5.2.3	Quat_to_Sky_Coords . . . . .	116
5.2.4	TOD_to_Sky_Coords . . . . .	117
5.3	Mapping Procedures . . . . .	119
5.3.1	REPROJ_HEALPIX . . . . .	119
5.3.2	HEALINFO . . . . .	120
5.3.3	HEALPIX_Nested_Vectors . . . . .	120
5.3.4	GRID_OVERLAY . . . . .	120
5.3.5	CIRCOPLT . . . . .	122
5.3.6	PLANET_OVERLAY . . . . .	124
5.4	Transformations . . . . .	125
5.4.1	TIMETRANSFORM . . . . .	125
5.4.2	COORTRANS . . . . .	126
5.5	Widgets . . . . .	127
5.5.1	MAP_DATE . . . . .	127
5.5.2	MAPVIEW . . . . .	128
5.6	WMAP IDL Procedures . . . . .	129
<b>6</b>	<b>Bibliography</b>	<b>135</b>
<b>A</b>	<b>Gain Model Parameters</b>	<b>140</b>
<b>B</b>	<b>Selected WMAP Log Entries</b>	<b>144</b>
<b>C</b>	<b>Mnemonics Lists</b>	<b>173</b>
C.1	Science Mnemonics . . . . .	174
C.2	Instrument Housekeeping Mnemonics . . . . .	175
C.2.1	Amplifier Drain Currents . . . . .	175
C.2.2	Radiometer RF Bias (Total Power) . . . . .	176
C.2.3	TRS Temperatures . . . . .	177
C.2.4	FPA Temperatures . . . . .	177

---

C.2.5 RXB Temperatures . . . . .	178
C.2.6 AEU Temperatures . . . . .	178
C.2.7 PDU Temperatures . . . . .	178
C.2.8 AEU Voltages and Reference Roads . . . . .	179
C.2.9 PDU Voltages . . . . .	179
<b>D Acronym List</b>	<b>180</b>

# List of Figures

1.1	Spacecraft Overview . . . . .	2
1.2	Radiometer Schematic . . . . .	5
1.3	HEMT Life Test Bias . . . . .	9
1.4	Cool-down Thermal Profile . . . . .	13
1.5	Distortion Model . . . . .	20
1.6	Nine Years Thermal Profile . . . . .	21
1.7	First Year Thermal Profile . . . . .	22
1.8	Second Year Thermal Profile . . . . .	23
1.9	Third Year Thermal Profile . . . . .	24
1.10	Fourth Year Thermal Profile . . . . .	25
1.11	Fifth Year Thermal Profile . . . . .	26
1.12	Sixth Year Thermal Profile . . . . .	27
1.13	Seventh Year Thermal Profile . . . . .	28
1.14	Eighth Year Thermal Profile . . . . .	29
1.15	Nineth Year Thermal Profile . . . . .	30
1.16	Instrument Temperature Rate Histograms . . . . .	31
1.17	PRT Noise Power Spectrum . . . . .	32
1.18	FPA and RXB Temperature Power Spectra . . . . .	34
1.19	Solar Array Temperature Profile . . . . .	36
1.20	Solar Flare Effects on the Observatory . . . . .	44
1.21	Battery Temperature and Voltage Over Time . . . . .	45
1.22	Telemetry Data Path . . . . .	47
3.1	Archive Record Timing . . . . .	101

# List of Tables

1.1	WMAP Optical System Parameters . . . . .	4
1.2	WMAP Feed Specifications . . . . .	4
1.3	WMAP Radiometer and HEMT Specifications . . . . .	5
1.4	WMAP Amplifier . . . . .	10
1.5	WMAP Amplifier Components . . . . .	11
1.6	WMAP Maneuver Summary . . . . .	15
1.7	Observing Mode Performance . . . . .	19
1.8	Data Cut Summary . . . . .	41
1.9	Solar Storms . . . . .	43
2.1	Nine-Year Release Cosmological Parameters Model/Dataset . . . . .	61
2.2	Nine-Year Release Cosmological Models . . . . .	62
2.3	Nine-Year Release Analyzed Data Sets . . . . .	62
2.4	Seven-Year Release Cosmological Parameters Model/Dataset . . . . .	63
2.5	Seven-Year Release Cosmological Models . . . . .	64
2.6	Seven-Year Release Analyzed Data Set . . . . .	64
2.7	Five-Year Release Cosmological Parameters Model/Dataset . . . . .	65
2.8	Five-Year Release Cosmological Models . . . . .	66
2.9	Five-Year Release Analyzed Data Set . . . . .	66
2.10	Three-Year Release Cosmological Parameters Model/Dataset . . . . .	67
2.11	Three-Year Release Cosmological Models . . . . .	68
2.12	Three-Year Release Analyzed Data Set . . . . .	68
2.13	Pixel Noise Coefficients . . . . .	72
2.14	MCMC Foregrounds . . . . .	85
2.15	Masks . . . . .	90
A.1	Gain Model Parameters - $T_o$ and $V_o$ . . . . .	141
A.2	Gain Model Parameters - $\beta$ and $\alpha$ . . . . .	142
A.3	Gain Model Parameters - $m$ and $c$ . . . . .	143

# Chapter 1

## Mission Explanatory Supplement

The *WMAP* (Wilkinson Microwave Anisotropy Probe) mission is designed to determine the geometry, content, and evolution of the universe via a 13 arcminute FWHM resolution full sky map of the temperature anisotropy of the cosmic microwave background radiation. The choice of orbit, sky-scanning strategy and instrument/spacecraft design were driven by the goals of uncorrelated pixel noise, minimal systematic errors, multifrequency observations, and accurate calibration. The skymap data products derived from the *WMAP* observations have 45 times the sensitivity and 33 time the angular resolution of the COBE DMR mission.

An overall description of the *WMAP* mission can be found in Bennett et al. (2003c). Details of the instrument design are described in Jarosik et al. (2003a), Page et al. (2003c), and Barnes et al. (2002). The basic results from the first year of *WMAP* observations are summarized in Bennett et al. (2003b). Results from the first three years of operation are described in Jarosik et al. (2007); Hinshaw et al. (2007); Page et al. (2007); Spergel et al. (2007); and Kogut et al. (2007). The results from the first five years of operation are described in Dunkley et al. (2009); Gold et al. (2009); Hill et al. (2009); Hinshaw et al. (2009); Komatsu et al. (2009); Nolta et al. (2009); and Wright et al. (2009). The results from the first seven years of operations are described in Jarosik et al. (2011); Gold et al. (2011); Larson et al. (2011); Bennett et al. (2011); Komatsu et al. (2011); and Weiland et al. (2011). A final summation of the nine year mission is documented in Bennett et al. (2012) and Hinshaw et al. (2012).

Jarosik et al. (2003b) describes the in flight performance of the *WMAP* radiometers. Characteristics of the telescope beam profiles and limits on systematic effects are provided in Page et al. (2003a); Barnes et al. (2003); Jarosik et al. (2007) and Hill et al. (2009). A summary of non-cosmological signals observed is presented in Bennett et al. (2003a). Hinshaw et al. (2003a); Jarosik et al. (2007), Hinshaw et al. (2009), and Gold et al. (2011) provide details on data processing for the mission and subsequent refinements.

The methods for obtaining cosmological parameters from the first year of data are described in Verde et al. (2003). Limits on non-Gaussian fluctuations are provided in Komatsu et al. (2003). The angular power spectrum and basic cosmological parameters resulting from *WMAP* are presented in Hinshaw et al. (2003b) and Spergel et al. (2003). The observed TE

polarization signal is described in Kogut et al. (2003). The implications of the above results for inflation is described in Peiris et al. (2003). A guide to understanding how cosmological parameters affect the the observed power spectra is provided in Page et al. (2003b). Weiland et al. (2011) discusses the utility of signals from the planets and other fixed astronomical sources as instrument calibrators of *WMAP* and potentially of other scientific instruments.

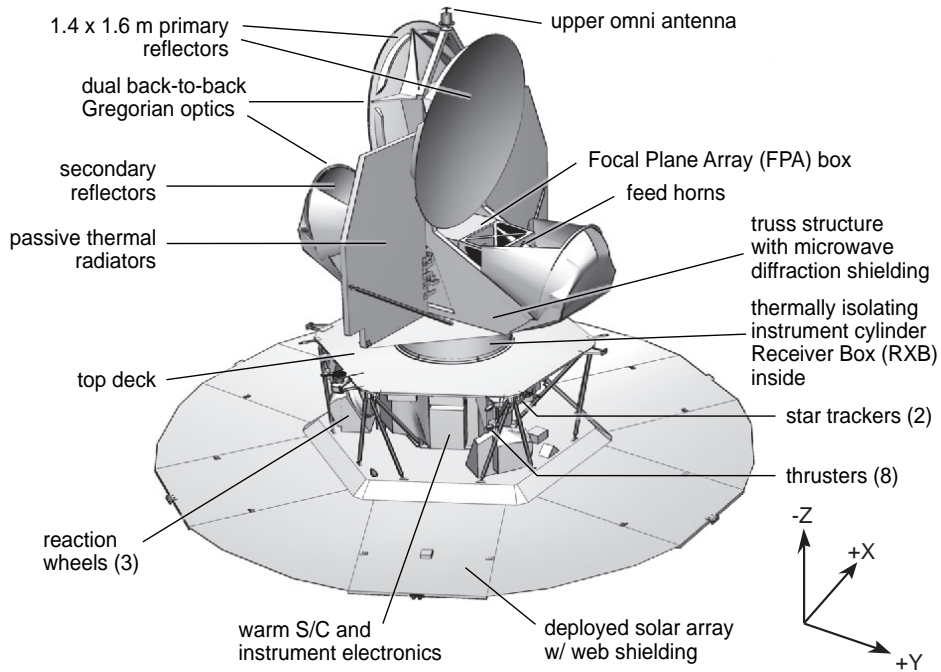


Figure 1.1: Spacecraft Overview. View of the spacecraft in the deployed configuration with major components labeled. The primary and secondary reflectors as well as the two thermal radiators are clearly visible in the upper portion of the image. The cold and warm section of the radiometers are housed in the FPA and RXB respectively and are located in the core of the spacecraft under the primary reflectors. All the support electronics (AEU, DEU, PDU, MAC, LMAC), gyros, star-trackers, and reaction wheels are mounted on the hexagonal hub at the base of the spacecraft. While at L2, the optics, instrument and support electronics are constantly in the shade of the solar array and never exposed to solar radiation.

## 1.1 The Observatory

The design of the *WMAP* observatory<sup>1</sup>, the choice of its orbit and its operational mode has been driven by the mission's science requirements of producing full sky maps of the cosmic microwave background radiation of unprecedented accuracy. Therefore the overall mission's

<sup>1</sup>The combination of the spacecraft and the instrument are referred to as the observatory throughout this document.

design philosophy has been to minimize and control systematic errors even at the expense of sensitivity, simplicity and cost. This choice has a profound effect not only in the design of the instrument but on the spacecraft as well. In particular, to minimize temperature variations in the optics and the radiometers that could lead to systematic effects in the measured signals the thermal control is entirely passive. The heat generated by the instrument is radiatively dissipated by two large radiators mounted in the upper part of the spacecraft (see Figure 1.1) while all the support systems (battery, analog and digital electronics, etc.) are mounted around an open hexagonal hub in the lower part of the spacecraft and dissipate their excess heat through individual radiating surfaces which are part of their enclosures.

## 1.2 The Instrument

The WMAP instrument is basically made by two separate but highly interdependent components:

- **The Optics** focus the incoming radiation in the focal plane.
- **The Radiometers** amplify and convert the microwave signal into a measurable voltage proportional to the received power.

In the following section we briefly describe the basic details of each of this components, we will also briefly describe the spacecraft's thermal design.

### 1.2.1 The Optics

The WMAP optical system consists of two back-to-back shaped offset Gregorian telescopes (see Figure 1.1). This is a highly symmetrical and compact optical design allows efficient placement of the feeds and radiometers while at the same time meeting all the science requirements. A summary of the optical system basic parameters is given in Table 1.1. The WMAP's optical system design and characterization is described in detail in Page et al. (2003c).

Two mirror-symmetric arrays of corrugated feeds couple the radiation from WMAP's two telescopes to the inputs of the differential receivers. Corrugated feeds were chosen because of their low emissivity, symmetric beam pattern, and low sidelobes. A summary of the feed basic parameters is given in Table 1.2. The WMAP's feeds design, manufacturing methods, and characterizations are described in details in Barnes et al. (2003).

### 1.2.2 The Radiometers

The 20 differential radiometers that make up the WMAP instrument cover 5 frequency bands and share the same design: they are pseudo-correlation differential radiometers with High Electron Mobility Transistor (HEMT) amplifiers passively cooled to  $\sim 90$  K. A summary of the WMAP radiometers design parameters and a schematic of an individual radiometer are given in Table 1.3 and Figure 1.2 respectively. The WMAP radiometers are described in detail in Jarosik et al. (2003a).

Band	K	Ka	Q	V	W	
Optical System			Gregorian			[‐]
Primary Dimensions			1.4 × 1.6			[m]
Secondary Dimensions			0.8 × 0.8			[m]
Focal length			90			[cm]
Beam Size	0.88	0.66	0.51	0.35	0.22	deg
Max Edge Taper	-13	-20	-21	-21	-16/-20	[dB]
Forward Beam Efficiency	0.960	0.986	0.986	0.996	0.996/0.999	[‐]

Table 1.1: *WMAP* Optical System Parameters. The beam patterns are not Gaussian, and thus are not simply specified. The size given here is the square-root of the beam solid angle. The value reported for the edge taper is the maximum for the center of the band. As the feeds are not illuminating the reflectors symmetrically, most of the edge has a substantially smaller taper. The beam efficiency is the integral of the beam in the area around 2° from the minimum divided by  $4\pi$ ; a value of 0.960 means that 4% of solid angle is scattered into the sidelobes.

Band	K	Ka	Q	V	W
Waveguide (WR)	42	28	22	15	10
$\nu$ (GHz)	19.5–25	28–37	35–46	53–69	82–106
$\nu_{gv}$ (GHz)	22	25.9	32.5	49.1	90.1
Length (mm)	536.4	542.1	567.6	569.6	603.3
Throat $\oslash$ (mm)	12.50	8.34	6.68	4.41	2.97
Aperture $\oslash$ (mm)	109.37	89.92	89.88	59.89	39.92
Mass (g)	1010	650	615	325	214
$N_{gv}$	116	169	217	329	533
$N_s$	1	1	3	4	5
$\theta_{fwhm}$ (deg)	10.1–7.7	8.9–6.7	7.8–6.0	8.8–7.4	9.7–8.3
Gain (dBi)	24.9–28.1	26.1–29.1	27.3–30.8	26.0–28.8	25.0–27.2

Table 1.2: *WMAP* Feed Specifications. The waveguide bands listed are for the rectangular commercial standard designations used in the radiometer,  $\nu_{gv}$  is the hybrid frequency,  $N_{gv}$  is the total number of corrugations, and  $N_s$  is the number of sections (1 meaning made in one piece). The antenna beam width and the gain values range from the lower to the higher ends of the band.

WMAP Band Designation	K	Ka	Q	V	W
<hr/>					
Radiometers Specifications					
Frequency Range (GHz)	20 – 25	28 – 36	35 – 46	53 – 69	82 – 106
$\Delta\nu_{eff}$ (GHz)	4	5	8	13	19
Number of Radiometers	2	2	4	4	8
Sensitivity (mK sec <sup>1/2</sup> )	0.65	0.78	0.92	1.13	1.48
$T_{sys}$ (K)	29	39	59	92	145
<hr/>					
HEMTs Specifications					
Noise temperature @300K (K)	~100	~115	~150	~260	~370
Noise temperature @85K (K)	30±2	33±3	48±5	64±7	96±7
Gain @300K (dB)	33	32	31	31	32
Gain @85K (dB)	34	34	34	35	35
Gain flatness (dB)	±1.5	±1.0	±1.5	±2.5	±3.0

Table 1.3: WMAP Radiometer and HEMT Amplifiers Specifications. The sensitivity is per radiometer. Sensitivity and  $T_{sys}$  values are given in Rayleigh-Jeans temperature.

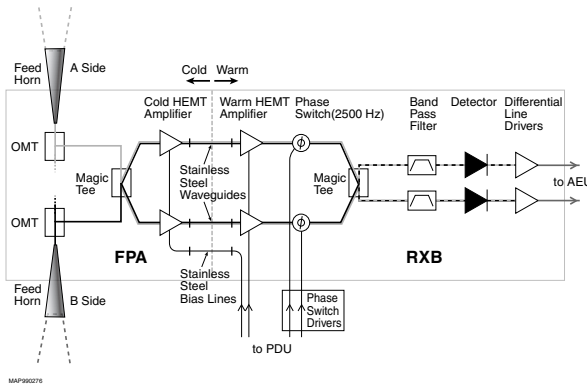


Figure 1.2: Layout of an Individual WMAP Radiometer. Components on the cold (left) side of the stainless steel waveguides are housed in the FPA where they passively cooled to  $\sim 90$  K through thermal links to the radiator panels. The components in the RXB achieve a balance temperature of  $\sim 290$  K.

### 1.2.3 The HEMT Amplifiers

The amplifier build for the WMAP satellite was carried out by the National Radio Astronomy Observatory Central Development Laboratory (NRAO/CDL) in Charlottesville, Virginia. See:

<http://www.nrao.edu/engineering/amplifiers.shtml>

Specific details of the amplifier design which were driven by the mission and the instrument's flight environment can be found in Bennett et al. (2003c); Jarosik et al. (2003a). Technical details regarding the design, development, and measured performance of this family of low noise 0.1 micron InP HEMT amplifiers can be found in: Nguyen et al. (1992); Pospieszalski (1989); Pospieszalski et al. (1993, 1995, 1997); Wollack (1995); Pospieszalski et al. (1994); Wollack & Pospieszalski (1998); Pospieszalski et al. (2000).

#### 1.2.3.1 WMAP Amplifier Build, Qualification and Testing

Here, we briefly outline the manufacture, qualification, and test flow used to produce high reliability millimeter wave amplifiers in the quantities required for the flight instrument. The NASA Technical Workmanship and MIL standards were used in specification of the fabrication and in process inspection criteria. A summary of the development sequence and applicable references used for the mission are given in Table 1.4. The amplifier designs were qualified for thermal stress/shock, vibration, gain/bias stability, RF/ionizing radiation exposure, and extended life. Thermal and vibration test criteria for the final assemblies were derived from the General Environmental Verification Specification (GEVS). The phase, gain, noise, and stability as a function bias at the extremes of the flight environment were verified prior to and after amplifier level vibration and thermal cycling for each flight unit.

The NASA/GSFC provided quality assurance support for the component selection and the flight build. The use of commercial components with augmented testing was employed where suitable military grade product lines could not be identified. Each component type was procured as a single lot and subjected to additional testing during their manufacture to monitor their suitability for the intended end use. This arrangement enabled components with known performance heritage in existing NRAO cryogenic amplifier designs to be qualified and used if appropriate. Prior to onsite acceptance by NRAO, the components were visually inspected, samples were tested for bondability and electrical/mechanical tolerances were verified. Vendors willing to manufacture several key components required for the MIC (Microwave Integrated Circuit) amplifier design could not be identified. To meet these design needs, custom components were processed, delivered as wafers, and the final dicing steps were performed at NRAO. Samples of these parts were subsequently inspected by the NASA/GSFC materials branch prior to use. See Table 1.5 for a summary of the electrical components and vendors used for the amplifier build.

### 1.2.3.2 Ionizing Radiation Testing

An amplifier was radiation tested as an assembly at the levels anticipated over the mission (Bennett et al., 2003c) while under the nominal flight bias. A cobalt 60 source was used to produce total ionizing doses of 0, 2, 4, 8, 16, and 32 krad at incremental rates of 1.90, 1.90, 1.61, 2.04, and 6.50 krad/min, respectively. The anticipated total dose over the course of the *WMAP* mission is 2.3 krad-Si. The noise, gain, gain stability, and voltage/current bias points for each device in the amplifier were tested prior to and after exposure at a fixed temperature. Within the calibration errors, the amplifier response was unchanged. No measurable change in the amplifier electrical bias performance was observed over the course of the three week irradiation test duration. No change in amplifier noise temperature or gain was observed after exposure. (Comment: The unit was visually inspected before exposure and after the 32 krad-Si total dose. An essentially cosmetic darkening of the clear epoxy (GC Electronics, P/N 10-114) used to bond the LEDs to the exterior of the amplifier assembly cover was noted. The volume of this material used to stake wires internal to the amplifier body is effectively shielded by  $\sim 5\text{mm}$  of brass was unaffected). The influence of ionizing radiation on the noise spectrum of the red LED's used to illuminate the amplifier channel were also tested and found to be independent of the exposure.

### 1.2.3.3 Amplifier Life Testing

Life testing was preformed on an engineering model amplifier in parallel with the construction of the *WMAP* observatory. A double temperature regulated enclosure was instrumented to monitor the amplifier temperature and each stage of a precision power supply which generated the gate and drain voltage and currents. To minimize the influence of diurnal changes in the laboratory ambient temperature the entire fixture was mounted on a heat exchanger coil which circulated coolant regulated to  $\sim 1\text{K}$ . The amplifier was mounted on the interior temperature stage which had a regulation error  $\lesssim 20\text{ mK}$ . The computer, data acquisition, and HEMT bias boards were run off an uninterruptible power supply. Data taken the brief period of time where thermal regulation exceeds this window on the interior stage were flagged and removed during analysis. For the duration of the test, the input and output of the amplifier were terminated in waveguide loads and the LEDs were illuminated. Pre- and post-test noise, gain, and stability were consistent within the experimental calibration error limit (*i.e.*,  $dT_n \simeq 3\text{K}$ ,  $dG \simeq 0.08\text{dB}$ ). A summary of the bias data is presented in Figure 1.3.

The instrument housing keeping data for the first three years of the mission were scrutinized for potential aging effects in the 80 amplifiers used in flight. To carry out this analysis, the drain current monitor data for each channel was corrected for the change in the instrument temperature which experienced as the satellite's distance from the sun changes. The pre-L2 flight data, which data contains amplifier 'burn-in' response (*e.g.*, see Figure 1.3 and Jarosik et al. (2003a)) and initial instrument cool down response, was cut. The residuals to the resulting data set fit contain two terms which are largely degenerate: the secular increase in drain current arising from the degradation of the thermal control surfaces and the potential increase in device current due to device aging. To delve further we use the temperature

sensitivity for derived from the thermally driven orbital variations for each channel to remove an estimate of the influence of the secular increase in observatory temperature with time. We find that the response is consistent with the ground life test data and are unable to detect amplifier aging with the present data set. Based upon these observations and the inferred change in spacecraft's effective emissivity we estimate that > 10 years of instrument operation will elapse before aging of the active components will produce a measurable impact on the radiometer performance. Through out the duration of the WMAP mission, the operational characteristics of all amplifier channels remain within nominal parameter ranges.

#### 1.2.3.4 Safe Operating Bias and Power Levels

In a conventional room temperature high frequency amplifier the bias power is typically regulated from a higher level down to the desired safe operating point close to the devices. In operation this provides noise immunity and added protection unintentional external threats such as electrostatic and internal discharge. The thermal power dissipation associated with this approach on the cold stage can be unacceptably high in applications where the device is cooled to reduce the Johnson noise and increase gain. In such cryogenic applications the bias lines for the devices are passively filtered internal to the amplifier housing. In this configuration the harness, power supply, and amplifier must be considered from a system perspective to achieve the desired noise margin on the bias, stability, and protection from external threats. In addition, this places higher demands upon the required harness integrity and power supply sequencing required to safely operate the active devices without damage.

A fundamental tradeoff exists between breakdown voltage and speed for a given semiconductor material – roughly speaking – the carrier speed in a given material is a constant, to make faster transistor, the distance the electrons travel is minimized which ultimately reduces the breakdown voltage (Hadaway et al., 1995). In the case of the *WMAP* 0.1 micron InP devices the maximum safe operating voltage to  $\sim 2$  volts across the amplifier bias input terminals (*i.e.*, referenced to the device the drain-source voltage less than 1.5V is recommended (Nguyen et al., 1992)). The nominal instrument operating bias of  $V_{ds} \sim 1.5$  volts and  $-0.2 < V_{gs} < 0$  volts only leaves a modest margin against device stress due to bias transients. To deal with this issue the power distribution unit regulated outputs are limited by voltage clamps, the power on sequence does not allow an overshoot of the target bias, and the high frequency transients are filtered by a passive network at the amplifier housing. The immunity of this configuration against anticipated RF power, ESD, and IESD were verified against anticipated flight threat levels. From our laboratory testing of the engineering models we derived the following RF exposure limits for the amplifier inputs: 1) Green Limit:  $< -5\text{dBm}$  (e.g., safe RF device exposure regime for power / voltage-stress), 2) Yellow Limit:  $< 0\text{dBm}$  (e.g., onset of increased but recoverable gate leakage behavior due to the device 'burn-in'), 3) Red Limit:  $< 10\text{dBm}$  (maximum tested exposure CW limit at 300K, no permanent influence upon noise; temporary gate voltage shift). These operational limits were used throughout the mission's I&T (Integration and Test) and Launch phases. The testing methods and comments found in Lilie (1989) and Chen (2000) may be of potential value in establishing such operational guidelines.

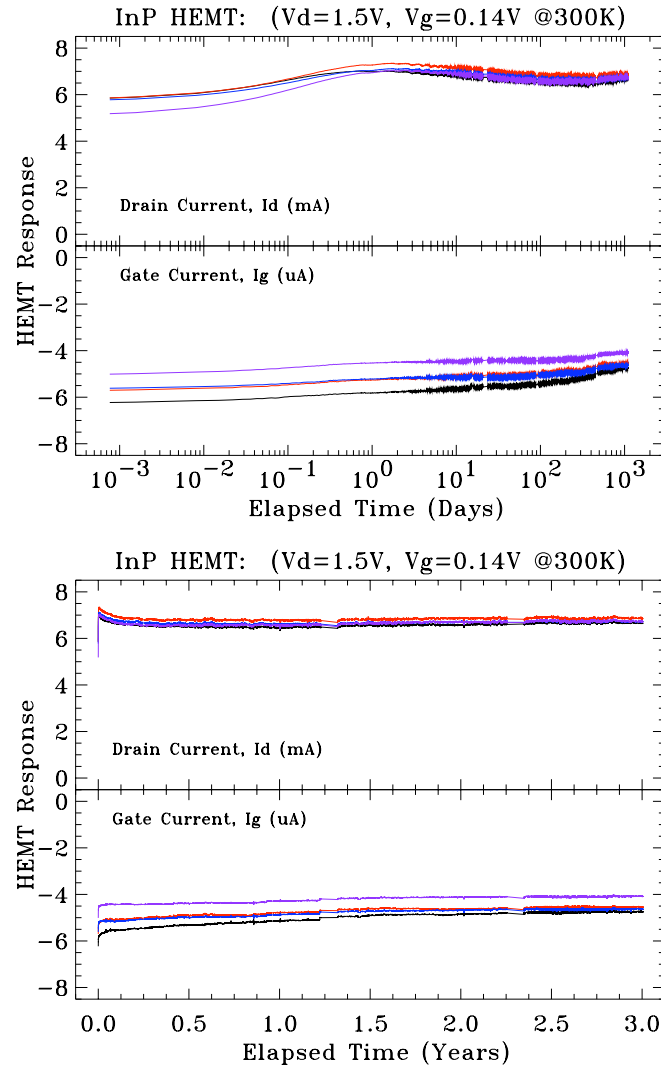


Figure 1.3: HEMT Life Test Bias Data (4-stage Q-Band Amplifier). The bias data from the amplifiers display an initial transient upon power on which repeatable and dependent upon the device thermal, illumination, RF power levels, and bias history. The timescale of this ‘power-on’ or ‘burn-in’ effect is device dependent and correlated with the gate leakage measured during initial screening of the wafer. A logarithmic axis is chosen in the top figure to emphasize this characteristic. In the bottom figure this influence is seen to die to a negligible level in several months. This characteristic behavior is typical of the observed response for the flight devices. From an instrument perspective this introduces a slow gain drift which is removed from the system during the calibration of the flight data. This life test data set was acquired in the laboratory with a specially instrumented test set that enabled a full characterization of each amplifier stage.

Topic	Activity Description	Comments
Mil-Specification:	General Workmanship and Compatibility: <ul style="list-style-type: none"><li>• Electroplating</li><li>• Wire Bonding</li><li>• Electrical Component Incoming Inspection</li><li>• Wave-guide Flange Type and Configuration</li><li>• Electrostatic Discharge &amp; Charging (ESD/IESD)</li><li>• Electromagnetic Interference (EMI/EMC)</li></ul>	(a), Bondable and Bright Gold (b), Modify for RF Bond Strain Relief (b) (c), Modify Pinning Detail (d-g) (h,f)
NASA Technical Workmanship Standards:	General Workmanship: <ul style="list-style-type: none"><li>• Adhesive Bonds</li><li>• Hand Soldering</li><li>• Assembly Cleaning</li></ul>	NASA Handbooks (NHB)
NRAO/WMAP: Specific	Storage / Shipping / Humidity: Test Equipment Calibration: Material Selection / Qualification: <ul style="list-style-type: none"><li>• Cryogenic Thermal Performance/Cycle/Shock</li><li>• Out-Gassing</li><li>• Ionizing Radiation</li><li>• ESD / IESD</li><li>• Bias / Stability</li><li>• Life Test</li><li>• Complex Gain</li><li>• Gain Stability</li><li>• Noise</li><li>• Vibration</li><li>• Thermal Cycling</li><li>• Wire Bond Pull Strength</li><li>• Adhesive Cure</li><li>• Adhesive Peel Strength</li><li>• Ionic Contamination</li></ul> Amplifier Fabrication / Test Sequence: <ul style="list-style-type: none"><li>• Mechanical Tolerance</li><li>• Electrical Tolerance</li><li>• Plating Quality / Thickness</li><li>• Component (Wire) Bondibility</li><li>• Cleanliness / Ionic Contamination</li></ul> NASA/GSFC In Process Inspection Point <ul style="list-style-type: none"><li>• Acceptance Testing/Debug</li><li>• Gain/Phase</li><li>• Noise</li><li>• Device Bias/Stability</li><li>• Vibration</li><li>• Final Electrical Characterization</li></ul> NASA/GSFC Final Inspection Point <ul style="list-style-type: none"><li>• Delivery for integration into receiver assemblies</li><li>• Monitor and record amplifier bias and radiometer gain trend data throughout I&amp;T</li></ul>	Amplifier Assembly Selected Materials (g-j) LEDs, Powered Amplifier (d-g) Amplifier/Harness/Power Supply Engineering Units/Flight Assembly Engineering Units Flight Units; Warm/Cryogenic Engineering Units; Warm/Cryogenic Flight Units; Warm/Cryogenic (j) Flight Units; Un-Powered Flight Units / Coupons Process Coupons Process Coupons Process Coupons Process Coupons Process Coupons Inspection and Test per NRAO Inspection and Test per NRAO Inspection and Test per NRAO Inspection and Test per NRAO Inspection and Test per NRAO RF Trend Data 300K / 80K Ambient Temperature 300K / 80K Ambient Temperature 300K / 80K Ambient Temperature (j) RF Trend Data before/after Test RF Trend Data Pre-Cap Inspection / Data Review RF Trend Data DC and Radiometer Trend Data

Table 1.4: WMAP Amplifier: Fabrication, Integration and Test Flow

- a) MIL-G-45204C, Gold Plating, Electrodeposited.
- b) MIL-STD-883E, Method 2010.10, Visual Inspection; Method 2011.7, Destructive Bond Strength; Method 2023.5, Non-Destructive Bond Pull.
- c) MIL-F-3922, Waveguide Flange Specification.
- d) MIL-STD-462, Transient EMC (pulse is ~10ms wide while an ESD pulse is on the order of 10-to-100ns).
- e) MIL-STD-1541A, Transient ESD Source.
- f) MIL-STD-883, Method 3015, V-Zap ESD Test.
- g) NASA Technical Handbook, "Avoiding Problems Caused by Spacecraft on-Orbit Internal Charging Effects", NASA-HDBK-4002, February 17, 1999.
- h) NASA Technical Standards for Space Flight and Mission Critical Ground Support Hardware, see <http://www.hq.nasa.gov/office/codeq/qdoc.pdf>
- i) J.L., Barth, et al., "MAP Radiation Analysis," X-900-97-006, August, 1997, Table 7.
- j) J.S. Milne, 'General Environmental Verification Specification for STS and EVL Payloads, Subsystems, and Components,' 1996, NASA GSFC, System Reliability & Safety Office, Greenbelt, Maryland.

Component Envelope X×Y×Z (inches)	Part Designation	Part Vendor
Solder-to-Wire Bond Transition 0.110 × 0.040 × 0.010	Au/Cu/Cr on Alumina (NRAO Custom Design)	American Technical Ceramics, Corporation, Thin Films Products, Jacksonville, FL 32216.
Capacitor, 680 pF 0.055 × 0.055 × 0.055	CDR11BP681AJNS (700A681JCA50X)	American Technical Ceramics, Corporation, Huntington, Station, NY 11746-2102.
Resistor Divider Network 0.034 × 0.034 × 0.010	MSMT125ST-55000J-GB	Mini-Systems, Inc, Thin Films Division, Attleboro, MA 02703-0028
Resistor, 10 ohm 0.016 × 0.020 × 0.010	MSMW122AT10R00J-GB	Mini-Systems, Inc, Thin Films Division, Attleboro, MA 02703-0028
Resistor, 10 ohm 0.013 × 0.032 × 0.013	H0302AP100JG (Alternate Component)	State of the Art, Inc., State College, PA 16803-1797.
Capacitor, 16 pF 0.055 × 0.055 × 0.055	CDR11BP160AJNS (700A160JCA150X)	American Technical Ceramics, Corporation, Huntington, Station, NY 11746-2102.
Resistor, 50 ohm 0.016 × 0.020 × 0.010	MSMW122AT50R00J-GB	Mini-Systems, Inc, Thin Films Division, Attleboro, MA 02703-0028.
Resistor, 50 ohms 0.013 × 0.032 × 0.013	H0302AP500JG (Alternate Component)	State of the Art, Inc., State College, PA 16803-1797.
Termination Resistor, 50 ohm 0.007 × 0.033 × 0.005	Quartz, NiCr 25 ohm/sq. (NRAO Custom Design)	Filtran Microcircuits, Inc., Ottawa, Ontario, K1H8P5.
RF Stabilization Network 0.008 × 0.0125 × 0.005	Quartz, NiCr 25 ohm/sq. (NRAO Custom Design)	Filtran Microcircuits, Inc., Ottawa, Ontario, K1H8P5.
Capacitor, 0.8 pF 0.025 × 0.025 × 0.008	D25CG0R8B1PC	Dielectric Labs, Cazenovia, NY 13035.
Capacitor, 0.2 pF 0.015 × 0.015 × 0.006	D15CF0R2P5PC	Dielectric Labs, Cazenovia, NY 13035.
Cuflon Substrate XXX × 0.028 × 0.003	CF-A-3-5-6-G3 (NRAO Custom Design)	Crane/Polyflon, New Rochelle, NY 10801.
InP HEMT, 0.1 μm Gate 0.010 × 0.013 × 0.004	Wafer Number I448A/S514-026	Hughes Research Laboratory, Malibu, CA 90625.
Coupling Capacitor XXX × 0.0065 × 0.003	Metalized Quartz (NRAO Custom Design)	NRAO Central Development Laboratory, Charlottesville, VA 22903.
Red LED	521-9186 (RL-50/MV-50)	Dialight Corporation, Corporation, Manasquan, NJ 08736.
Bias Connector, Micro-D	M83513/01-BN	ITT/Cannon, Santa Ana, CA 92705-6500.
LED Connectors	GM2, -Round (Male) GF2, -Round (Female)	Microtech, Boothwyn, PA 19061-2199.

Table 1.5: WMAP Amplifier Components Summary.

## 1.3 The Journey

This section summarizes the events and the environment encountered by the observatory from days immediately preceding launch to the moment of the lunar swing-by that provides the gravity assist to reach its final orbital position around L2.

### 1.3.1 Time Line

The WMAP observatory was powered on and tested for the last time at GSFC on April 6, 2001 before being shipped to Kennedy Space Center (KSC) on April 18 where it arrived two

days later. In the approximately two months following its arrival at KSC, the observatory underwent further testing, integration with the launch vehicle 3rd stage and finally integration with the rest of the launch vehicle. The launch vehicle was a Boeing Delta II 7425. This was the 286<sup>th</sup> Delta launch. A summary of these events are included in the log in Appendix B which also covers the rest of the mission to the end of the first year of science observations.

### 1.3.2 Launch

On June 30, 2001 at 19:29 GMT the GSFC control team gave its approval to proceed with the terminal count-down. Approximately 10 minutes later the observatory was switched to internal power and at 19:46:46 GMT it lifted off from launch pad 17B at the Eastern Range Space Launch Complex – the first step in a journey that took it three times around the Earth (phasing loops) and close to the Moon (fly-by) before it reached its intended observational position around L2.

Five minutes after launch, the Delta II first-stage engine cut off and the fairing jettisoned, exposing the observatory for the first time to the full space environment. Although the launch vehicle was tracked by radar station and its telemetry was received by the Boeing launch team, there was no contact with the observatory itself during launch and ascent. At approximately 21:00 GMT the signal from of WMAP's omni-directional was picked up by NASA's TDRS-W satellite and relayed to the ground, confirming that the payload was in good health and that all parameters were nominal. The WMAP payload was successfully inserted in a  $\sim 185$  km elliptical parking orbit with a  $\sim 28.7^\circ$  inclination.

### 1.3.3 Deployment and Instrument Power On

From the moment the observatory was switched to internal power, 5 minutes before launch, until deployment of the solar array panels, the observatory relies on power provided by the battery. At 21:03 GMT an on-board procedure triggered the deployment of the solar array. Immediately after this event the spacecraft oriented itself along the Sun-line maximizing the electrical power being generated by the array and, at the same time, protecting the instrument from the solar radiation.

At 21:43 GMT the WMAP instrument was powered in flight for the first time: housekeeping data was monitored as the instrument cooled and the flight burn-in phase was completed as scheduled. All science signals were within nominal limits during the cool down period. HEMT drain currents and RF radiometer total power were similar to the modeled response based upon the thermal environment and the radiometric flux presented to the instrument. The RXB temperature peaked at  $\sim 293$  K before cooling as anticipated due to the instrument power on time, thermal loads, and cooling profile. No anomalies were noted in the instrument electronics system (AEU/DEU and PDU) performance.

A platinum resistance thermometer (PRT) on top of the thermal reflector system radiator (DTAMXTOPRADT) failed on 2001:185:1100 GMT. From the flight telemetry we conclude that the sensor failed open and remains in this state. This failure was not completely unexpected, a similar sensor at the same location had failed during ground testing. Two days

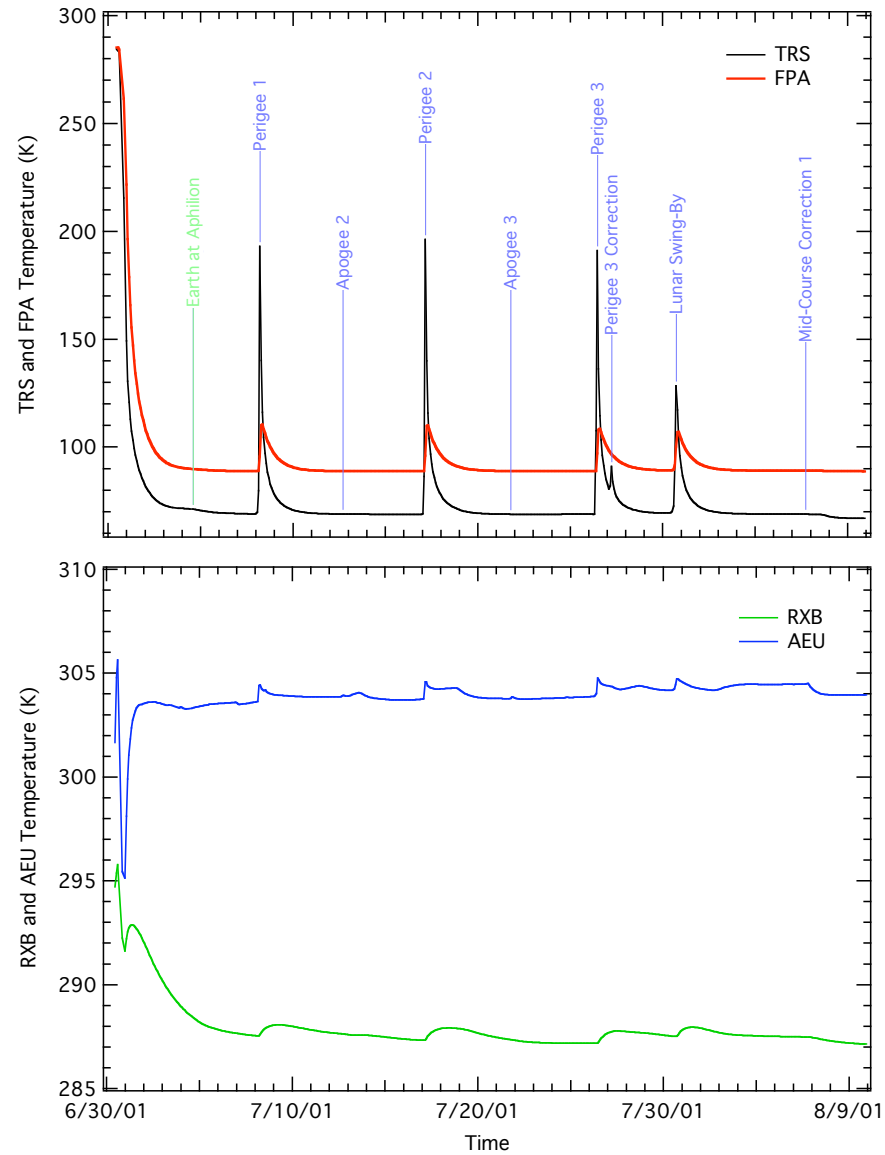


Figure 1.4: Cool-down Thermal Profile. Thermal profile of major instrument subsystems (TRS, FPA, RXB and AEU) from the launch to the beginning of the observations used for the first year maps.

after deployment on July 2, 2001 at 19:18 GMT the spacecraft entered observing mode for the first time.

### 1.3.4 Observatory Checkout

From June 30, 2001, when *WMAP* was launched, to August 17, 2001 the *WMAP* spacecraft and instrument underwent a period of formal checkout. During this period the spacecraft was contacted through the Deep Space Network (DSN) multiple times each day and all subsystem were tested thoroughly. The end of the in-flight checkout marked the beginning of normal mission operations; during this time the spacecraft is constantly in observing mode with one DSN contact per day. The spacecraft exits observing mode only for the planned station keeping maneuvers (see section 1.3.10) or if an unexpected event (see Table 1.9) puts it in “Safehold”. Details of the spacecraft in-flight checkout are presented in Jackson (2002).

### 1.3.5 Phasing Loops

Three orbital phasing loops and a lunar gravity assist were employed to perform the transfer to the mission’s operational orbit – a Lissajous orbit about the Sun-Earth L2 Lagrange point,  $\sim 1.5$  million km from Earth in the anti-Sun direction. To fine tune the spacecraft trajectory in preparation for the Lunar Fly-by, 7 burns were performed while at Earth’s perigee (4) and apogee (3).

Thruster calibration maneuvers were performed at apogees. This allowed calibration of the propulsion system using the thruster configurations for the phasing loop and station keeping burns.

A summary of the phasing loops maneuvers as well as all the other maneuvers performed during the first year of the *WMAP* observatory’s operations are given in Table 1.6. The first perigee burn (P1) was the first of a series of incremental adjustments of the satellite’s orbital energy and phasing for the final lunar assist. The second perigee burn (P2) provided a slight correction in preparations for the critical final perigee burns. The velocity boost provided by the final perigee (P3) and final correction (P3c) burns tuned the orbit for a lunar encounter at the desired time and location to achieve the desired eclipse free trajectory (i.e. an orbit that does not cross Earth-shadow’s cone). The temperatures of the primary reflectors exhibited significant transients during the perigee passes (see Figure 1.4) as they were exposed to both Earth IR inputs and edge-on solar inputs to the upper portion of their +X sides. This was an anticipated aspect of the mission design.

The phasing loops were also used to measure the far side-lobe response of the *WMAP* optical system. See Barnes et al. (2003) for details. In particular during the first orbital phasing loop (July 2-8, 2001), while the Moon was close enough to be a significantly bright thermal source, the spacecraft was operated in a scanning pattern very similar to the flight observing mode with the Moon sweeping through the optical system far side-lobes.

Event	yyyy:ddd:hhmm GMT	$\Delta V$ (m/s)	Burn (s)	Altitude (km)
Apogee 1	2001:185:1322	1.921	106	299,478 (E)
Perigee 1	2001:189:0433	20.194	1274	3,098 (E)
Apogee 2 (+Z Cal)	2001:193:1611	0.254	41	347,891 (E)
Perigee 2	2001:198:0336	2.514	177	2,955 (E)
Apogee 3 (-Z Cal)	2001:202:1854	0.296	40	356,012 (E)
Perigee 3	2001:207:1029	7.410	546	4,741 (E)
Perigee 3 Correction	2001:208:0430	0.308	24	158,306 (E)
Lunar Swing-By	2001:211:1637	N/A	N/A	5,279 (M)
Mid-Course Correction 1	2001:218:1637	0.103	18	755,736 (E)
Mid-Course Correction 2	2001:257:1551	0.042	6	1,402,107 (E)
Station Keeping 1	2002:016:1650	0.428	72	(L2)
Station Keeping 2	2002:128:1603	0.348	49	(L2)
Station Keeping 3	2002:211:1638	0.460	66	(L2)
Station Keeping 4	2002:309:1921	0.564	96	(L2)
Station Keeping 5	2003:071:1350	0.321	50	(L2)
Station Keeping 6	2003:316:1511	0.251	42	(L2)
Station Keeping 7	2004:069:1524	0.663	112	(L2)
Station Keeping 8	2004:224:1748	0.326	56	(L2)
Station Keeping 9	2004:349:1926	0.218	66	(L2)
Station Keeping 10	2005:094:1142	0.326	56	(L2)
Station Keeping 11	2005:208:1504	0.399	63	(L2)
Station Keeping 12	2005:314:1101	0.232	37	(L2)
Station Keeping 13	2006:066:1528	0.233	48	(L2)
Station Keeping 14	2006:165:1552	0.164	29	(L2)
Station Keeping 15	2006:313:1619	0.179	31	(L2)
Station Keeping 16	2007:067:1445	0.046	7	(L2)
Station Keeping 17	2007:178:0001	0.447	69	(L2)
Shadow Avoidance	2007:248:1438	8.200	623	(L2)
Shadow Avoidance Corr.	2007:269:1359	0.157	25	(L2)
Station Keeping 18	2008:023:1424	0.232	36	(L2)
Station Keeping 19	2008:156:1635	0.588	91	(L2)
Station Keeping 20	2008:282:1402	0.509	79	(L2)
Station Keeping 21	2009:042:2126	0.357	66	(L2)
Station Keeping 22	2009:197:1608	0.488	77	(L2)
Station Keeping 23	2010:020:1455	0.723	113	(L2)
Station Keeping 24	2010:133:1738	0.642	121	(L2)
Deorbit Maneuver 1	2010:251:1520	6.737	1205	(L2)
Deorbit Maneuver 2	2010:264:1810	35.749	3624	(HS)
Deorbit Maneuver 3	2010:273:1540	32.114	3655	(HS)
Deorbit Maneuver 4	2010:292:2020	17.245	3851	(HS)

Table 1.6: *WMAP* Maneuver Summary. The altitude in the last column is measured either respect to the surface of the Earth (E) or it indicates that the satellite starts at L2, or it has left L2 for its final heliospheric orbit (HS).

### 1.3.6 Earth IR and Outgassing

The materials and processes used in the construction of the *WMAP* Observatory result in a small mass loss due to outgassing. Outgassing from and re-deposition of materials on space-craft surfaces are anticipated in flight due to the loss of volatile materials and the pre-flight exposure to the ambient environment. Outgassing products emitted and re-encountered by spacecraft have a finite capture probability which increases upon cooling. Pre-flight contamination estimates did not indicate a concern for critical passively-cooled elements and optical sensors. In-flight performance of these subsystems are consistent with these estimates. In flight, outgassing by-products resulted in a small but detectable perturbation on the system's total angular momentum during perigee maneuvers (Starin et al., 2002). This observation may be of potential interest to the mission design of spacecraft with large cold surfaces.

Prior to each perigee maneuver, *WMAP* was in its nominal science observing mode. The first command to prepare for a burn maneuver placed the system into Inertial Mode. Once in this configuration for the perigee pass, the spacecraft and its solar array panels were oriented approximately 45-to-50 degrees from the Sun-line and the instrument was directed toward the nadir. This placed the thrusters in the proper orientation for the burn. These conditions also result in an attitude profile which allows the Sun to briefly heat portions of the instrument and the Earth albedo to illuminate the anti-solar side of the array before perigee. At the first perigee, a torque of 0.004 Nm and a peak system momentum of 2 Nms were noted before the ASC returned to nominal state. (Note: The maximum allowed wheel torque and momentum are 0.215 Nm and 10 Nms respectively. If these values are exceeded then the on-board software invokes "Safehold" mode. The wheels can store a total momentum of  $\pm 75$  Nms. The event did not pose a performance problem for the ACS at any time.)

To understand this small perturbation on the ACS response, we recall that once the solar arrays are deployed the heavily insulated backside, which forms a solar shield for the instrument, rapidly cools to space. By design, this protects the *WMAP* telescopes from millimeter wave emission from the Sun and reduces the instrument's thermal load to facilitate passive cooling. The solar shield fills approximately one-third of the spacecraft central truss field-of-view. As a result, these cooled surfaces serve as a collection point for outgassing by-products from the central hub electronics, blanketing, and vent paths from the warm portions of the instrument. Based upon the pre-launch configuration, we estimate a mass of  $\sim 0.8$  kg settles on the back of the solar shield in flight. The dominant outgassing component, water, has sufficient energy to be liberated in high vacuum when warmed above 130 K.

Thermal sensors indicate that the Earth infrared exposure was sufficient to sublime water on the back of the solar shield during the perigee maneuvers. Due to shadowing of Earth IR by the instrument and central hub, the release of the material on the back of the solar array panel was delayed in time. The resultant imbalance in the sublimation rate across the array is consistent with the observed torque magnitude and profile. This basic hypothesis is supported by telemetry from the coarse sun sensors (CCS) and subsequent analysis of *WMAP*'s trajectory. The mass of the sublimate material for each perigee event and  $\sim 9$  day outgassing time constant derived from the telemetry are compatible with the anticipated range of parameters for the *WMAP* observatory. The time between perigee maneuvers and

subsequent heating events enabled  $\sim 97\%$  of the outgassing products to be dumped from the solar shield before proceeding to L2.

### 1.3.7 Lunar Fly-by

Although the propulsion system was passive during the lunar swing-by, the encounter has a large influence on the satellite's final trajectory. On July 30, 2001 at 16:37 the lunar swing-by occurred as planned.

### 1.3.8 Mid-course Correction

To correct the growth of errors from the nominal trajectory to the L2 Lissajous orbit, two mid-course correction (MCC1 and MCC2) burns were planned and executed prior to the first Jupiter beam calibration season. This approach allowed minimal propellant usage and minimized the potential disruption during main beam mapping using Jupiter. The thermal stability of the observatory was sufficiently stable to begin collection of science data on 2001:222 (08/10/2001).

### 1.3.9 Observing Mode

The spacecraft has six operational modes (Bennett et al., 2003c) but it spends more than 99% of the time in observing mode. While in observing mode, the spacecraft spins around its vertical (Z) axis every 129.3 s while the Z axis precess around the Sun-line every 1 hour described by cone with an half-angle of  $22.5^\circ$ . This compound motion is achieved varying the speeds of the 3 reaction wheels mounted symmetrically around the spacecraft's lower deck (see Figure 1.1). Excess momentum is unloaded during the station keeping maneuvers.

### 1.3.10 Station Keeping

Station keeping burns are performed to maintain the desired orbit. During these maneuvers the satellite is de-spun to operate in Delta-V mode. Station keeping maneuvers are designed to minimize thermal disturbance and duration. The science data is suitably flagged in the archive to indicate these activities. A list of the station keeping maneuvers is included in Table 1.6.

During the first attempt at SK17, June 25, 2007, it was discovered that the thrusters did not fire as commanded. Investigation into the anomaly determined that the most likely cause was a single event upset in the Solid State Power Controller (SSPC) that switches power to the thrusters; the thrusters were powered off even though the telemetry indicated that it was powered on. During the second attempt at this maneuver the next day, the SSPC was commanded to power the thrusters off and then on; this cleared the anomaly and the thrusters fired normally. These steps were added to the standard procedure for later station keeping maneuvers.

In September of 2007, two maneuvers were performed to prevent WMAP from being eclipsed by the Earth. The first was maneuver, of 623 seconds duration, adjusted the orbit

to avoid the Earth's shadow. The second, 25 second, maneuver was performed three weeks later to fine-tune the orbit.

On August 1, 2008, *WMAP* was partially eclipsed by the Moon. The shadow would occult no more than 4% of the sunlight so it was decided to simply fly through the shadow instead of maneuvering to avoid it.

### 1.3.11 Pointing

The *WMAP* observatory orientation is controlled by a redundant attitude control system (ACS) which integrates the signals from multiple sensors through a Kalman filter and acts upon a set of reaction wheels and thrusters to maintain the desired spacecraft operational mode. The attitude control system sensors component suite includes:

- Course Sun Sensor (CCS)
- Digital Sun Sensor (DSS)
- 2 Two-Axis Rate Assemblies (TARAs) or Gyroscopes
- 2 Autonomous Star Trackers (ASTs) [Lockheed-Martin AST201 Star Trackers]

Three reaction wheels provide attitude control and an eight thruster (2 roll, 2 pitch, 2 yaw, and 2 backups) propulsion system provides the orbit adjustment capabilities needed to achieve and maintain the correct L2 trajectory. The eight thrusters are also used for attitude control during the orbit maneuvers and for unloading any system momentum buildup on the spacecraft.

*WMAP*'s ability to reconstruct a full map of the sky from a series of differential measurements depends greatly upon the observatory capability of maintaining a stable highly, inter-linked observing pattern. The motion of the *WMAP* observatory is specified in terms of 3-1-3 Euler angles and rotations specified in *WMAP*'s rotating sun reference (RSR) frame. Because the Z axis of the RSR frame is defined as the vector from *WMAP* to the Sun, the three Euler angles are defined as follows:  $\phi$ , the precession angle about the Sun-line;  $\theta$ , the angle between the spacecraft Z axis and the Sun-line; and  $\psi$ , the spin angle about the spacecraft Z axis. The performance requirements for observing mode are specified in terms of the  $\phi$  and  $\psi$  rates and the  $\theta$  angle. Table 1.7 shows the observing mode requirements and the in-flight measured performance.

#### 1.3.11.1 Pointing Correction

Variations in the telescope pointing reconstruction at the level of  $\sim 0.5$  minute of arc between the various Jupiter observational seasons were noted. By investigating the quaternions derived from the A and B star trackers, this systematic variation was traced to a thermally driven change in the tracker mounting geometry. Tracker mount sensitivities of  $\sim 8$  arcsec/K correlated with the physical temperature of the solar array are observed. Corrections based

upon a simple spacecraft thermal model (see section 1.4.4) are applied to the data to remove this residual effect as a smooth function of the orbital phase.

The origin of this effect can be traced to the geometry of the spacecraft hex hub structure used for mounting the trackers (Bennett et al., 2003c, Figure 2). As the observatory proceeds along its orbit, the lower deck temperature is slowly modulated by  $\sim \pm 3\text{K}$  due to changes in the sun-to-spacecraft separation distance (see section 1.4). Meanwhile, the passively cooled anti-solar portion of the observatory remains at essentially constant temperature. Due to thermal expansion of the spacecraft structure, the warm end of the hex hub walls rotate toward the  $-z$  axis by an angle of order:

$$\begin{aligned}\delta\theta &= R_{hex}\alpha_{Al}\Delta T/H_{hex} \\ &\approx (0.4m)(0.22 \times 10^{-4}/K)(6K)/0.6m \sim 8.8 \times 10^{-5}\text{rad}\end{aligned}$$

If uncorrected, this induces an apparent change in tracker elevation of order  $\delta\theta_{tracker} \sim 2\delta\theta_{wall} \sim 1.8 \times 10^{-4}$  radians. The pointing error observed in practice,  $\sim 1.5 \times 10^{-4}$  radians, is consistent with the results of a thermal-mechanical Finite Element Model (FEM) model of the observatory's flight configuration.

Pointing corrections are applied early in the processing pipeline, such that the quaternions in all released TOD files have been corrected for thermal flexure. The estimated angular correction takes the form:

$$\delta\theta = \alpha\Delta T \quad (1.1)$$

where  $\alpha$  is a constant with units  $''/K$  and  $\Delta T$  is the difference in spacecraft temperature between the time of observation and day 222 of 2001.

For the first-year and three-year data releases, only small angular corrections in elevation were applied to the quaternions using  $\alpha_{el} = 2.615''/K$ . For the five- and seven-year releases, the elevation correction was retained, and a successive corrective azimuthal rotation was also applied, with  $\alpha_{az} = -1.3''/K$ . Spacecraft temperature for these releases was computed using the model for the damper described in section 1.4.4.

For the nine-year release, angular corrections in both elevation and azimuth were updated, and a separate measure of spacecraft temperature was used for each. For elevation,  $\alpha_{el} = 2.816''/K$  and  $\Delta T$  is interpolated from the damper1 thermistor on-board. For azimuth,  $\alpha_{az} = -4.024''/K$ , using the MAC baseplate thermistor.

Euler States	Requirements	Pre-Calibration	Post-Calibration
$\phi$ precession rate (deg/s)	$-0.1 \pm 6.3\%$	$-0.1 \pm 9\%$	$-0.1 \pm 3.6\%$
$\theta$ (deg)	$22.5 \pm 0.25$	$22.5 \pm 0.064$	$22.5 \pm 0.0234$
$\psi$ spin rate (deg/s)	$2.784 \pm 5\%$	$2.784 \pm 0.32\%$	$2.784 \pm 0.13\%$

Table 1.7: Observing Mode Performance. The pre-calibration data where measured in flight but using the default calibration coefficients loaded in the ACS before launch. The post-calibration coefficients were uploaded on August 9, 2001, at the end of the in-flight checkout.

### 1.3.12 End of Mission

Nominal science operations ended on 10 August 2010. For the following ten days, operations continued using different precession angles to characterize the sun shade performance.

On 8 September 2010, a maneuver was performed to remove WMAP from L2 on its way to its final heliospheric orbit. A total of four burns were performed, using 42.88kg of the fuel on board and resulting in a heliospheric parking orbit far removed from L2. The final command to shut down the spacecraft transmitter was sent on 28 October 2010 at 21:44 and the operations component of the mission was declared over at 21:45.

## 1.4 The Thermal Environment

While a platform at L2 is certainly a much better place than Earth orbit for conducting CMB observations, it is still slightly affected by some solar induced disturbances. In this section we describe such disturbances and the effects that they have on the instrument stability.

Thermal data from the WMAP observatory not only provides a means of monitoring the health and safety of the various on-board systems, but enables one to search for and understand potential instrumental systematic effects. Detailed knowledge of the thermal performance of the observatory in flight is important in assessing the quality of the end data products.

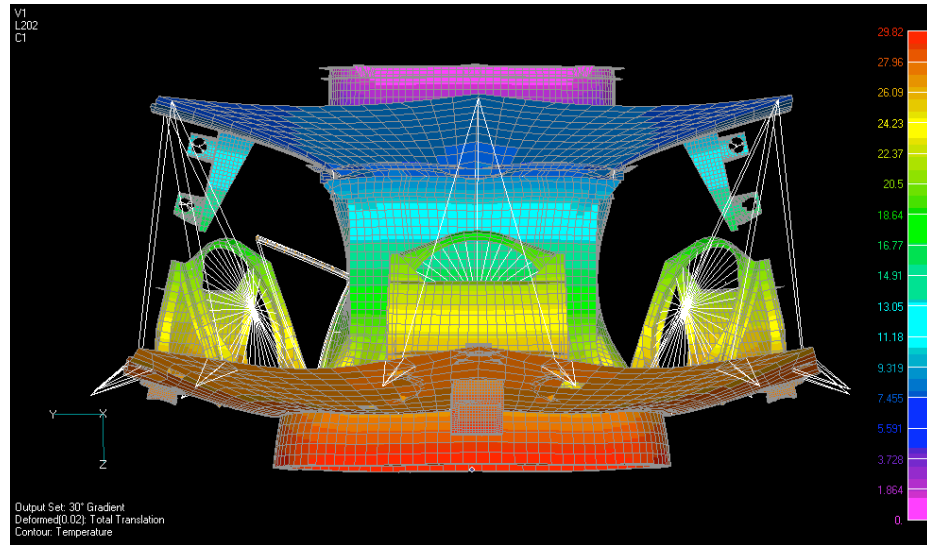


Figure 1.5: WMAP Thermal-Mechanical Distortion Finite Element Model (30 K Thermal gradient along spacecraft's z axis. Distortions are overly exaggerated for visualization purposes.

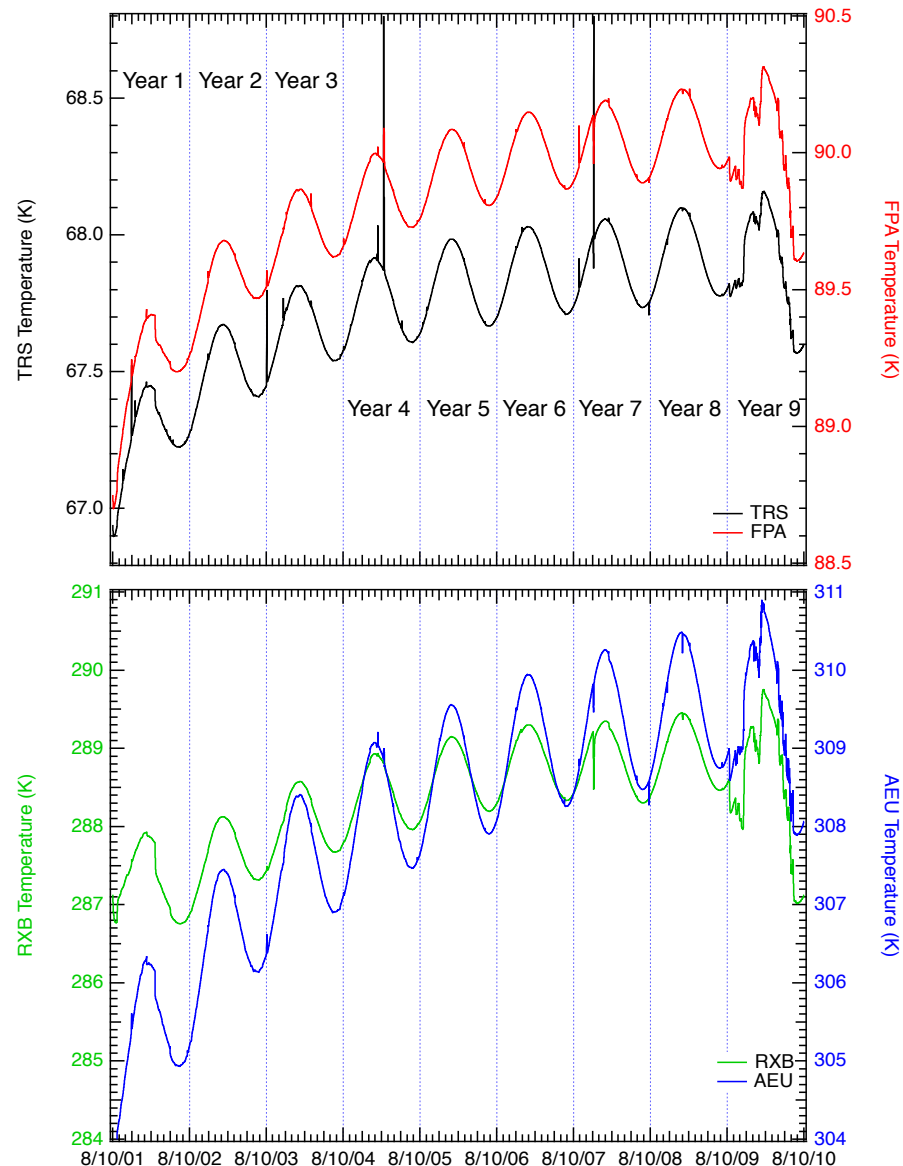


Figure 1.6: Nine Years Thermal Profile. The measured thermal profile for the cumulative nine years of operation covers 2001:222 (08/10/2001) to 2010:222 (08/10/2010). Expanded plots and details are shown in Figures 1.7, 1.8, 1.9, 1.10, 1.11, 1.12, 1.13, 1.14 and 1.15.

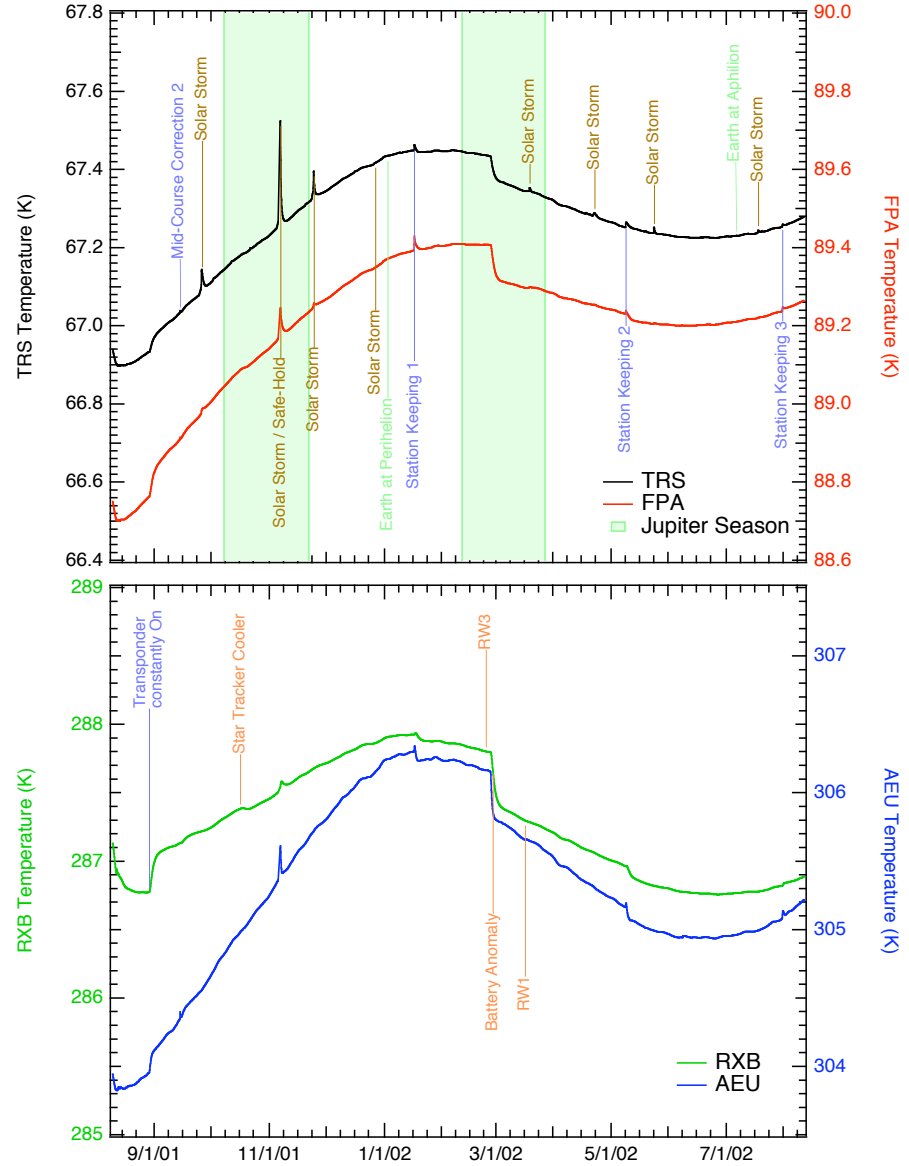


Figure 1.7: First Year Thermal Profile. The measured thermal profile for the first year of operation covers 2001:222 (08/10/2001) to 2002:222 (08/10/2002). Transient events are noted. Modulation from the eccentricity of Sun-Earth L2 orbit is clearly visible. RW1 and RW3 indicate times when there were thermal perturbations due to small changes in reaction wheel drag. See Appendix B for additional details.

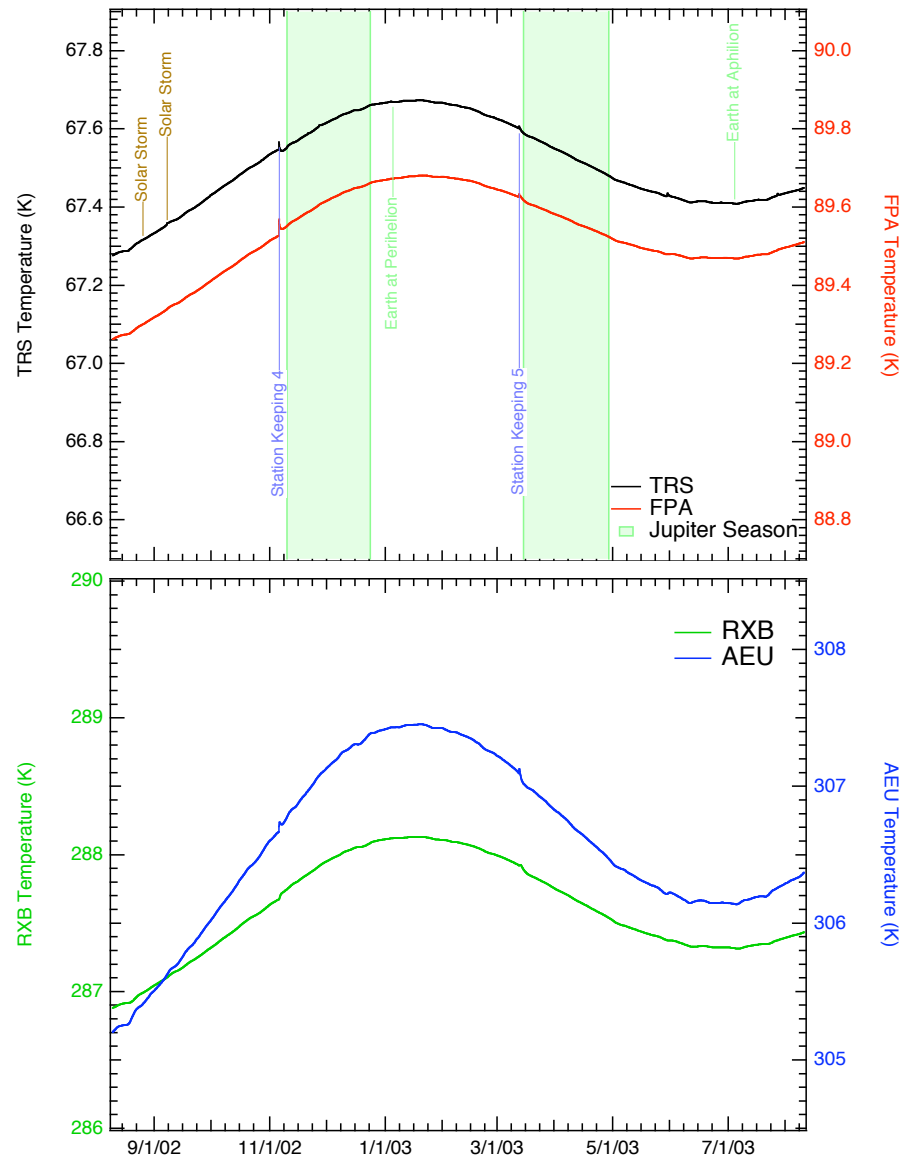


Figure 1.8: Second Year Thermal Profile. The measured thermal profile for the second year of operation covers 2002:222 (08/10/2002) to 2003:222 (08/10/2003). Transient events are noted. Modulation from the eccentricity of Sun-Earth L2 orbit is clearly visible. See Appendix B for additional details.

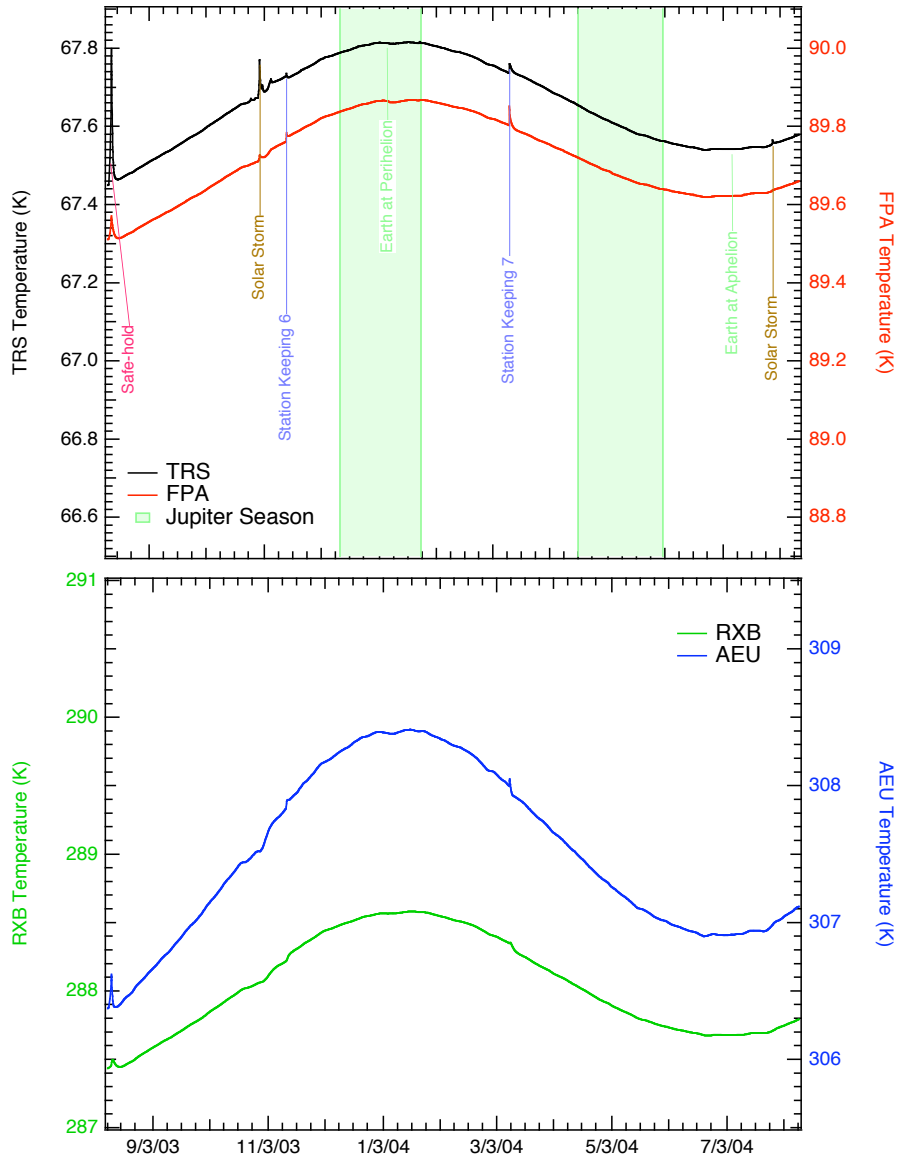


Figure 1.9: Third Year Thermal Profile. The measured thermal profile for the third year of operation covers 2003:222 (08/10/2003) to 2004:222 (08/09/2004). Transient events are noted. Modulation from the eccentricity of Sun-Earth L2 orbit is clearly visible. See Appendix B for additional details.

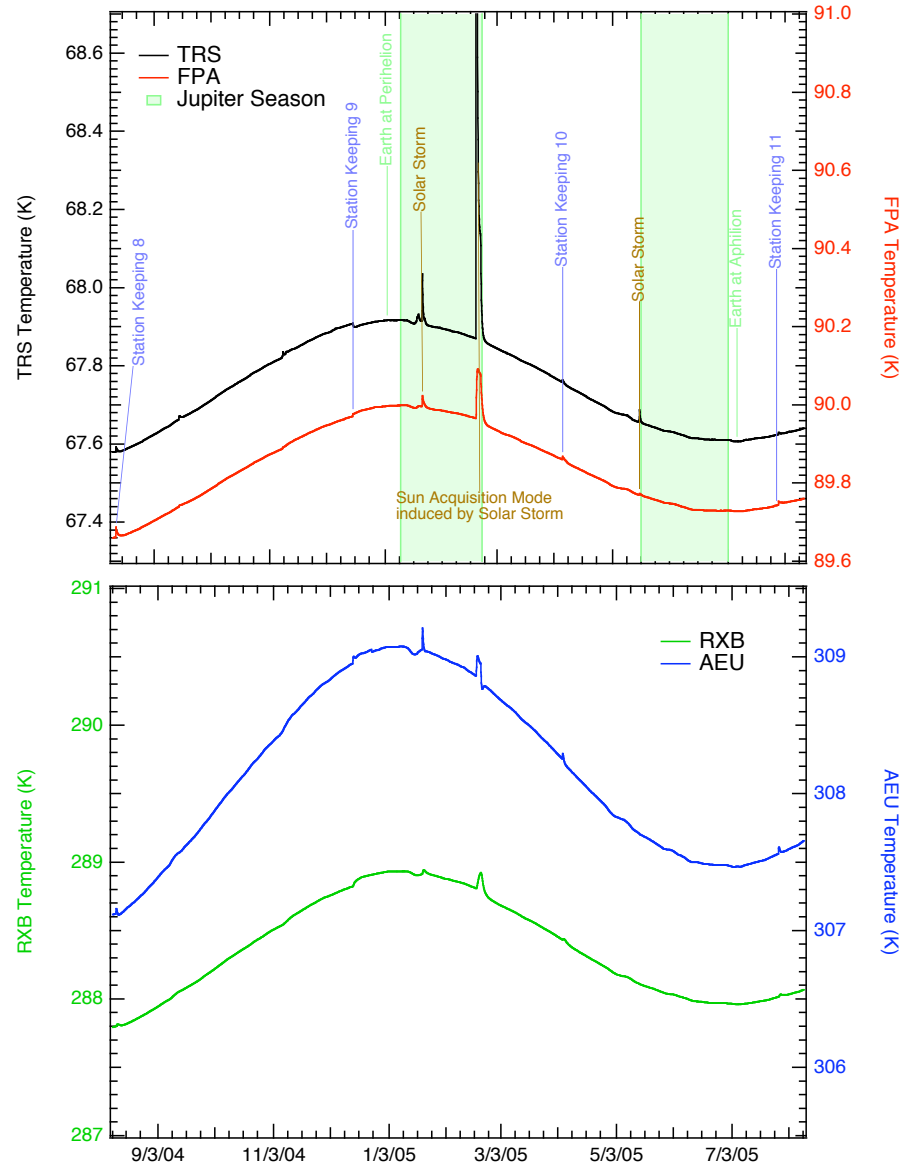


Figure 1.10: Fourth Year Thermal Profile. The measured thermal profile for the fourth year of operation covers 2004:222 (08/09/2004) to 2005:222 (08/10/2005). Transient events are noted. Modulation from the eccentricity of Sun-Earth L2 orbit is clearly visible. See Appendix B for additional details.

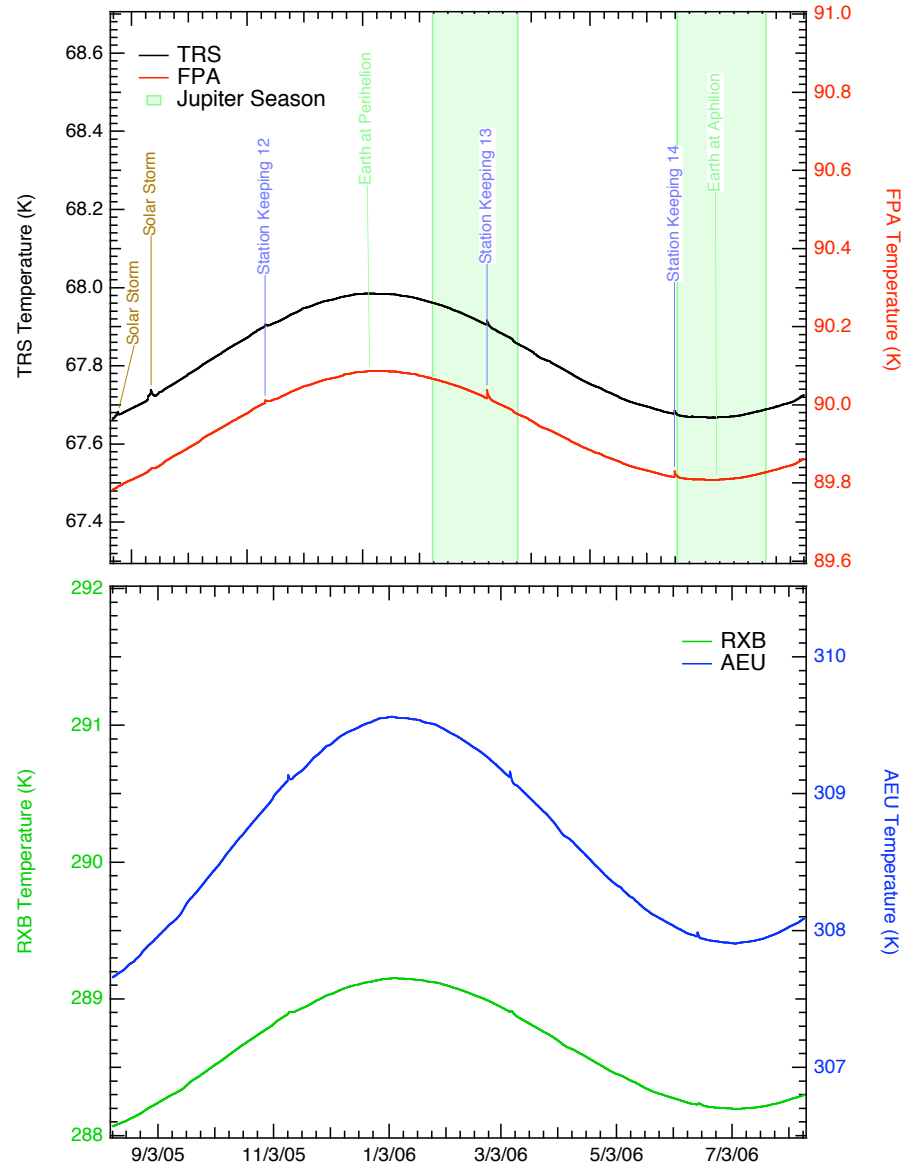


Figure 1.11: Fifth Year Thermal Profile. The measured thermal profile for the fifth year of operation covers 2005:222 (08/10/2005) to 2006:222 (08/10/2006). Transient events are noted. Modulation from the eccentricity of Sun-Earth L2 orbit is clearly visible. See Appendix B for additional details.

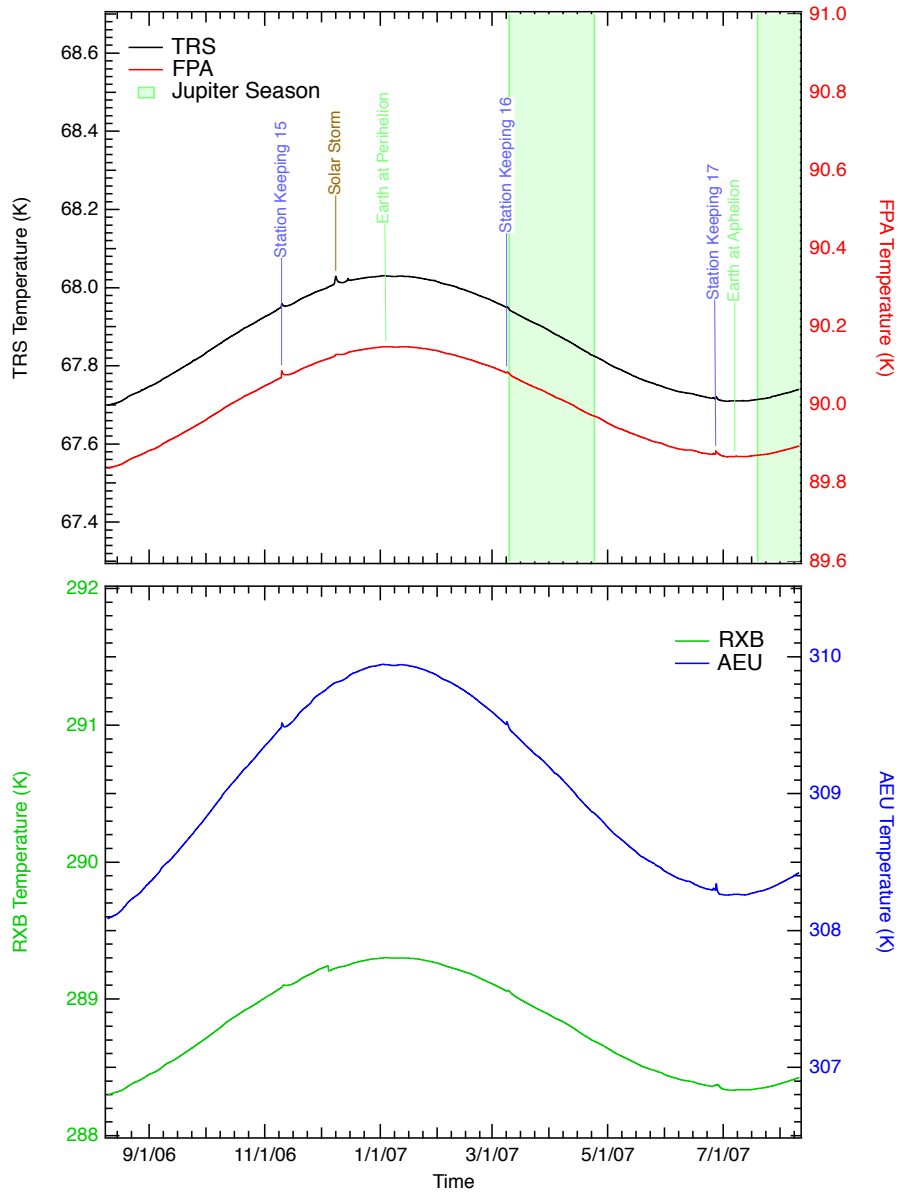


Figure 1.12: Sixth Year Thermal Profile. The measured thermal profile for the sixth year of operation covers 2006:222 (08/10/2006) to 2007:222 (08/10/2007). Transient events are noted. Modulation from the eccentricity of Sun-Earth L2 orbit is clearly visible. See Appendix B for additional details.

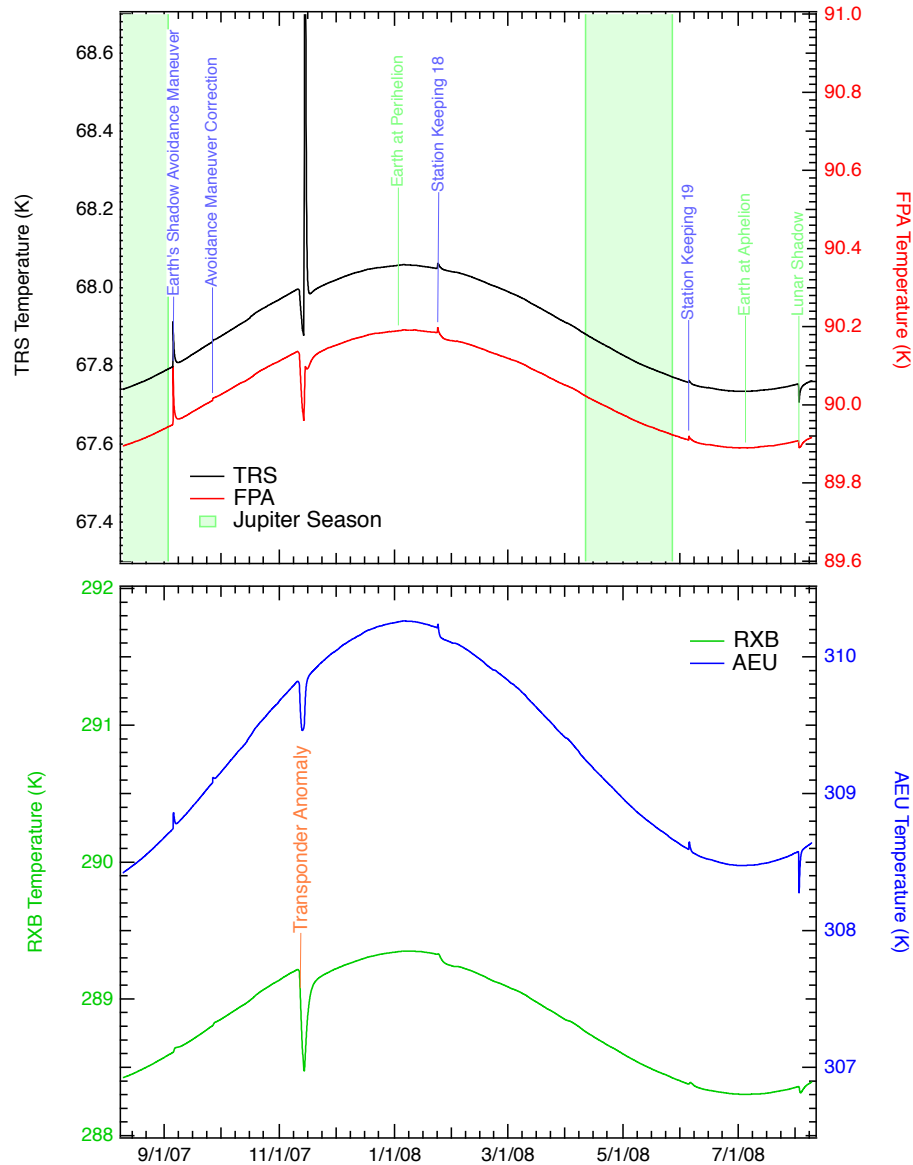


Figure 1.13: Seventh Year Thermal Profile. The measured thermal profile for the seventh year of operation covers 2007:222 (08/10/2007) to 2008:222 (08/09/2008). Transient events are noted. Modulation from the eccentricity of Sun-Earth L2 orbit is clearly visible. See Appendix B for additional details.

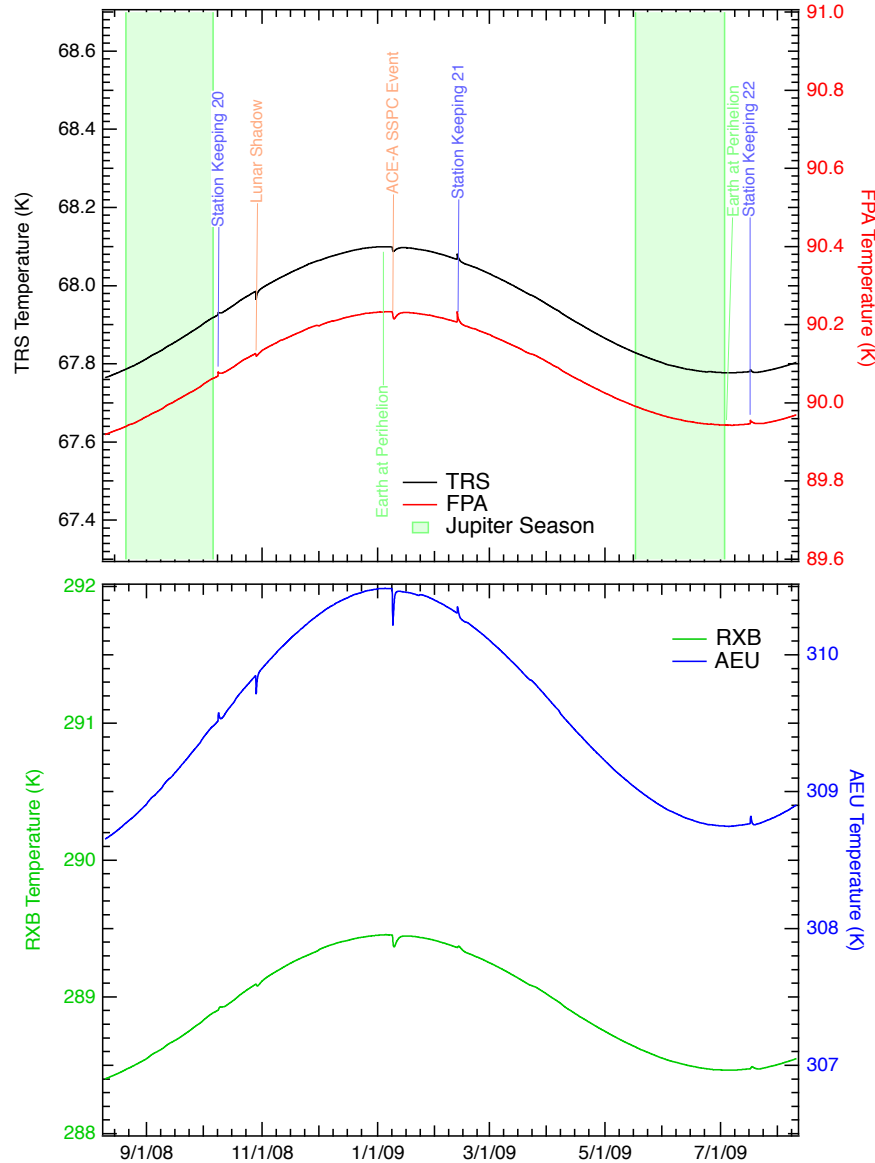


Figure 1.14: Eighth Year Thermal Profile. The measured thermal profile for the eighth year of operation covers 2008:222 (08/09/2008) to 2009:222 (08/10/2009). Transient events are noted. Modulation from the eccentricity of Sun-Earth L2 orbit is clearly visible. See Appendix B for additional details.

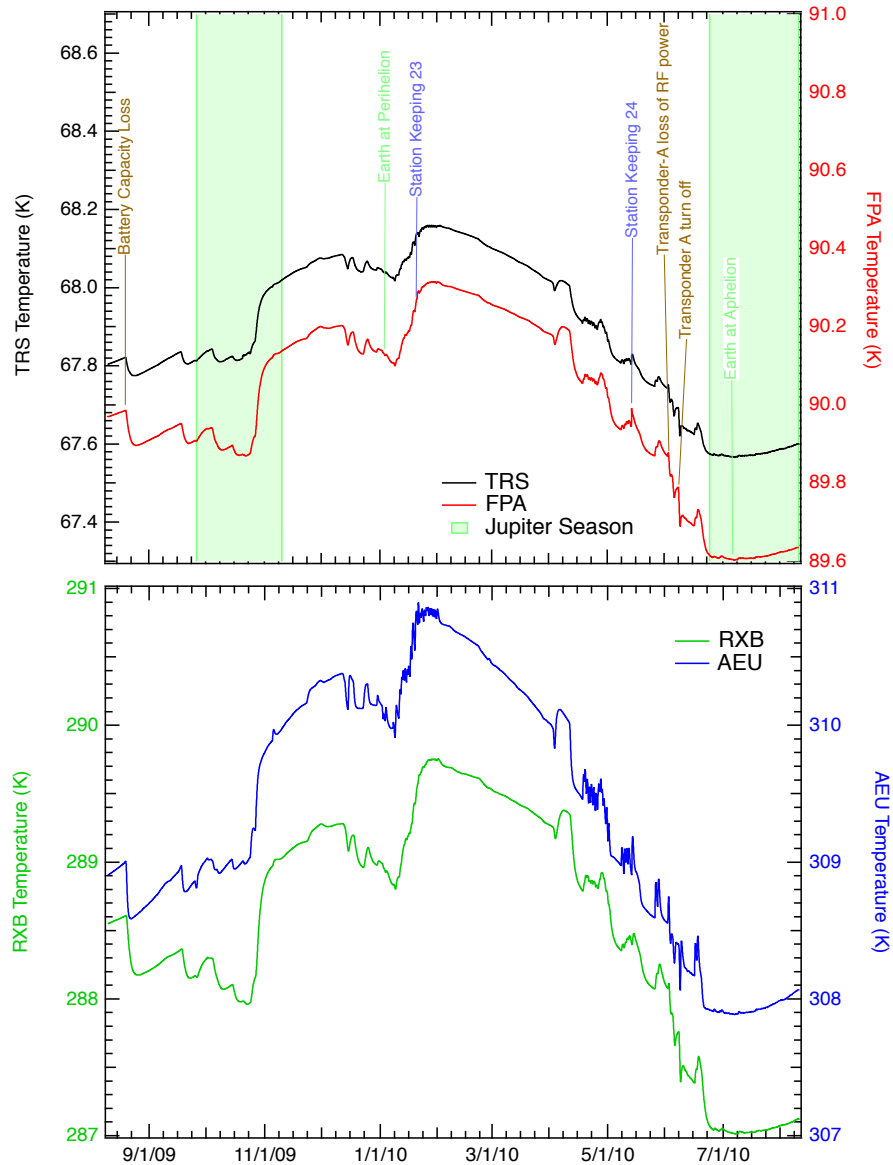


Figure 1.15: Nineth Year Thermal Profile. The measured thermal profile for the nineth year of operation covers 2009:222 (08/10/2009) to 2010:222 (08/10/2010). Transient events are noted. Modulation from the eccentricity of Sun-Earth L2 orbit is clearly visible. See Appendix B for additional details.

In practice, *WMAP* maintains thermal equilibrium by balancing the absorbed solar radiation input and on-board electrical power dissipation with passive radiative cooling to space. The temperature of the entire spacecraft is extremely uniform due to the vehicle's orbital geometry, constant spin/precession rates and stable power draw. The dominant mechanism that drives changes in the system's temperature is the variation of spacecraft-to-sun separation as a function of orbital position; however, operationally induced changes in spacecraft power dissipation, aging or contamination of the thermal control coatings (e.g., insulating blankets, emissive coatings, reflective surfaces, etc), and solar flare events can also induce measurable thermal effects.

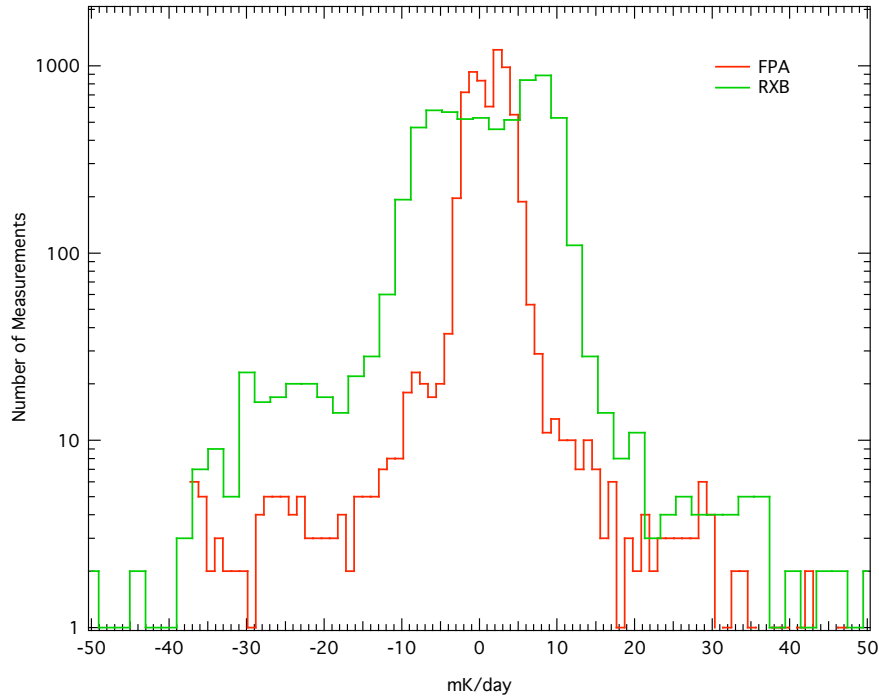


Figure 1.16: Instrument Temperature Rate Histograms. Histograms of the FPA and RXB temperature rates during the first year of science data. The widths of the distributions are  $3.9 \pm 0.2$  mK/day and  $11.2 \pm 0.6$  mK/day for FPA and RXB respectively.

*WMAP*'s thermal performance is monitored by a set of platinum resistance thermometers and thermistors (PRTs) which are installed at key locations throughout the system. A representative summary of the instrument's thermal history for the *WMAP* data is presented in Figures 1.7 - 1.9 and Figure 1.19.

#### 1.4.1 Temperature Monitor Architecture

The *WMAP* instrument temperature monitor system is designed to provide high sensitivity thermometry with sensitivity to temperature drifts and resolution of better than 0.25 mK over a temperature range from 40 K to 340 K. Absolute calibration is of secondary importance

with a requirement of  $\pm 1$  K accuracy. The primary purpose of the temperature monitor system is to permit the removal of any possible instrument or optics temperature driven offset drifts in the radiometers.

The system uses calibrated Rosemount<sup>2</sup> Platinum Resistance Thermometers (PRTs) energized with a 100  $\mu$ A rms sine-wave current at 195 Hz. The current is driven on a shielded twisted pair of wires of up to 10 m length. A second twisted pair within the same shield carries the voltage on the PRT back to a high-impedance, gain 100 differential receiver. Both the drive current and sense voltage are analog multiplexed with 30 PRTs and 2 calibration resistors per readout card and two cards for a total of 60 PRT circuits. WMAP used 57 PRT channels.

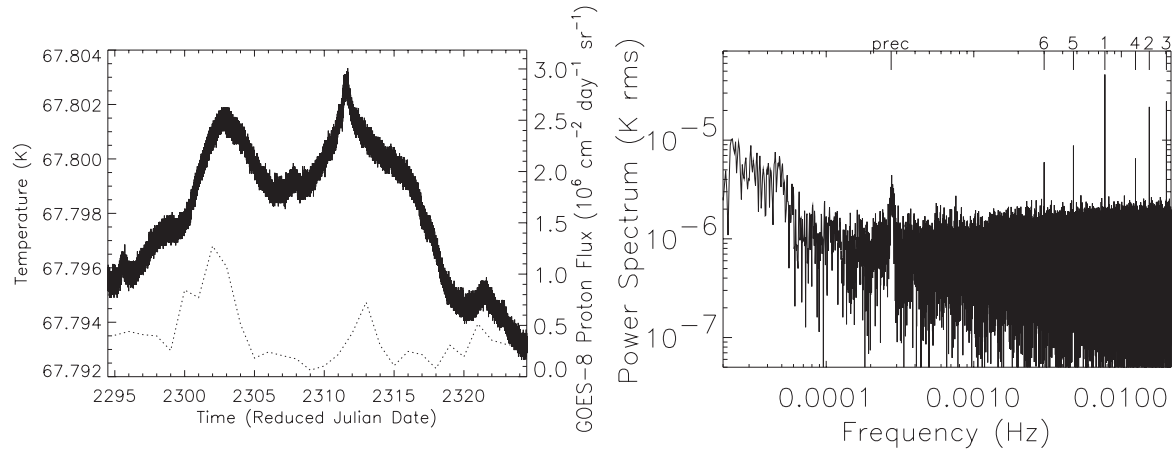


Figure 1.17: PRT Noise Power Spectrum. The left plot is the temperature of the top of the B-side primary mirror for a period of 30 days starting January 20, 2002. The temperature drift is driven by a combination of the changing distance to the sun and solar proton wind. The dotted line is the total solar proton flux as measured by the GOES-8 satellite scaled to the right axis. The right plot is the power spectrum of the temperature over the same period. The low frequency excess is due to the drifts seen on the left. The intrinsic thermometer drift is small relative to the thermal drifts in the system. Special frequencies are marked at the top with labels: “prec” is the spacecraft precession frequency and the numbers indicate the spin frequency harmonic. These are folded back by the Fourier transform. A 45  $\mu$ K RMS signal is seen at the spin harmonic and is the largest spin synchronous temperature signal seen on the spacecraft. The equivalent measurement noise of the thermometer system is about 1 mK $\sqrt{\text{s}}$ .

The PRT sensitivity is approximately  $2\Omega/\text{K}$ , constant over the range 40 to 360 K. The 100  $\mu$ A excitation gives voltage signal of about 200  $\mu$ V<sub>RMS</sub>/K. This signal is differenced with a reference sine wave derived from a reference resistor also in the 100  $\mu$ A current loop. The reference voltage amplitude is set with an 8 bit multiplying Digital to Analog Converter (DAC) which nulls the signal to within  $\pm 4$  K. The 8 nulling bits per PRT are stored in the

<sup>2</sup>Rosemount Aerospace, Inc., ”Rosemount Model 118MF Platinum Resistance Temperature Sensor,” 1989, Eagan, MN, technical specification.

DEU and set a PRT “window”. The windows overlap by 40%. The differenced signal is AC coupled, amplified and analog synchronously demodulated. The demodulated voltage is ripple filtered and integrated for 25 195 Hz cycles with a 16 bit synchronous charge-balance V/F ADC. The analog current and voltage sense multiplexers switch between PRTs after the sample integration is complete. Each PRT sample is therefore a 24 bit number including the 8 bits of window information. The gain is set so that the temperature resolution is 125  $\mu\text{K}/\text{ADC}$  unit. Each PRT is read once each 23 seconds (i.e.,  $\sim 4$  measurements per spin rotation) but not synchronously with the spin.

Assigning a resistance to the digital word for each thermometer sample requires the calibration of the ADC with the window DAC. Because the window DAC has differential non-linearity, the window sizes are not all identical. This leaves jumps in the calculated resistance when switching from one window to another. Because the purpose of the thermometry is largely to monitor temperature variations, these jumps are not important since no window transitions are expected once the temperatures stabilize during the data taking part of the mission. Because the windows overlap by 40%, a transition to the next window starts near the center of the new window minimizing window transitions. The correct window is found either with a binary search at startup, by command or after a saturated ADC samples two times in a row. The binary search is controlled by the DEU. During normal operations, a window transition is initiated when a PRT reading is within 10% of the edge of the current window.

#### 1.4.2 Temperature Monitor Performances

The sensitivity and stability of the temperature monitors is shown in Figure 1.17. Shown is a section of time where the solar input was not changing quickly because the observatory was at the minimum distance from sun and with no large solar flares to drive a thermal disturbance. The sensor shown is mounted to the top of the B-side primary mirror and shows the most thermal variation of any of the sensors. The power spectrum shows low-frequency power from the slow thermal drift of the changing distance to the sun and variations due to solar activity. There is also a  $\sim 45 \mu\text{K}$  RMS signal at the spin period of the spacecraft. The equivalent noise power spectral density is  $\sim 1 \text{ mK}\sqrt{\text{s}}$  for each of the thermometers.

Temperature calibration of the sensors is derived from the Rosemont calibration curves. Uncorrected offsets in the post-demodulation electronics and differential non-linearity in the window DAC result in an absolute temperature error of  $\pm 1 \text{ K}$ . The accuracy of temperature variations is derived from reference to precision resistors measured each multiplexing cycle.

Several of the thermal sensors in the FPA assembly exhibit variations which exceed that anticipated from an ideal PRT channel by a factor of several in flight on a time scale of hours. An example of interest is provided by DFW32FPATEET. See Figure 1.18 for power spectrum. In addition to the long-term overall thermal drifts, short-term variations of order 1 mK can be seen in the time order data on this sensor. One observes that this signature is reproduced with smaller amplitude in PRT channels DFW3AOMTT and DFW3BOMTT. This signature is consistent with the presence of a random variation in the physical temperature near this location. From the instrument’s thermal parameters, one estimates that this requires a

variation in power dissipation  $\sim 100\mu W$  in the vicinity of the W3A magic tee.

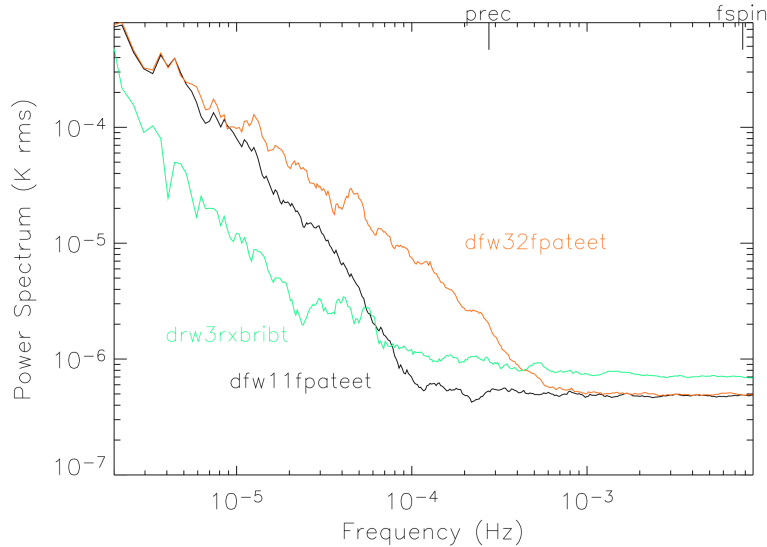


Figure 1.18: FPA and RXB Temperature Power Spectra. PRTs DFW32FPATEET and DFW11FPATEET are mounted on the cold hybrid tees of W32 and W11 radiometers respectively. DRW3RXBRIBT is mounted on an aluminum rib that supports the W3 DA inside the RXB. DFW32FPATEET shows sign of excess thermal variations as described in the text. These power spectra essentially define the envelope of the RXB and FPA temperature stability.

Data from the radiometer outputs and monitors were searched for signals correlated with the variance in DFW32FPATEET temperature sensor. We note that the resolution of the HEMT drain current monitor is sufficient to eliminate the possibility of a bias instability as the primary source of the fluctuations. This effect was not detected in the science data or instrument gain. In addition, the spacecraft housekeeping data were investigated for correlation with on-board activity and the observed effect. The non-detection of a source at the levels investigated suggests that the most likely candidate is a variation in one of the LED bias circuit channels. (note: The LEDs are used to illuminate the HEMT amplifier channel and are operated near saturation.) The fractional variations in the radiometer's total power monitor,  $dT_{sys}/T_{sys} \sim 6 \times 10^{-4}$ , dominate over the influence of thermal variations,  $dT_{amb}/T_{amb} \sim 1 \times 10^{-5}$ . This has a negligible influence on the instrument gain calibration model (Jarosik et al., 2003b). The presence of this noise source at this level has negligible impact upon the quality of the science data.

### 1.4.3 Sun Driven Yearly Temperature Changes

By design, the spacecraft has a large thermal gradient from its sunlit to dark-side. Temperatures for sensors range from  $\sim 330$  K for objects directly illuminated by the sun to  $\sim 60$  K for elements passively cooled to space. The variation in the satellite's distance from the sun as it progresses around its orbit at L2 changes the observatory's average temperature. To estimate the magnitude of this effect we consider the ratio of the solar flux intercepted at the maximum and minimum distance from the sun in the orbit. For a radiatively cooled object in an orbit with numerical eccentricity  $\varepsilon$ , one finds a relative change in the temperature on the sunlit side of order  $dT/T_{amb} \sim \varepsilon \ll 1$ . To a good approximation, for the WMAP orbit, the eccentricity is equal to that of the Earth,  $\varepsilon = 0.017$ , yielding an estimated orbital change with temperature of order  $\sim 5$  K for sensors well coupled to objects receiving direct illumination.

Over the course of the first year of observations, for directly illuminated objects, the component of the thermal signature correlated with the satellite-to-solar distance was  $\sim 4$  K. For objects shaded from the sun, the thermal isolation provided for in the design reduces the overall magnitude of this effect. For example, a typical electronics box mounted on the shaded side of the spacecraft hub experienced a temperature correlated with solar distance with amplitude of  $\sim 1$  K. Over the same period of time the thermal reflector system's temperature, which is shaded from direct solar input and well thermally tied to the radiator panels, was noted to change by less than  $\sim 0.2$  K. This is consistent with the performance anticipated from a detailed analysis of the thermal design.

### 1.4.4 Aging of Thermal Control Surfaces

In flight, exposure of the thermal control surfaces to ultraviolet radiation, charged particles, and surface contamination are anticipated to increase solar absorptance while leaving the infrared emittance essentially unchanged (Triolo et al., 1977; Gilmore & Bello, 1994). Published data on the degradation of materials in flight are essentially limited to the more tenuous GEO and LEO environments; however, qualitatively similar trends are anticipated for WMAP. Contamination by outgassing of volatile condensable materials, which are subsequently darkened by UV exposure, are anticipated to cause an initial modest increase in the effective aging rate for the first few months to year of the mission. As the outgassing rate tapers off, a slow and monotonic degradation of the coating performance is expected. Such a trend is consistent with the observed thermal performance of the WMAP observatory over the first year as presented in Figure 1.19 after taking into account contributions arising from the modest changes in the spacecraft's internal power dissipation.

A simple model of the long term temperature profile of the spacecraft can be written as the product of two term: a sinusoidal one accounting for the change in temperature due to the L2 motion around the Sun and an exponential one accounting for the change in absorptance due to the degradation of the spacecraft's surfaces. This can be written as

$$T(t) = T_o \left( 1 + \frac{\delta a}{4a_o} \left( 1 - e^{-t/\tau} \right) \right) \left( 1 + \frac{\delta R}{2R_o} \sin(\omega t + \phi) \right),$$

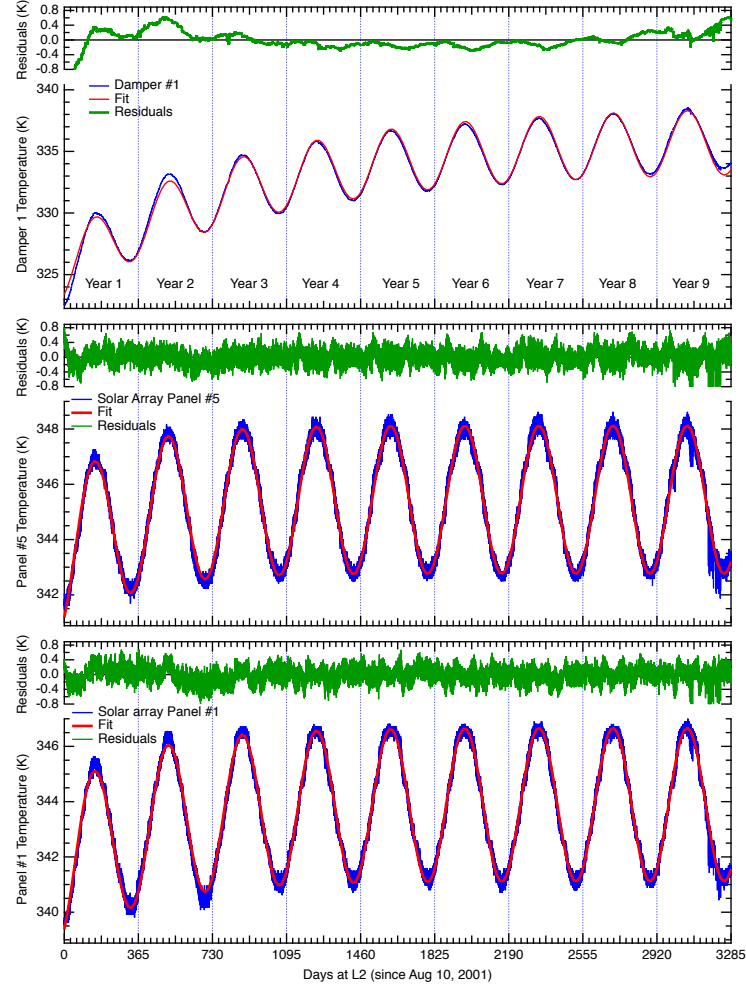


Figure 1.19: Solar Array Temperature Profile. The Damper sensor is mounted on the hinge's damper of solar array panel 1 while the two panel sensors are mounted directly on solar panel 1 and 2. These two sensors are thermistors and are not part of the instrument's temperature monitoring system described in section 1.4.1, the excess noise in the solar array sensors is due to the spacecraft temperature readout. Both datasets have been edited to remove spikes induced by the maneuvers and other singular events. Fits to the model described in the text are also displayed.

Damper	1 year	2 years	3 years	4 years	5 years	6 years	7 years	8 years	9 years	
$T_o$	324.6	324.5	324.7	324.9	325.0	325.2	325.3	325.4	325.5	[K]
$\delta R/R_o$	-0.018	-0.017	-0.017	-0.016	-0.016	-0.016	-0.016	-0.016	-0.016	[-]
$\delta a/a_o$	0.143	0.102	0.110	0.117	0.122	0.125	0.126	0.128	0.130	[-]
$\tau$	679	417	507	602	695	758	808	868	930	[days]
$\phi$	2.14	2.17	2.16	2.16	2.16	2.17	2.17	2.17	2.17	[rad]

Panel #1	1 year	2 years	3 years	4 years	5 years	6 years	7 years	8 years	9 years	
$T_o$	341.65	341.3	341.5	341.6	341.6	341.6	341.6	341.6	341.6	[K]
$\delta R/R_o$	-0.017	-0.017	-0.017	-0.016	-0.016	-0.016	-0.016	-0.016	-0.016	[-]
$\delta a/a_o$	0.034	0.025	0.026	0.026	0.026	0.027	0.027	0.027	0.027	[-]
$\tau$	519	198	294	345	384	384	376	384	390	[days]
$\phi$	2.14	2.20	2.19	2.19	2.19	2.19	2.19	2.19	2.19	[rad]

Panel #5	1 year	2 years	3 years	4 years	5 years	6 years	7 years	8 years	9 years	
$T_o$	343.41	343.21	343.31	343.32	343.34	343.30	343.3	343.3	343.4	[K]
$\delta R/R_o$	-0.015	-0.016	-0.016	-0.016	-0.016	-0.016	-0.016	-0.016	-0.016	[-]
$\delta a/a_o$	0.0280	0.023	0.024	0.024	0.024	0.024	0.024	0.024	0.024	[-]
$\tau$	401	210	270	281	292	284	289	297	300	[days]
$\phi$	2.16	2.19	2.19	2.19	2.19	2.19	2.19	2.19	2.19	[rad]

where  $T_o$  is the initial equilibrium temperature of the spacecraft,  $a_o$  the initial absorptance,  $\delta a$  the change in absorptance over a time large compared to the surface degradation time constant  $\tau$ ,  $\delta R$  is the departure from a circular orbit of radius  $R_o$  and we assume that  $\delta a/a_o$  and  $\delta R/R_o$  are small compared to unity. Setting  $\omega$  equal to  $2\pi$  over 1 year and fitting for all the other parameters we obtain:

The value of  $\delta R/R_o$  is in good agreement with Earth's orbit eccentricity (0.0167) and a 10% change in absorptance is also consistent with previous observations of surface degradation (Gilmore & Bello, 1994).

#### 1.4.5 Operationally Induced Disturbances

Control over the spacecraft's solar absorptance, radiative cooling, and dissipated power density are used to maintain a stable operational temperature for the various components. During nominal operation, changes in the power dissipation in the various electronics boxes have, by design, a negligible impact on the instrument performance. As a rule, as described in Bennett et al. (2003c), passive thermal control is employed for normal observing mode. Survival heaters, which are nominally "off", are engaged by mechanical thermostats in case of an emergency and the star tracker Peltier coolers which have an internal set point will actively adjust.

Slight changes in WMAP's power dissipation were encountered in maintaining the system. A summary of the instrument's thermal performance is presented in Figures 1.7 - 1.9. Several operationally induced disturbances of potential interest from the events log (Appendix B) are

indicated. The dominant thermal disturbances in this time frame result from the decision to leave the transponder on and a partial short of a battery cell which subsequently resulted a change in the power system's nominal voltage. During station keeping maneuvers it is necessary to change in *WMAP*/Sun-line angle. Secondary thermal perturbation sources which occur during these periods include pre-heating the thrusters to operate with approximately optimal and known efficiency, changes in reaction wheel dissipation after momentum unload, and autonomous changes in the power system solar array configuration. Maneuvers and other operationally induced thermal events which may induce noise in the calibration, are flagged. See Table 1.8. A long term late mission battery anomaly is discussed in Section 1.6.

#### 1.4.6 Radiometric Baselines Discontinuities

During the first year of observations 21 sudden step-like changes in the radiometers outputs were observed. These events have been identified as small changes in the properties of several microwave components resulting from the sudden release of internal stress and are presumably thermally driven. The observed step-like shifts in output are not correlated with changes in HEMT bias. These small steps in radiometer output can be categorized and their point of origin in the system understood by the symmetry of the observed response:

- Waveguide Creep Mode: Differential-mode change in radiometric output (i.e., science signals move with equal and opposite magnitude) induced by slight change in waveguide loss or reflectively prior to input magic-tee. Signature mimics a small but sudden change in noise temperature.
- Phase Switch Mode: Common-mode step in science output of both radiometer diode readout channels (i.e., science signals move with equal and common magnitude). Can induce second order common mode RF bias. Motion of phase matched waveguide sections could produce similar signatures; however, given the mounting geometry, one anticipates that this would produce relatively slow changes in response rather than producing a sudden step.
- Filter Mode: Step in RF bias of a single diode channel. Signature is consistent with small change total power (i.e., shift in detector diode responsively or band-pass filter bandwidth) after second magic tee.

A typical event is of order  $\sim 1$  mK in amplitude and one's knowledge of the transition time is limited by the data sample rate. In practice, these small events do not cause a discernible change in the DA gain or noise properties. Given the calibration time scale for the system,  $\sim 1$  hour of data on either side of the event is removed, each cut is additionally padded by 1.2 hours on each side by the baseline fitting routine (Hinshaw et al., 2003a). A data loss of  $\sim 0.1\%$  is incurred in processing these events. In flight, steps have been observed in radiometer channels W12, W11, Q12 Q11, K11, Ka11 in decreasing order of frequency of event occurrence. Of the 21 events, 2 affected more than one radiometer channel. The most probable cause of coupling between nearly coincident events is due to the mechanical

layout of the radiometer mounting structures. From the band-to-band and channel-to-channel consistency of the maps we conclude that all channels have similar statistical properties after removal of the baseline steps in processing (Hinshaw et al., 2003a).

Cut From yyyy:ddd:hhmm	To yyyy:ddd:hhmm	DA Flag	Notes
2001:223:1800	2001:223:2130	[0,0,1,0,0,0,0,0,0,0]	Q1 dT glitch
2001:230:1600	2001:230:2010	[0,0,0,0,0,0,1,0,0,0]	W12 dT glitch
2001:245:1930	2001:246:0110	[0,0,1,0,0,0,0,0,0,0]	Two close Q1 dT glitches
2001:249:0600	2001:249:1010	[0,0,0,0,0,0,1,0,0,0]	Small W12 dT glitch
2001:257:1500	2001:258:0900	[1,1,1,1,1,1,1,1,1,1]	Mid-Course correction #2
2001:282:1700	2001:282:2030	[0,0,0,0,0,0,1,0,0,0]	Small W12 dT glitch
2001:309:1630	2001:311:0000	[1,1,1,1,1,1,1,1,1,1]	Solar Storm Induced Safe-hold
2001:316:2300	2001:317:0300	[0,0,1,0,0,0,0,0,0,0]	Small Q12 dT glitch
2002:013:0810	2002:013:1130	[0,0,0,0,0,0,1,0,0,0]	W12 dT glitch
2002:016:1500	2002:016:2330	[1,1,1,1,1,1,1,1,1,1]	Station Keeping #1 (SK1)
2002:053:0500	2002:053:1000	[0,0,0,0,0,0,1,0,0,0]	W12 dT glitch
2002:053:1700	2002:053:2030	[0,0,0,0,0,0,1,0,0,0]	W12 dT glitch
2002:057:0200	2002:057:1022	[1,1,1,1,1,1,1,1,1,1]	Change to VT0
2002:066:2000	2002:067:0000	[0,0,0,0,0,0,1,0,0,0]	W12 dT glitch
2002:068:2230	2002:069:0200	[0,0,0,0,0,0,1,0,0,0]	W12 dT glitch
2002:082:2000	2002:082:2300	[0,0,0,0,0,0,1,0,0,0]	W12 dT glitch
2002:085:0100	2002:085:0400	[0,1,0,0,0,0,0,0,0,0]	Ka123 RF bias glitch
2002:092:1140	2002:092:1530	[0,0,0,0,0,0,1,0,0,0]	W12 dT glitch
2002:097:1005	2002:097:1410	[0,1,0,0,0,0,0,0,0,0]	Ka114 dT and RF bias glitch
2002:100:0600	2002:100:0930	[0,0,0,0,0,0,1,0,0,0]	W12 dT glitch
2002:100:2210	2002:101:0200	[0,0,0,0,0,0,1,0,0,0]	W12 dT glitch
2002:123:0200	2002:123:0530	[0,0,0,0,0,0,1,0,0,0]	W12 dT glitch
2002:128:1400	2002:129:0000	[1,1,1,1,1,1,1,1,1,1]	Station Keeping #2 (SK2)
2002:211:1456	2002:212:0100	[1,1,1,1,1,1,1,1,1,1]	Station Keeping #3 (SK3)
2002:269:0202	2002:269:0426	[1,0,0,0,0,0,0,0,0,0]	K11 dT and RF bias glitch
2002:273:0822	2002:273:1046	[0,1,0,0,0,0,0,0,0,0]	Ka11 dT and RF bias glitch
2002:309:1805	2002:310:0405	[1,1,1,1,1,1,1,1,1,1]	Station Keeping #4 (SK4)
2002:314:0720	2002:314:1040	[0,0,0,0,0,0,1,0,0,0]	W12 dT glitch (marginal)
2002:321:0450	2002:321:0812	[0,0,0,0,0,0,1,0,0,0]	W12 dT glitch (marginal)
2003:071:1235	2003:071:2315	[1,1,1,1,1,1,1,1,1,1]	Station Keeping #5 (SK5)
2003:081:0130	2003:081:0600	[0,0,1,0,0,0,0,0,0,0]	Q12 dT glitch
2003:085:0945	2003:085:1400	[0,0,1,0,0,0,0,0,0,0]	Q12 dT glitch
2003:145:0644	2003:145:0940	[1,1,1,1,1,1,1,1,1,1]	Recorder overflow
2003:156:0848	2003:156:1412	[0,0,0,0,0,0,1,0,0,0]	W12 dT step, plus assoc W11
2003:222:1530	2003:225:0112	[1,1,1,1,1,1,1,1,1,1]	MV reset induced SafeHold
2003:301:2245	2003:302:0420	[1,1,1,1,1,1,1,1,1,1]	Solar activity induced switch to ASTB
2003:316:1335	2003:317:0000	[1,1,1,1,1,1,1,1,1,1]	Station Keeping #6 (SK6)
2004:069:1400	2004:070:0100	[1,1,1,1,1,1,1,1,1,1]	Station Keeping #7 (SK7)
2004:178:1639	2004:178:1903	[0,0,0,0,0,0,1,0,0,0]	W12 dT glitch
2004:224:1610	2004:225:0300	[1,1,1,1,1,1,1,1,1,1]	Station Keeping #8 (SK8)
2004:238:1115	2004:238:1339	[0,0,0,1,0,0,0,0,0,0]	Q21 dT and RF bias step
2004:248:1746	2004:248:2010	[0,0,0,0,0,0,1,0,0,0]	W12 dT glitch
2004:349:1740	2004:350:0430	[1,1,1,1,1,1,1,1,1,1]	Station Keeping #9 (SK9)
2005:019:1700	2005:019:1924	[0,0,0,0,0,0,1,0,0,0]	W12 dT glitch

Continued on next page

Cut From yyyy:ddd:hhmm	To yyyy:ddd:hhmm	DA Flag	Notes
2005:020:0600	2005:021:2000	[1,1,1,1,1,1,1,1,1,1]	Solar activity induced SunAcq mode
2005:048:2100	2005:053:0000	[1,1,1,1,1,1,1,1,1,1]	Fault protection circuitry trips RWA1 off
2005:094:1030	2005:094:2130	[1,1,1,1,1,1,1,1,1,1]	Station Keeping #10 (SK10)
2005:114:1117	2005:114:1341	[0,0,0,0,0,0,1,0,0,0]	W12 dT step, plus assoc W11
2005:154:1800	2005:159:1200	[0,0,1,0,0,0,0,0,0,0]	Q12 dT dip
2005:155:1533	2005:155:1757	[0,1,0,0,1,1,1,0,0,0]	Ka11,Ka12,Q12,V11 dT glitch, marginal in V12,V21,W12
2005:208:1340	2005:209:0040	[1,1,1,1,1,1,1,1,1,1]	Station Keeping #11 (SK11)
2005:232:0133	2005:232:0357	[0,0,0,1,0,0,0,0,0,0]	Q21 step, very hard to see
2005:252:2328	2005:253:0152	[0,0,0,1,0,0,0,0,0,0]	Q21 step, very hard to see
2005:314:0915	2005:314:2100	[1,1,1,1,1,1,1,1,1,1]	Station Keeping #12 (SK12)
2006:054:0515	2006:054:0739	[0,0,0,0,0,0,1,0,0,0]	W12 dT glitch
2006:066:1345	2006:067:0310	[1,1,1,1,1,1,1,1,1,1]	Station Keeping #13 (SK13)
2006:142:1726	2006:142:1950	[0,1,0,0,0,0,0,0,0,0]	Ka12 step, very hard to see
2006:151:0624	2006:151:0848	[0,0,0,0,0,0,1,0,0,0]	W12 step
2006:165:1405	2006:166:0430	[1,1,1,1,1,1,1,1,1,1]	Station Keeping #14 (SK14)
2006:229:2038	2006:229:2302	[0,0,0,0,0,0,0,0,0,1]	W42 step
2006:255:0432	2006:255:0656	[0,0,1,0,0,0,0,0,0,0]	Q12 step
2006:298:0340	2006:298:0604	[0,0,0,0,0,0,0,0,0,1]	W42 step
2006:313:1430	2006:314:0455	[1,1,1,1,1,1,1,1,1,1]	Station Keeping #15 (SK15)
2007:013:0241	2007:013:0505	[0,0,0,0,0,0,1,0,0,0]	W12 step
2007:048:1759	2007:048:2023	[0,0,0,0,0,0,1,0,0,0]	W12 step
2007:067:1300	2007:068:0400	[1,1,1,1,1,1,1,1,1,1]	Station Keeping #16 (SK16)
2007:125:2017	2007:125:2241	[0,0,1,0,0,0,0,0,0,0]	Q12 step
2007:176:1100	2007:176:2000	[1,1,1,1,1,1,1,1,1,1]	Station Keeping #17 (SK17, part 1)
2007:177:2200	2007:178:1300	[1,1,1,1,1,1,1,1,1,1]	Station Keeping #17 (SK17, part 2)
2007:248:1230	2007:249:1330	[1,1,1,1,1,1,1,1,1,1]	Shadow Avoidance Maneuver (SAM)
2007:269:1200	2007:270:0300	[1,1,1,1,1,1,1,1,1,1]	Shadow Avoidance Correction Maneuver
2007:271:2126	2007:271:2350	[0,0,0,0,0,0,1,0,0,0]	W12 step
2007:314:1400	2007:320:0000	[1,1,1,1,1,1,1,1,1,1]	Thermal effects from XB problem
2008:023:1235	2008:023:2235	[1,1,1,1,1,1,1,1,1,1]	Station Keeping #18 (SK18)
2008:156:1443	2008:157:0500	[1,1,1,1,1,1,1,1,1,1]	Station Keeping #19 (SK19)
2008:194:0020	2008:194:0244	[0,0,0,0,0,0,1,0,0,0]	W11,W12 step
2008:198:0810	2008:198:1034	[0,1,1,1,1,1,0,0,1,0]	Ka11,Ka12,Q12,V11,W32 step, marginal in Q21,V12,V21. Small spike in TRS A-side temp DTAMIDPRIT
2008:214:1700	2008:216:0400	[1,1,1,1,1,1,1,1,1,1]	4% Lunar Shadow ride-through
2008:279:1000	2008:279:1300	[0,1,1,0,1,0,1,0,1,0]	Small step in Ka12, Q12, V11, W12, W32, small spike in TRS Bside temperature DTBMIDPRIT
2008:282:1220	2008:282:2350	[1,1,1,1,1,1,1,1,1,1]	Station Keeping #20 (SK20)
2008:300:0738	2008:300:1002	[0,0,0,0,0,0,0,0,1,0]	W32 step
2008:302:1000	2008:302:2240	[1,1,1,1,1,1,1,1,1,1]	Second lunar shadow ride-through
2009:008:1020	2009:009:1230	[1,1,1,1,1,1,1,1,1,1]	ACE-A SSPC Event
2009:042:1940	2009:043:1000	[1,1,1,1,1,1,1,1,1,1]	Station Keeping #21 (SK21)

Continued on next page

Cut From yyyy:ddd:hhmm	To yyyy:ddd:hhmm	DA Flag	Notes
2009:055:0248	2009:055:0512	[1,1,1,0,1,0,0,0,1,0]	Step in K11, Ka11, Ka12, Q12, V11, W31, W32, small spike in DTBMIDPRIT
2009:182:2203	2009:184:0027	[0,0,1,0,0,0,1,0,0,0]	Step in Q11, Q12, W11, W12
2009:197:1422	2009:198:0220	[1,1,1,1,1,1,1,1,1,1]	Station Keeping #22 (SK22)
2009:244:0408	2009:244:0632	[0,0,0,0,0,1,0,0,0]	Marginal step in W12
2009:263:2118	2009:263:2342	[0,0,0,0,0,1,0,0,0]	Step in W12
2009:264:1430	2009:264:1654	[0,0,0,0,0,1,0,0,0]	step in W12
2010:020:1315	2010:021:0915	[1,1,1,1,1,1,1,1,1,1]	Station Keeping #23 (SK23)
2010:045:1553	2010:045:1817	[0,0,0,0,0,1,0,0,0]	Step in W12
2010:078:0348	2010:078:0612	[0,0,1,0,1,0,0,0,1,0]	Step in Q12, V11, W32, small spike in DTAMIDPRIT
2010:133:1600	2010:134:0830	[1,1,1,1,1,1,1,1,1,1]	Station Keeping #24 (SK24 w/preceding battery charge)
2010:153:0100	2010:154:1330	[1,1,1,1,1,1,1,1,1,1]	Transponder A loss of RF power - first incident
2010:158:0900	2010:159:1800	[1,1,1,1,1,1,1,1,1,1]	Transponder A turn-off and mkup heater tests

Table 1.8: Data Cut Summary. Each line consists of a start time, a stop time and ten element array indicating which DAs are affected, ( $[1,0,0,0,0,0,0,0,0,0] = \text{K1}$ ,  $[0,1,0,0,0,0,0,0,0,0] = \text{Ka1}$ , etc.). Each cut is additionally padded by 1.2 hours on each side by the baseline fitting software. Additional cuts are made for Jupiter, Saturn, Mars, Uranus and Neptune if the planet lies near a DA's line-of-sight on either the A- or the B-side; more information concerning this can be found in Jarosik et al. (2011).

## 1.5 The Radiation Environment

### 1.5.1 Plasma Environment

The Earth's auroral tail is collimated by the solar wind and has a nominal radius of  $\sim 20R_E$  at L2. Variations in the solar wind velocity and direction drive fluctuations of the auroral tail from its average position by up to a few tail radii in extent. In an idealized picture, the magnetospheric lobes are relatively small and the magnetosheath has higher density than the lobes but less than the solar wind. Streaming plasma in this region will see essentially open magnetic field lines and it is easier to exhaust out the end than confine the plasma in this region.

To place this in perspective for *WMAP*, we recall the Earth's angular extent as viewed from  $\sim 240R_E$  at the L2 halo orbit is in the range of  $1^\circ < \theta < 10^\circ$ . Based upon these inputs we estimate the major and minor axis of the *WMAP* orbit to be  $\sim 4R_E$  and  $\sim 40R_E$  respectively. Thus, at L2, the spacecraft will experience the auroral tail, lobes, magnetosheath, and solar wind plasma. In principle, the halo orbit places the satellite inside the magnetosheath for extended periods of time; however, in reality, rotation of Earth's magnetic field and solar wind drive large perturbations from the simple static picture. The surface and internal charge

control design described in Bennett et al. (2003c) are compatible with these anticipated environmental conditions.

### 1.5.2 Spacecraft Charge Control

If the accumulation of charge in an electromagnetic structure exceeds the dissipation rate, a discharge occurs when the critical field strength of the configuration is exceeded. In the space environment, such events can be initiated by sudden changes in electromagnetic field, plasma density, or mechanical stress. The resultant rapid release of electromagnetic energy can induce spurious electrical responses or result in damage to components. In this context, faults in spacecraft performance can result from several basic mechanisms (Frederickson, 1996b,a; Adamo & Matarrese, 1983; Leung et al., 1986; Mizera, 1983).

- Coupling to circuitry increases noise and corrupts desired signal.
- Field strength exceeds dielectric strength and induces mechanical failure.
- Localized heating induces stress which exceeds material strength.

Such discharges can be conducted along wires or ground planes, radiated through free space to a structure that acts as a pick-up antenna, or be directly injected into a circuit. For these reasons, the control of surface and internal charge by proper coating selection, return impedance level, and shielding against electromagnetic and ionizing radiation must be considered for reliable spacecraft operation.

In the case of the *WMAP* observatory, all susceptible circuits are enclosed by an equivalent stopping power of 0.16 cm of aluminum. Grounded lead and copper foils were used to locally augment the available shielding where required in the system. For particularly sensitive subsystems, the signal lines in the harness were filtered or clamped with diode limiters to improve overall immunity. Addition charge control mitigation approaches are outlined in Bennett et al. (2003c).

For the charging environment experienced in the phasing loop portion of the mission *WMAP*, surface discharges can potentially induce electrical transients in the system. Such considerations are of particular interest for elements of the system with a low damage threshold to electrostatic discharge. Charge control objectives were achieved while simultaneously satisfying the thermal design goals by using appropriate dissipative surfaces ( $< 10^9 \Omega/\square$ ) in electrical contact with the spacecraft ground. Materials employed included dissipative paints, indium-tin-oxide films, carbon loaded polymers, thin SiO<sub>x</sub> coatings on metallic substrates, and conductive tapes. The use of low loss dielectrics exposed to the ambient space plasma in un-illuminated regions is limited to unavoidable patches with area  $< 10^{-3}$  of the total surface area. In regions of the spacecraft where photoemission is present, larger dielectric regions can be and are employed. Radiated electromagnetic threats are broadband in nature (Leung & Plamp, 1982) and band-limited by the input waveguide cutoff or input circuitry.

### 1.5.3 Solar Flares: Charged Particle Heating

Particle heating by the solar wind can produce a small time variable thermal load on the spacecraft (see for example, Jimenez (1988); Vampola et al. (1989)). This effect is a concern when the power deposited by the incident charged particle flux approaches the cooling power available to the system. In practice, this is predominantly a concern for surfaces cooled to low temperatures. Since the *WMAP*'s optics have relatively large thermal mass and operate at a physical temperature around 70 K this is a negligible but measurable effect. In fact, by correlating the GOES-8 proton monitor (<http://www.swpc.noaa.gov/today.html>) with the precision thermal sensors data from the *WMAP* instrument package, we note that such an effect is observable on the TRS and outer bulk heads of the FPA.

Event Date	$E_p \geq 1\text{MeV}$ p/cm <sup>2</sup> sr day	$E_p \geq 10\text{MeV}$ p/cm <sup>2</sup> sr day	$E_p \geq 100\text{MeV}$ p/cm <sup>2</sup> sr day	Reflectors $\Delta T(\text{mK})$
09/26/01	$1.40 \times 10^{+09}$	$2.70 \times 10^{+08}$	$1.80 \times 10^{+06}$	60
11/06/01	$2.40 \times 10^{+09}$	$6.20 \times 10^{+08}$	$3.60 \times 10^{+06}$	–
11/24/01	$2.30 \times 10^{+09}$	$3.80 \times 10^{+08}$	$2.00 \times 10^{+05}$	70
12/27/01	$6.80 \times 10^{+07}$	$2.40 \times 10^{+07}$	$6.20 \times 10^{+05}$	3
03/18/02	$2.90 \times 10^{+08}$	$1.90 \times 10^{+06}$	$3.50 \times 10^{+03}$	12
04/22/02	$3.30 \times 10^{+08}$	$1.30 \times 10^{+08}$	$1.20 \times 10^{+06}$	10
05/23/02	$2.60 \times 10^{+08}$	$6.80 \times 10^{+06}$	$2.80 \times 10^{+03}$	16
07/17/02	$2.50 \times 10^{+08}$	$6.40 \times 10^{+06}$	$4.20 \times 10^{+03}$	8
08/25/02	$7.00 \times 10^{+07}$	$6.80 \times 10^{+06}$	$2.10 \times 10^{+04}$	0
09/07/02	$1.00 \times 10^{+08}$	$2.10 \times 10^{+06}$	$3.20 \times 10^{+03}$	5
10/29/03	$3.00 \times 10^{+09}$	$7.70 \times 10^{+08}$	$5.20 \times 10^{+06}$	95
07/27/04	$2.70 \times 10^{+08}$	$9.50 \times 10^{+06}$	$2.10 \times 10^{+03}$	12
09/14/04	$4.60 \times 10^{+08}$	$8.50 \times 10^{+06}$	$2.70 \times 10^{+03}$	8
11/09/04	$3.00 \times 10^{+08}$	$1.10 \times 10^{+07}$	$7.00 \times 10^{+04}$	13
01/17/05	$6.20 \times 10^{+08}$	$1.10 \times 10^{+08}$	$6.10 \times 10^{+06}$	30
05/15/05	$6.70 \times 10^{+08}$	$2.20 \times 10^{+07}$	$8.00 \times 10^{+03}$	30
08/24/05	$2.60 \times 10^{+08}$	$1.70 \times 10^{+07}$	$1.10 \times 10^{+04}$	12
09/11/05	$1.10 \times 10^{+09}$	$7.40 \times 10^{+07}$	$4.60 \times 10^{+05}$	18
12/13/06	$7.00 \times 10^{+08}$	$6.70 \times 10^{+07}$	$1.80 \times 10^{+06}$	25

Table 1.9: Solar Storms. Major storms encountered by the observatory from launch to the end of the current data release. The proton data are from the GOES-8 and GOES-11 satellites. The spacecraft went into safe-hold mode during the November 6, 2001 solar storm.

As an illustrative example we consider the heating of the *WMAP* primary reflector that occurred during September 26, 2001 solar proton event. This is an example of a severe solar storm with the  $> 10$  MeV proton flux reaching  $10^5$  times nominal levels. During the event, a thermal change with amplitude  $dT \sim 0.06$  K correlated with the event was observed in the

primary reflector sensors. From the thermal properties of the TRS in its flight configuration, a change in power loading on the reflector of  $\sim 6$  mW was inferred. One notes for an effective thickness,  $dt > 0.5$  mm of aluminum, essentially all incident particles with an energy  $< 10$  MeV, dissipate their energy in the composite structure.

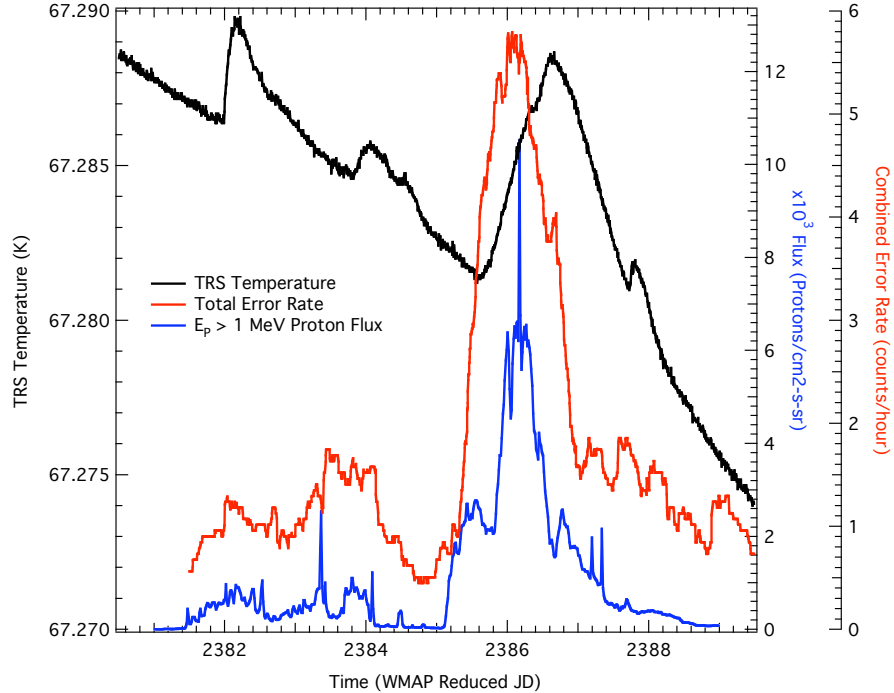


Figure 1.20: Solar Flare Effects on the Observatory. This plot shows the effects of a solar flare (April 17, 2002) on the TRS temperature and on the combined (on-board computer and data recorder) single-bit error rate. The proton data are from the GOES-8 satellite.

In effect, this portion of the system acts as a bolometric particle detector: the primary reflector serves as an absorber for low energy particles from the solar wind, the PRT is a thermal sensor element, and passive cooling to the sky serves as weak link to the thermal reservoir. A calibration of this bolometric response can be derived from the observed change in temperature which resulted from the removal of RF power to the Z omni antenna (see Appendix B WMAP Events Log, 2001:219). The cable which runs through the cavity formed by the back-to-back reflectors on the TRS provides a known ohmic load for calibration. The observed thermal response is consistent with the power deposition by the incident particle flux. We conclude that the instrument's observed thermal behavior is consistent with the absorption of an enhanced number of low energy particles encountered during the solar proton event. Given the mm-wave emissivity of the reflector surfaces (Page et al., 2003c), magnitude, and timescale of the thermal response, the resultant differential microwave emission is insufficient to influence the science data.

## 1.6 Battery Capacity Loss

The WMAP power system (Bennett et al., 2003c) employs an 11-cell nickel-hydrogen Common Pressure Vessel (CPV) battery. During the first year of operation a shift in the battery operating point was indicative of a sudden cell loss. This signature was attributed to a battery-manufacturing defect when initially observed (i.e., see operational log entry 2002054 in Appendix B). In the fall of 2009, sudden and periodic drops in the battery voltage were encountered. Evaluation of the available telemetry revealed that these events were associated with transient thermal load increases that were correlated with a step reduction in voltage. The differential voltage telemetry indicated the events randomly occurred in the battery and only one cell within a given CPV was affected. If left unchecked the progressive bus voltage loss was anticipated to drop below the level necessary to maintain the Observatory's full capabilities on orbit. Operationally, it was found that high rate pulsed charging of the battery enabled temporarily recovery of these cells; however, the efficacy of this approach was limited in practice by the battery's safe operating temperature and radiator heat rejection.

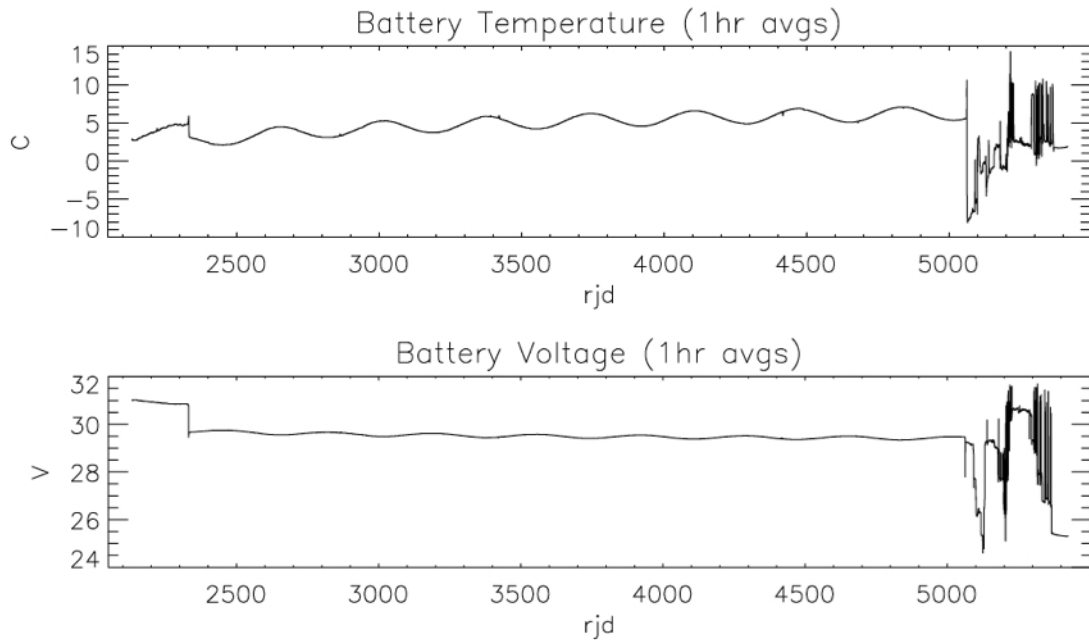


Figure 1.21: Upper Panel: Battery Temperature, Lower Panel: Battery Voltage, as a function of Reduced Julian Day (JD - 2450000)

Subsequent ground testing of the flight spare battery was able to successfully duplicate the voltage collapse signature displayed on-orbit, as well as isolate potential mechanisms behind the observed behavior (Keys, D., and team, 2010). These tests enabled aging and other normal battery degradation effects to be discounted as contributing to the phenomenon observed in flight. The most probable cause was determined to be an internal voltage-driven potassium

hydroxide (KOH) electrolyte creep and subsequent establishment of bridging between the cells within the CPV. These conditions enabled an ionic current flow that irreversibly depleted the battery's capacity of one of the two internal cells within a shared pressure vessel (Manzo, M. A., and team, 2010)(Keys, D., and team, 2011). Since the power system architecture was not designed to recondition the battery, cell imbalances could not be corrected.

The system impact largely presented an operational challenge, which in retrospect, could have been eliminated by an operational pressure sensor or reduced via a larger battery radiator that would have allowed a higher trickle charge rate. The mitigation scheme devised—suitable battery operational point, trickle charge, and high rate pulsed charge recovery—enabled the operations team to limit further battery degradation and extend the life of the mission for a full year to complete its planned activities. WMAP completed its scheduled science operations on 19 August 2010. In October of 2010 with its mission objectives finished the WMAP spacecraft was placed in a graveyard parking orbit (O'Neill, 2010).

From a ‘lessons learned’ perspective it is interesting to briefly consider several interrelated design factors that contributed to this outcome for this shared pressure cell battery configuration. The desire to have a thermally stable platform for the mission favored a power system design with constant power dissipation. However, late in the integration of the spacecraft an EMI/EMC problem with the battery pressure vessel pressure transducer readout was uncovered and necessitated either correction or disabling this portion of the circuitry. The role of the pressure sensor signal was intended to provide the power system a means of monitoring the battery state of charge and protect the battery from overcharge and damage. Upon re-viewing the options, a battery operational mode was identified which avoided overcharging by reducing the trickle charge rate to the lower end of the recommended range. Post anomaly analysis of the pre-flight data revealed that the battery trickle current employed in-flight was inadequate to counteract the self-discharge current within the cells. Without sufficient potential within a cell electrolyte bridging the two cells created a conductive path within a common pressure vessel discharging one of the cells. The data at hand would suggest that this effect does not occur in single pressure vessel cell battery architectures. This is consistent with the detailed battery geometry, the observed failure mechanism, and subsequent controlled studies in the laboratory. Thus, in striving to circumvent a known operational issue (overcharging) the solution employed entered an operational regime where experts and practitioners possessed limited experience regarding potential undercharge failure modes (cell electrolyte bridging).

## 1.7 Telemetry

WMAP data are transmitted to Earth as a stream of packets. There are many types of packets, each containing a collection of measurements with a common theme. In general, there are four types of packets:

- Analog Instrument Housekeeping (AIHK) data consists of measurements describing the current state of the instrument portion of the satellite, consisting primarily of temper-

ature and electrical (voltage and current) measurements from the Analog Electronics Unit (AEU). There is a single AIHK packet definition, containing two complete sets, or sweeps, of measurements. A single sweep requires 23.04 seconds to poll all the readouts; therefore a single AIHK packet is transmitted every 46.08 seconds.

- Digital Instrument Housekeeping (DIHK) data consists of the Digital Electronics Unit (DEU) voltages and temperatures, plus a number of status and error codes. There is a single DIHK packet definition; this packet is transmitted 11.52 seconds, or four times for each AIHK packet.
- Science data consists of the measurements from the radiometers. There are two science data packets, each of which is transmitted every 1.536 seconds, or thirty times for each AIHK packet. One packet contains only the W-radiometer data; the other packet contains the other radiometer data. Observations last for an integral number of 25.6 msec blocks; the number of blocks per observation depends upon the observed frequency; the higher frequencies require fewer blocks. Unlike the other packets, the time recorded in a science data packet represents the end of the first 25.6 msec observation as opposed to the actual start of the set of observations.
- Observatory Housekeeping (OBHK) data consists of the remaining measurements and status information from the satellite. There are many different packets with a variety of download rates.

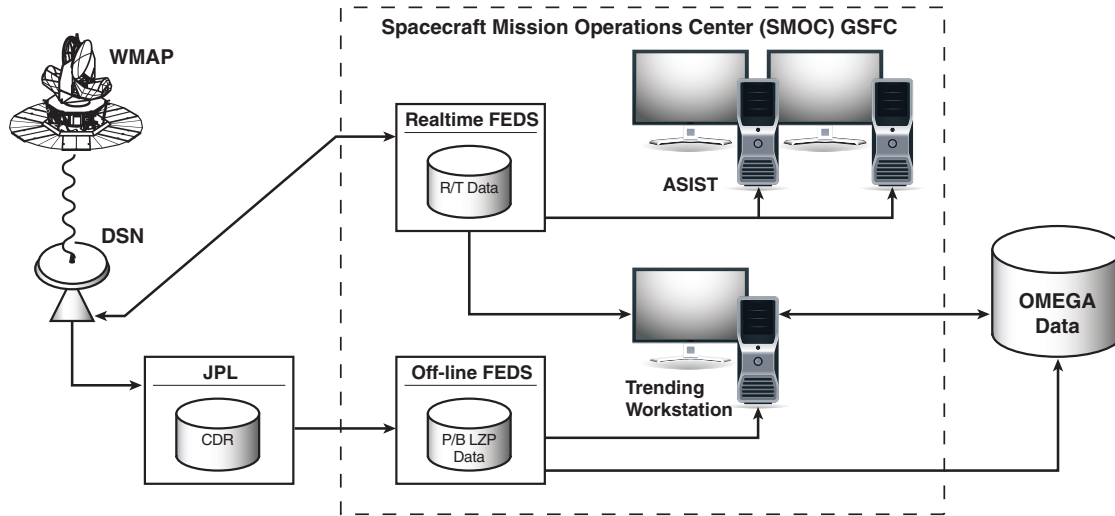


Figure 1.22: Telemetry Data Path. This figure shows the path that data from the satellite follow.

Ground-based timing tests indicate that the relative accuracy of times recorded in telemetry packets is 30  $\mu$ sec. Figure 1.22 shows the path that the telemetry packets follow from the satellite to the Science and Mission Operations Center (SMOC) and to the Office of the

MAP Experiment General Archive (OMEGA, also the science data analysis facility). Data are accumulated on board until the satellite is commanded to transmit it to Earth. There is on average one pass per day. Data is transmitted from the satellite to the Deep Space Network (DSN).

During each pass, the DSN transmits a subset of the data in real time directly to the realtime Front End Data System (FEDS) in the SMOC. The realtime FEDS distributes this data to the ASIST workstations and to a trending workstation. The ASIST systems are Linux workstations that are used to display the data in realtime and to construct and send commands to the satellite. The trending workstation is a Linux system configured much like the systems used in the OMEGA; this system is used to generate plots of the realtime data over time, allowing trends in the data to be more easily identified.

The DSN also transmits all of the data accumulated since the last pass to the Jet Propulsion Laboratory (JPL) for quality checking, archiving, and formatting. Within four hours, JPL transmits it to the offline processing FEDS in the SMOC. This FEDS categorizes the packets and sorts them in time. Four files of telemetry packets are produced: one science data (INSC) file, one instrument housekeeping (INHK) file, and two observatory (or space-craft) housekeeping (OBHK and OBHX) files. Of the two observatory housekeeping files, the OBHK file contains the bulk of the packets; the OBHX file contains only a few types of packets. An additional file containing processing notes in a binary format is also delivered (OBEM). Finally, a set of quality assurance files (QA) containing a text summary of the data delivered are also delivered; there is one QA file for each telemetry file.

The offline FEDS transmits the data it receives to OMEGA in two waves. The first wave of files, known internally as quicklook data, is transmitted essentially as-is from JPL. This allows the science team to look at the housekeeping data for potential anomalies within a few hours of data transmission. The second wave consists of daily files. There is a delay of two or three days in the delivery of the daily files; this allows holes in the data to be retransmitted (either from JPL or the spacecraft, depending upon the problem). This second wave of files are known as the Level Zero (LZ), or Level Zero Processing (LZP), files; these are the files used to construct the WMAP time-ordered data archive (see Section 3).

## Chapter 2

# Data Products

Each section of this chapter contains the description of a particular delivered data product and contain at least the following information:

- Description of the data
- Data format
- Quick summary of the methodology use to obtain the data set
- References to papers describing the more technical details.

Time-ordered data are described in Chapter 3. Telemetry data are described in Chapter 4. More information on how to read both maps and time-ordered data are contained in Chapter 5 and in Appendix C. All the data can be downloaded at:

<http://lambda.gsfc.nasa.gov/>

## 2.1 Derived CMB Products

### 2.1.1 Combined TT Power Spectra

<b>Units</b>	$\mu\text{K}^2$
<b>Format</b>	ASCII
<b># of Files</b>	2

The nine year TT power spectrum is produced by combining the Maximum Likelihood estimated spectrum from  $l = 2 - 10$  with the pseudo- $C_l$  based cross-power spectra for  $l > 32$ . The pseudo- $C_l$  estimate uses only V- and W-band data, with a uniform pixel weight applied for  $l \leq 500$  and  $N_{obs}$  weights for  $l > 500$ .

The complete (unbinned) TT power spectrum data are provided as an ASCII table containing the following columns:

- The multipole moment  $l$
- The power spectrum in units of  $\mu\text{K}^2$
- The error derived from the diagonal elements of the covariance matrix in units of  $\mu\text{K}^2$
- The portion of column 3 attributed to measurement errors in units of  $\mu\text{K}^2$
- The portion of column 3 attributed to cosmic variance in units of  $\mu\text{K}^2$ , assuming the best-fit  $\Lambda\text{CDM}$  model.

The diagonal elements provide an estimate of the error, but should not be used as exact error bars. The complete Fisher matrix should be used for that purpose.

The numbers in this file (and specifically the error bars) are derived from the following values, calculated at each  $l$ : the power spectrum,  $l(l+1)C_l^{TT,data}/(2\pi)$ , the noise  $l(l+1)N_l/(2\pi)$ , the effective sky fraction  $f_{\text{sky},l}$ , and a best fit theory spectrum,  $C_l^{TT,th}$ . Column 3 above is the total diagonal error at each  $l$ :

$$\sigma \left( \frac{l(l+1)}{2\pi} C_l^{TT,data} \right) = \frac{l(l+1)}{2\pi} \sqrt{\frac{2 \left( C_l^{TT,th} + N_l^{TT} \right)^2}{(2l+1)f_{\text{sky},l}^2}} \quad (2.1)$$

Column 4 is the error mostly from noise:

$$\sigma_{\text{noise}} \left( \frac{l(l+1)}{2\pi} C_l^{TT,data} \right) = \frac{l(l+1)}{2\pi} \sqrt{\frac{2 \left[ 2C_l^{TT,th}N_l^{TT} + (N_l^{TT})^2 \right]}{(2l+1)f_{\text{sky},l}^2}} \quad (2.2)$$

Column 5 is the error from only cosmic variance:

$$\sigma_{\text{CV}} \left( \frac{l(l+1)}{2\pi} C_l^{TT,data} \right) = \frac{l(l+1)}{2\pi} \sqrt{\frac{2 \left( C_l^{TT,th} \right)^2}{(2l+1)f_{\text{sky},l}^2}} \quad (2.3)$$

These are defined so that  $\sigma_{\text{noise}}^2$  and  $\sigma_{\text{CV}}^2$  add to  $\sigma^2$ . For discussion of error bars on the TT power spectrum, see for example Hinshaw et al. (2003b); Verde et al. (2003); Hinshaw et al. (2007).

A binned version of the power spectrum is also available in a separate file with the following columns:

- The mean multipole moment  $l$
- The smallest  $l$  contributing to the bin
- The largest  $l$  contributing to the bin
- The power spectrum in units of  $\mu\text{K}^2$
- The error derived from the diagonal elements of the covariance matrix in units of  $\mu\text{K}^2$
- The portion of column 5 attributed to measurement errors in units of  $\mu\text{K}^2$
- The portion of column 5 attributed to cosmic variance in units of  $\mu\text{K}^2$ , assuming the best-fit  $\Lambda\text{CDM}$  model.

The binning is unweighted; the mean value of  $l(l+1)C_l^{TT,\text{data}}/(2\pi)$  is reported for each bin. For the purposes of this file, errors at each  $l$  before binning are assumed to be uncorrelated and Gaussian and are propagated under the assumption of unweighted binning.

More details may be found in Larson et al. (2011), Dunkley et al. (2009), Hinshaw et al. (2009) and Nolta et al. (2009).

### 2.1.2 TE, TB, EE, and BB Power Spectra

Units	$\mu\text{K}^2$
Format	ASCII
# of Files	8

The TE, TB, EE, and BB power spectra are computed using a pseudo- $C_l$  estimator for the region outside the nine-year polarization mask in P and outside the analysis mask in T. The foreground-cleaned V band with uniform weighting is used for T. The combined foreground-cleaned Q and V bands are used for P. Polarization weighting uses the full  $N_{inv}$  weighting for  $l \leq 16$  and  $N_{obs}$  weighting for  $l > 16$ .

Unbinned TE, TB, EE, and BB, power spectra are provided as ASCII tables containing the following columns:

- The multipole moment  $l$
- The power spectrum in units of  $\mu\text{K}^2$
- The error derived from the diagonal elements of the covariance matrix in units of  $\mu\text{K}^2$
- The portion of column 3 attributed to measurement errors in units of  $\mu\text{K}^2$
- The portion of column 3 attributed to cosmic variance in units of  $\mu\text{K}^2$ , assuming the best-fit  $\Lambda\text{CDM}$  model.

For the TB spectrum, the theoretical expected value is zero, so there is no cosmic variance. The noise in that spectrum is therefore all instrument noise, and so columns 4 and 5 are not reported.

The diagonal elements provide an estimate of the error, but should not be used as exact error bars. The complete Fisher matrix should be used for that purpose.

The error bars are calculated using the following quantities at each  $l$ : the power spectra,  $l(l+1)C_l^{TE,data}/(2\pi)$ ,  $l(l+1)C_l^{TB,data}/(2\pi)$ ,  $l(l+1)C_l^{EE,data}/(2\pi)$ , and  $l(l+1)C_l^{BB,data}/(2\pi)$ ; the noise power spectra  $l(l+1)N_l^{TT}/(2\pi)$  and  $l(l+1)N_l^{EE}/(2\pi)$ ; the effective sky fractions  $f_{\text{sky},l}^{TE}$ ,  $f_{\text{sky},l}^{TB}$ ,  $f_{\text{sky},l}^{EE}$ , and  $f_{\text{sky},l}^{BB}$ ; and the best fit theory power spectra  $C_l^{TT,th}$ ,  $C_l^{TE,th}$ , and  $C_l^{EE,th}$ .

We first describe the TE power spectrum. Column 3 above is the total diagonal error at each  $l$ :

$$\sigma \left( \frac{l(l+1)}{2\pi} C_l^{TE,data} \right) = \frac{l(l+1)}{2\pi} \sqrt{\frac{(C_l^{TT,th} + N_l^{TT})(C_l^{EE,th} + N_l^{EE}) + (C_l^{TE,th})^2}{(2l+1) [f_{\text{sky eff},l}^{TE}]^2}} \quad (2.4)$$

Column 4 is the error mostly from noise:

$$\sigma_{\text{noise}} \left( \frac{l(l+1)}{2\pi} C_l^{TE,data} \right) = \frac{l(l+1)}{2\pi} \sqrt{\frac{C_l^{TT,th} N_l^{EE} + C_l^{EE,th} N_l^{TT} + N_l^{TT} N_l^{EE}}{(2l+1) [f_{\text{sky eff},l}^{TE}]^2}} \quad (2.5)$$

Column 5 is the error from only cosmic variance:

$$\sigma_{\text{CV}} \left( \frac{l(l+1)}{2\pi} C_l^{TE,\text{data}} \right) = \frac{l(l+1)}{2\pi} \sqrt{\frac{C_l^{TT,\text{th}} C_l^{EE,\text{th}} + (C_l^{TE,\text{th}})^2}{(2l+1) [f_{\text{sky eff},l}^{TE}]^2}} \quad (2.6)$$

The error bars for the TB spectrum are very similar, with B replacing E above, except we also assume  $C_l^{TB,\text{th}} = 0$ , and  $C_l^{BB,\text{th}} = 0$ . This gives us only one error column, since cosmic variance is zero under these assumptions.

$$\sigma \left( \frac{l(l+1)}{2\pi} C_l^{TB,\text{data}} \right) = \frac{l(l+1)}{2\pi} \sqrt{\frac{(C_l^{TT,\text{th}} + N_l^{TT}) N_l^{BB}}{(2l+1) [f_{\text{sky eff},l}^{TB}]^2}} \quad (2.7)$$

Next we describe the EE spectrum error bars. Column 3 is the total diagonal error at each  $l$ :

$$\sigma \left( \frac{l(l+1)}{2\pi} C_l^{EE,\text{data}} \right) = \frac{l(l+1)}{2\pi} \sqrt{\frac{(C_l^{EE,\text{th}} + N_l^{EE})^2}{(2l+1) [f_{\text{sky eff},l}^{EE}]^2}} \quad (2.8)$$

Column 4 is the error mostly from noise:

$$\sigma_{\text{noise}} \left( \frac{l(l+1)}{2\pi} C_l^{EE,\text{data}} \right) = \frac{l(l+1)}{2\pi} \sqrt{\frac{2 [2C_l^{EE,\text{th}} N_l^{EE} + (N_l^{EE})^2]}{(2l+1) [f_{\text{sky eff},l}^{EE}]^2}} \quad (2.9)$$

Column 5 is the error from only cosmic variance:

$$\sigma_{\text{CV}} \left( \frac{l(l+1)}{2\pi} C_l^{EE,\text{data}} \right) = \frac{l(l+1)}{2\pi} \sqrt{\frac{2 (C_l^{EE,\text{th}})^2}{(2l+1) [f_{\text{sky eff},l}^{EE}]^2}} \quad (2.10)$$

The BB spectrum error bars are computed exactly as above, with BB replacing EE. In this case we allow  $C_l^{BB,\text{th}}$  to be slightly nonzero due to gravitational lensing of the EE spectrum into BB. It can be seen that has a negligible effect on the total error bar—noise dominates over cosmic variance at all  $l$  for the BB spectrum.

Error bars are defined so that  $\sigma_{\text{noise}}^2$  and  $\sigma_{\text{CV}}^2$  add to  $\sigma^2$ . The total error formulas (column 3 in the above files) are listed in Appendix C3 of Page et al. (2007).

A binned version of each power spectrum are also available in separate ASCII files containing the columns:

- The mean multipole moment  $l$

- The smallest  $l$  contributing to the bin
- The largest  $l$  contributing to the bin
- The power spectrum in units of  $\mu\text{K}^2$
- The error derived from the diagonal elements of the covariance matrix in units of  $\mu\text{K}^2$
- The portion of column 5 attributed to measurement errors in units of  $\mu\text{K}^2$
- The portion of column 5 attributed to cosmic variance in units of  $\mu\text{K}^2$ , assuming the best-fit  $\Lambda\text{CDM}$  model.

Again, the TB spectrum is assumed to have no cosmic variance, so the last two columns for that file are omitted.

Note that for the binned cross spectra, TE and TB, the units are  $(l + 1)C_l/(2\pi)$  in  $\mu\text{K}^2$ , instead of  $l(l + 1)C_l/(2\pi)$  in  $\mu\text{K}^2$ . One factor of  $l$  is removed, to make plots easier to read.

More details may be found in Larson et al. (2011), Hinshaw et al. (2009), Dunkley et al. (2009) and Nolta et al. (2009).

### 2.1.3 Cosmological Parameter Table

Analysis of the *WMAP* data involved the computation of cosmological parameters assuming a variety of models and including a variety of datasets in addition to the *WMAP* datasets. The various model/dataset combinations that were tested are displayed in Tables 2.10, 2.7, 2.4, and 2.1. In the equivalent table available on the LAMBDA web site the combinations that were analyzed have links in the corresponding cells to individual display pages that show the cosmological parameters computed using that combination of model and dataset. A printable version of each list of parameters is made available as a Postscript file through a link to its corresponding individual model-data combination display page; these Postscript files list the error information associated with each parameter.

In the nine year data analysis, the BAO and  $H_0$  datasets were included to refine the parameters computed from the displayed model/dataset combinations; independent chains for these two datasets were not created. Therefore the parameters derived from BAO and  $H_0$  are reported with those from the displayed datasets; separate pages are not provided.

When available, Monte Carlo Markov Chains and best-fit  $C_l$  spectra are provided for model/dataset combinations; links to these files are provided through the individual parameter display pages described above.

The Markov Chains are supplied in compressed tarballs; each contains a README file describing the contents. In the seven-year release, some of the chains are flagged as “post-processed.” These chains have been constructed from chains originally run with a different data combination. Importance sampling (Lewis & Bridle, 2002) was used to reweight the original chain for the new dataset. The new distribution was checked against the original chain to determine if the statistics can be trusted.

The nine-year *WMAP* chains can contain files with the following names. Some of the below files will be missing from some chains; for example, if the chain does not use the SPT likelihood, then files related to that likelihood will not be present.

**2011hubble\_neglnlike** In the few cases where the  $H_0$  prior from Riess et al. (2011) is directly included in the chain (as opposed to being used for reweighting the chain), this gives the negative natural logarithm of the  $H_0$  likelihood.

**2012bao\_neglnlike** In the few cases where the BAO likelihood combination used in Hinshaw et al. (2012) is directly included in the chain (as opposed to being used for reweighting the chain), this gives the negative natural logarithm of the BAO likelihood used.

**a002** This is  $10^9 \Delta_{\mathcal{R}}^2$ , where  $\Delta_{\mathcal{R}}^2$  is the power of scalar fluctuations at  $k = 0.002 \text{ Mpc}^{-1}$ , as mentioned in e.g. Komatsu et al. (2009).

**ac** The amplitude  $A$  of correlated clusters, for both the ACT and SPT likelihoods. The amount that correlated clusters contribute to the TT spectrum is assumed to be  $Al(l+1)C_l^{\text{clusters}}/2\pi$ , where the cluster template scales with  $l$  as  $l(l+1)C_l^{\text{clusters}}/2\pi \propto l^{0.8}$  and it is normalized so that  $l(l+1)C_l^{\text{clusters}}/2\pi = 1 \mu\text{K}^2$  at  $l = 3000$ .  $A$  is therefore the amplitude of the template in  $\mu\text{K}^2$  at  $l = 3000$ .

**actlens\_neglnlike** The negative natural logarithm of the ACT gravitational lensing likelihood.

**act\_v2a1s\_neglnlike** The negative natural logarithm of the ACT 148 GHz TT power spectrum likelihood, version v2a1s.

**age** The age of the universe in billions of years (Gigayears).

**agestar** The age of the universe,  $t_*$ , (years) at the redshift of last scattering. This redshift  $z_*$  is determined by the fitting formula of Hu & Sugiyama (1996).

**ap\_act** The amplitude  $A$  of poisson distributed point source foregrounds, in the ACT likelihood. The amount that point sources contribute to the ACT TT spectrum is assumed to be  $Al(l+1)C_l^{\text{ps}}/2\pi$ , where the point source template scales with  $l$  as  $l(l+1)C_l^{\text{ps}}/2\pi \propto l^2$  and it is normalized so that  $l(l+1)C_l^{\text{ps}}/2\pi = 1 \mu\text{K}^2$  at  $l = 3000$ .  $A$  is therefore the amplitude of the template in  $\mu\text{K}^2$  at  $l = 3000$ .

**ap\_spt** The amplitude  $A$  of poisson distributed point source foregrounds, in the SPT likelihood. The amount that point sources contribute to the SPT TT spectrum is assumed to be  $Al(l+1)C_l^{\text{ps}}/2\pi$ , where the point source template scales with  $l$  as  $l(l+1)C_l^{\text{ps}}/2\pi \propto l^2$  and it is normalized so that  $l(l+1)C_l^{\text{ps}}/2\pi = 1 \mu\text{K}^2$  at  $l = 3000$ .  $A$  is therefore the amplitude of the template in  $\mu\text{K}^2$  at  $l = 3000$ .

**asz** Amplitude of the Sunyaev Zel'dovich template. The same scale factor scales the templates for WMAP, ACT, and SPT. The SZ templates for the three experiments have been scaled for the frequencies of 61, 148, and 150 GHz, respectively.

**c220** The amplitude of the TT power spectrum at  $l = 220$ , as generated by CAMB and including the lensing approximation used by CAMB, but not including the SZ effect or any contaminating foregrounds. The value given is  $l(l+1)C_l/(2\pi)$  in  $\mu\text{K}^2$ .

**daeq** The comoving angular diameter distance  $d_A(z_{\text{eq}})$  to the redshift of matter-radiation equality.

**dastar** The comoving angular diameter distance  $d_A(z_*)$  in Mpc to the redshift of last scattering. This redshift is determined by the fitting formula of Hu & Sugiyama (1996).

**description.txt** The chains released are typically a concatenation of several statistically identical chains. This file describes how many chains were run and how they were combined into the released files.

**eta** This is  $\eta$ , the baryon to photon ratio. It was calculated assuming a CMB temperature of 2.72548 Kelvins (Fixsen, 2009) today (410.719 photons per cubic centimeter) and assuming all baryons have the mass of a proton.

**H0** The Hubble constant, in units of  $\text{km s}^{-1} \text{Mpc}^{-1}$ .

**h0\_like** The likelihood of  $H_0$ , given by Riess et al. (2011). This has been used for reweighting chains.

**keq** This is  $a_{\text{eq}}H(a_{\text{eq}})$ , where  $a_{\text{eq}}$  is the scale factor at matter-radiation equality.

**leq** This is  $a_{\text{eq}}H(a_{\text{eq}})d_A(z_*)$ .

**lstar** The multipole moment  $l_* \equiv \pi/\theta_*$ , where  $\theta_*$  is measured in radians. See **thetastar** for  $\theta_*$ .

**mnu** The sum of neutrino masses,  $\sum m_\nu$ . Units are electron volts.

**nb** The physical density of baryons in the universe today, in units of  $10^{-7}$  proton masses per cubic centimeter. See also **omegabh2**.

**neglnlike** The negative natural logarithm of the likelihood used for generating the chain points. This includes the *WMAP* nine-year likelihood and possibly ACT, SPT, or SNLS3 likelihoods. In a few cases, this also includes BAO and  $H_0$  likelihoods.

**neglnlike\_including\_2012bao** The negative natural logarithm of the product of likelihoods used in the chain, added to the negative natural logarithm of the BAO likelihood used in Hinshaw et al. (2012). The BAO likelihood is included by post-processing the chain.

**neglnlike\_including\_2012bao\_h0** The negative natural logarithm of the product of likelihoods used in the chain, added to the negative natural logarithm of the BAO likelihood used in Hinshaw et al. (2012) and the negative natural logarithm of the  $H_0$  prior from Riess et al. (2011). BAO and  $H_0$  likelihoods are included by post-processing the chain.

**neglnlike\_including\_h0** The negative natural logarithm of the product of likelihoods used in the chain, added to the negative natural logarithm of the negative natural logarithm of the  $H_0$  prior from Riess et al. (2011). The  $H_0$  likelihood is included by postprocessing the chain.

**ns002** The spectral index  $n_s$  for the scalar power spectrum.

**omegab** This is  $\Omega_b$ , the baryonic matter density today as a fraction of the critical density of the universe.

**omegabh2** This is  $\Omega_b h^2$ , the physical baryonic matter density of the universe today. Units are  $1.123 \times 10^{-5}$  proton masses per cubic centimeter or  $1.878 \times 10^{-29}$  grams per cubic centimeter. Units are calculated from  $\frac{3}{8\pi G} (100 \text{ km s}^{-1} \text{ Mpc}^{-1})^2$ . See also **nb**.

**omegac** This is  $\Omega_c$ , the cold dark matter density today as a fraction of the critical density of the universe.

**omegach2** This is  $\Omega_c h^2$ , the physical cold dark matter density of the universe today. Units are  $1.123 \times 10^{-5}$  proton masses per cubic centimeter or  $1.878 \times 10^{-29}$  grams per cubic centimeter.

**omegal** This is  $\Omega_\Lambda$ , the dark energy density today as a fraction of the critical density of the universe.

**omegam** This is  $\Omega_m$ , the matter (both cold and baryonic) density of the universe today as a fraction of the critical density of the universe.

**omegamh2** This is  $\Omega_m h^2$ , the physical matter (both cold and baryonic) density of the universe today. Units are  $1.123 \times 10^{-5}$  proton masses per cubic centimeter or  $1.878 \times 10^{-29}$  grams per cubic centimeter.

**omeganh2** This is  $\Omega_\nu h^2$ , the physical neutrino density of the universe today. Units are  $1.123 \times 10^{-5}$  proton masses per cubic centimeter or  $1.878 \times 10^{-29}$  grams per cubic centimeter.

**rsdrag** The comoving distance  $r_s(z_d)$  that a sound wave can propagate in the early universe, up until the baryons are released from the photons. The value is given in comoving Mpc. The relevant redshift  $z_d$  is listed in **zdrag**, using the formula given by Eisenstein & Hu (1998).

**rsdvz0106** The quantity  $r_s(z_d)/D_v(z = 0.106)$ . See also **rsdrag** for  $r_s(z_d)$ .

**rsdvz02** The quantity  $r_s(z_d)/D_v(z = 0.2)$ . See also **rsdrag** for  $r_s(z_d)$ .

**rsdvz035** The quantity  $r_s(z_d)/D_v(z = 0.35)$ . See also **rsdrag** for  $r_s(z_d)$ .

**rsdvz044** The quantity  $r_s(z_d)/D_v(z = 0.44)$ . See also **rsdrag** for  $r_s(z_d)$ .

**rsdvz054** The quantity  $r_s(z_d)/D_v(z = 0.54)$ . See also **rsdrag** for  $r_s(z_d)$ .

**rsdvz057** The quantity  $r_s(z_d)/D_v(z = 0.57)$ . See also **rsdrag** for  $r_s(z_d)$ .

**rsdvz06** The quantity  $r_s(z_d)/D_v(z = 0.6)$ . See also **rsdrag** for  $r_s(z_d)$ .

**rsdvz073** The quantity  $r_s(z_d)/D_v(z = 0.73)$ . See also **rsdrag** for  $r_s(z_d)$ .

**rsstar** The comoving distance  $r_s(z_*)$  that a sound wave could propagate in the early universe, up until  $z_*$ , given by Hu & Sugiyama (1996). See also **zstar**.

**shift** This is  $d_A(z_*)\sqrt{\Omega_b + \Omega_c + \Omega_\nu} H_0/c$ , where  $c$  is the speed of light.

**sigma8** The standard deviation of matter fluctuations in the universe, once the distribution has been convolved with a spherical top-hat function of radius 8 Megaparsecs. This is also known as  $\sigma_8$ .

**snls3\_neglnlike** The negative natural logarithm of the SNLS3 likelihood. The bug found after publication of the SNLS3 likelihood, which read **zcmb** and **zhel** in the wrong order in **SNLS.f90**, has been corrected. (This causes the current SNLS3 likelihood code not to exactly match the SNLS3 published chains.)

**snls\_alpha** The  $\alpha_{\text{SNLS}}$  parameter to describe Supernovae, over which we marginalize in the SNe chains.

**snls\_beta** The  $\beta_{\text{SNLS}}$  parameter to describe Supernovae, over which we marginalize in the SNe chains.

**sptlens\_neglnlike** The negative natural logarithm of the south pole telescope gravitational lensing likelihood.

**spt\_neglnlike** The negative natural logarithm of the south pole telescope likelihood, for the 150 GHz TT power spectrum.

**tau** The optical depth due to reionization.

**thetastar** The angle  $\theta_*$  in radians subtended by the sound horizon at a comoving angular diameter distance  $d_A(z_*)$ . This is calculated for a redshift of  $z_*$  given by the fitting formula of Hu & Sugiyama (1996).

**trec** Conformal time to recombination,  $\tau_{\text{rec}}$ , as calculated by CAMB.

**weight** The number of times the Markov chain attempted to move to another point and failed, plus 1. When computing histograms of parameters, this contains weight to give to each point.

**weight\_including\_2012bao** The weight of the Markov chain, multiplied by a scale factor to reweight the chain by the combination of BAO likelihoods described in Hinshaw et al. (2012). This is used instead of **weight**, to postprocess the chain with the BAO prior.

**weight\_including\_2012bao\_h0** The weight of the Markov chain, multiplied by a scale factor to reweight the chain by the combination of BAO likelihoods described in Hinshaw et al. (2012), as well as the  $H_0$  prior given by Riess et al. (2011). This is used instead of **weight**, to postprocess the chain with the BAO and  $H_0$  priors.

**weight\_including\_h0** The weight of the Markov chain, multiplied by a scale factor to reweight the chain by the  $H_0$  prior given by Riess et al. (2011). This is used instead of **weight**, to postprocess the chain with the  $H_0$  prior.

**wmap\_neglnlike** The negative natural logarithm of the WMAP nine-year likelihood.

**zdrag** The drag redshift,  $z_d$ , which describes “the time at which the baryons are released from the Compton drag of the photons, in terms of a weighted integral over the Thompson scattering rate” (Eisenstein & Hu, 1998). This is computed directly from the fitting formula given in that paper.

**zeq** The redshift of matter-radiation equality,  $z_{\text{eq}}$ .

**zrec** The redshift of recombination,  $z_{\text{rec}}$ , as calculated by CAMB.

**zreion** The redshift of reionization,  $z_{\text{reion}}$ , as calculated by CAMB.

**zstar** The redshift of last scattering,  $z_*$ , as determined by the fitting formula of Hu & Sugiyama (1996).

The best fit  $C_l$  files are text files containing four or five columns. Scalar files contain four columns: l, TT, EE, and TE. Tensor and total files contain five columns: l, TT, EE, BB, and TE. The columns are scaled

$$T_0^2 l(l+1) C_l / 2\pi$$

and are reported in  $\mu\text{K}^2$ .

Nine-Year Data Release					
Model	Data Sets				
	wmap9+		wmap9+		
	wmap9	spt+ act	wmap9+ snls3	spt+ act+	act+ snls3
	wmap9				
lcdm	✓	✓	✓	✓	✓
lcdm+run	✓	✓	✓	✓	✓
lcdm+tens	✓	✓	✓	✓	✓
lcdm+run+tens	✓	✓	✓	✓	✓
lcdm+iso+corr	✓	✓	✓	✓	✓
lcdm+iso+uncorr	✓	✓	✓	✓	✓
lcdm+mnu	✓	✓	✓	✓	✓
lcdm+nrel	✓	✓	✓	✓	✓
lcdm+yhe	✓	✓	✓	✓	✓
lcdm+nrel+yhe		✓			
olcdm	✓	✓	✓	✓	✓
olcdm+mnu	✓	✓		✓	
wacdm		✗		✗	
wcdm	✓	✓	✓	✓	✓
wcdm+mnu	✓	✓	✓	✓	✓
owcdm	✓	✗	✓	✓	✓

Table 2.1: Combinations model/dataset for which the cosmological parameters have been evaluated. The various models and data sets are briefly described in Table 2.2 and Table 2.3 respectively. The model/data set combinations flagged with a ✓ have a chain for the indicated model and data set. The same chain is re-weighted with BAO and/or  $H_0$  to provide additional data set combinations. The model/data set combinations flagged with a ✗ have chain that also includes includes BAO and  $H_0$ , to facilitate convergence.

Model	Description
lcdm	$\Lambda$ CDM
wcdm	Dark energy equation of state ( $w$ ) allowed to vary
olcdm	$\Omega_k$ allowed to vary
owcdm	$\Omega_k$ and $w$ allowed to vary
wacdm	Time-dependent dark energy equation of state, given by $w(a) = w_0 + w_a(1 - a)$
yhe	$\Lambda$ CDM with a variable primordial Helium fraction
iso+corr	Anticorrelated CDM isocurvature
iso+uncorr	Uncorrelated CDM isocurvature
mnu	Massive neutrinos
nrel	Number of relativistic species
run	Running scalar spectral index
tens	Tensor Modes

Table 2.2: Description of the cosmological model components listed in Table: 2.1

Data Set	Description
wmap9	WMAP nine year data set
act	Atacama Cosmology Telescope (Both power spectrum and lensing measurements)
bao	Baryonic Acoustic Oscillations (Combination described in Hinshaw et al. (2012))
h0	Hubble constant (Riess et al., 2011)
snls3	Supernova Legacy Survey three year sample (Conley et al. (2011); Sullivan et al. (2011))
spt	South Pole Telescope (Both power spectrum and lensing measurements)

Table 2.3: Description of the Data sets listed in Table: 2.1

Seven-Year Data Release							
Model all '+sz+lens'	wmap7	Data Sets					
		wmap7+					
		bao+ h0	bao+ snsalt	snconst	bao+ snconst	h0+ tdel	lrg+ h0
lcdm	✓	✓	✓				
lcdm+delz	✓						
lcdm+run	✓	✓				✓	
lcdm+tens	✓	✓	✓			✓	
lcdm+run+tens	✓	✓					
lcdm+iso1	✓	✓				✓	
lcdm+iso2	✓	✓				✓	
lcdm+mnu	✓	✓				✓	✓
lcdm+yhe	✓						✓
wcdm+mnu	✓	✓				✓	✓
lcdm+nrel	✓	✓					✓
lcdm+nrel> 3	✓	✓					✓
olcdm	✓	✓	✓			✓	
wcdm	✓	✓		✓	✓	✓	
owcdm	✓	✓		✓	✓	✓	
		lrg+ h0+ snconst	acbar+ lrg+h0+ cmb	cmb	bao	h0	lrg
lcdm				✓	✓	✓	✓
lcdm+delz							
lcdm+run				✓			
lcdm+tens					✓		
lcdm+tens+run							
lcdm+iso1							
lcdm+iso2							
lcdm+mnu		✓					
lcdm+yhe			✓				
wcdm+mnu			✓				
lcdm+nrel			✓				
lcdm+nrel> 3							
olcdm							
wcdm							
owcdm							

Table 2.4: Combinations model/dataset for which the cosmological parameters have been evaluated. The various models and data sets are briefly described in Table 2.5 and Table 2.6 respectively.

Model	Description
lcdm	$\Lambda$ CDM
wcdm	Dark energy equation of state ( $w$ ) allowed to vary
olcdm	$\Omega_K$ allowed to vary
owcdm	$\Omega_K$ and $w$ allowed to vary
lens	Turn on lensing when computing CMB spectrum
sz	Floating amplitude for SZ spectrum
delz	$\Lambda$ CDM with a variable width reionization epoch, $\Delta z$
yhe	$\Lambda$ CDM with a variable primordial Helium fraction
iso1	Anticorrelated CDM isocurvature
iso2	Uncorrelated CDM isocurvature
mnu	Massive neutrinos
nrel	Number of relativistic species
run	Running scalar spectral index
tens	Tensor Modes

Table 2.5: Description of the cosmological model components listed in Table: 2.4

Data Set	Description
wmap7	WMAP seven year data set
acbar+quad	Small-scale CMB observations from ACBAR and QUAD
bao	Baryonic Acoustic Oscillations (Percival et al., 2010)
h0	Hubble constant (Riess et al., 2009)
lrg	Sloan Luminous Red Galaxy Sample (Reid et al., 2010)
snconst	Type Ia supernovae from the Constitution dataset (Hicken et al., 2009)
snsalt	Type Ia supernovae from the extended SDSS dataset (Kessler et al., 2009)
time	Time delay measurements (Suyu et al., 2010)

Table 2.6: Description of the Data sets listed in Table: 2.4

Five-Year Data Release								
Model (all +sz+lens)	wmap5	Data Sets						
		wmap5+						
		2df	acb	bao	bao+ small	bao+ hst	bao+ snall+	bao+ hst+
lcdm	✓	✓	✓	✓	✓			✓
lcdm+iso1	✓				✓			
lcdm+iso2	✓				✓			
lcdm+mnu	✓				✓			
lcdm+mnu+run	✓							
lcdm+mnu+tens	✓							
lcdm+nrel	✓					✓	✓	
lcdm+run	✓		✓		✓			✓
lcdm+run+tens	✓		✓		✓			✓
lcdm+tens	✓		✓		✓			✓
lcdm+xe	✓							
ocdm	✓			✓	✓			
owcdm	✓			✓	✓			
wcdm	✓			✓	✓			✓
wcdm+mnu	✓				✓			
ebao+								
		cmb	ebao	small	hst	lrg	sdss	snall
lcdm		✓				✓	✓	✓
lcdm+iso1								
lcdm+iso2								
lcdm+mnu								
lcdm+mnu+run								
lcdm+mnu+tens								
lcdm+nrel		✓						
lcdm+run		✓						
lcdm+run+tens		✓						
lcdm+tens		✓						
lcdm+xe								
ocdm					✓			✓
owcdm				✓	✓			✓
wcdm					✓			✓
wcdm+mnu								

Table 2.7: Combinations model/dataset for which the cosmological parameters have been evaluated. The various models and data sets are briefly described in Table 2.8 and Table 2.9 respectively.

Model	Description
lcdm	$\Lambda$ CDM
wcdm	Dark energy equation of state (w) allowed to vary
ocdm	$\Omega_K$ allowed to vary
owcdm	$\Omega_K$ and w allowed to vary
lens	Turn on lensing when computing CMB spectrum
sz	Floating amplitude for SZ spectrum
iso1	Anticorrelated CDM isocurvature
iso2	Uncorrelated CDM isocurvature
mnu	Massive neutrinos
nrel	Number of relativistic species
run	Running scalar spectral index
tens	Tensor Modes
xe	Two step reionization model

Table 2.8: Description of the cosmological model components listed in Table: 2.7

Data Set	Description
wmap5	WMAP five-year data set
2df	2dF Galaxy Redshift Survey, (Cole et al., 2005)
sdss	Sloan Digital Sky Survey, (Tegmark et al., 2004), (Eisenstein et al., 2005)
acb	ACBAR complete data set, (Reichardt et al., 2009)
bao	Baryonic Acoustic Oscillations, (Eisenstein et al., 2005)
snall	Supernova “Gold Sample” (Riess et al., 2004), Supernova Legacy Survey (Astier et al., 2006), and SNEssence
hst	Hubble Space Telescope Key Project, (Freedman et al., 2001)
cmb	Boomerang + CBI + VSA + Acbar 2006
lrg	Sloan Luminous Red Galaxy Sample
lyapost	Post-processed with the Lyman-alpha forest data, (Seljak et al., 2006)

Table 2.9: Description of the Data sets listed in Table: 2.7

Three-Year Data Release										
Model	wmap	Data Sets								
		wmap+								
		2df	bao	boom+	cbi+	sn	sn	all	wl	gold
lcdm	✓	✓	✓	✓	✓	✓	✓	✓	✓	✓
lcdm+kcutlin	✓									
lcdm+kcutlog	✓									
lcdm+mnu	✓		✓				✓			✓
lcdm+mnu+nrel			✓				✓			✓
lcdm+nrel			✓				✓			✓
lcdm+ns=1	✓									
lcdm+run	✓	✓		✓	✓		✓		✓	✓
lcdm+run+tens	✓	✓		✓	✓		✓		✓	✓
lcdm+tau=0	✓									
lcdm+tens	✓	✓		✓	✓		✓		✓	✓
lcdm+xelstep	✓									
ocdm	✓	✓	✓			✓	✓	✓		
ocdm+omegac=0	✓									
ocdm+omegal=0	✓									
ocdm+w										✓
pkrec	✓									
wcdm+mnu										✓
wcdm+nopert	✓	✓				✓	✓	✓		✓
wcdm+pert	✓	✓				✓	✓	✓		✓

Table 2.10: Combinations model/dataset for which the cosmological parameters have been evaluated. The various models and data sets are briefly described in Table 2.11 and Table 2.12 respectively.

Model	Description
lcdm	$\Lambda$ CDM
lcdm+kcutlin	$\Lambda$ CDM + primordial spectrum with sharp cutoff and linear prior
lcdm+kcutlog	$\Lambda$ CDM + primordial spectrum with sharp cutoff and log prior
lcdm+mnu	$\Lambda$ CDM + massive neutrinos
lcdm+mnu+nrel	$\Lambda$ CDM + massive neutrinos + number of relativistic species
lcdm+nrel	$\Lambda$ CDM + number of relativistic species
lcdm+ns=1	$\Lambda$ CDM + scale invariant fluctuations ( $n_s = 1$ )
lcdm+run	$\Lambda$ CDM + running scalar spectral index
lcdm+run+tens	$\Lambda$ CDM + running spectral index + Tensor Modes
lcdm+tau=0	$\Lambda$ CDM + no reionization ( $\tau = 0$ )
lcdm+tens	$\Lambda$ CDM + Tensor Modes
lcdm+xelstep	$\Lambda$ CDM + step reionization
ocdm	Open CDM
ocdm+omegac=0	Open CDM + No Dark Matter ( $\Omega_c = 0, \Omega_\Lambda \neq 0$ )
ocdm+omegal=0	Open CDM + No Cosmological Constant ( $\Omega_c \neq 0, \Omega_\Lambda = 0$ )
ocdm+w	Open CDM + $w$ , ( $w = constant$ )
pkrec	primordial spectrum freely varying in 15 bins in k space
wcdm+mnu	$w$ CDM + massive neutrinos, ( $w = constant$ )
wcdm+nopert	$w$ CDM + no perturbations, ( $w = constant$ )
wcdm+pert	$w$ CDM + perturbations, ( $w = constant$ )

Table 2.11: Description of the cosmological models listed in Table: 2.10

Data Set	Description
wmap	WMAP three-year data set
2df	2dF Galaxy Redshift Survey (Cole et al., 2005)
bao	Baryonic Acoustic Oscillations (Eisenstein et al., 2005)
boom+acbar	BOOMERanG + ACBAR (Montroy et al., 2006),(Kuo et al., 2004)
cbi+vsa	CBI + VSA (Readhead et al., 2004),(Dickinson et al., 2004)
hst	Hubble Space Telescope Key Project (Freedman et al., 2001)
sdss	Sloan Digital Sky Survey, (Tegmark et al., 2004), (Eisenstein et al., 2005)
sn astier	Supernova Legacy Survey (SNLS) (Astier et al., 2006)
sn gold	Supernova "Gold Sample"(Riess et al., 2004)
wl	Weak Lensing (Semboloni et al., 2005; Hoekstra et al., 2006)
all	All data sets combined, excluding wl, hst and bao

Table 2.12: Description of the Data sets listed in Table: 2.10

### 2.1.4 Likelihood Code

**Format** FORTRAN 90

**# of Files** 2

Proper assignment of errors to points in the CMB angular power spectra requires the use of a Fisher matrix. Since some components that go into making the Fisher matrix are model dependent, we provide FORTRAN 90 code which, given an input CMB model power spectrum, will compute the likelihood of that model fit to *WMAP* data and optionally return the inverse Fisher matrix.

Two versions are supplied. One contains only the software while the other contains the software plus the supporting data. More details may be found in the readme file bundled with in the distribution, Bennett et al. (2012), Larson et al. (2011), Dunkley et al. (2009), Hinshaw et al. (2003b) and Verde et al. (2003).

### 2.1.5 Predicted Sunyaev-Zeldovich Power Spectrum

<b>Units</b>	$\mu\text{K}^2$
<b>Format</b>	ASCII
<b># of Files</b>	3

The angular power spectrum due to the Sunyaev-Zeldovich effect as adapted from Battaglia et al. (2010) are supplied for three frequencies: 61 GHz (WMAP), 148 GHz(ACT), and 150 GHz(SPT).

The spectra are supplied in three ASCII text files each with two columns. The first column is the multipole moment  $l$ . The second is the spectrum in  $\mu\text{K}^2$ .

The spectra were computed with the following parameter assumptions:

$$\begin{aligned}\Omega_m &= 0.258 \\ \Omega_l &= 0.742 \\ \Omega_b &= 0.0441 \\ h &= 0.722 \\ n_s &= 0.972 \\ \sigma_8 &= 0.8005\end{aligned}$$

They are supplied in the form:

$$\frac{l(l+1)C_l^{TT}}{2\pi}$$

## 2.2 Sky Maps

Iterative algorithms are used to create skymaps from the calibrated differential time-ordered WMAP data for each of the ten differencing assemblies. Each pixel in a map represents a sky temperature. The CMB dipole has been removed from the Stokes I maps.

Frequency band maps were created by computing a weighted, pixel-by-pixel, mean of the individual differencing assemblies comprising each bandpass.

Foreground reduced maps have been produced by removing a foreground model from the ‘unreduced’ maps using the Foreground Template Model discussed in (Bennett et al., 2012). The cleaning algorithm for Stokes I was updated for the nine-year data set. The Stokes I cleaning algorithm for previous data releases is described in (Hinshaw et al., 2007). The Stokes Q and U cleaning algorithm is as described in (Bennett et al., 2012) and (Page et al., 2007); this algorithm hasn’t changed significantly for the nine-year data release. Briefly, synchrotron, free-free, and dust emission templates were modeled and then subtracted from the single year ‘unreduced’ maps. The goal was to produce a set of maps with the foreground removed while retaining WMAP’s noise characteristics.

K and Ka maps were used to produce the Stokes I foreground cleaned maps; therefore only the Q, V, and W frequency bands are provided for this product. K maps were used to produce the Stokes Q and U foreground cleaned maps, so only Ka, Q, V, and W frequency bands are provided.

Nine-year coadded maps that were smoothed to 1 deg resolution are provided. The smoothing takes place using symmetrized window function in harmonics space.

A new product was developed for the nine-year data release. A set of Stokes I maps were processed to reduce the asymmetry of the effective beam; the process deconvolves the maps using only the asymmetric component of the beam. The resulting map contains the true sky signal effectively convolved with a circularly symmetric beam. See (Bennett et al., 2012) for details.

All WMAP maps are pixelized using the HEALPix system. The full resolution maps are provided at either Res 9 (NSide=512; 3,145,728 pixels) or Res 10 (NSide=1024; 12,582,912 pixels). The HEALPix pixelization scheme Gorski et al. (2005), initially developed by K. Górski, B. Wandelt, and E. Hivon, is a hierarchical equal area isolatitude pixelisation of the sphere. More information and a suite of Fortran and IDL software tools for working with HEALPix format maps is available from the HEALPix web site at:

<http://healpix.jpl.nasa.gov/>

The maps are stored in FITS binary table extensions. The maps are stored in the first extension in a file; the number of columns in this table depends upon whether polarization maps have been included in the file. Some files also contain the polarization covariance matrices for the maps; if supplied these matrices are stored in a second binary table extension. Column names for the Stokes I, Q, U, and N\_OBS were selected to be compatible with existing HEALPix software. Some maps will contain a bandpass mismatch component, the so-called S, or spurious signal, map. These columns are:

Stokes Parameter	$\sigma_0$ For Each Differencing Assembly									
	K1	Ka1	Q1	Q2	V1	V2	W1	W2	W3	W4
I	1.429	1.466	2.245	2.131	3.314	2.949	5.899	6.562	6.941	6.773
Q,U, uncleaned	1.435	1.472	2.254	2.140	3.324	2.958	5.912	6.577	6.958	6.795
Q,U, cleaned	N/A	2.166	2.710	2.572	3.534	3.144	6.157	6.850	7.246	7.076
	$\sigma_0$ For Each Frequency Band									
	K	Ka	Q	V	W					
I	1.429	1.466	2.188	3.131	6.544					
Q,U, uncleaned	1.435	1.472	2.197	3.141	6.560					
Q,U, cleaned	N/A	2.166	2.641	3.339	6.832					

Table 2.13: Pixel Noise Coefficients: cleaned indicates foreground cleaned.

TEMPERATURE	The Stokes I, or temperature, measurement.
Q_POLARISATION	The Stokes Q measurement.
U_POLARISATION	The Stokes U measurement.
SPUR_SIGNAL	The bandpass mismatch, or S, component.
N_OBS	The effective number of observations.

The same I, Q, U, and N\_OBS data are used to construct I,Q,U and I,Q,U,S files; the only difference is in the bandpass mismatch component and in the additional covariance matrices table (if one is included in the file).

I, Q, U, and S data are provided in thermodynamic mK. N\_OBS is provided in counts.

Pixel noise in mK may be evaluated from N\_OBS using the expression  $\sigma = \sigma_0 / \sqrt{N_{obs}}$ ; see Table 2.13 for these coefficients.

Files that contain polarization maps may contain a second FITS binary table containing the polarization noise covariance matrices for the pixels in the maps of the first FITS extension. These matrices are used in the map-making process and characterize the noise properties of the polarization maps. See (Bennett et al., 2012), (Jarosik et al., 2007) and (Hinshaw et al., 2009) for more details. There are two forms of this matrix, depending upon whether or not the bandpass mismatch term (S map) has been included in the file.

If the map file contains only I, Q, and U, then the covariance matrices table will contain the following columns:

N_OBS	The effective number of observations.
QQ	The QQ covariance term in units of N_OBS-style counts.
QU	The QU covariance term in units of N_OBS-style counts.
UU	The UU covariance term in units of N_OBS-style counts.

The N\_OBS columns in each table are the same.

The covariance matrix for each pixel is then a 2x2 symmetric matrix with the form:

$$\begin{matrix} \text{QQ} & \text{QU} \\ \text{QU} & \text{UU} \end{matrix}$$

If the map file contains I, Q, U, and S, then the covariance matrices table will contain the following columns:

N_OBS	The effective number of observations.
M11	The SS covariance term in units of N_OBS-style counts.
M12	The SQ covariance term in units of N_OBS-style counts.
M13	The SU covariance term in units of N_OBS-style counts.
M22	The QQ covariance term in units of N_OBS-style counts.
M23	The QU covariance term in units of N_OBS-style counts.
M33	The UU covariance term in units of N_OBS-style counts.

The N\_OBS columns in each table are the same.

The covariance matrix for each pixel is then a 3x3 symmetric matrix with the form:

$$\begin{matrix} \text{M11} & \text{M12} & \text{M13} \\ \text{M12} & \text{M22} & \text{M23} \\ \text{M13} & \text{M23} & \text{M33} \end{matrix}$$

### 2.2.1 Coadded Nine Year Sky Maps

These full nine year maps were produced by performing a weighted, pixel-by-pixel, mean of the nine single year maps; the `N_OBS` measurement was used to weight this mean. The zero point of each nine year Stokes I map has been set using a Galactic  $csc|b|$  model, as described in Bennett et al. (2012). The `N_OBS` measurements were added together to produce the final `N_OBS` measurement.

See Section 2.2 for general details.

Coadded Nine Year Map Products	
Product	# files
I Maps per DA	10
I Maps per Freq. Band	5
Deconvolved I Maps per DA	10
Deconvolved I Maps per Freq. Band	5
Foreground Reduced I Maps per DA	8
Foreground Reduced I Maps per Freq. Band	3
Smoothed I Maps per DA	10
Smoothed I Maps per Freq. Band	5
Smoothed Deconvolved I Maps per DA	10
Smoothed Deconvolved I Maps per Freq. Band	5
I,Q,U Maps per DA	10
I,Q,U Maps per Freq. Band	5
Smoothed I,Q,U Maps per DA	10
Smoothed I,Q,U Maps per Freq. Band	5
I,Q,U,S Maps per DA	10
I,Q,U,S Maps per Freq. Band	5

### 2.2.2 Full Resolution Individual Year Sky Maps

These maps were each constructed using only a single year of data; they are used both for direct analysis and to construct the nine year maps discussed in Section 2.2.1. The dates bounding each year are:

Year	Start (GMT)	End (GMT)
1	2001:222 0:00	2002:222 0:00
2	2002:222 0:00	2003:222 0:00
3	2003:222 0:00	2004:222 0:00
4	2004:222 0:00	2005:222 0:00
5	2005:222 0:00	2006:222 0:00
6	2006:222 0:00	2007:222 0:00
7	2007:222 0:00	2008:222 0:00
8	2008:222 0:00	2009:222 0:00
9	2009:222 0:00	2010:222 0:00

The start date of the first year, 2001:222, corresponds to WMAP's arrival at L2.

See the general description of skymap format and creation in Section 2.2.

Individual Year Map Products	
Product	# files
I Maps per DA	90
Deconvolved I Maps per DA	90
High Resolution I Maps per DA	90
Foreground Reduced I Maps per DA	72
High Resolution Foreground Reduced I Maps per DA	72
I,Q,U Maps per DA	90
Foreground Reduced Q,U Maps per DA	81
I,Q,U,S Maps per DA	90

### 2.2.3 Reduced Resolution Sky Maps

These low resolution maps are supplied at HEALPix Res 4 (Nside=16; 3072 pixels) and are used primarily for foreground analysis on the polarization component of the WMAP data.

See the general descriptions of skymap format and creation in Section 2.2.

In some cases, the noise covariance matrices used with the higher resolution maps described in the previous sections are supplied with these maps. If the file contains only Stokes Q and U, then the `N_OBS` column is not supplied in this second table.

However, these noise covariance matrices do not fully characterize the pixel-to-pixel noise in these lower resolution maps. Therefore a accurate and much larger inverse covariance matrix is supplied for each map as a separate product. These are supplied in one of two forms.

The first, more common, form consists of a 6144x6144 matrix containing four 3072x3072 blocks representing Q–U covariance with the form:

$$\begin{matrix} \text{QQ} & \text{QU} \\ \text{QU} & \text{UU} \end{matrix}$$

The second form, supplied for the single year IQUS maps per differencing assembly, consists of a 12288x12288 matrix containing sixteen 3072x3072 blocks representing I–Q–U–S covariance with the form:

$$\begin{matrix} \text{II} & \text{IQ} & \text{IU} & \text{IS} \\ \text{IQ} & \text{QQ} & \text{QU} & \text{QS} \\ \text{IU} & \text{QU} & \text{UU} & \text{US} \\ \text{IS} & \text{QS} & \text{US} & \text{SS} \end{matrix}$$

These inverse covariance matrices are supplied in the primary header/data unit for a FITS file.

The elements corresponding to the Galactic plane pixels as defined by the standard processing mask are set to zero. therefore, the matrices as supplied are singular. To make them non-singular, the rows and the columns corresponding to each zero element of the diagonal should be deleted.

A small effect due to transmission imbalance between the A side and the B side of the instrument has been projected out of the inverse covariance matrices as described in Section 3.5.1 of (Jarosik et al., 2007).

Low Resolution Map Products	
Product	# files
Single Year Q,U Maps per DA	90
Inverse Covariance Matrices for Single Year Q,U Maps per DA	90
Single Year I,Q,U,S Maps per DA	90
Inverse Covariance Matrices for Single Year I,Q,U,S Maps per DA	90
Single Year Foreground Reduced Q,U Maps per DA	81
Inverse Covariance Matrices for Single Year Foreground Reduced Q,U Maps per DA	81
Nine Year Coadded Q,U Maps per Freq. Band	5
Inverse Covariance Matrices for Nine Year Coadded Q,U Maps per Freq. Band	5
Nine Year Coadded Foreground Reduced Q,U Maps per Freq. Band	4
Inverse Covariance Matrices for Nine Year Coadded Foreground Reduced Q,U Maps per Freq. Band	4

#### 2.2.4 Loss Imbalance Templates

<b>Coord System</b>	Galactic
<b>Projection Type</b>	HEALPix Nested
<b>Res/N<sub>side</sub></b>	4/16
<b>N<sub>pix</sub></b>	3072
<b>Resolution</b>	0.23° – 0.93°
<b>Units</b>	mK (Thermodynamic)
<b>Format</b>	FITS
<b># of Files</b>	10

WMAP data processing takes into account the small transmission imbalance between the A side and the B side of the instrument. The imbalance has been measured for each radiometer using WMAP flight data, with an uncertainty of 20% (Jarosik et al., 2011). This uncertainty could lead to significant artifacts in the polarization skymaps. Spatial patterns in the Stokes Q and U maps that correspond to this uncertainty have been determined by comparing results of data simulations in which the transmission imbalance factors have been varied. See section 2.9 of Jarosik et al. (2011). In one case, a simulation with these factors increased by 20% for both radiometers in each DA was compared with a simulation using nominal values. In a second case, the imbalance was increased by 10% for radiometer 1 and decreased by 10% for radiometer 2 in each DA. This yielded two sets of Q,U templates, which we provide as HEALPix Nside=16 (Res 4) maps in mK for each DA. Section 3.5.1 of Jarosik et al. (2007) describes how these templates can be projected out of the inverse covariance matrices so that transmission imbalance uncertainty will not affect subsequent analyses. The calculation is done using equation 27 of Jarosik et al. (2007):

$$\hat{\Sigma}^{-1} = \Sigma^{-1} - \frac{\Sigma^{-1}v \otimes \Sigma^{-1}v}{v^T \Sigma^{-1} v}$$

where  $\Sigma^{-1}$  is the  $6144 \times 6144$  QU inverse covariance matrix for a given DA in  $\text{mK}^{-2}$  and  $v$  is the 6144 element QU transmission imbalance template for the DA in  $\text{mK}$ .

## **2.3 Derived Foreground Products**

### 2.3.1 Internal Linear Combination (ILC) Map

<b>Coord System</b>	Galactic
<b>Projection Type</b>	HEALPix Nested
<b>Res/<math>N_{side}</math></b>	9/512
<b><math>N_{pix}</math></b>	3145728
<b>Resolution</b>	1°
<b>Units</b>	mK (Thermodynamic)
<b>Format</b>	FITS
<b># of Files</b>	2

The Internal Linear Combination (ILC) map is formed from a weighted linear combination of 5 Smoothed I Maps in which the weights are chosen to maintain the CMB anisotropy signal while minimizing the Galactic foreground contribution. The weights are determined by minimizing the variance of the measured temperatures with the additional constraint that sum of the weights is equal to 1. To account for the spatial variation of the spectral indices of the various foreground components across the sky and in particular in the Galactic plane, the sky is divided into 12 regions: 11 regions within the Galactic plane and 1 covering the outer Galactic plane and high Galactic latitudes. The weights are calculated for each of the 12 regions and a full-sky ILC map is generated using the obtained coefficients after smoothing the region boundaries with a 1.5 degree kernel. As a final step, a ‘bias correction’ based on Monte Carlo simulations is applied to the ILC map.

On angular scales greater than  $\sim 10$  degrees, we believe that the nine-year ILC map provides a reliable estimate of the CMB signal, with negligible instrument noise, over the full sky. However, we caution that on smaller scales there is a significant structure in the bias correction map that is still uncertain.

In addition to the ILC map, we provide a FITS-format map which defines the 12 sky regions used to construct the ILC. Full documentation is contained in the FITS header.

### 2.3.2 Point Source Catalog

**Format** ASCII

**# of Files** 2

This is a catalog of 501 point sources detected in the nine year *WMAP* sky maps independently from any previous surveys. The sources listed in the catalog were detected as  $\geq 5\sigma$  sigma peaks in *WMAP* maps that have been weighted by the square root of the number of observations and optimally filtered for point source detection. The position of each source is obtained by fitting a Gaussian profile plus a baseline to each detected peak. Of the 501 detected sources, 463 have one or more possible 5 GHz counterparts. Of the sources with no 5 GHz identification, some are close to the detection threshold and may be spurious. The catalog lists the following parameters for each source:

Column	Parameter
1 – 2	Right Ascension and Declination (2000)
3 – 4	Galactic Longitude and Latitude
5 – 9	<i>WMAP</i> Flux (Jy)
10 – 14	Flux Error (Jy)
15 – 16	5 GHz Identification
17	Flag for multiple 5 GHz identifications
18	<i>WMAP</i> DR1 Identification Number
19	<i>WMAP</i> Spectral Index
20	<i>WMAP</i> Spectral Index Error
21	Bitmask indicating bands where $\text{SNR} \geq 5$

The CMB-free method identifies 502 point sources in a linear combination map formed from Q, V, and W band maps using weights such that CMB fluctuations are removed and flat-spectrum point sources are retained. Source fluxes are then estimated by integrating the Q, V, and W temperature maps within 1.25 degrees of each source position and applying a correction for Eddington bias due to noise. The catalog lists the following parameters for each source:

Column	Parameter
1 – 2	Right Ascension and Declination (2000)
3 – 4	Galactic Longitude and Latitude
5 – 7	<i>WMAP</i> Flux for Q, V, and W (Jy)
8 – 10	<i>WMAP</i> Flux Error for Q, V, and W (Jy)
11 – 12	5 GHz Identification
13	M for sources with multiple 5 GHz IDs
14	<i>WMAP</i> Source ID

The right ascension and declination are formatted hhmmss.s and dddmmss.

### 2.3.3 Point Source Variability Table

**Format** ASCII

**# of Files** 1

This table lists flux densities for each year of the *WMAP* mission for each of the 501 sources in the five-band nine-year *WMAP* point source catalog. For each source, the yearly flux variation with respect to the nine-year mean flux was obtained by fitting a Gaussian to the (individual year minus nine-year) difference map for each year 1–9. The position of the Gaussian is fixed to the source position in the nine-year catalog and the width of the Gaussian is fixed to the beam width. The only free parameters are the Gaussian peak brightness and the baselevel. The table lists yearly flux densities obtained by adding the nine-year mean flux to the yearly flux variation. The error values can be used with year-to-year flux differences to estimate the significance of variability. For bands in which a nine-year flux is not listed in the point source catalog, the yearly fluxes and errors in this table are set to -9.99.

Column	Parameter
1	Source Name
2 – 3	Galactic Longitude and Latitude
4	Year of <i>WMAP</i> Mission
5 – 9	Yearly Flux (Jy) in K-W bands
10 – 14	Uncertainty in Yearly Flux Variation (Jy)
15	5 GHz Identification
16	Flag for multiple 5 GHz identifications
17	<i>WMAP</i> DR1 Identification Number

### 2.3.4 Foregrounds Derived from Maximum Entropy Method

This description applies to any of the three foregrounds recovered using the Maximum Entropy Method: synchrotron, free-free thermal dust, and spinning dust.

<b>Coord System</b>	Galactic
<b>Projection Type</b>	HEALPix Nested
<b>Res/<math>N_{side}</math></b>	7/128
<b><math>N_{pix}</math></b>	786432
<b>Resolution</b>	1°
<b>Units</b>	mK (Antenna)
<b>Format</b>	FITS
<b># of Files</b>	21

The Maximum Entropy Method (MEM) is used to derive all-sky maps of the synchrotron, free-free, spinning dust, and thermal dust foregrounds at each of the 5 *WMAP* frequencies. Using the Smoothed I Maps minus the ILC map as input, representations of each of the foregrounds are fit to each pixel independently. The synchrotron, free-free and dust spectral indices are assumed to be constant over the sky. The shape of the spinning dust spectrum is also assumed constant, but the model includes a frequency scale factor for the spinning dust spectrum for pixels where the spinning dust prior is brighter than 0.1 mK. The MEM technique fits for the separate components and the frequency scaling of the spinning dust spectrum by minimizing an entropy functional using priors based on the listed templates:

Component	Prior
Synchrotron	408 GHz Haslam Map
Free-Free	Scattering corrected, extinction corrected H $\alpha$ Map
Spinning Dust	SFD Dust Map
Thermal Dust	FDS Map

The model foregrounds are provided in separate files for each of the five *WMAP* frequencies. Note that the model temperatures are in mK, antenna temperature, rather than in thermodynamic units. A map of the peak frequency of spinning dust emission is also supplied.

### 2.3.5 Foregrounds Derived from an MCMC Method

<b>Coord System</b>	Galactic
<b>Projection Type</b>	HEALPix Nested
<b>Res/<math>N_{side}</math></b>	6/64
<b><math>N_{pix}</math></b>	49152
<b>Resolution</b>	1°
<b>Units</b>	mK (Antenna)
<b>Format</b>	FITS
<b># of Files</b>	14

These maps were generated from the MCMC fit described in Gold et al. (2009) and Bennett et al. (2012). The inputs are the one degree smoothed maps per frequency band, binned to  $N_{side} = 64$ . There is an MCMC chain for each pixel which is used to estimate the likelihood for all the parameters. The maps provided for each parameter are:

- The best-fit parameter from each chain.
- The main parameter over the chain.
- The marginalized variance.

Four sets of maps are provided: a “base” model, a synchrotron model, and a shifted spinning dust model with two additional variants. Each model has a slightly different set of parameters that are allowed to vary.

The base model consists of a three-component power-law model (synchrotron, free-free, and dust) where the synchrotron and dust indices are free parameters.

The shifted spinning dust model is a four-component model (synchrotron, free-free, dust, and spinning dust) where the synchrotron index is fixed to -3, the spinning dust spectrum is fixed to the Cold Neutral Medium spectral form from Silsbee et al. (2011) with a shift parameter of 0.7, and dust is a free parameter. This will be referred to as the spinning dust model.

The first variant uses the spinning dust model but makes the synchrotron spectral index a free parameter. the spinning dust spectrum uses a shift parameter of 0.84. This will be referred to as the free synchrotron model.

The final variant is based upon the free synchrotron model just discussed by constrains the synchrotron spectral index to follow that specified in Strong et al. (2011) instead of a pure power law. This will be referred to as the strong synchrotron model.

The following parameters are reported:

Temperatures in mK are in antenna units except for the CMB maps, which are provided in thermodynamic units.

The reduced  $\chi^2$  are the best-fit  $\chi^2$  divided by the number of degrees of freedom determined from the chain using the “effective complexity”.

Parameter	Notes
CMB temperature	All four models.
CMB Stokes Q	All four models.
CMB Stokes U	All four models.
Free-free temperature at K-band	All four models.
Synchrotron temperature at K-band	All four models.
Synchrotron Stokes Q at K-band	All four models.
Synchrotron Stokes U at K-band	All four models. Not an independent parameter.
Synchrotron spectral index	Not present in the spinning dust model.
Dust temperature at W-band	All four models.
Dust Stokes Q at W-band	All four models.
Dust Stokes U at W-band	All four models. Not an independent parameter.
Dust spectral index	All four models.
Spinning Dust Temperature at K-band	Not present in the base model.
Error flags.	All three models. Each pixel is bit-coded: 0 - no error 1 - did not find a good adaptive stepsize in the “prechain” for that pixel, but the chain was run anyway 2 - the chain for that pixel failed the convergence test 4 - not used 8 - not used 16 - pixel was masked before processing, no fit was done
Best fit reduced $\chi^2$	All four models.

Table 2.14: MCMC Foregrounds

### 2.3.6 Foregrounds Templates

<b>Coord System</b>	Galactic
<b>Projection Type</b>	HEALPix Nested
<b>Res/<math>N_{side}</math></b>	9/512
<b><math>N_{pix}</math></b>	786432
<b>Resolution</b>	1°
<b>Units</b>	mK (Antenna)
<b>Format</b>	FITS
<b># of Files</b>	3

For most cosmological analyses one must retain the well-defined noise characteristics of the WMAP frequency band maps. To achieve this, low-noise model templates for each foreground emission component (dust, free-free, and synchrotron) were created and fit to the maps at each frequency band; these fits were then subtracted from the skymaps. Regions that could not be reliably cleaned were masked, and thereby essentially discarded from later analysis.

The dust emission templates were created from "Model 8" from the Finkbeiner et al. (1999) (FDS 1999) analysis of IRAS and COBE data. The FDS 94GHz map was used as the dust emission template for Stokes I/temperature analysis and can be found on LAMBDA. A separate dust template was developed for Q and U polarization analysis, combining information from the FDS intensity map and starlight polarization maps. This latter template is stored in a standard HEALpix FITS map file with the Q and U templates stored in the **Q\_POLARISATION** and **U\_POLARISATION** columns of the first binary table extension; the **TEMPERATURE** and **N\_OBS** columns of this extention are set to zero and one, respectively.

The free-free emission template was developed from the full-sky H $\alpha$  map compiled by Finkbeiner (2003) with corrections for dust extinction and scattered H $\alpha$  (Bennett et al. (2003c); Bennett et al. (2012)).

The synchrotron template used for temperature analysis was computed from the difference of the WMAP K and Ka Stokes I maps in thermodynamic units, using the maps smoothed to 1° resolution. The procedure for creating the template is described in detail in Hinshaw et al. (2007). K band data was used for the polarized synchrotron emission template as described by Page et al. (2007).

More details may be found in Bennett et al. (2012), Hinshaw et al. (2009), Jarosik et al. (2007), Hinshaw et al. (2007), Page et al. (2007), Spergel et al. (2007), Bennett et al. (2003c), Finkbeiner (2003) and Finkbeiner et al. (1999).

### 2.3.7 Smoothed Single Year K1 and Ka1 Sky Maps

<b>Coord System</b>	Galactic
<b>Projection Type</b>	HEALPix Nested
<b>Res/<math>N_{side}</math></b>	9/512
<b><math>N_{pix}</math></b>	786432
<b>Resolution</b>	1°
<b>Units</b>	mK (Antenna)
<b>Format</b>	FITS
<b># of Files</b>	18

See the Foregrounds Templates section (2.3.6) for a discussion of this product. These are the smoothed maps used to construct the synchrotron template.

## **2.4 Ancillary Data**

### 2.4.1 Masks

<b>Coord System</b>	Galactic
<b>Projection Type</b>	HEALPix Nested
<b>Res/N<sub>side</sub></b>	9/512
<b>N<sub>pix</sub></b>	3145728
<b>Resolution</b>	N/A
<b>Units</b>	N/A
<b>Format</b>	FITS
<b># of Files</b>	6

A number of *WMAP* data analysis applications use pixel masks to exclude foreground-contaminated portions of the sky from the analysis. Diffuse emission in Stokes I (temperature) is masked using a combination of cuts in the K band and Q band maps, as described in (Bennett et al., 2012). Diffuse emission in Stokes Q and U is masked using cuts in K band polarized intensity combined with a model of thermal dust emission. Point sources are masked based on a combination of external catalog data and *WMAP*-detected sources. The source exclusion radius is 0.6 degree for the intensity masks and 1.0 degrees for all but one source in the polarization masks. The exception is Cen A, which is masked to a radius of 3 degrees in polarization.

Mask values for each map pixel are provided in the N\_OBS field of the data file (the verb—TEMPERATURE— field should be disregarded). A mask value of zero means the pixel is rejected; a value of one means the pixel is accepted. For temperature analysis, we provide two cut levels: the standard cut ("temperature\_analysis") corresponds roughly to the "Kp2" cut in the three-year data release; the extended cut ("extended temperature analysis") corresponds roughly to the "Kp0" cut in the three-year data release. For all the masks we provide the data at multiple pixel resolutions. For all but the polarization analysis mask, the cut is defined at the lowest supplied resolution and all higher resolution versions mask the same sky area. The polarization analysis mask is defined at Nside=512 (r9) but we also provide a degraded version at Nside=16 (r4) for low-l analysis. For this mask, an r4 pixel is included (set to one) if more than 50% of its daughter r9 pixels are set to one.

The point source catalog mask was used to exclude Galactic plane and Magellanic cloud regions in making the *WMAP* nine-year point source catalogs. The region outside of this mask consists of pixels that are either outside of the diffuse component of the nine-year temperature analysis mask or outside of the nine-year point source catalog mask.

More details may be found in Bennett et al. (2012).

Mask File	%	Nside	Description
wmap_temperature_kq75_analysis_mask_r9_9yr_v5.fits	68.8	512	Extended temperature analysis mask
wmap_temperature_kq75_analysis_mask_r10_9yr_v5.fits	68.8	1024	Extended temperature analysis mask
wmap_temperature_kq85_analysis_mask_r9_9yr_v5.fits	74.8	512	Primary temperature analysis mask
wmap_temperature_kq85_analysis_mask_r10_9yr_v5.fits	74.8	1024	Primary temperature analysis mask
wmap_polarization_analysis_mask_r9_9yr_v5.fits	73.2	512	Polarization analysis mask
wmap_polarization_analysis_mask_r4_9yr_v5.fits	73.4	16	Polarization analysis mask

Table 2.15: Masks. The % column indicates the amount of the sky admitted.

#### 2.4.2 Beam Transfer Functions

<b>Units</b>	see text
<b>Format</b>	ASCII
<b># of Files</b>	10

Beam transfer functions are computed from the Legendre transform of the binned hybrid radial beam profile. The window function applicable to power spectra is the square of the beam transfer function.

Window functions are presented as ASCII tables, with the first column being multipole moment  $l$  and the second column the transfer function (amplitude) normalized to 1.0 at  $l = 1$ .

More details may be found in Bennett et al. (2012).

### 2.4.3 Beam Maps

<b>Coord System</b>	Focal Plane
<b>Projection Type</b>	Rectilinear, pixelized at $2.4'(0.04^\circ)$
<b>Resolution</b>	$0.23^\circ - 0.93^\circ$ (frequency dependent)
<b>Units</b>	mK (Thermodynamic)
<b>Format</b>	FITS
<b># of Files</b>	12

The main and near-sidelobe response of each of the 20 WMAP antenna feeds has been mapped in-flight using observations of Jupiter. The nine-year release is comprised of 17 Jupiter observing seasons: Oct/Nov 2001, Feb/Mar 2002, Nov/Dec 2002, Mar/Apr 2003, Dec 2003/Jan 2004, Apr/May 2004, Jan/Feb 2005, May/Jun 2005, Feb/Mar 2006, Jun/Jul 2006, Mar/Apr 2007, Jul/Aug 2007, Apr/May 2008, Aug/Sep 2008, May/Jun 2009, Oct/Nov 2009, and Jul/Aug 2010. As a prelude to beam analysis, an archive of calibrated time-ordered observations is constructed, consisting of Jupiter passages within roughly 7.0, 5.5, 5.0, 4.0 and 3.5 degrees of either the A- or B-side beam center for K, Ka, Q, V and W bands respectively. The time-ordered observations are corrected to a fiducial Jupiter distance of 5.2 AU, background subtracted and corrected for aberration. To constrain low signal-to-noise beam pedestals, a hybrid TOD archive is then constructed in which model predictions ((Bennett et al., 2012), (Hill et al., 2009)) are substituted for data at the 2, 3, 5, 6 and 9 dBi levels of K,Ka,Q,V and W respectively. This hybrid beam archive serves as the basis for beam map and window function analysis.

For purposes of constructing beam maps, the data in the hybrid beam TOD archive are assigned to 2.4 arcminute bins on a coordinate grid centered on either the A or B-side focal plane axis. The beam response for each feed is computed from the average temperature in each bin. No correction has been made for the side-A vs. side-B input transmission imbalance. These beam maps are convenient for some applications, but are not used in the computation of the flight beam transfer functions. The 2.4 arcminute binning acts as a smoothing kernel which filters high frequency spatial content. The pixelization transfer function may be estimated from the Legendre transform of the symmetrized radial profile of the binning kernel. Assuming a square pixel of 0.04 degrees on a side centered on the origin, the symmetrized radial profile of the binning function may be represented as

$$\begin{aligned} f(r) &= 1.0 && \text{for } r < R \\ &= 1.0 - \frac{4}{\pi} \cos^{-1}(R/r) && \text{for } R \leq r \leq R\sqrt{2} \end{aligned}$$

where  $R = 0.02$  deg. Both the pixelization profile and pixelization transfer function are provided as a useful reminder of the limitations of the 2.4 arcminute binning.

Beam maps are provided in 10 FITS image format files, one file for each differencing assembly. Each file contains:

- Beam map for the A side, in mK (antenna temperature)

- Statistical errors of each bin of the A and B sides beam maps, in mK (antenna temperature). The statistical error are based on the number of observations in each bin. Model points are assigned 100% error.
- Beam map for the B side, in mK (antenna temperature)
- Statistical errors of each bin of the A and B sides beam maps, in mK (antenna temperature)

The beam coordinates form an equal area rectangular coordinate system centered on the optic axis of the spacecraft. They are related to coordinates  $\theta$  (elevation from optic axis) and  $\phi$  (azimuth about optic axis) as follows:

$$\begin{aligned}X_{beam} &= 2 \sin(\theta/2) \cos(\phi) \\Y_{beam} &= 2 \sin(\theta/2) \sin(\phi)\end{aligned}$$

More details may be found in Bennett et al. (2012), Hill et al. (2009), Hinshaw et al. (2009) and Jarosik et al. (2007).

#### 2.4.4 Beam Radial Profiles

**Units** see text

**Format** ASCII

**# of Files** 10

For each differencing assembly, an azimuthally symmetrized radial beam profile is computed by binning the ensemble of individual A- and B- side hybridized Jupiter observations. A constant bin size of 0.25 arcmin is used, and the straight mean of all hybrid samples within a radial bin represents the value for that bin.

More details may be found in Hill et al. (2009) and Hinshaw et al. (2009).

### 2.4.5 Far-Sidelobe Maps

<b>Coord System</b>	Spacecraft
<b>Projection Type</b>	HEALPix Nested
<b>Res/<math>N_{side}</math></b>	7/128
<b><math>N_{pix}</math></b>	196608
<b>Resolution</b>	N/A
<b>Units</b>	[ $\cdot$ ]
<b>Format</b>	FITS
<b># of Files</b>	10

Low resolution (res 7) maps of the antenna gain response over  $4\pi$  steradians for each of the 10 *WMAP* detector assemblies. While *WMAP*'s optical system gain drops very rapidly when moving away from the main beam line-of-sight, the emission of the extended Galactic foreground can be 1000 times brighter than the fluctuations of the CMB and can cover very large solid angles. It is therefore extremely important to fully characterize the antenna gain response. The Far-Sidelobe Maps are based on compilations of data from the following sources:

- GSFC anechoic chamber antenna range
- Princeton outdoor antenna range
- In flight lunar data
- Physical optics code theoretical predictions

The gain pattern is presented in spacecraft coordinates, such that the X axis is parallel to the plane of the radiators, -Z is the anti-sun direction of the spin axis, and Y is perpendicular to both. The gain,  $4\pi/\Omega^S$ , is relative to isotropic in dimensionless units where  $\Omega^S$  is the symmetrized beam solid angle. Positive values refer to A-side pickup, and negative values to B-side pickup.

These maps are in units of directive gain,  $g_i$ , where  $i$  is a pixel; these are the linear units that correspond to dBi. The normalization is such that  $\sum_i(|g_i|) = 2N_{pix}$ , or it would equal  $2N_{pix}$  if the full antenna pattern were represented rather than being cut off at the radius chosen to define the main beam/far-sidelobe boundary.

More details may be found in Bennett et al. (2012), Hill et al. (2009) and Barnes et al. (2003).

#### 2.4.6 Bandpass Frequency Response

**Units** see text

**Format** ASCII

**# of Files** 20

The frequency response of the two detectors in each of *WMAP*'s twenty radiometers (two per differencing assembly) are provided in this dataset; there is one file for each radiometer. Each file contains three columns:

- The first column contains the frequency in GHz.
- The second and third columns contain the frequency response for the two detectors comprising the radiometer. These values are in Rayleigh-Jeans units that have since been normalized to one, so these columns are dimensionless.

In principal the bandpass data for the two detectors should be weighted by their response to a thermal spectrum corresponding to how the *WMAP* data is calibrated in flight. In practice, weighting this bandpass data based upon the area beneath each response curve should be sufficient. It is worth noting that the center frequencies have drifted over time; the effective frequency calculator on the LAMBDA's *WMAP* software page and the corresponding IDL procedures in the delivered IDL library apply a correction factor to account for this drift.

These are the same files released in the fourth *WMAP* data release.

More details may be found in Jarosik et al. (2003a), Jarosik et al. (2003b) and Jarosik et al. (2007).

## **2.5 Time-Ordered Data**

### 2.5.1 Calibrated Time-Ordered Data

**Units** mK  
**Format** FITS  
**# of Files** 2554

This is a set of time-ordered data containing the scientific measurements and the most important instrument and spacecraft housekeeping measurements. The scientific data have been calibrated using the final *WMAP* calibration parameters and are, therefore, supplied in millikelvin. Each pair of radiometer channels have been coadded together, so each observation consists of two measurements.

These data will be described in detail in Chapter 3.

### 2.5.2 Uncalibrated Time-Ordered Data

**Units** mK  
**Format** FITS  
**# of Files** 2554

This is a set of time-ordered data containing the scientific measurements and the most important instrument and spacecraft housekeeping measurements. The scientific data have not been calibrated and are, therefore, supplied in counts. All four radiometer channels have been provided.

These data will be described in detail in Chapter 3.

### 2.5.3 Optimal Time-Domain Filters

<b>Units</b>	dimensionless
<b>Format</b>	FITS
<b># of Files</b>	7

The optimal time-domain filters are used in the creation of the first estimate of the *WMAP* maximum likelihood sky map solution:

$$(M^T N^{-1} d)^{-1}$$

also known as the iteration zero (it0) map. Final maps are produced by multiplying the it0 maps by

$$(M^T N^{-1} M)^{-1}$$

through an iterative process.

The  $N^{-1}$  term represents the inverse radiometer noise correlation matrix and is computed using the inverse noise correlation function; this correlation function is the optimal time-domain filter.

There are seven FITS files containing the collection of filters, one for each year of data, and with each file containing filters for all ten differencing assemblies. Each differencing assembly filter is written to its own FITS binary table extension, so there are ten such extensions in each file. The first column represents the lag time measured in samples of that radiometer. The remaining two columns supply the filters for each radiometer.

More details may be found in Jarosik et al. (2007).

## Chapter 3

# Time Ordered Data (TOD)

Three complete time-ordered data archives are supplied with the latest *WMAP* data release; two archives contain calibrated data while the third contains uncalibrated (or raw) data. Each archive is delivered through a collection of compressed tar files; each tar file contains twenty daily telemetry files. The daily files are written using the Flexible Image Transport Standard (FITS) format.

Archive	# of FITS Files	Size (GB)	# of Tar Files	Size (GB)
Calibrated (2 channel)	2554	256.7	164	376.9
Calibrated (4 channel)	2554	256.7	164	491.0
Uncalibrated	2554	485.7	164	185.8

The uncalibrated and one of the calibrated archives contain all four radiometer channels for each observation. The other calibrated archives have been coadded into two radiometer channels to reduce the size.

*WMAP*'s Telemetry data consists of many packet types; each packet type contains several measurements with some sort of common theme (see Section 1.7). Once on the ground and delivered to the data analysis facility, these packets are sorted and a subset are combined into records spanning 46.08 seconds; these records comprise the time-ordered data (TOD) archive. This archive is maintained in a collection of files, each spanning one day of data.

The 46.08 second record length is driven by the packet frequency of the analog instrument housekeeping (AIHK) data, which is recorded every 46.08 seconds. There are four digital instrument housekeeping (DIHK) packets and thirty science records (telemetered in two packets per record) for each AIHK packet. The science records are frequently referred to as major science frames.

The TOD archive is distributed to the public through daily files written FITS format. Each file contains five binary FITS tables:

1. Meta Data Table
2. Science Data Table

3. Analog Instrument Housekeeping Data Table
4. Digital Instrument Housekeeping Data Table
5. Line-Of-Sight Data Table

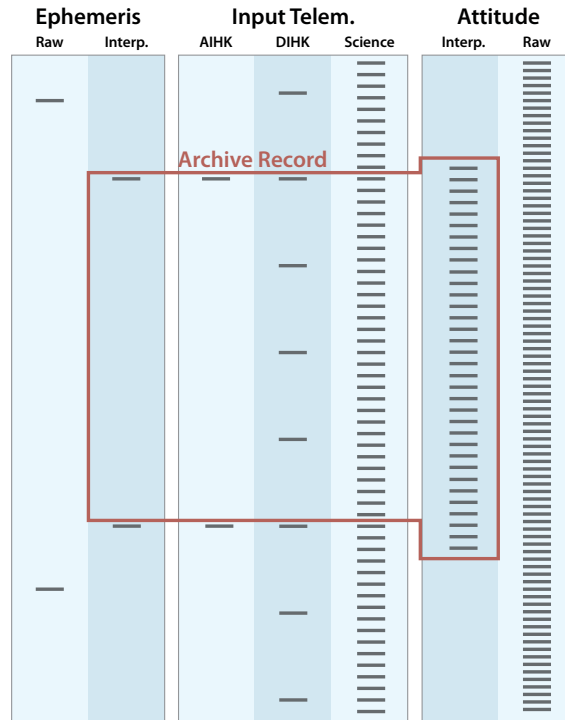


Figure 3.1: Shows how the different components of an archive record interrelate in time.

In four of the five tables, each row has a time associated with it. This time is reported in a modified reduced Julian day format. Packet times require precision to better than one tenth of a millisecond, so in order to retain sufficient precision in the numerical representation of the time, it is necessary to modify the definition of the reduced Julian day. To convert a modified reduced Julian day to a Julian day, add 2,450,000 to its value. Figure 3.1 shows how record components relate in time.

A discussion of each table, followed by a very brief discussion of FITS headers, follows. In these discussions, records refer to TOD records and packets refer to the telemetry packets received from *WMAP*.

### 3.1 The Meta Data Table

The meta data table contains general information describing each record in the time ordered data archive for that day. Each row corresponds to one 46.08 second record; each column

represents:

Name	Description
TIME	The time of the start of the record, represented as a modified reduced Julian day.
POSITION	A three element Cartesian vector supplying the position (in kilometers) of <i>WMAP</i> at the start of the record. It is measured from the Sun with the +X axis in the J2000 0hr right ascension direction and the +Z axis in the J2000 +90deg. declination direction.
VELOCITY	A three element Cartesian vector supplying the velocity (in km/sec) of <i>WMAP</i> at the start of the record, using the same coordinate system as the POSITION vector.
GEOPOS	A three element Cartesian vector supplying the position (in kilometers) of <i>WMAP</i> at the start of the record. It is measured in the same coordinate system as the POSITION vector, centered on the Earth instead of the Sun.
GEOVEL	A three element Cartesian vector supplying the velocity (in km/sec) of <i>WMAP</i> at the start of the record, using the same coordinate system as the GEOPOS vector.
QUATERN	A $4 \times 33$ array containing a four element quaternion for the start of each major science frame plus one for the preceding science frame and one for each of the two following science frames.
NSCI	The number of major science frames in the record. There will usually be thirty [the maximum number of frames allowed in a record].
NDIHK	The number of digital instrument housekeeping packets there are in the record. There will usually be four [the maximum number of frames allowed in a record].

Position and velocity data are received from the spacecraft every 60 seconds. The positions and velocities recorded in the time-ordered data archive have been interpolated to the time recorded in each record. These are the packets referred to as Ephemeris data in Figure 3.1.

Attitude data are transmitted from the spacecraft every second. The thirty quaternions corresponding to the science data frames have been interpolated to the start time of the corresponding science frame. The preceding quaternion was interpolated to a time 1.536 seconds prior to the first science frame. The two following quaternions were interpolated in 1.536 second intervals following the thirtieth science frame. In the rare event of a missing science frame, a quaternion is generated for the expected time and stored in this table. These are the Attitude data referred to in Figure 3.1.

The slowly varying position and velocity data have been interpolated to the time recorded in the Meta Data Table row. The rapidly-varying quaternions have been specifically inter-

polated to the start time of each 1.536 sec science frame. When using the quaternions to determine the attitude of the spacecraft, and therefore the pointing for each observation, the 33 quaternions should be used to interpolate a quaternion at the midpoint of the individual science observation of current interest. The line-of-site boresights provided in the LOS Table can then be used to determine the pointing for each observation.

## 3.2 The Science Data Table

The science data table contains the major science frames recorded for that day. Each frame consists of two science data telemetry packets that have been combined into a single data structure.

A single TOD record contains thirty 1.536 second major science frames. The data has been calibrated and are reported in millikelvin. Each row corresponds to one frame; each column represents:

Name	Description
TIME	The time of the start of the science frame, represented as a modified reduced Julian day.
K1	The K-band differencing assembly array.
KA1	The KA-band differencing assembly array.
Q1	The first Q-band differencing assembly array.
Q2	The second Q-band differencing assembly array.
V1	The first V-band differencing assembly array.
V2	The second V-band differencing assembly array.
W1	The first W-band differencing assembly array.
W2	The second W-band differencing assembly array.
W3	The third W-band differencing assembly array.
W4	The fourth W-band differencing assembly array.
GenFlags	A set of bit-coded quality flags describing the entire science frame [the general flags].
DAFlags	An array of ten sets of bit-coded quality flags, each describing one differencing assembly.
Error1	A two bit-coded error code transmitted by <i>WMAP</i> describing the science frame. There are two—one for each science telemetry packet.
Error2	A bit-coded error code transmitted by <i>WMAP</i> describing the science frame. There are two—one for each science telemetry packet.
FrmInd	The index within the day of the time-ordered data record containing this science frame.
SciInd	The index of the science frame within its time-ordered data record.

Each differencing assembly (DA) array consists of four channels measured N times where N depends upon the bandpass. For the first data release, however polarization data are not available and the four channels are averaged together,<sup>1</sup> so each differencing assembly array consists of N observations for each DA per channel per major science frame. N for each bandpass is:

K	Ka	Q	V	W
12	12	15	20	30

For the three-year data release the calibrated TOD include polarization data as two separate polarization vectors. The average polarization estimate for the detectors is reported. For the uncalibrated data all four detector channels are provided; this data are reported in counts instead of millikelvin. The bit-coded quality flags are set during processing. These flags are:

#### General Flags

- Bit 0 There is a problem with the spacecraft attitude for this science frame.
- Bit 1 A filler telemetry packet (science, instrument, or space-craft) affects this science frame. A filler packet is an empty frame that replaces a missing packet.
- Bit 2 The transmitter is on. Since the transmitter is now always on this flag will not be implemented.
- Bit 3 WMAP is not in observing mode.
- Bit 4 There is no science data in this frame. Not implemented.
- Bit 5 The sun is visible over the sun shield. In other words, the angle between the sun and the +Z axis is greater than some angle (see programs.pars for the shield angle).
- Bit 6 The Earth is visible over the sun shield. In other words, the angle between the Earth and the +Z axis is greater than some angle (see programs.pars for the shield angle).
- Bit 7 The moon is visible over the sun shield. In other words, the angle between the moon and the +Z axis is greater than some angle (see programs.pars for the shield angle).

#### DA Specific Flags

---

<sup>1</sup>The IDL procedure `pckt2mnemonic` (see section 5.2.2) provided with the WMAP software package is designed to be compatible with future data releases and will accept as input any of the four channels but will always return the same average value.

Bit 0	This flag indicates that the data in the frame is suspect. An ASCII log file is used to flag time ranges that contain suspect data.
Bit 1	Mars is visible in the A-side beam.
Bit 2	Mars is visible in the B-side beam.
Bit 3	Jupiter is visible in the A-side beam.
Bit 4	Jupiter is visible in the B-side beam.
Bit 5	Saturn is visible in the A-side beam.
Bit 6	Saturn is visible in the B-side beam.
Bit 7	Uranus is visible in the A-side beam.
Bit 8	Uranus is visible in the B-side beam.
Bit 9	Neptune is visible in the A-side beam.
Bit 10	Neptune is visible in the B-side beam.

Finally, the bit-coded error codes in the science telemetry packets shown below are extracted from the internal WMAP document: “MAP DEU Flight Command and Telemetry Packets Definition,” by Carlos Trujillo of NASA/GSFC.

#### Error 1

Bit 0	Unused.
Bit 1	Band Buffer Overflow. The memory location where the pointer to the next available storage location inside the Band buffer has been corrupted. In order to avoid writing science data outside the boundaries of the Band buffer, this check is performed prior to storage of the next 40 science data samples into the Band buffer. A detected overflow condition is handled by not storing science data into the Band buffer. Correction of this error is done during science data packetization (the pointer value is cleared as part of cleaning operations).
Bit 2	K-Band Accumulation Buffer Overflow. The memory location where the pointer to the next available storage location for the K-Band Accumulation buffer has been corrupted. In order to avoid writing science data outside the boundaries of this buffer, this check is performed prior to calculation of the next K-Band accumulated result. If the overflow condition is detected, accumulation data will not be processed nor stored.

- Bit 3      Ka-Band Accumulation Buffer Overflow. The memory location where the pointer to the next available storage location for the Ka-Band Accumulation buffer has been corrupted. In order to avoid writing science data outside the boundaries of this buffer, this check is performed prior to calculation of the next Ka-Band accumulated result. If the overflow condition is detected, accumulation data will not be processed nor stored.
- Bit 4      Q-Band Accumulation Buffer Overflow. The memory location where the pointer to the next available storage location for the Q-Band Accumulation buffer has been corrupted. In order to avoid writing science data outside the boundaries of this buffer, this check is performed prior to calculation of the next Q-Band accumulated result. If the overflow condition is detected, accumulation data will not be processed nor stored.
- Bit 5      V-Band Accumulation Buffer Overflow. The memory location where the pointer to the next available storage location for the V-Band Accumulation buffer has been corrupted. In order to avoid writing science data outside the boundaries of this buffer, this check is performed prior to calculation of the next V-Band accumulated result. If the overflow condition is detected, accumulation data will not be processed nor stored.
- Bit 6      W-Band Accumulation Buffer Overflow. The memory location where the pointer to the next available storage location for the W-Band Accumulation buffer has been corrupted. In order to avoid writing science data outside the boundaries of this buffer, this check is performed prior to calculation of the next W-Band accumulated result. If the overflow condition is detected, accumulation data will not be processed nor stored.
- Bit 7      Science Pointers Out of Spec - The values for all the storage and retrieval pointers for Band and Accumulation buffers are examined at the end of each Science Data Cycle. The FSW can be fooled into believing that a Science Data Cycle ended (corruption of Timing.SciDataCycles counter) and attempt an early packetization of the science data. This attempt will be accepted, but the condition is flagged. Clearing all science data cycle counters and pointers (therefore correcting any corrupted memory locations) recovers from this error.

**Error 2**

Bits 1–15 Non-matching channel address counter - For each science data sample collected from the AEU the actual reported address of the sample (0 through 39) is verified against the address value requested by the FSW. Any non-matching address values will void the science data sample collected and a value of 0 will be stored in the expected Band buffer location.

### 3.3 The Analog Instrument Housekeeping (AIHK) Data Table

The AIHK data table contains the AIHK packets recorded for that day. This data represents physical measurements [such as temperatures, voltages, and currents] of the instrument indicating its current state.

A single TOD record contains one AIHK telemetry packet consisting of two 23.04 second sweeps. Each row in the table corresponds to one sweep; each column represents:

Name	Description
TIME	The time of the start of the telemetry packet, represented as a modified reduced Julian day. This time will be reported twice in the table—once for each sweep extracted from an AIHK packet.
PDU	The Power Distribution Unit (PDU) data block of 97 elements.
AEU1	The Analog Electronics Unit (AEU) #1 data block of 57 elements.
AEU2	The Analog Electronics Unit (AEU) #2 data block of 57 elements.
AWIN1	The 16 element window range block corresponding to AEU1.
AWIN2	The 16 element window range block corresponding to AEU2.
Counters	Five status counters. There is actually only one set of these counters in the telemetry packet; each sweep has a copy in its table row.
FrmInd	The index within the day of the time-ordered data record containing this science frame.
Sweep	The sweep within the telemetry packet represented by this row (1 or 2).

The two AEU data blocks contain 32 elements that require more dynamic range than a single two byte integer can provide. For each of these elements, a one byte window element

is provided in the AWIN blocks that essentially adds another byte of dynamic range to those measurements.

### 3.4 The Digital Instrument Housekeeping (DIHK) Data Table

The DIHK data table contains the DIHK packets recorded for that day. This data primarily represents digital status information relating to commands received and current status codes. Physical measurements regarding the digital electronics unit are also transmitted through this packet.

A single TOD record contains four 11.52 second DIHK telemetry packets. A row in the table represents one packet; each column represents:

Name	Description
TIME	The time of the start of the telemetry packet, represented as a modified reduced Julian day.
Data	The DIHK data portion of the packet consisting of 42 elements.
FrmInd	The index within the day of the time-ordered data record containing this science frame.
DihkInd	The index of the DIHK packet within its time-ordered data record.

### 3.5 The Line-Of-Sight (LOS) Table

The LOS table provides unit vectors describing the line-of-sight for each microwave horn in spacecraft coordinates. The position and attitude data [attitude provided through the quaternions] may be used with these unit vectors to determine the pointing of *WMAP* at any given time.

This table consists of a single row of twenty columns. Each column contains a three element unit vector describing the pointing of a single differencing assembly horn on either the A or B side of the spacecraft. The column names are:

K1A	K1B	KA1A	KA1B	Q1A	Q1B	Q2A	Q2B	V1A	V1B
V2A	V2B	W1A	W1B	W2A	W2B	W3A	W3B	W4A	W4B

### 3.6 Headers

Each FITS header in the file contains the conversion constant used to transform the reduced Julian day into a standard Julian day; the header keyword is TIME2JD. The primary header also contains:

- The start (keyword STIME) and end (keyword ETIME) times of the data contained by the file in a GMT text format:

YYYYDDDhhmmss

where YYYY is the year, DDD is the day of the year, hhmmss is the GMT hour, minute, and second of the day.

- The data release date (keyword RELEASE) in the same GMT format.
- The number of TOD records (keyword NUMREC) is stored in the file.

# Chapter 4

## Telemetry Data

In the all but the final *WMAP* data release, a limited set of housekeeping data was released as part of the time-ordered data archives. The final data release will include a much larger collection of telemetry data.

*WMAP* data was transmitted from the satellite in NASA's CCSDS format; each day of data was supplied in four files:

- INHK Instrument housekeeping
- OBHK Spacecraft (or observatory) housekeeping
- OBHX Extended spacecraft housekeeping
- INSC Science data

The housekeeping data consists of several different packets of data; each packet is identified with an application identifier (or apid). Each packet has a time stamp associated with it and contains multiple data points, each identified by a unique mnemonic. Several 'pseudotelemetry' packets were also defined; the mnemonics from these 'packets' are computed from data extracted out of multiple telemetry packets.

This format is no longer used by NASA missions, having been replaced with a new format. Therefore, to spare the user from having to parse out the contents of these files and then converting this data from the original form into something more useful (counts to volts, for example), selected measurements from these files have been rewritten into a single FITS file for each day.

Each FITS file contains 58 binary FITS tables. The first five tables contain the science data, one table for each differencing assembly. Many of the rest of these tables contain data from a single apid/packet. The rest are one or more pseudotelemetry mnemonics that share the same timestamps. The underlying feature of all the data within a given table is that contents of each row in the table share the same time. Within each binary table, the first column contains a time in *WMAP* Reduced Julian day (Julian day less 2,450,000; this allows precision to the submillisecond level); a column follows for each mnemonic. The header contains a brief description of each mnemonic.

# Chapter 5

## Software

The WMAP IDL<sup>®</sup><sup>1</sup> library is a collection of IDL<sup>®</sup> procedures to assist with reading, manipulating and displaying the WMAP data products. The library can be downloaded at:

<http://lambda.gsfc.nasa.gov/>

As described in Chapter 2 all the WMAP maps are pixelized using the HEALPix system. The HEALPix pixelization scheme Gorski et al. (2005), initially developed by K. Górski, B. Wandelt, and E. Hivon, is a hierarchical equal area isolatitude pixelisation of the sphere. More information and a suite of Fortran and IDL software tools for working with HEALPix format maps is available from the HEALPix web site at:

<http://healpix.jpl.nasa.gov/>

### 5.1 FITS Readers

The following routines will read skymaps and time-ordered data.

#### 5.1.1 FITS\_READ\_MAP

The FITS\_READ\_MAP routine reads any of WMAP maps data products (I maps, foreground maps, etc., except for map files containing polarization data – to read polarization data products use READ\_COMBINED\_MAP available through the software page) into a R\*4 array. See individual data products for details.

```
CALLING SEQUENCE:  
    FITS_READ_Map, File_Name, T, N_obs, [ EHeader, PHeader= ]  
INPUTS:  
    File_Name - Character name of archive map FITS file, scalar string  
    A .fits extension is optional. Compressed files (with a  
    .gz extension) are allowed.
```

---

<sup>1</sup>IDL<sup>®</sup> is a trademark of ITT Visual Information Solutions, 4990 Pearl East Circle, Boulder, CO 80301:  
<http://www.ittvis.com>

**OUTPUTS:**

T - R\*4 array with temperature of each pixel  
 N\_obs R\*4 array with number of observations of each pixel

**OPTIONAL OUTPUT:**

EHeader - FITS header with map information, string array. This is the FITS header associated with the FITS binary table that contains the map.

**OPTIONAL KEYWORD OUTPUT:**

Pheader - Primary FITS header, string array

**EXAMPLE:**

```
Read the first year K band map
IDL> fits_read_map,'wmap_imap_r9_yr1_K1_v2.fits',t,N_obs,h
```

**5.1.2 READ\_COMBINED\_MAP**

The READ\_COMBINED\_MAP routine reads all of WMAP maps data products containing polarization data into a R\*4 array. See individual data products for details.

**CALLING SEQUENCE:**

```
Read_Combined_Map, FileName, Imap, Qmap, UMap [, Smap]
```

**INPUTS:**

FileName - The name of the FITS file.

**OUTPUTS:**

Imap - The Stokes I map.  
 Qmap - The Stokes Q map.  
 Umap - The Stokes U map.  
 Smap - The spurious signal map, if available.

**OUTPUT KEYWORDS:**

N\_Obs - The N\_Obs column.  
 PolWtArr - The polarization weights matrix. This will be a 2x2xN or 3x3xN array depending upon the contents of the weights binary table. The 3x3xN option will be accompanied by an Smap array.

PriHdr - The primary FITS header.

StokesHdr - The Stokes data binary table FITS header.

PolWtHdr - The weights matrix binary table FITS header.

**COMMENTS:**

'mrdfits.pro' is used to read the contents of the file.

Two spellings of the Q and U columns are supported:  
 p\_POLARIZATION and p\_POLARISATION

The relevant binary FITS tables must be the first two extensions in the file, but the order of these two is irrelevant.

**EXAMPLE:**

```
Read the three year Q1 band map
IDL> fits_read_map,'wmap_iqumap_r9_3yr_Q1_v2.fits',t,q,u,s,N_obs=n,...
```

### 5.1.3 FITS\_READ\_TOD

Read a WMAP time-ordered data FITS file (e.g. `map_q_imap_yr1_v1.fits`) into an IDL® structure.

CALLING SEQUENCE:

```
FITS_READ_TOD, file, arch, [/NOHK]
```

INPUTS:

file - The name of the FITS file to read.

OUTPUTS:

arch - The TOD data structure. See the function `TOD_FORMAT()` for additional information about this structure

OPTIONAL INPUT KEYWORD:

/NOHK - If set, Then no housekeeping information is Returned, and only the time stamp and science data are defined in the output structure

EXAMPLE:

```
Read the time-ordered data for day 221 of year 2002 into an output  
structure  
IDL> file ='MAP_tod_20022202357_20022212357.fits'  
IDL> FITS_READ_TOD, file, arch
```

COMMENTS:

The `sci` array in the archive record contains the science data; there are thirty major science frames in each record; each of the frequency bands has some number of observations in each of these frames; the number of observations will be mentioned below.

Further, the science data in each archive record assumes a four-channel form for each observation of each differencing assembly (DA). If the file contains a single channel for each DA, each of the four channels of an observation for the DA will contain the same single value.

If the file contains two channels for each DA, the first two channels will contain the first channel from the file; the second two channels will contain the second channel from the file. Finally, if the file contains four channels for each DA then each channel in the output structure will contain a separate value.

The science data is stored in the output structure by bandpass (K, Ka, Q, V, and W). These bandpass arrays map to the DAs as follows:

```
arch.sci.k [ 0: 3,nobs] -- K1 (nobs=12)  
arch.sci.ka[ 0: 3,nobs] -- Ka1 (nobs=12)  
arch.sci.q [ 0: 3,nobs] -- Q1 (nobs=15)  
arch.sci.q [ 4: 7,nobs] -- Q2 (nobs=15)  
arch.sci.v [ 0: 3,nobs] -- V1 (nobs=20)  
arch.sci.v [ 4: 7,nobs] -- V2 (nobs=20)  
arch.sci.w [ 0: 3,nobs] -- W1 (nobs=30)  
arch.sci.w [ 4: 7,nobs] -- W2 (nobs=30)  
arch.sci.w [ 8:11,nobs] -- W3 (nobs=30)  
arch.sci.w [12:15,nobs] -- W4 (nobs=30)
```

## 5.2 Time-Ordered Data Access

The following routines can be used to extract specific fields or manipulate the time-ordered data.

The WMAP pointing direction for any given observation in the time-ordered data can be computed using the `TOD_to_Sky_Coords` (see section 5.2.4) IDL procedure; see the discussion of that procedure below for more details.

### 5.2.1 Interpolate\_Quaternions

This is procedure interpolate quaternions extracted from WMAP time-ordered data.

#### CALLING SEQUENCE:

```
Interpolate_Quaternions, input_q, offset, interp_q [, status]
```

#### INPUTS:

`input_q` - Set of 4 evenly-spaced quaternions (in a 4x4 array).

See the COMMENTS section for how this array should be arranged.

`offset` - Dimensionless time offset relative to the first quaternion.

#### OUTPUTS:

`interp_q` - The interpolated quaternion.

`status` - A status code:

0=normal interpolation,

-1=normal extrapolation--low,

-2=normal extrapolation--high,

1=offset out of bounds--low,

2=offset out of bounds--high,

#### KEYWORDS:

`ExtLimit` - The dimensionless extrapolation limit; it defines the permitted range in Offset. If this optional parameter is not supplied then it defaults to 1.0, resulting in a permitted range in Offset of -1 to 4 (0 to 3 indicates interpolation while anything outside that range indicates extrapolation).

`Transpose` - If present and nonzero, the transpose of the `input_q` array is used.

`Dmax` - Sets the maximum allowed displacement between adjacent q's.

Physically,  $|\Delta_q|^2 = |\omega \cdot \Delta_t/2|^2$ , the default

is  $0.02 \text{ rad}^2$  ( $\omega \sim 10 \text{ deg/sec}$ ,  $\Delta_t = 1.536 \text{ sec}$ )

which should cover all map applications. Any displacements larger than `Dmax` will produce an error condition.

`Verbose` - If present and nonzero, the input and intermediate quaternions and the result will be printed.

#### COMMENTS:

This routine expects a uniformly sampled set of quaternions Q1,Q2,Q3,Q4. It interpolate a quaternion for any time between Q1 and Q4, inclusive. The output is calculated at a time `T_Out`, expressed in terms of the sampling of the input quaternions:

```
T_Out = T(Q1)
Offset = -----
```

$T(Q2) - T(Q1)$

where  $T(Q1)$  is the time at quaternion  $Q1$ , and so forth. That is, the time for the output quaternion (variable `OFFSET`) should be a number in the range -1.000 to 4.000 inclusive. Input values outside that range result in an error. Input values outside 0.0 to 3.0 result in extrapolation instead of interpolation.

In other words, `Offset` is essentially a floating point subscript, similar to those used by the IDL intrinsic routine `INTERPOLATE`.

For optimal results, `OFFSET` should be in the range [1.0, 2.0] -- that is, the input quaternions  $Q1\dots Q4$  should be arranged such that 2 come before the desired output and 2 come after.

This routine expects `input_q` to be ordered as follows, where  $Q1\dots Q4$  are the 4 input quaternions:

`input_q = [[Q1], [Q2], [Q3], [Q4]]`

i.e., the Y subscript selects a quaternion and the X subscript selects an element.

If passing

`input_q = transpose([[Q1], [Q2], [Q3], [Q4]])`

i.e., so that the X subscript selects a quaternion, and the Y subscript selects an element, then use the `Transpose` keyword.

All computations are performed in double precision, and a double precision quaternion is returned regardless of the data type of the input quaternions.

### 5.2.2 Pckt2Mnemonic()

This is a procedure to extract data for a given mnemonic from a packet in the time-ordered data (include both digital and analog housekeeping data as well as science data)

CALLING SEQUENCE:

```
data = Pckt2Mnemonic(Pckt, Mnemonic [, Status])
```

INPUTS:

Pckt - IDL structure giving Time-ordered data, e.g. as read by  
`FITS_READ_TOD`

Mnemonic - scalar string giving the mnemonic to extract, e.g. 'DK113'

OUTPUTS:

Status - A status code: 0=success, -1=error.

RETURNED:

data - The extracted data.

OPTIONAL INPUT KEYWORDS:

/TIME - If present and nonzero, the data returned as `DLBARR[N,2]`  
 where `data[*,0]` gives the WMAP reduced Julian date, and  
`data[*,1]` gives the extracted data. It is usually preferable

to use the TJ output keyword to obtain the Julian dates.

**NFRAMES** - The number of major frames over which to average detector data or produce an rms of detector data. Only applies to science data mnemonics beginning with 'A' (average) or 'R' (rms). Default = 1 MF.

Other keywords are used by the various data extraction routines.

**OPTIONAL OUTPUT KEYWORD:**

TJ - vector of WMAP-reduced Julian dates associated with each data point

**EXAMPLE:**

After reading a TOD file the Pckt2Mnemonic procedure can be used to extract any of the mnemonics defined in Appendix B.

Extract the raw science data for channel K113 and its time base:

```
IDL> dk113_data = Pckt2Mnemonic(arch, 'dk113', tj=tj_sci)
```

Extract the major frame average for the same channel:

```
IDL> adk114_data = Pckt2Mnemonic(arch, 'adk114', tj=atj_sci)
```

Extract the temperature measured by the sensor at the top of the A side primary (dtatopprit):

```
IDL> trs = Pckt2Mnemonic(arch, 'dtatopprit', tj=tj_trs)
```

**5.2.3 Quat\_to\_Sky\_Coords**

This is a procedure to extract time series list of coordinates from an array of input quaternions.

**CALLING SEQUENCE:**

QUAT\_TO\_SKY\_COORDS, Q, DA\_str, [Res, ECL= , GAL=, CEL=, PIXEL = ]

**INPUTS:**

Q An array of quaternions of size 4xN.

**OPTIONAL INPUTS:**

DA\_str Case-insensitive string containing the DA to process:

'K1', 'Ka1', 'Q1', 'Q2', 'V1', 'V2', 'W1', 'W2', 'W3', 'W4'. If not supplied or set to '', then the mean optical axis is used.

Res Integer(1-13) giving the resolution of the returned nested Healpix pixel number. Only required if the output PIXEL keyword is supplied.

**OPTIONAL INPUT KEYWORD:**

Side - String -- either 'A' or 'B' or 'AB' specifying which side of the spacecraft to compute coordinates for. Default is 'AB' to compute for both sides.

**OUTPUT KEYWORDS:**

If only 1 side is specified, then the following output arrays will be N X 2 rather than N X 4

```

ECL      N X 4 array containing ecliptic long & lat for side A,
        ecliptic long & lat for side B.
GAL      N X 4 array containing galactic long & lat for side A,
        galactic long & lat for side B.
CEL      N X 4 array containing RA & Dec in degrees for side A,
        RA & Dec in degrees for side B.
PIXEL    N X 2 array containing pixel number for side A,
        pixel number for side B. The Side keyword is ignored.

```

**EXAMPLE:**

Find the Side A pointing of the K band in Galactic coordinates for the first science frame in a TOD file

```

IDL> fits_read_tod, 'MAP_tod_20022162357_20022172357.fits', tod
IDL> q = tod[0].quaternions ;Extract first 4 x 33 quaternion array
IDL> quat_to_sky_coords, q[*,1:30], 'K1',gal = gal

```

The subscripts [1:30] are used since the first quaternion is for the preceding science frame, and the last two are for the subsequent science frame

**PROCEDURES USED:**

COORTTRANS, Q2M	WMAP Library
VEC2PIX_NEST	HealPix Library
FTAB_EXT	IDLAstro Library

**5.2.4 TOD\_to\_Sky\_Coords**

This is a procedure to extract time series list of coordinates from an array of time-ordered data records.

**CALLING SEQUENCE:**

```
TOD_to_Sky_Coords, TOD, DA_str, [Res, Side=, /MajorFrm, /Center,
      ECL=, GAL=, CEL=, PIXEL= ]
```

**INPUTS:**

TOD An array of 'N' WMAP time-ordered data records, of  
the same structure as returned by READ\_TOD\_FITS.

**OPTIONAL INPUTS:**

DA\_str Case-insensitive string containing the DA to process:  
'K1', 'Ka1', 'Q1', 'Q2', 'V1', 'V2', 'W1', 'W2', 'W3', 'W4'. If not  
supplied or set to '', then the mean optical axis is used;  
this can be done ONLY if the MajorFrm keyword is set.

Res Integer(1-13) giving the resolution of the returned nested  
Healpix pixel number. Required if the output PIXEL  
keyword is supplied.

**OPTIONAL INPUT KEYWORD:**

Side A string containing either 'A' or 'B' or 'AB' specifying which  
side of the spacecraft to compute coordinates for. Default  
is 'AB' to compute for both sides.

MajorFrm If present and non-zero the coordinates for a DA at the start  
of each major science frame are returned. See the comments  
section for more details.

Center If present and non-zero the coordinates returned are interpolated  
to the center of each observation. This keyword is ignored if

MajorFrm is set.  
OUTPUT KEYWORDS:  
If only one side is specified, then the following output arrays will be N x 30 x M x 2 rather than N x 30 x M x 4. More details concerning the output arrays is supplied below in COMMENTS.

ECL      Array containing ecliptic long & lat for side A,  
          ecliptic long & lat for side B.  
GAL      Array containing galactic long & lat for side A,  
          galactic long & lat for side B.  
CEL      Array containing RA & Dec in degrees for side A,  
          RA & Dec in degrees for side B.  
PIXEL    N x 30 x M x 2 array containing pixel number for side A,  
          pixel number for side B. The Side keyword is ignored.

EXAMPLE:

Find the Side A pointing of the K band in Galactic coordinates for the first science frame in a TOD file

```
IDL> fits_read_tod, 'MAP_tod_20022162357_20022172357.fits', tod  
IDL> tod_to_sky_coords, tod[0], 'K1', Gal=gal, /MajorFrm
```

COMMENTS:

This procedure is a wrapper to the Quat\_to\_Sky\_Coords procedure, encapsulating the second two steps in the example described in that procedure, and interpolating quaternions as necessary while setting the call up.

There are thirty major science frames (sci elements) in each TOD record (thus N x 30 x M x 4 output arrays); these are separated in time by 1.536 seconds. M is the number of observations for a DA:

K1 & Ka1 - 12  
Q1 & Q2 - 15  
V1 & V2 - 20  
W1 - W4 - 30

The coordinates returned at those at the start each observation unless the /Center keyword is specified; in that event the coordinates are interpolated to the center of each observation.

If the /MajorFrm keyword is specified then the coordinates returned are those of the start of each major science frame in each TOD record. In this event the arrays returned will be dimensioned N x 30 x 4 (N x 30 x 2 for the PIXEL array, and for the other arrays if only one side is specified).

When computing the coordinates for each observation of a DA, this procedure may take quite a while to return!

PROCEDURES USED:

Quat\_to\_Sky\_Coords, Interpolate\_Quaternions      WMAP Library

## 5.3 Mapping Procedures

The following routines will transform a temperature map in HEALPIX projection into a flat-map projection and allow the user to draw various overlays.

### 5.3.1 REPROJ\_HEALPIX

This procedure converts a HealPix image to a flat map projection without doing any intensity scaling, i.e., the pixel values are in their original units.

#### CALLING SEQUENCE:

```
REPROJ_HEALPIX, T, Proj, Subs, [COORD=[1-9], PROJECT=[1,2],
                                SIZE=[1-5], MASK= ]
```

#### INPUT ARGUMENT:

T - Vector giving input HEALPix pixel list, full sky.

#### OUTPUT ARGUMENT:

Proj	- Output reprojected map, 2-d array
Subs	- Subscripts that generate the projection from the HEALPix vector.

#### INPUT KEYWORDS

The following keywords are passed to GET\_HEAL\_LUT via \_EXTRA:  
User will be prompted for the following values if they are not  
supplied as keywords:

COORD - Scalar Integer (1-9) giving the coordinate system transformation

	Display		
	Galactic	Celestial	Ecliptic
<b>Native:</b>			
Galactic	1	2	3
Celestial	4	5	6
Ecliptic	7	8	9

PROJECT - Scalar integer (1 or 2) giving the type of projection:

- 1 - Mollweide
- 2 - Zenithal Equal Area

SIZE - Scalar integer giving the size of the output image described  
by the table:

- 1 -- Small (512 x 256)
- 2 -- Medium (1024 x 512)
- 3 -- Large (2048 x 1024)
- 4 -- X large (4096 x 2048)
- 5 -- XX large (8192 x 4096, mollweide, native  
coordinates only)

#### OUTPUT KEYWORD:

Mask - Mask outlining the data/nodata ellipse. Same size as  
the output proj parameter

EXAMPLE: Display the K band all-sky map in Galactic coordinates in a medium (1024 x 512) size Mollweide projection scaled between -0.2 and 1.3 mK.

```
IDL> fits_read_map,'map_k_imap_yr1_v1.fits',t,n
IDL> reproj_healpix,t,proj,coord=1,project=1,size=2
IDL> tv,bytscl(proj,-.2,1.3)
```

### 5.3.2 HEALINFO

This procedure prints or returns values describing HEALPix formats of varying resolution.

**INPUT ARGUMENTS:**

No positional arguments.

**INPUT KEYWORDS:**

RES:	Resolution (0 - 10)
NSIDE:	Number of divisions along edge of biggest HEALPix pixel (1, 2, ..., 1024)
NPIX:	Total number of pixels in full sky (12, 48, ..., 12582912)
SPACING:	Approximate mean linear spacing between pixel centers in degrees
/HELP:	Flag to display short help message.

**OUTPUT KEYWORDS:**

These mean the same thing as the corresponding input keywords, except they are used to return results.

GET\_RES  
GET\_NSIDE  
GET\_NPIX

### 5.3.3 HEALPIX\_Nested\_Vectors

Procedure to read Cartesian [X,Y,Z] direction vectors from (FITS) binary file for HEALPix pixel scheme, nested pixel order.

**CALLING SEQUENCE:**

HEALPIX\_Nested\_Vectors, resolution, Px, Py, Pz

**INPUTS:**

Resolution - Scalar integer (3-9) giving the HEALPix resolution

**OUTPUTS:**

Px, Py, Pz, - vectors giving the Cartesian direction vectors for the specified resolution. The number of elements will be 768, 3072, 12288, 49152, 196608, 786432 or 3145728 as the resolution is increased from 3 to 9.

### 5.3.4 GRID\_OVERLAY

Plot coordinate grid lines on a map projection.

## CALLING SEQUENCE:

```
grid_overlay, [ PROJ={'M','Z'}, IMCOORD={'G','E','C'},  
               GRCOORD={'G','E','C"}, COLOR =, /PS, IMAGE=,  
               LON= , LAT=, /ZBUFF ]
```

## INPUTS:

none required, if defaults are satisfactory.

## OUTPUTS:

output consists of a plot, either to screen or postscript file.

## OPTIONAL INPUT KEYWORDS:

proj - char string - Single character specifying the projection type  
of the plot. Either 'M' (Mollweide) or  
'Z' (Zenithal Equal Area) are allowed. Case  
insensitive. Defaults to 'M'.

imcoord - char string - Single character specifying the coordinate  
system of the image projection. Three systems are  
recognized: 'E' (Ecliptic J2000), 'G' (Galactic) or  
'C' (Celestial J2000). Case insensitive.  
Defaults to 'G'.

grcoord - char string - Single character specifying the coordinate  
system of the grid overlay. Three systems are  
recognized: 'E' (Ecliptic J2000), 'G' (Galactic) or  
'C' (Celestial J2000). Case insensitive.  
Defaults to 'G'.

color - byte - The color (range 0-255) used to plot the  
grid pattern. Defaults to 0.

/ps - value=0 or 1 - Set this keyword to direct the plot to a postscript  
file. The output file is named 'grid\_overlay.ps'.  
If not set, plot will be directed to the screen  
(windows device).

image - bytarr - A byte-scaled image over which the grid will  
be plotted. If not specified, the procedure will  
plot within the current window (screen) or plot  
a grid with no image to the postscript file (/ps).

lon - fltarr - lines of constant longitude, in degrees.  
Default is every 15 degrees centered on 0.  
Specifying lon=-1000. results in NO longitude lines.

lat - fltarr - lines of constant latitude, in degrees.  
Default is every 10 degrees centered on 0.  
Specifying lat=-1000. results in NO latitude lines.

/zbuff - value=0 or 1 - Set this keyword if plotting to the z buffer  
is desired.

**EXAMPLE:**

```
Plot ecliptic coordinates grid over the current image
IDL> grid_overlay, GRCOORD='E'

Plot a default grid (Mollweide, Galactic) over an image (Kmoll)
to a postscript file
IDL> grid_overlay,image=bytscl(Kmoll,0,300),/ps
```

**COMMENTS:**

The routine scales the overlay to fill the screen window. If the user is trying to overlay an image on the screen which does not fill the window, then the overlay will be scaled incorrectly. The user need not worry about this when creating a postscript image, as the image and overlay are scaled together automatically when producing the .ps file.

The Zenithal equal area plot has a hard time plotting the lat=0 edge border. This can be remedied by plotting lat=[-0.00000001,0.0000000001] in its place (and this is what the code does by default).

**5.3.5 CIRCOPLOT**

Plots a circle of user-requested radius over an image projection. Circle is centered on the cursor position specified either by the user clicking the left mouse button (screen) or providing a coordinate list (postscript). Option also exists to indicate WMAP-visible portions of circle.

**CALLING SEQUENCE:**

```
circoplot [,radius=radius] [,proj={'M','Z'} [,color=num]
           [/visible] [,coord={'G','E','C'},
           [/ps [,image=image] [,ctable=num] [,coorlist=coorlist]
```

**INPUTS:****Screen mode:**

User positions cursor over image and clicks left mouse button to specify circle center.  
Routine remains active until the user clicks the right mouse button.

**Postscript mode:**

User provides a list of centers via coorlist keyword.

**OUTPUTS:****Screen mode:**

Output consists of a circle outline overlaid on an already existing image. A small cross is drawn at the requested the circle center position. Multiple circles may be drawn during the one call to circoplot. Click on right mouse button while the cursor is on the image to exit. If /visible is specified, triangles are plotted over the WMAP-visible segments of the circle.

**Postscript mode:**

Outputs similar to screen mode and written to file circoplot.ps.

Plot symbols have been tailored for hardcopy.  
Postscript is written in portrait deliberately to allow user the option  
of using eps and preview options within ghostview.

## KEYWORDS:

radius - float - Radius of the circle, in degrees.  
Default value = 141 deg.

proj - char string - Single character specifying the projection type  
of the underlying image. Either 'M' (Mollweide) or  
'Z' (Zenithal Equal area) are allowed. Case  
insensitive. Defaults to 'M'.

color - byte - The color (range 0-255) used to plot the  
circle and plot symbols. Defaults to 0

/visible - Set this keyword to have circoplot indicate those  
portions of the circle in which the spin axis  
is within 22.5 deg of the ecliptic.  
The result is coordinate system  
dependent -- see the coord keyword.

coord - char string -THIS KEYWORD IS MEANINGFUL ONLY IF /VISIBLE  
IS SPECIFIED.  
Single character specifying the coordinate  
system of the projection. Three systems are  
recognized: 'E' (Ecliptic J2000), 'G' (Galactic) or  
'C' (Celestial J2000). Case insensitive.  
Defaults to 'G'.

ps - value=0 or 1 - Set this keyword to direct the plot to a postscript  
file. The output file is named 'circoplot.ps'.  
If not set, plot will be directed to the screen  
(windows device).

coorlist - fltarr - A list of circle center coordinates, in the  
coordinate system OF THE UNDERLYING IMAGE.  
Format is [2,N] where N is the number of centers.  
Must be present when /ps is requested, and is only  
implemented for ps at present.

image - bytarr - A byte-scaled image over which the circles will  
be plotted. At present, only implemented for  
/ps, since user can already plot over an existing  
image on the screen.

ctable - long - A number specifying which standard IDL color table  
to load. Only implemented for /ps.

## EXAMPLE:

```
IDL> circoplot, radius=10, proj='Z', color=20
```

---

```
IDL> circoplot,/vis,color=100,coord='e'
IDL> circoplot,image=myimage,coorlist=[[120,50],[130,80]],/ps
```

### 5.3.6 PLANET\_OVERLAY

Plot a cross at the position of the chosen planet over an existing image within a screen window.

**CALLING SEQUENCE:**

```
planet_overlay,gmt=gmt,jd=jd [,planet=planet] [,coord={'G','E','C'}]
[,proj={'M','Z'}] [,color=color]
```

**INPUTS:**

At minimum, use must specify a time, using either the GMT or JD keywords (but not both).

**OUTPUTS:**

output consists of a plot to screen.

**KEYWORDS:**

gmt - char string - WMAP GMT time for which the planet position is to be computed, e.g., '200034500000'. Valid GMTs lie between 1 Nov 2000 and 20 April 2003. Do not specify GMT if you are already using the JD keyword.

jd - scalar or vector - Julian date for which the planet position is to be computed. Only JDs between 2451849.5 and 2452749.5 are accepted. It is acceptable to input a reduced Julian date with values between 1849.4 and 2749.5. Do not specify JD if you are already using the GMT keyword.

planet - char string - Name of the planet. Only one planet may be specified. Valid planet names are 'mars', 'jupiter', 'saturn', 'uranus', 'neptune'. Default planet = 'jupiter'.

proj - char string - Single character specifying the projection type of the plot. Either 'M' (Mollweide) or 'Z' (Zenithal Equal Area) are allowed. Case insensitive. Defaults to 'M'.

coord - char string - Single character specifying the coordinate system of the projection. Three systems are recognized: 'E' (Ecliptic J2000), 'G' (Galactic) or 'C' (Celestial J2000). Case insensitive. Defaults to 'G'.

color - byte - The color (range 0-255) used to plot the

---

scan pattern. Defaults to 0.

**COMMON BLOCKS:**

None.

**ROUTINES CALLED:**

`is_ieee_big()`, `gmt2jul`, `coortrans`, `mollweide_xy`, `zea_xy`

**EXTERNAL FILES REFERENCED:**

The FITS file JPLEPH.405 \\${MAP\_REF}/planet\_overlay/ provides the JPL DE405 ephemeris (as Chebyshev polynomials).

**EXAMPLE:**

To overplot Jupiter's positions for 500 days on a Galactic Mollweide projection:

```
IDL> jd0= 1850.0
IDL> planet_overlay,jd=jd0+dindgen(500)
```

**COMMENTS:**

The routine scales the overlay to fill the screen window. If the user is trying to overlay an image on the screen which does not fill the window, then the overlay will be scaled incorrectly.

## 5.4 Transformations

The following routines can be used to convert between different time systems or projections.

### 5.4.1 TIMETRANSFORM

Converts one time format into another.

**CALLING SEQUENCE:**

`TimeTransform, input [, output], TransKeyword`

**INPUTS:**

`input` - The input time. (See KEYWORDS for details.)

**OUTPUTS:**

`output` - The converted time. (See KEYWORDS for details.)

**INPUT KEYWORDS:**

`/Date2Jul` - Converts a Gregorian date into reduced Julian day.

Input should be a 3-6 element array containing the date: [year, month, day, hour, minute, second]. Time of day elements are optional.

`/DayOfYear` - Returns the day of the year for a given date. Input should be a 3-5 element array containing the date: [year, month, day, hour, minute]

`/DispGMT` - Converts a GMT string into a more readable string.

`/DispTS` - Converts a WMAP timestamp into a more human readable format

`/DOY2Date` - Determines the date from day-of-year and year. Input should be a 2 element array containing the day of year

and year. Output will be a 5 element array containing the date: [year, month, day, hour, minute]

- /DOY2Jul - Determines the reduced Julian day from day-of-year and year. Input should be a 2 element array containing the day of year and year.
- /GMT2Jul - Converts a WMAP GMT date/time string into a Julian day.
- /GMT2TS - Converts a WMAP GMT into a WMAP timestamp.
- /GMT2YMD - Converts the YYYYDDD portion of a GMT string to the format YYYY:MM:DD.
- /Jul2Date - Converts a reduced Julian day into a Gregorian date and time. Output consists of a 6 element array containing the date: [year, month, day, hour, minute, second].
- /Jul2GMT - Converts a reduced Julian day into a WMAP GMT date/time .
- /Jul2Tel - Converts a reduced Julian day into a telemetry structure timestamp. The telemetry structure must already exist!
- /Tel2Jul - Converts a packet time stamp into a reduced Julian day.
- /TS2GMT - Converts a WMAP timestamp into a WMAP GMT.
- /TS2Jul - Converts an array of time stamps into reduced Julian days.

Reference - The timestamp reference time in GMT format.

/Verbose - If present and nonzero, the output value is written to the screen.

\_EXTRA - IDL keyword inheritance. Keywords required by the conversion routines can be passed directly to them simply by specifying them in the call to this routine.

**COMMENTS:**

A conversion keyword indicating the type of conversion MUST be specified.

Reduced Julian days referred to here are WMAP Reduced Julian days:  
Full Julian day - 2450000

**EXAMPLE:**

Covert the WMAP reduced Julian day extracted using Pckt2mnemonic into a GMT string YYYYDDDhhmmsscccc000

```
IDL> adk114_data = pckt2mnemonic(arch, 'adk114', tj=atj_sci)
IDL> TimeTransform, atj_sci, GMT_string, /jul2gmt
IDL> print, GMT_string[0]
20013612359350260000
```

**5.4.2 COORTRANS**

Transforms between various J2000 coordinate systems. No precession is performed.

**CALLING SEQUENCE:**

```
coortrans,coor_in,coor_out,code [, /lonlat ]
```

**INPUTS:**

coor\_in - fltarr OR dblarr - The input coordinates, specified either as (lon,lat) pairs or unit vector arrays.  
Unit vectors must be of dimension (N,3).

Lonlat pairs must be of dimension (N,2).

```
code - char string - Character string specifying the desired
                     coordinate transformation. Only ONE code
                     may be requested at a time. Valid codes are:
                     'c2e' - in = celestial    out = ecliptic
                     'e2c' - in = ecliptic    out = celestial
                     'g2e' - in = galactic    out = ecliptic
                     'e2g' - in = ecliptic    out = galactic
                     'c2g' - in = celestial    out = galactic
                     'g2c' - in = galactic    out = celestial
                     'u2ll' - in = unit vector out = lon,lat
                     'll2u' - in = lon,lat     out = unit vector
```

#### OUTPUTS:

`coor_out` - dblarr - The output coordinates, returned as unit vectors unless `/lonlat` is set by the user.  
 Unit vectors are returned with dimension (N,3).  
 Lonlat pairs are returned with dimension (N,2).

#### OPTIONAL INPUT KEYWORDS:

`/lonlat` - Set this keyword to get output coordinates returned as longitude,latitude pairs.  
 (Superfluous if `code = 'u2ll'`).

#### COMMON BLOCKS:

None.

#### ROUTINES CALLED:

`get_rot_matrix()`

#### EXAMPLE:

Transform from celestial unit vectors ( $x,y,z$ ) to Galactic (lon,lat):

```
coortrans,[[x],[y],[z]],galcoor,'c2g',/lonlat
```

#### COMMENTS:

The routine does some rudimentary checking to ensure the input and output formats agree with the requested transformation code.  
 It also will bounce out if the unit vectors are not normalized.

Rotation matrices are computed by the routine `get_rot_matrix()`.

## 5.5 Widgets

### 5.5.1 MAP\_DATE

This widget computes and displays dates and times in the various systems used internally by the WMAP project. The widget has two modes: continuous update, and calculator. The

default mode is to update to the current time once per second. To enter your own data for computations, you need to stop the update, which you can do using the button **Press for Calculator Mode**.

Click on text fields to enter values in them. When you hit the **Enter** key on your keyboard, the changes will propagate through all the quantities in a reasonable way. Self-contradictory data will not mess up the computation, because the program will just use the last type of date and time that you altered. Because continuous update mode is based on system (local) time, the time zone needs to be selected with the dropdown at the upper right.

### 5.5.2 MAPVIEW

This widget displays a HEALPix sky map, and lets the user zoom in on regions of the map on the fly.

```
IDL> mapview,file='map_w1_imap_yr1_v1.fits'
```

The widget displays two images on the right: the upper image is an all-sky map (a Mollweide projection in Galactic coordinates), with a circle drawn over the zoomed region. The lower 512 x 512 image displays the zoomed region. The images are manipulated using the mouse cursor and the control panels on the left.

The Control panel functions are (from top to bottom)

1. **Select Map** – Choose whether to display temperature or number of observations
2. **Cursor Info** – Informational panel giving the Galactic coordinates, Healpix pixel number and pixel value of the current cursor position in either the all-sky or zoomed image. (The panel is disabled if the cursor is not over either image.)
3. **Color Scaling** - lets the user choose linear, logarithmic or histogram equalization scaling, and a color lookup table. Note temperature maps may appear entirely black with a linear scaling.
4. **Zoom Region** - User can type in the Galactic coordinates of the region to be zoomed, and then press the draw button. Alternatively, if the zoom region is selected on the all-sky map with the cursor, then the chosen coordinates are displayed. A slider allows the user to choose the area of the zoomed region; the larger the region, the smaller the zoom factor. The actual pixel scale of the zoomed region is displayed at the terminal.
5. **Quit button** - exits the widget

The mouse cursor functions are as follows: move the cursor over either the all-sky or zoomed image to have values displayed in the **Cursor Info** panel. Press any mouse button on the all sky image to define a new center for the zoomed image. Press any mouse button on the zoomed image to move that position to the center of the zoomed image.

## 5.6 WMAP IDL Procedures

A list of the available WMAP IDL procedures.

AIHK_Arch2Mnemonic()	Returns the physical value associated with an analog instrument housekeeping mnemonic, extracting the data from an AEU sweep from a time-ordered
AIHK_GetMnemonic()	Returns a physical value associated with a mnemonic, extracting the data out of a sweep of analog instrument housekeeping telemetry data.
AIHK_Pckt2Mnemonic()	Return the physical value associated with an analog instrument housekeeping mnemonic, extracting the data from a DEU telemetry sweep.
AIHK_Mnem2Serial	Return the serial number of an analog instrument housekeeping (AIHK) PRT.
AIHK_Mnem2Serial_List	Returns an array of structures that associates mnemonics with serial numbers for sensor ids.
AIHK_MnemTime	Returns the time offset into a AIHK packet for the measurement of a given mnemonic.
AIHK_MnemTimeStamp	Returns an array of time stamps for a given mnemonic in an array of analog instrument housekeeping (AIHK) elements.
AIHK_Mnem_Coefs	Returns the conversion coefficients associated with an analog instrument housekeeping mnemonic.
AIHK_Mnemonic	Returns the array index of an analog instrument housekeeping mnemonic.
CircOplot	Overplots a circle of requested radius on a Mollweide or Zenithal equal area projection.
CoorTrans	Transforms input J2000 coordinates into the requested J2000 output coordinate system.
CW_ImageDraw()	Defines a compound widget containing a scrollable draw widget to be used to display images.
CW_ImageFull()	Define a compound widget containing a draw widget to be used to display entire images at reduced resolution.
CW_ImageBoth()	Define a compound widget to contain both a full resolution image in a scrollable draw widget and a compressed image

Date2Jul()	Converts a Gregorian date and time into a reduced Julian date.
Day0fYear	Determines the day-of-year for a date.
DefTSRef()	Return the default WMAP timestamp reference GMT
DIHK_GetMnemonic()	Returns a physical value associated with a mnemonic, extracting the data out of an array of digital instrument housekeeping telemetry data.
DIHK_Pckt2Mnemonic()	Returns the physical value associated with a digital instrument housekeeping mnemonic, extracting the data from a DEU telemetry packet.
DIHK_Mnemonic()	Returns the array index of a digital instrument housekeeping mnemonic.
DIHK_Mnem_Coefs	Returns the conversion coefficients associated with a digital instrument housekeeping (DIHK) mnemonic. Automatically written.
DispGMT()	Converts a time formatted as a WMAP GMT into a more human-readable form.
DispTS()	Converts a WMAP timestamp into a more human readable format.
DOY2Date	Converts a year and day-of-year into a five element date vector. This is the reverse of dayofyear.pro
DOY2Jul	Converts a year and day-of-year into a WMAP Reduced Julian day.
extract_band_index	Extracts the frequency band and array index value from an input channel string. Supporting routine for sci_getmnemonic.
frame_avg()	Computes single or multiple frame averages of science data. Supporting routine for sci_getmnemonic.
frame_rms()	Computes single or multiple frame rms of science data. Supporting routine for sci_getmnemonic.
FITS_Read_Combined_Map	Read a WMAP HEALPIX formatted combined map FITS file
FITS_Read_Map	IDL procedure to read WMAP archive-format temperature sky maps
FITS_Read_TOD	Read timeordered archive data from a binary FITS table.

FITS_Reproj_Healpix	Convert a HealPix image to a flatmap projection in a FITS file with World Coordinate System (WCS) information
FSC_FileSelect()	Widget to select a file name (from David Fanning's Library)
Get_DEU_Int_Temp	Converts DEU internal temperature from counts to degrees Centigrade via a lookup table.
Get_Heal_LUT	Procedure to read and return a user-selectable look-up table.
Get_Heal_RES()	Function to compute the resolution of a heal-pixelized sky map, given the number of map pixels.
Get_PRT_Temp	Converts PRT resistance in ohms to temperature in Kelvin, given the PRT serial number.
Get_Rot_Matrix()	Returns rotation matrix for conversion between the specified input and output coordinate systems.
GMT2Jul()	Converts a WMAP GMT date/time string into a reduced Julian date.
GMT2TS	Converts a WMAP GMT into a WMAP timestamp.
GMT2YMD	Converts the YYYYDDD portion of a WMAP GMT string into a string of format YYYYMM-DDD.
Grid_Overlay	Overplots coordinate grid on a Mollweide or Stereographic projection.
HEALinfo	IDL procedure to return or print information on HEALPix resolutions.
HEALPIX_Nested_Vectors	IDL procedure to read Cartesian [X,Y,Z] direction vectors from binary file for HEALPIX pixel scheme, nested pixel order.
Healpix_to_Image	Convert a 1-d Healpix map into a 2-d byte-scaled image ready for display
Interpolate_Quaternions	Interpolate quaternions extracted from WMAP time-ordered data
Jul2Date	Converts a reduced Julian date into a Gregorian date and time. Unlike a classic reduced Julian date, the full Julian date is recovered by adding 2450000.
Jul2GMT ()	Converts a WMAP GMT date/time string into a Julian date.

<code>Jul2Tel</code>	Converts a <i>WMAP</i> Reduced Julian day into a telemetry structure timestamp.
<code>Jul2TS()</code>	Converts a <i>WMAP</i> Reduced Julian day into a time stamp.
<code>KeyArray()</code>	Breaks a string containing a number of comma-delimited elements into an array of strings.
<code>KeyFile</code>	Reads a file containing keyword/value pairs into an array of structures, each element of which contains a keyword/value pair.
<code>KeyParse</code>	Breaks a string into a keyword/value pair.
<code>LoadCT_012</code>	load a standard IDL color table with the first three colors reserved as white, black and grey
<code>Load_MAP_Params</code>	Reads the contents of the general <i>WMAP</i> program parameters file into an IDL structure.
<code>MAP_Date</code>	Widget to convert the various <i>WMAP</i> time and date formats
<code>MAPView</code>	Interactive widget to display and zoom a Healpix map
<code>Mnem_Type()</code>	Function to return the type of mnemonic associated with an input mnemonic, eg. 'AIHK', 'SCI', etc.
<code>mollweide()</code>	Computes Mollweide angle theta from input latitudes.
<code>mollweide_xy</code>	Converts longitude and latitude coordinates to x,y positions on a Mollweide projection.
<code>Now2Jul()</code>	Returns the current system time as a <i>WMAP</i> Reduced Julian day.
<code>Pckt2Mnemonic()</code>	Returns the physical value associated with a <i>WMAP</i> telemetry mnemonic. This is a wrapper routine that calls the appropriate specific routine depending on mnemonic type.
<code>Planet_Overlay</code>	Plots a planet's position on an existing skymap within a screen window.
<code>projxy2coord</code>	Converts (x,y) positions on a Mollweide or Zenithal Equal Area projection to longitude and latitude.
<code>rotx()</code>	Computes rotation matrix for rotation about x axis.
<code>rotz()</code>	Computes rotation matrix for rotation about z axis.
<code>Q2M</code>	Convert quaternions to rotation matrices

Quat_to_Sky_Coords	Extract a time series of coordinates from an array of input quaternions
Reproj_HEALPIX	Convert a HealPix image to a flatmap projection
Scan_Overlay	Plot the WMAP scan path for a specified time using quaternion data
Sci_GetMnemonic()	Extracts a channel of radiometer data from an array of sciencepackets. Depending on mnemonic prefix, the routine can also return a frame average or rms.
Sci_Mnemonic()	Tests whether or not a given science mnemonic is valid.
ScrTV	Displays an image in a scrollable draw widget. This allows the user to examine a full resolution portion of the image, using the scrollbars to navigate around.
Reproj_HealPix	Convert a HealPix image to a flatmap projection
spread_pckt_tjul()	Propagate science packet times in reduced Julian format to each observation within a packet. Supporting routine for sci_getmnemonic.
Tel2Jul()	Converts a WMAP telemetry structure time stamp into a reduced Julian date.
TextRead	TextRead reads a non-empty record/line from an open text file. Lines are read until a nonzero length string is read.
TimeStamp_AddTime timestamp_diff()	Adds to a WMAP Omega time stamp. Determine the diffence between two time stamps.
TimeTransform tod_format()	Converts one time format into another. Defines the time-ordered data (TOD) structure format
Tod_to_Sky_Coords	Extract a time series of coordinates from an array of time-ordered data records
TS2GMT	Converts a WMAP timestamp into a WMAP GMT.
TS2Jul()	Converts a time stamp into a WMAP Reduced Julian day.
Xcolors	Interactively change color tables (from David Fanning's Library)

**zea\_xy** Converts longitude and latitude coordinates to x,y positions on a Zenithal equal area projection.

# Chapter 6

## Bibliography

- Adamo, R. C. & Matarrese, J. R. 1983, *J Spacecraft*, 20(5), 432
- Astier, P., et al. 2006, *A&A*, 447, 31
- Barnes, C., et al. 2002, *ApJS*, 143, 567
- . 2003, *ApJS*, 148, 51
- Battaglia, N., Bond, J. R., Pfrommer, C., Sievers, J. L., & Sijacki, D. 2010, *ApJ*, 725, 91
- Bennett, C. L., et al. 2003a, *ApJS*, 148, 97
- . 2003b, *ApJS*, 148, 1
- . 2003c, *ApJ*, 583, 1
- . 2011, *ApJS*, 192, 17
- Bennett, C. L., et al. 2012, Submitted to *ApJS*, 0, 0
- Chen, Y. C. 2000, in IEEE MTT-S International Microwave Symposium Digest, Vol. 3, 1917–1920
- Cole, S., et al. 2005, *MNRAS*, 362, 505
- Conley, A., et al. 2011, *ApJS*, 192, 1
- Dickinson, C., et al. 2004, *MNRAS*, 353, 732
- Dunkley, J., et al. 2009, *ApJS*, 180, 306
- Eisenstein, D. J. & Hu, W. 1998, *ApJ*, 496, 605
- Eisenstein, D. J., et al. 2005, *ApJ*, 633, 560

- Finkbeiner, D. P. 2003, ApJS, 146, 407, accepted (astro-ph/0301558)
- Finkbeiner, D. P., Davis, M., & Schlegel, D. J. 1999, ApJ, 524, 867
- Fixsen, D. J. 2009, ApJ, 707, 916
- Frederickson, A. R. 1996a, IEEE Transactions on Nuclear Science, 43, 2454
- . 1996b, IEEE Transactions on Nuclear Science, 43(2), 426
- Freedman, W. L., et al. 2001, ApJ, 553, 47
- Gilmore, D. G. & Bello, M. 1994, Satellite Thermal Control Handbook (El Segundo, CA: The Aerospace Corporation Press)
- Gold, B., et al. 2009, ApJS, 180, 265
- . 2011, ApJS, 192, 15
- Gorski, K. M., Hivon, E., Banday, A. J., Wandelt, B. D., Hansen, F. K., Reinecke, M., & Bartlemann, M. 2005, ApJ, 622, 759
- Hadaway, R. et al. 1995, in Gallium Arsenide Manufacturing Technology, 1316
- Hicken, M., Wood-Vasey, W. M., Blondin, S., Challis, P., Jha, S., Kelly, P. L., Rest, A., & Kirshner, R. P. 2009, ApJ, 700, 1097
- Hill, R. S., et al. 2009, ApJS, 180, 246
- Hinshaw, G., et al. 2003a, ApJS, 148, 63
- . 2003b, ApJS, 148, 135
- . 2007, ApJS, 170, 288
- . 2009, ApJS, 180, 225
- . 2012, Submitted to ApJS, 0, 0
- Hoekstra, H., et al. 2006, ApJ, 647, 116
- Hu, W. & Sugiyama, N. 1996, ApJ, 471, 542
- Jackson, C. 2002, Microwave Anisotropy Probe (MAP) Observatory Launch & In-Orbit Checkout (L&IOC) Phase, Volume I: Summary Report, Tech. rep., NASA/GSFC
- Jarosik, N., et al. 2003a, ApJS, 145, 413
- . 2003b, ApJS, 148, 29
- . 2007, ApJS, 170, 263

- . 2011, ApJS, 192, 14
- Jimenez, R. D. 1988, Natural Environment Charged Particle Heating of Spacecraft Cryogenics Components, Tech. Rep. TOR-088(3062)-3, The Aerospace Corporation
- Kessler, R., et al. 2009, ApJS, 185, 32
- Keys, D., and team. 2010, Wilkinson Microwave Anisotropy Probe (WMAP) Battery Operations Problem Resolution Team (PRT), Technical Assessment Report RP-10-00608, NASA/GSFC
- . 2011, Nickel-Hydrogen ( $\text{NiH}_2$ ) Common Pressure Vessel (CPV) Cell Capacity Loss and Voltage Collapse, Technical Bulletin 11-01, NASA/GSFC
- Kogut, A., et al. 2003, ApJS, 148, 161
- . 2007, ApJ, 665, 355
- Komatsu, E., et al. 2003, ApJS, 148, 119
- . 2009, ApJS, 180, 330
- . 2011, ApJS, 192, 18
- Kuo, C. L., et al. 2004, ApJ, 600, 32
- Larson, D., et al. 2011, ApJS, 192, 16
- Leung, P. & Plamp, G. 1982, IEEE Transactions on Nuclear Science, 29(6), 1610
- Leung, P., Whittlesey, A. C., Garrett, H. B., & Robinson, P. A. 1986, Journal of Spacecraft and Rockets, 23, 323
- Lewis, A. & Bridle, S. 2002, Phys. Rev. D, 66, 103511
- Lilie, P. A. 1989, X-Band HEMT Burnout Test, Tech. rep., NRAO/VLA
- Manzo, M. A., and team. 2010, Effects of a Simulated Electrolyte Bridge in a Common Pressure Vessel (CPV) Nickel Hydrogen Cell, Tech. Rep. ATR-2010 (5175)-1, Aerospace
- Mizera, P. F. 1983, Journal of Spacecraft and Rockets, 20, 438
- Montroy, T. E., et al. 2006, ApJ, 647, 813
- Nguyen, L. D. et al. 1992, IEEE Transactions on Electron Devices, 39, 2007
- Nolta, M. R., et al. 2009, ApJS, 180, 296
- O'Neill, I. 2010, Mission Complete! WMAP Fires Its Thrusters for the Last Time, <http://news.discovery.com/space/mission-complete-wmap-fires-its-thrusters-for-the-last-time.html>

- Page, L., et al. 2003a, ApJS, 148, 39
- . 2003b, ApJS, 148, 233
- . 2003c, ApJ, 585, 566
- . 2007, ApJS, 170, 335
- Peiris, H. V., et al. 2003, ApJS, 148, 213
- Percival, W. J., et al. 2010, MNRAS, 401, 2148
- Pospieszalski, M. W. 1989, IEEE Trans. Microwave Theory Tech., MTT-37, 1340
- Pospieszalski, M. W., Lakatos, W. J., Nguyen, L. D., Le, M., Lui, M., & Lui, T. 1997, in IEEE MTT-S International Microwave Symposium Digest, 1285–1288
- Pospieszalski, M. W., Lakatos, W. J., Nguyen, L. D., Lui, M., Lui, T., Le, M., Thompson, M. A., & Delaney, M. J. 1995, in IEEE MTT-S International Microwave Symposium Digest, 1121–1125
- Pospieszalski, M. W., Wollack, E. J., Bailey, N., Thacker, D., Webber, J., Nguyen, L. D., Le, M., & Lui, M. 2000, in IEEE MTT-S International Microwave Symposium Digest, ed. V. 1, Boston, MA, 25 – 28
- Pospieszalski, M. W. et al. 1993, in IEEE MTT-S International Microwave Symposium Digest, 515–518
- Pospieszalski, M. W. et al. 1994, IEEE MTT-S Digest, 1345
- Readhead, A. C. S., et al. 2004, ApJ, 609, 498
- Reichardt, C. L., et al. 2009, ApJ, 701, 1958
- Reid, B. A., et al. 2010, MNRAS, 404, 60
- Riess, A. G., et al. 2004, ApJ, 607, 665
- . 2009, ApJ, 699, 539
- . 2011, ApJ, 730, 119
- Seljak, U., Slosar, A., & McDonald, P. 2006, JCAP, 0610, 014
- Semboloni, E., et al. 2005, ArXiv Astrophysics e-prints
- Silsbee, K., Ali-Haïmoud, Y., & Hirata, C. M. 2011, MNRAS, 411, 2750
- Spergel, D. N., et al. 2003, ApJS, 148, 175

- 
- . 2007, ApJS, 170, 377
- Starin, S. R., O'Donnell, Jr., J. R., Ward, D. K., Wollack, E. J., Bay, P. M., & Fink, D. R. 2002, in AIAA Symposium, Monterey, CA
- Strong, A. W., Orlando, E., & Jaffe, T. R. 2011, A&A, 534, A54
- Sullivan, M., et al. 2011, ApJ, 737, 102
- Suyu, S. H., Marshall, P. J., Auger, M. W., Hilbert, S., Blandford, R. D., Koopmans, L. V. E., Fassnacht, C. D., & Treu, T. 2010, ApJ, 711, 201
- Tegmark, M., et al. 2004, ApJ, 606, 702
- Triolo, J. J., Heaney, J. B., & Hass, G. 1977, in Optics in Adverse Environments, Vol. 121, SPIE, 46
- Vampola, A. L., Jimenez, R. D., & Cox, J. E. 1989, Journal of Spacecraft and Rockets, 26(6), 474
- Verde, L., et al. 2003, ApJS, 148, 195
- Weiland, J. L., et al. 2011, ApJS, 192, 19
- Wollack, E. J. 1995, Rev. Sci. Instrum., 66, 4305
- Wollack, E. J. & Pospieszalski, M. W. 1998, IEEE MTT-S International Microwave Symposium Digest, 669
- Wright, E. L., et al. 2009, ApJS, 180, 283

# Appendix A

## Gain Model Parameters

The gain model is described by Eq. 2 of Jarosik et al. (2007) with modifications discussed in Bennett et al. (2012) and Hinshaw et al. (2009). Combining these, the form of the nine-year gain model is

$$G = \alpha \frac{\bar{V} - V_o - \beta(T_{\text{RXB}} - 290)}{T_{\text{FPA}} - T_o} + (m\Delta t + c) \quad (\text{A.1})$$

The gain model is evaluated for each detector channel, for a total of 40 channels.  $T_{\text{RXB}}$  is the temperature (in K) of the RXB thermistor closest to the detector. Similarly,  $T_{\text{FPA}}$  is the FPA temperature as measured from the nearest thermistor.  $\bar{V}$  are the radio frequency bias powers on the detectors.  $\Delta t$  is the mission elapsed time in days, starting from day 222 of 2001, 00:00 UT.

The fitted parameters are  $T_o$ ,  $V_o$ ,  $\beta$ ,  $\alpha$ ,  $m$ , and  $c$ .  $T_o$  characterizes the variation of the noise temperature on the input amplifiers with physical temperature.  $V_o$  characterizes compression (nonlinear response) of the amplifiers and detectors.  $\alpha$  normalizes the overall gain.  $\beta$  accounts for the variation of the compression of the amplifiers and square law diode detectors with their physical temperature. In the nine year analysis, the gain model was augmented by adding a time-dependent linear trend term,  $m\Delta t + c$  to account for the aging of the radiometers.

The values of the gain model parameters are given below.

DA	$T_o(13)$	$T_o(14)$	$T_o(23)$	$T_o(24)$
K1	$5.3235 \times 10^{+01}$	$5.3235 \times 10^{+01}$	$1.0000 \times 10^{+04}$	$1.0000 \times 10^{+04}$
Ka1	$5.2827 \times 10^{+02}$	$5.2827 \times 10^{+02}$	$5.4573 \times 10^{+01}$	$5.4573 \times 10^{+01}$
Q1	$2.3070 \times 10^{+01}$	$2.3070 \times 10^{+01}$	$4.2921 \times 10^{+01}$	$4.2921 \times 10^{+01}$
Q2	$3.6824 \times 10^{+01}$	$3.6824 \times 10^{+01}$	$5.0227 \times 10^{+01}$	$5.0227 \times 10^{+01}$
V1	$4.4834 \times 10^{+01}$	$4.4834 \times 10^{+01}$	$5.2905 \times 10^{+01}$	$5.2905 \times 10^{+01}$
V2	$5.5982 \times 10^{+01}$	$5.5982 \times 10^{+01}$	$5.4309 \times 10^{+01}$	$5.4309 \times 10^{+01}$
W1	$-6.8283 \times 10^{+01}$	$-6.8283 \times 10^{+01}$	$-9.4980 \times 10^{+01}$	$-9.4980 \times 10^{+01}$
W2	$-1.0486 \times 10^{+02}$	$-1.0486 \times 10^{+02}$	$-1.8059 \times 10^{+02}$	$-1.8059 \times 10^{+02}$
W3	$8.3914 \times 10^{+01}$	$8.3914 \times 10^{+01}$	$-2.7692 \times 10^{+02}$	$-2.7692 \times 10^{+02}$
W4	$8.8408 \times 10^{+01}$	$8.8408 \times 10^{+01}$	$4.9238 \times 10^{+01}$	$4.9238 \times 10^{+01}$

DA	$V_o(13)$	$V_o(14)$	$V_o(23)$	$V_o(24)$
K1	$-5.5125 \times 10^{-01}$	$-5.4203 \times 10^{-01}$	$3.7781 \times 10^{-02}$	$2.1017 \times 10^{-02}$
Ka1	$5.9338 \times 10^{-02}$	$-6.9249 \times 10^{-01}$	$-7.7285 \times 10^{-01}$	$-6.7187 \times 10^{-01}$
Q1	$-1.4283 \times 10^{+00}$	$-1.2100 \times 10^{+00}$	$-4.9191 \times 10^{-01}$	$-5.5483 \times 10^{-01}$
Q2	$-6.9106 \times 10^{-01}$	$-8.1238 \times 10^{-01}$	$-9.0155 \times 10^{-01}$	$-8.0719 \times 10^{-01}$
V1	$-1.0074 \times 10^{+00}$	$-9.1457 \times 10^{-01}$	$-9.4576 \times 10^{-01}$	$-8.4200 \times 10^{-01}$
V2	$-7.2614 \times 10^{-01}$	$-7.4866 \times 10^{-01}$	$-5.4468 \times 10^{-01}$	$-5.5098 \times 10^{-01}$
W1	$2.1695 \times 10^{-01}$	$2.1132 \times 10^{-01}$	$5.8038 \times 10^{-02}$	$2.1856 \times 10^{-01}$
W2	$7.3005 \times 10^{-02}$	$7.4144 \times 10^{-02}$	$-2.8921 \times 10^{-01}$	$4.5801 \times 10^{+00}$
W3	$-9.8113 \times 10^{-01}$	$-1.0860 \times 10^{+00}$	$-4.8598 \times 10^{-01}$	$4.2550 \times 10^{+00}$
W4	$-9.6705 \times 10^{-01}$	$-1.0058 \times 10^{+00}$	$3.1577 \times 10^{+00}$	$2.6937 \times 10^{+00}$

Table A.1: Nine-Year Gain Model Parameters:  $T_o$  and  $V_o$ .

DA	$\beta(13)$	$\beta(14)$	$\beta(23)$	$\beta(24)$
K1	$-7.2200 \times 10^{-04}$	$-8.1810 \times 10^{-04}$	$-3.3609 \times 10^{-03}$	$-3.8992 \times 10^{-03}$
Ka1	$-5.7981 \times 10^{-03}$	$-5.3344 \times 10^{-03}$	$-4.1879 \times 10^{-03}$	$-3.8811 \times 10^{-03}$
Q1	$-1.0056 \times 10^{-02}$	$-8.6515 \times 10^{-03}$	$-4.1582 \times 10^{-03}$	$-4.8031 \times 10^{-03}$
Q2	$-1.6922 \times 10^{-03}$	$-3.2459 \times 10^{-03}$	$-4.2172 \times 10^{-03}$	$-3.5610 \times 10^{-03}$
V1	$-2.3861 \times 10^{-03}$	$-1.2643 \times 10^{-03}$	$-5.5404 \times 10^{-03}$	$-3.3018 \times 10^{-03}$
V2	$-3.1608 \times 10^{-03}$	$-3.6054 \times 10^{-03}$	$-2.7406 \times 10^{-03}$	$-2.7447 \times 10^{-03}$
W1	$-6.0973 \times 10^{-03}$	$-6.7467 \times 10^{-03}$	$-5.1466 \times 10^{-03}$	$-5.1031 \times 10^{-03}$
W2	$-6.5581 \times 10^{-03}$	$-6.5886 \times 10^{-03}$	$-5.2498 \times 10^{-03}$	$-1.9643 \times 10^{-03}$
W3	$-5.5403 \times 10^{-03}$	$-5.5063 \times 10^{-03}$	$-6.8111 \times 10^{-03}$	$-5.1315 \times 10^{-03}$
W4	$-8.1677 \times 10^{-03}$	$-9.2725 \times 10^{-03}$	$-1.9976 \times 10^{-02}$	$-1.9998 \times 10^{-02}$

DA	$\alpha(13)$	$\alpha(14)$	$\alpha(23)$	$\alpha(24)$
K1	$4.4619 \times 10^{+01}$	$-4.4559 \times 10^{+01}$	$1.1323 \times 10^{+04}$	$-1.1571 \times 10^{+04}$
Ka1	$4.8441 \times 10^{+02}$	$-5.0538 \times 10^{+02}$	$3.7418 \times 10^{+01}$	$-3.8655 \times 10^{+01}$
Q1	$-4.0577 \times 10^{+01}$	$4.2335 \times 10^{+01}$	$-3.6833 \times 10^{+01}$	$3.6559 \times 10^{+01}$
Q2	$4.5121 \times 10^{+01}$	$-4.5240 \times 10^{+01}$	$3.0466 \times 10^{+01}$	$-3.0895 \times 10^{+01}$
V1	$-2.1649 \times 10^{+01}$	$2.2453 \times 10^{+01}$	$1.5654 \times 10^{+01}$	$-1.5397 \times 10^{+01}$
V2	$1.6423 \times 10^{+01}$	$-1.6519 \times 10^{+01}$	$-1.6287 \times 10^{+01}$	$1.6504 \times 10^{+01}$
W1	$-3.7419 \times 10^{+01}$	$3.8530 \times 10^{+01}$	$-4.1983 \times 10^{+01}$	$3.5166 \times 10^{+01}$
W2	$4.7740 \times 10^{+01}$	$-4.8479 \times 10^{+01}$	$-9.4100 \times 10^{+01}$	$6.1097 \times 10^{+01}$
W3	$1.4261 \times 10^{+00}$	$-1.6321 \times 10^{+00}$	$3.4478 \times 10^{+01}$	$-6.3356 \times 10^{+01}$
W4	$-3.5820 \times 10^{-01}$	$3.6791 \times 10^{-01}$	$-2.7352 \times 10^{+00}$	$2.9615 \times 10^{+00}$

Table A.2: Nine-Year Gain Model Parameters:  $\alpha$  and  $\beta$

---

DA	$m(13)$	$m(14)$	$m(23)$	$m(24)$
K1	$-2.7274 \times 10^{-07}$	$-6.2135 \times 10^{-07}$	$0.0000 \times 10^{+00}$	$0.0000 \times 10^{+00}$
Ka1	$0.0000 \times 10^{+00}$	$1.5675 \times 10^{-06}$	$1.7431 \times 10^{-06}$	$-1.3445 \times 10^{-06}$
Q1	$2.0934 \times 10^{-06}$	$-1.8049 \times 10^{-06}$	$-9.2557 \times 10^{-07}$	$7.1961 \times 10^{-07}$
Q2	$-3.3999 \times 10^{-07}$	$-1.0739 \times 10^{-07}$	$5.7370 \times 10^{-07}$	$-4.4217 \times 10^{-07}$
V1	$-2.1019 \times 10^{-07}$	$5.4817 \times 10^{-07}$	$-6.2039 \times 10^{-08}$	$9.9114 \times 10^{-08}$
V2	$-2.7905 \times 10^{-07}$	$2.5047 \times 10^{-07}$	$-3.6946 \times 10^{-07}$	$5.0953 \times 10^{-08}$
W1	$0.0000 \times 10^{+00}$	$0.0000 \times 10^{+00}$	$0.0000 \times 10^{+00}$	$0.0000 \times 10^{+00}$
W2	$0.0000 \times 10^{+00}$	$0.0000 \times 10^{+00}$	$0.0000 \times 10^{+00}$	$-8.0626 \times 10^{-07}$
W3	$-2.7841 \times 10^{-07}$	$-2.7470 \times 10^{-07}$	$4.3525 \times 10^{-07}$	$-6.9075 \times 10^{-07}$
W4	$-4.8415 \times 10^{-08}$	$7.2104 \times 10^{-08}$	$0.0000 \times 10^{+00}$	$0.0000 \times 10^{+00}$

DA	$c(13)$	$c(14)$	$c(23)$	$c(24)$
K1	$-6.7556 \times 10^{-01}$	$6.6748 \times 10^{-01}$	$0.0000 \times 10^{+00}$	$0.0000 \times 10^{+00}$
Ka1	$0.0000 \times 10^{+00}$	$-8.3667 \times 10^{-01}$	$-8.5769 \times 10^{-01}$	$7.5598 \times 10^{-01}$
Q1	$1.0102 \times 10^{+00}$	$-8.9222 \times 10^{-01}$	$3.3920 \times 10^{-01}$	$-3.8851 \times 10^{-01}$
Q2	$-6.0343 \times 10^{-01}$	$7.1256 \times 10^{-01}$	$-6.7279 \times 10^{-01}$	$6.0873 \times 10^{-01}$
V1	$4.8502 \times 10^{-01}$	$-4.4017 \times 10^{-01}$	$-4.3453 \times 10^{-01}$	$3.8182 \times 10^{-01}$
V2	$-3.6244 \times 10^{-01}$	$3.7857 \times 10^{-01}$	$2.5173 \times 10^{-01}$	$-2.6329 \times 10^{-01}$
W1	$0.0000 \times 10^{+00}$	$0.0000 \times 10^{+00}$	$0.0000 \times 10^{+00}$	$0.0000 \times 10^{+00}$
W2	$0.0000 \times 10^{+00}$	$0.0000 \times 10^{+00}$	$0.0000 \times 10^{+00}$	$9.9539 \times 10^{-01}$
W3	$-2.4797 \times 10^{-01}$	$2.7258 \times 10^{-01}$	$-1.9858 \times 10^{-01}$	$-6.6823 \times 10^{-01}$
W4	$2.2624 \times 10^{-01}$	$-2.3324 \times 10^{-01}$	$0.0000 \times 10^{+00}$	$0.0000 \times 10^{+00}$

Table A.3: Nine-Year Gain Model Parameters:  $m$  and  $c$

## Appendix B

# Selected WMAP Log Entries

This appendix consists of selected entries from the events log that the members of the Science Working Group have kept throughout the mission. This particular subset of the log lists all major events from the beginning of the Pre-ship Functional Test (April 6, 2001) to the end of nine years of flight operations.

---

#### Selected WMAP Satellite Pre-Flight Preparations:

---

...  
GMT 20010961125 GSFC: Pre-Ship Functional Test (GSFC)  
GMT 20011161100 SAEF-2: Post-Ship Functional and CPT (KSC)  
GMT 20011621058 SAEF-2: Instrument Contingency Tests (KSC)  
GMT 20011721430 SLC17B: Pre-Fairing Pad Functional Test (KSC)  
GMT 20011780851 SLC17B: Post-fairing Pad Functional Test (KSC)  
GMT 20011791200 SLC17B: Load Vehicle Oxidizer  
GMT 20011811013 SLC17B: Instrument Pre-Flight Burn-in  
GMT 20011811803 SLC17B: Load Vehicle LOX  
GMT 20011811925 SLC17B: Poll to go to Launch Decision Authority (KSC/GSFC)  
GMT 20011811929 SLC17B: GSFC poll to Proceed with Terminal Count (GSFC)  
GMT 20011811939 SLC17B: Proceed to internal power (KSC/GSFC)

---

#### Selected WMAP Satellite Launch and In-Orbit Checkout (IOC):

---

GMT 20011811946 WMAP Launch Time: 2001181194646.183  
GMT 20011811951 Main engine cutoff/fairing separation...  
GMT 20011812000 SECO-I cutoff -- trajectory is on course...  
GMT 20011812100 WMAP Transmitter detected by TDRS...  
GMT 20011812103 Solar arrays deployed...  
GMT 20011812138 Star trackers powered...  
GMT 20011812143 WMAP Instrument powered...  
GMT 20011821515 Gyro calibration slews...  
GMT 20011830744 WMAP Thruster Tests...  
GMT 20011831918 Enter observing mode for the first time:  
CMB Dipole/galaxy visible in science data

---

Begin mapping sidelobes with Moon as source  
 GMT 20011842201 Top Radiator PRT (DTAMXTOPRADT) fails open.  
 GMT 20011890153 P1 - First Perigee Maneuver  
 GMT 20011890244 End mapping sidelobes with Moon as source  
 GMT 20011980143 P2 - Second Perigee Maneuver  
 GMT 20012021758 A3 - Second Apogee Maneuver (third apogee)  
 GMT 20012070832 PF - Final Perigee Maneuver  
 GMT 20012080330 PF'- Final Perigee Correction  
 GMT 20012080200 PF"-- Final Perigee Correction  
 GMT 20012111639 Lunar Swing-by  
 GMT 20012181551 Mid-Course Correction #1  
 GMT 20012181819 W411 Bias Adjustment.  
 GMT 20012191300 Turn off the omni antenna and switch to the  
medium gain antenna. FPA is observed to accelerate  
its cooling. Leave transmitter power to allow ranging.  
 GMT 20012191807 W411 Returned to Nominal Bias Setting.  
 GMT 20012210306 W12 Science Output Jump: Sudden jump of W12 science  
output, both channels W123 and W124 jumped of about  
35-40 counts in opposite directions. When calibrated  
the jump is about 100mK. The jump is essentially  
instantaneous, it happens across just one sample and  
the dipole is visible before and after the jump. No  
changes in drain currents or RF bias are present at the  
time of the output jump. No change noted in other science  
channels. Observed radiometric signature is consistent  
with relief of thermally induced stress in radiometer and  
is anticipated in this phase of mission operations. This  
and any other subsequent suspect data to be flagged in  
time stream data mask.

---

-----  
START: WMAP YEAR-ONE SCIENCE DATA  
-----

---

-----  
Transmitter Make-Up Heater Tests

---

GMT 20012212000 Turn off transmitter: Today we turn off the transmitter  
for the first time in flight and will turn on the  
transponder make-up heater when the transmitter is off.  
 GMT 20012410810 After flying with the transmitter make-up heater for  
several days, we conclude that the daily thermal cycling  
seen in the instrument boxes is probably worse than the  
potential "RFI", and wear on tear on the transmitter. The  
transmitter will now remain on for the duration of the  
mission, effective with this pass. Continue the cruise to  
L2 in this configuration.

---

-----  
Mid-Course Correction #2

---

GMT 20012571620 Start Mid-course correction #2: This is a very small

maneuver of about 4.3 cm/sec Delta V. Thrusters #1&2 will be fired for about 6.44sec.

The burn will occur at 16:37 GMT.

Exit observing mode. Command to spin down at the desired precession angle. Sun angle remains at 22.5 degrees for now. The S/C will shortly be commanded to the desired spin angle.

GMT 20012571625      Command S/C to inertial - this sets up the command to the correct spin angle and will result in a short excursion from 22.5 degrees during the slew.  
 GMT 20012571627      Actual slew to the correct spin angle.  
 GMT 20012571635      Slew to 19 degrees in preparation for the burn.  
 GMT 20012571637      Burn starts and stops. 6.4 seconds.  
 GMT 20012571639      Return to inertial hold.  
 GMT 20012571640      Disable thrusters. Enable ACS rate checks.  
 GMT 20012571641      Slewing back to 22.5 degrees.  
 GMT 20012571644      Disable thrusters. Restart TSMs.  
 GMT 20012571701      Send command to resume observing mode.

---

End Mid-Course Correction #2

---

#### Solar Proton Storm

---

GMT 20012671200      A severe solar storm has occurred with >10 MeV proton fluxes reaching  $10^5$  times normal levels. We are observing a heating of the cold stage of several tens of millikelvins with a heating slope that appears to be well correlated with the proton flux. Since this thermal perturbation is larger than the mid-course correction #2 we may want to cut a period of data about this time. The storm itself will likely last for a few days.

---

#### ASTB Thermal Change

---

GMT 200128900      Star tracker crosses internal thermal threshold of CCD thermo-electric cooler. ASTB baseplate cools 4C from 30C to 26C. Change in thermal distribution causes RXB to cool by ~10mK.

---

#### Solar Proton Storm

---

GMT 20013100258      The second severe solar storm since WMAP's launch has occurred with >10 MeV proton fluxes reaching  $>10^5$  times normal levels. This is more severe than the previous storm on 2001267. This storm caused an apparent single event upset (possibly on the power-up reset circuit in the MAC) which caused a power-up cold restart of the Mongoose. All recorded data was lost from the start of the previous

---

pass to the time of the reset.  
Telemetry Lost: 20013100258 - 20013101635.

GMT 20013101430 The entry into safehold was noticed on the subsequent pass which started at 20011430. After spending some time diagnosing the problem, we are preparing to exit safehold and reenter observing mode "20013101830. The telemetry from the time of the reset until the clock was re-jammed at 20013101542 has a time stamp in 1994.

GMT 20013101742 Command out of safehold to sun-acquisition mode.

GMT 20013101823 Command back to inertial mode.

GMT 20013101825 Slew to 22.5 degrees off the Sun line.

GMT 20013101834 Command to observing mode.

GMT 20013101838 Achieved observing mode.

GMT 20013101903 Adjust clock 1Hz deviation.

GMT 20013101913 Complete clock adjustment.

GMT 20013101943 Return to normal operations.

---

#### Solar Proton Storm

---

GMT 200132800 A severe solar storm has occurred with >10 MeV proton fluxes reaching  $10^5$  times normal levels. We are observing a heating of the cold stage of several tens of millikelvins with a heating slope that appears to be well correlated with the proton flux. Since this thermal perturbation is larger than the mid-course correction #2 we may want to cut a period of data about this time. The storm itself will likely last for a few days.

---

#### Station-Keeping Maneuver #1 (SK1)

---

GMT 20020161620 This is a small maneuver of 42.8 cm/sec delta V that will last for 72 sec.  
Thrusters #3&4 will be fired at 16:50 GMT.  
Turn on catbed heaters in preparation for the burn.

GMT 20020161624 Brief drop-out of telemetry.

GMT 20020161633 Exit observing mode. Command to spin down at the desired precession angle. Sun angle remains at 22.5 degrees for now. The S/C will shortly be commanded to the desired spin angle.

GMT 20020161638 Command to go inertial - this sets up the command to the correct spin angle and will result in a small excursion from 22.5 degrees during the slew.

GMT 20020161639 Actual slew to the correct spin angle.

GMT 20020161648 Slew to 19 degrees in preparation for the burn.

GMT 2002016165055 Burn starts, lasts 72 seconds, as planned.

GMT 20020161652 Return to inertial hold.

GMT 20020161653 Disable thrusters. Enable ACS rate checks.

GMT 20020161656 Return to observing mode 5 minutes after burn.

---

End Station-Keeping Maneuver #1 (SK1)

---



---



---

Reaction Wheel 3 Temperature Increase

---

GMT 2002054      Reaction Wheel 3 bearing temperature increased by about 1.2K and the corresponding wheel's flange by about ~1K. ACS attributes this behavior to movement of the bearings' lubricant. Previous flight experience with this design suggests that this behavior is anticipated.

---

Battery Anomaly

---

GMT 2002054      Around this day the battery differential voltage started to deviate from its nominal value. Evidence suggests that effect is due to a partially shorted cell.

GMT 2002058      The S/C responds to the continuous raise of the differential voltage by resetting the battery VT curve to VT0 per design.

---

Reaction Wheel 1 Temperature Increase

---

GMT 2002075      At ~20020750445 the drag torque level and the temperatures of both bearing and flange of RWA stepped up by about 0.002 Nm 1 C respectively. Have seen similar changes in the past and they are not considered an anomaly.

---

Station-Keeping Maneuver #2 (SK2)

---

GMT 20021281533    This is a small maneuver of 34.8 cm/sec delta V that will last for 49 sec.  
Thrusters #1&2 will be fired at 16:03 GMT.  
Turn on catbed heaters in preparation for the burn.

GMT 20021281546    Exit observing mode. Command to spin down at the desired precession angle. Sun angle remains at 22.5 degrees for now. The S/C will shortly be commanded to the desired spin angle.

GMT 20021281551    Command to go inertial -- this sets up the command to the correct spin angle and will result in a small excursion from 22.5 degrees during the slew.

GMT 20021281552    Actual slew to the correct spin angle.

GMT 20021281601    Slew to 19 degrees in preparation for the burn.

GMT 2002128160327   Burn starts, lasts 49 seconds, as planned.

GMT 20021281604    Return to inertial hold.

GMT 20021281609    Disable thrusters. Enable ACS rate checks.

GMT 20021281610    Slew back to 22.5 degrees in preparation for observing mode.

GMT 20021281612    Return to observing mode 5 minutes after burn.

---

---

End Station-Keeping Maneuver #2 (SK2)

---

GMT 20021582120 Shift in nominal AEU/DEU temperature of ~28mK observed in PRTs sensors. Source localized near DVA223\_4AMPT PRT sensor from spatial and temporal evolution of observed event. Estimate change in card power dissipation of~+0.1% Correlated response in science data is not detected.

---

Station-Keeping Maneuver #3 (SK3)

---

GMT 20022111608 This is a small maneuver of 45.98 cm/sec delta V that will last for 66 sec.  
Thrusters #1&2 will be fired at 16:38:45 GMT.  
Turn on catbed heaters in preparation for the burn.

GMT 20022111621 Exit observing mode. Command to spin down at the desired precession angle. Sun angle remains at 22.5 degrees for now. The S/C will shortly be commanded to the desired spin angle.

GMT 20022111626 Command to go inertial - this sets up the command to the correct spin angle and will result in a small excursion from 22.5 degrees during the slew.

GMT 20022111627 Actual slew to the correct spin angle.

GMT 20022111635 Disable RTS 181, system rate checks.

GMT 20022111636 Slew to 19 degrees in preparation for the burn.

GMT 2002211163845 Burn starts, lasts 66 seconds, as planned.

GMT 20022111640 Return to inertial hold.

GMT 20022111642 Disable thrusters. Enable ACS rate checks.

GMT 20022111642 Disable catbed heaters.

GMT 200221116425 Slew back to 22.5 degrees in preparation for observing mode.

GMT 20022111646 Return to observing mode 4 minutes after burn, 26 minutes after leaving observing mode.

---

End Station-Keeping Maneuver #3 (SK3)

---

GMT 2002222 End of year-one data

---

END: WMAP YEAR-ONE DATA

---



---

Recorder Memory Mask Update

---

During this pass, modification to the solid state recorder memory map to mask out 3 bits that have repeatedly shown single bit errors will be uploaded.

GMT 20022951830 Perform a retransmit of the VR3 DS1 data set to minimize the amount of lost data.

---

GMT 20022951843    Modify data storage quota table #28.  
 GMT 20022951854    Commit Data Storage Segment Table #27 to mask the offending bits in the recorder. This clears all existing recorder memory.  
 GMT 20022951900    Modify Memory Scrub Segment Table #19. This will cause the memory scrub routine to skip the offending bits of recorder memory.  
 GMT 20022951910    Estimate that 16-18 VCDUs of data were lost during operation (~9 seconds).  
 GMT 20022951937    The first cycle of the memory scrub skipped over the first masked bit address, as planned.

---

End Recorder Memory Mask Update

---



---

Station-Keeping Maneuver #4 (SK4)

---

This is a small maneuver of 56.4 cm/sec delta V that will last for 95.5 sec. Thrusters #3&4 will be fired at 19:20:43 GMT. Thruster scale factor (TSF) 0.951.

GMT 20023091850    Turn on catbed heaters in preparation for the burn.  
 GMT 20023091904    Exit observing mode. Command to spin down at the desired precession angle. Sun angle remains at 22.5 degrees for now. The s/c will shortly be commanded to the desired spin angle.  
 GMT 20023091908    Command to go inertial - this sets up the command to the correct spin angle and will result in a small excursion from 22.5 degrees during the slew.  
 GMT 20023091909    Actual slew to the correct spin angle.  
 GMT 20023091916    Disable RTS 181, system rate checks, enable thrusters.  
 GMT 20023091918    Slew to 19 degrees in preparation for the burn.  
 GMT 2002309192043    Burn starts, lasts 95.5 seconds, as planned.  
 GMT 20023091922    Back to inertial hold.  
 GMT 20023091923    Disable thrusters. Enabling ACS system rate checks.  
 GMT 20023091924    Disable catbed heaters.  
 GMT 20023091925    Slew back to 22.5 degrees in preparation for observing mode.  
 GMT 20023091926    Return to observing mode 6 minutes after burn, 22 minutes after leaving observing mode.  
 GMT 20023091936    Turn off iso-valve driver power.

---

End Station-Keeping Maneuver #4 (SK4)

---



---

Update Solar Ephemeris

---

GMT 20023092005    The solar ephemeris table used for on board navigation is being updated with a new polynomial fit. The new ephemeris will cause a ~30 arcsec jump in the solar position. Such an update is estimated to be required approximately annually.

---

End Update Solar Ephemeris

---

---

Station Keeping Maneuver #5 (SK5)

---

This is a small maneuver of 32.07 cm/sec delta V that will last for 50 sec. Thrusters #1&2 will be fired at 13:50:13 GMT. Thruster scale factor (TSF) 0.983.

GMT 20030711320 Turn on catbed heaters in preparation for the burn.  
GMT 20030711332 Command to spin down. Spin down completed ~13:39.  
GMT 20030711341 Disable RTS 181, system rate checks, enable thrusters.  
GMT 20030711350 Thrusters firing. Burn duration nominal.  
GMT 20030711352 Disable all thrusters. Turn catbed heaters off 13:52:45.  
GMT 20030711353 Slew to 22.5 deg.  
GMT 20030711355 Go to observing mode 13:54:48.  
Primary temperature max increase by ~8 mK at ~13:49:30 as result of maneuver.

---

End Station Keeping Maneuver #5 (SK5)

---

GMT 2003222 End of year-two data

---

END: WMAP YEAR-TWO DATA

---

---

Safehold Event

---

GMT 2003223 The Mongoose V apparently experienced a Power-On type of restart similar to the event that occurred on November 6, 2001. The routine scheduled pass on Day 223 had a BOT of 1615 UT with station D43. At BOT the station had lock on a carrier signal but there was no data lock. The S/C's attitude control was verified as being in the safehold mode and the apparent Mongoose V Power-On restart identified.

The elapsed time from the routine scheduled pass during which the anomaly was identified until Observing mode was re-established was 7 hours 23 minutes 50 seconds. The VR1 (housekeeping) data loss covers the time from the last successful playback until the time the restart finished and was 20 hours 52 minutes 51 seconds. The VR3 (science) data loss covers the time from the last successful playback until Observing mode was re-established and was 31 hours 5 minutes 36 seconds.

---

GMT 20032231942 Ready to try to go back to B-side.  
 GMT 20032231950 Reconfigured DSN to get back to B-side, communicating with  
     MGA at 666 Kbps 1/4 rate, carrier locked at DSN Canberra.  
 GMT 20032235520 We are receiving data.  
 GMT 20032232256 Completed uploading changes (patches, procs, limits, etc.),  
     leaving safehold.  
 GMT 20032232259 Going to Sun acquisition.  
 GMT 2003223232700 Going inertial  
 GMT 2003223232833 Slewing to 22.5 degrees  
 GMT 2003223233350 Inertially holding at 22.5 degs  
 GMT 2003223233455 Going to Observing mode  
 GMT 2003223233515 Spinning up  
 GMT 20032232348 Switching to mission filter table  
 GMT 20032232340 Dumping data

---

End of Safehold Event

---



---

Solar Flare Supplemental Passage

---

GMT 200330202 This passage was scheduled because we undergoing a  
     severe solar storm. High energy ( $>100$  MeV) proton flux has  
     reached  $2e10 \text{ Pcm}^{-2}\text{s}^{-1}\text{sr}^{-1}$  comparable to the flux that  
     put the Spacecraft in safehold on 20013100258

Spacecraft is not in safehold but there are 19 bus errors  
     on ASTA and the Tracker switched from AST A to B at  
     00:03:03 GMT. Dumped the recorders.

GMT 2003302030357 Reset the AST to the A side and clear errors  
     Back on AST A tracker. System appears nominal.

---

End Solar Flare Supplemental Passage

---



---

Station-keeping Maneuver #6 (SK6)

---

This is a small maneuver of 25.06 cm/sec delta V that  
     will last for 42.22 sec. Thrusters #3&4 will be fired  
     at 15:10:56 GMT. Thruster scale factor (TSF) 0.9502.

GMT 20033161440 Turn on catbed heaters in preparation for the burn.  
 GMT 20033161454 Command to spin down. Spin down completed ~14:56.  
 GMT 20033161459 Go to inertial mode.  
 GMT 20033161500 Slew #1 to commanded quaternion @22.5 degree Sun angle.  
 GMT 20033161506 Disable RTS 181, system rate checks, enable thrusters.  
 GMT 20033161509 Slew #2 to commanded quaternion @19 degree Sun angle.  
 GMT 20033161510 Thrusters firing @15:10:56. Burn duration nominal.  
 GMT 20033161513 Disable all thrusters. Turn catbed htrs off 15:13:30.  
 GMT 20033161515 Slew #3 to commanded quaternion @22.5 degree Sun angle.

---

GMT 20033161519 Go to observing mode after delta-t = 25 min 7 sec  
Primary temperatures increased by ~30 mK at ~15:12:32  
as result of maneuver.

---

End Station-keeping Maneuver #6

---

Station-keeping Maneuver #7 (SK7)

---

This is a small maneuver of 66.3 cm/sec delta V that  
will last for 112 sec. Thrusters #3&4 will be fired  
at 15:24:56 GMT. Thruster scale factor (TSF) 0.95.

GMT 20040691525 Thrusters firing @15:24:56. Burn duration nominal.

---

End Station-keeping Maneuver #7 (SK7)

---

GMT 2004222 End of year-three data

---

END: WMAP YEAR-THREE DATA

---

Station-keeping Maneuver #8

---

This is a small maneuver about half the size of SK7;  
primarily in +Z (thrusters 3&4). Planned burn  
duration is 55.6255 sec. TSF = 0.94187 based on  
exponential fit. Solar ephemeris update will occur  
after maneuver when back in observing mode.

GMT 2004224164800 ATS started.

GMT 2004224171615 First command.

GMT 20042241721 Catbed htrs turned on

GMT 2004224173559 Spin down complete; go to inertial mode.

GMT 2004224174357 Slewing complete; inertial hold.

GMT 2004224174528 Thrusters enabled

GMT 2004224174722 Slew to 19 degree sun angle

GMT 2004224174830 Thrusters firing. Primary temperature deltaT ~ 35 mK at 17:48:35

GMT 2004224175210 Catbed htrs off. Thrusters disabled a little earlier.

GMT 2004224175430 Going to observing mode. We were out of observing  
mode for 26.0 min.

GMT 2004224182212 Ephemeris update upload started; complete at ~18:23:55  
Resulted in a ~20 arcsec position jumplet in S/C Z axis  
(from AST residuals plots). Not really a position  
change but a sensed velocity change which disappears  
when get the next points.

---

End Station-keeping Maneuver #8

---

---

Station-keeping Maneuver #9

---

This is a small maneuver primarily in -Z.

GMT 20043491926    Disabling thrusters, catbeds going off.  
Time out of observing mode = 25m 43s.

Post Housekeep Analysis Note: SA switched segment 3 transitioned from 'on' to 'off' as a result of this event (as it does for some station keeping maneuvers). There is some minor thermal disturbance to observatory as a result.

---

End Station-keeping Maneuver #9

---



---

Solar Storm Induced Sun Acquisition Mode

---

GMT 200502000    Sun Acquisition Mode induced by solar flare ~ 07:30 GMT.  
Recovery to nominal mission observing mode ~13:30 GMT.

Note: A large solar flare associated with region 0720 has been ongoing since Jan 15 ~09:00 GMT picking at

4000 P/cm<sup>2</sup>/s/sr for P>10MeV  
30 P/cm<sup>2</sup>/s/sr for P>100MeV

around Jan 17 at 18:00. After about a day of slow decay to towards normal levels it flared again on Jan 20 at around ~06:30 GMT, with a much harder spectrum, rapidly reaching level of

2000 P/cm<sup>2</sup>/s/sr for P>10MeV  
500 P/cm<sup>2</sup>/s/sr for P>100MeV

Today pass found the Spacecraft in sun Acquisition Mode. From the playback messages, the ASTs began to be significantly impacted at 05-020-07:09:21 UT which is the occurrence of the first TSM 85 (No AST Updates) failing which reset the Kalman filter. The actual transition from Observing mode to Sun Acquisition mode occurred at 07:35:35 UT. Our routinely scheduled pass for today was at 1240 UT (BOT). Station D43 was able to come up early for us and also extend the pass 65 minutes to allow us to reconfigure the S/C.

Return to Observing mode at 13:40:30 UT.  
Total time out of observing mode was 06:04:55.

---

End Solar Storm Induced Sun Acquisition Mode

---



---

FIFO Underflow Status Bit

---

---

Note: On Thursday 2/10/05, telemetry indicated that the XRSN-B low rate fifo had an underflow and loss of synchronization condition. Although a software error counter that should have incremented for this condition did not change. This appears to have been a single event or transient condition since the low rate data appeared to be nominal during the pass, this event occurred after the previous realtime pass but prior to today's pass.

---

#### RWA1 Power-Off Anomaly

---

- GMT 2005048220552 Power to RWA1 turned off. Spacecraft attitude starts to wander. Several ACS FDC tests failed within about 15 seconds (system momentum and reaction wheel torque/tach comparison tests) because the wheel is still spinning down but the tachometer reads ~0. WMAP enters Safehold/CSS mode where it sits normal to the sun line.
- GMT 20050482210 Sun line passes beyond 30 degrees, the point at which the top of the A-side primary is exposed to sunlight. The top of the primary starts heating rapidly.
- GMT 20050482214 Sun reaches a maximum angle of ~40 degrees off the s/c +z axis (instrument is in the -z hemisphere) at an azimuth of ~15 degrees off the +y axis.
- GMT 20050482215 A-side primary reaches a peak temperature of 165.5 K, from an ambient temperature of 67.9 K prior to the event. All other sensors in the primaries and secondaries remain below 80 K throughout.
- GMT 20050482219 Sun angle returns to less than 30 degrees, primary is back in shadow, temperature drops to 120 K. Primary spends <9 minutes in sunlight and ~35 minutes at >100 K. The FPA and RXB temperatures only changed by 0.1 K during the entire event.
- 

#### RWA1 Recovery Pass

---

Attempt to restart wheel #1 under the hypothesis that the power to it was shut off by a spike in the SSPC.

- GMT 20050510720 Start RWA1 recovery
- GMT 20050510726 TSM 55 enabled
- GMT 2005051072915 Power on RWA1. Current up by 0.3 A on bus. Vreg appears nominal. Baseplate temp warming.
- GMT 20050510733 Clear FDC's
- GMT 20050510734 Enable SSPC FDC. Start sequence of RTSs. Also re-enable AST sync pulses at this point, a deviation from the written procedure.
- GMT 2005051074035 Switch back to ACE-B for telemetry only. ACE-A is still controlling the s/c.
- GMT 20050510744 Command to IRU safehold
- GMT 20050510747 Clear FDC's and reset stats.
- GMT 2005051075150 Switch back to ACE-B for controlling the s/c (XOR 1). We have been switched back to ACE-A by the s/c because

---

of improper RTS configuration. Disable TSM 64, 65, 66.

GMT 20050510801 Disable TSM 64, 65, 66.

GMT 20050510804 Disable TSM 154,155.

GMT 20050510808 Enable TSM 71, 72.

GMT 20050510810 Switch back to ACE-B for controlling the s/c (XOR 1).

GMT 20050510810 Enable TSM 55.

GMT 20050510812 Enable Kalman filter.

GMT 2005051081529 Disable safehold, go to SunAq.

GMT 20050510820 Go to inertial mode. Complete the default TSM configuration first before trying the slew.

GMT 20050510826 Turn on EVD#1 and latch valve.

GMT 20050510827 Turn on EVD#2 and latch valve.

GMT 2005051082802 Primary EVD power monitor.

GMT 2005051082854 Redundant EVD power monitor.

GMT 2005051083000 Open iso-valve. First time it has been cycled in flight.  
This was closed because of a momentum-anomaly-induced safehold.

GMT 20050510833 Turn off iso-valve driver.

GMT 20050510834 Start TSM/RTS config proc for default flight config.

GMT 20050510841 Slew around sun line. All 3 wheels look nominal,  
~200 rpm each during slew.

GMT 20050510846 Slew scan angle to 22.5 degrees.

GMT 2005051085630 Go to observing mode - system nominal.

GMT 20050510900 Reconfigure to safehold IRU.

---

End RWA1 recovery pass

---



---

Station-keeping Maneuver #10

---

This is a small maneuver about half the size of SK7;  
primarily in +Z (thrusters 3&4). Planned burn  
duration is 55.6255 sec. TSF = 0.94187 based on  
exponential fit.

GMT 20050941109 ATS started.

GMT 20050941109 First command - close data sets.

GMT 20050941112 Catbed htrs turned on. Power on iso-valve driver.

GMT 2005094112514 Commence spin down.

GMT 20050941130 Spin down complete; go to inertial mode.

GMT 2005094113513 Slewing to desired azimuth; inertial hold.

GMT 2005094113807 Thrusters enabled, disable RTS 181.

GMT 2005094114027 Slew to 19 degree sun angle.

GMT 2005094114056 Slewing complete; inertial hold.

GMT 2005094114223 Thrusters firing.

GMT 2005094114320 Thruster firing ends. Primary temperature change ~8 mK.

GMT 2005094114444 Thrusters disabled a little earlier.

GMT 2005094114515 Catbed htrs off.

GMT 2005094114549 Going to 22.5 degrees in inertial mode.

GMT 2005094114720 Going to observing mode. We were out of observing

mode for 22 min.

---

End Station-keeping Maneuver #10

---

---

Station-keeping Maneuver #11

---

This is a typical maneuver, primarily in -Z (thrusters 1&2). Commanded burn duration is 57.334 sec (expected duration is 62.64 sec). Planned delta-v is 39.94 cm/sec using TSF = 0.983851 based on the fit to the exponential thermal model.

GMT 20052081431 ATS started.

GMT 2005208143125 First command - close data sets.

GMT 2005208143425 Catbed htrs turned on. Power on iso-valve driver.

GMT 2005208144725 Commence spin down.

GMT 2005208145225 Spin down complete; go to inertial mode.

Enable safehold to use IRU rates.

GMT 2005208145325 Slewing to desired azimuth; inertial hold.

GMT 2005208145955 Thrusters enabled, disable system rate checks.

GMT 2005208150225 Slew to 19 degree sun angle.

GMT 2005208150315 Slewing complete; inertial hold.

GMT 2005208150425 Thrusters firing.

GMT 2005208150535 Thruster firing ends. Primary temperature change ~5 mK.

GMT 2005208150700 Thrusters disabled.

GMT 2005208150725 Catbed htrs off.

GMT 20052081508 Going to 22.5 degrees in inertial mode.

GMT 20052081510 Going to observing mode. Out of observing mode for 25:40 min.

---

End Station-keeping Maneuver #11

---

---

Modify Data Storage Memory Map (CCR-018)

---

The data storage table is being modified to map out a bit of memory that has been producing repeated single bit errors. This will reduce the memory by 1 block.

GMT 20052081543 Table upload was performed after a fresh recorder dump. A few seconds of data was lost between the dump and the new table upload.

---

End Modify Data Storage Memory Map (CCR-018)

---

---

Station-keeping Maneuver #12

---

---

This is a typical maneuver, primarily in -Z (thrusters 1&2). Commanded burn duration is 33.855 sec (expected duration is 37.31 sec). Planned delta-v is 23.24 cm/sec using TSF = 0.963883 based on previous experience with SK11.

GMT 20053141028 ATS started.  
GMT 2005314102937 First command - close data sets.  
GMT 2005314103137 Catbed htrs turned on. Power on iso-valve driver.  
GMT 2005314104437 Commence spin down.  
GMT 2005314104937 Spin down complete; go to inertial mode.  
Enable safehold to use IRU rates.  
GMT 2005314105037 Slewing to desired azimuth; inertial hold.  
GMT 2005314105707 Thrusters enabled, disable system rate checks.  
GMT 2005314105937 Slew to 19 degree sun angle.  
GMT 20053141100 Slewing complete; inertial hold.  
GMT 2005314110137 Thrusters firing.  
GMT 2005314110214 Thruster firing ends. Primary temperature change was 6 mK on the B side.  
GMT 2005314110330 Thrusters disabled.  
GMT 2005314110345 Catbed htrs off.  
GMT 20053141104 Going to 22.5 degrees in inertial mode.  
GMT 2005314110537 Going to observing mode. Out of observing mode for 24:53 min.

---

End Station-keeping Maneuver #12

---

---

-----  
Modify data storage memory map (CCR-019)

---

GMT 20053141120 Upload a new solar ephemeris.

The data storage table is being modified to map out a bit of memory that has been producing repeated single bit errors. This will reduce the memory by 1 block.

GMT 20053141130 Table upload was performed after a fresh recorder dump. A few seconds of data was lost between the dump and the new table upload.

---

End Modify Data Storage Memory Map (CCR-019)

---

---

-----  
Common-mode drift in W32 baseline

---

GMT 2006033 Long-term trending of detector counts showed a common-mode, relatively rapid rise in baseline for W32. This is a long-term event and continues to be monitored.

---

End common-mode drift in W32 baseline

---



---



---

Station-keeping Maneuver #13

---

This is a typical maneuver in +Z (thrusters 3&4). Commanded burn duration is 45.123 sec (expected duration is 45.8 sec). Planned delta-v is 23.26 cm/sec using TSF = 0.94

GMT 2006066145850 Catbeds on  
 GMT 2006066151135 Commence spindown  
 GMT 2006066151635 Inertial hold  
 GMT 2006066151735 Slew  
 GMT 2006066152405 Thrusters enabled  
 GMT 2006066152428 Disable RTS  
 GMT 2006066152648 Slew to 19 degrees  
 GMT 2006066152835 Burn starts  
 GMT 2006066152939 Back to inertial  
 GMT 2006066153040 Disabling thrusters  
 GMT 2006066153104 Catbeds off  
 GMT 2006066153213 Slew back to 22.5 degrees.  
 GMT 2006066153256 Initiate return to observing mode  
     Max temp change on primary, B side = 33 mK  
 GMT 20060661600 Starting proc prior to table71 upload.  
 GMT 2006066160245 Loading table 71, Ephemeris upload.  
 GMT 2006066160414 Load complete, checksum confirmed.  
     Total time out of observing mode = 25 min 15 sec.

---

End Station-keeping Maneuver #13 and Ephemeris Upload.

---



---



---

Station-keeping Maneuver #14

---

This is a typical maneuver, primarily in +Z (thrusters 3&4). Commanded burn duration is 28.892 sec (expected duration is 28.92 sec). Planned delta-v is 16.38 cm/sec based on previous experience.

GMT 20061651519 First command - close data sets.  
 GMT 2006165151931 ATS started.  
 GMT 2006165152231 Catbed htrs turned on. Power on iso-valve driver.  
 GMT 2006165153531 Commence spin down.  
 GMT 2006165154031 Spin down complete; go to inertial mode.  
     Enable safehold to use IRU rates.  
 GMT 2006165154131 Slewing to desired azimuth; inertial hold.  
 GMT 2006165154801 Thrusters enabled, disable system rate checks.  
 GMT 2006165155031 Slew to 19 degree sun angle.  
 GMT 2006165155115 Slewing complete; inertial hold.  
 GMT 2006165155231 Thrusters firing.  
 GMT 2006165155300 Thruster firing ends. Primary temperature change was 23 mK on the A side.

---

GMT 2006165155400 Thrusters disabled.  
GMT 2006165165450 Catbed htrs off.  
GMT 2006165165530 Going to 22.5 degrees in inertial mode.  
GMT 2006165165630 Going to observing mode. Out of observing mode for 21:00 min.

---

End Station-keeping Maneuver #14

---

GMT 2006222 End of year-five data

---

END: WMAP YEAR-FIVE DATA

---

Station-keeping Maneuver #15

---

This is a typical manuever, primarily in +Z (thrusters 3&4). Commanded burn duration is 31.64 sec (expected duration is 31.4 sec). Planned delta-v is 17.89 cm/sec using TSF = 0.931 based on previous experience.

GMT 20063131546 ATS started.  
GMT 2006313154610 First command - close data sets.  
GMT 2006313154910 Catbed htrs turned on. Power on iso-valve driver.  
GMT 2006313160210 Commence spin down.  
GMT 2006313160710 Spin down complete; go to inertial mode.  
Enable safehold to use IRU rates.  
GMT 2006313160810 Slew to desired azimuth; inertial hold.  
GMT 2006313161010 Thrusters enabled, disable system rate checks.  
GMT 2006313161710 Slew to 19 degree sun angle.  
GMT 2006313161325 Slew complete; inertial hold.  
GMT 2006313161910 Thrusters firing.  
GMT 2006313161941 Thruster firing ends. Primary temperature change was 23 mK on the A side.  
GMT 2006313162100 Thrusters disabled.  
GMT 2006313162100 Catbed htrs off.  
GMT 2006313162400 Going to 22.5 degrees in inertial mode.  
GMT 2006313162645 Going to observing mode. We were out of observing mode for 24:35 min.

---

End Station-keeping Maneuver #15

---

Station-keeping Maneuver #16

---

This is a typical manuever, primarily in -Z (thrusters 1&2). Commanded burn duration is 7.057 sec (expected duration is 7.29 sec). Planned delta-v is 4.59 cm/sec using TSF = 0.953 based on previous experience.

---

GMT 2007067141216 ATS started.  
 GMT 2007067141216 First command - close data sets.  
 GMT 2007067141516 Catbed htrs turned on. Power on iso-valve driver.  
 GMT 2007067142816 Commence spin down.  
 GMT 2007067143316 Spin down complete; go to inertial mode.  
     Enable safehold to use IRU rates.  
 GMT 2007067143416 Slewing to desired azimuth; inertial hold.  
 GMT 2007067144046 Thrusters enabled, disable system rate checks.  
 GMT 2007067144316 Slew to 19 degree sun angle.  
 GMT 2007067144346 Slewing complete; inertial hold.  
 GMT 2007067144516 Thrusters firing.  
 GMT 2007067144523 Thruster firing ends. Primary temperature change  
     was 5 mK on the B side.  
 GMT 2007067144600 Thrusters disabled.  
 GMT 2007067144630 Catbed htrs off.  
 GMT 2007067144721 Going to 22.5 degrees in inertial mode.  
 GMT 2007067144930 Going to observing mode. We were out of observing  
     mode for 21:00 min.

---

End Station-keeping Maneuver #16

---

Station-keeping Maneuver #17

---

This is a typical manueuver, primarily in -Z (thrusters 1&2).  
 Commanded burn duration is 67 sec. Planned delta-v is  
 44 cm/sec based on previous experience.

GMT 2007176120548 ATS started.  
 GMT 2007176120548 First command - close data sets.  
 GMT 2007176120848 Catbed htrs turned on. Power on iso-valve driver.  
 GMT 2007176122148 Commence spin down.  
 GMT 2007176122648 Spin down complete; go to inertial mode.  
     Enable safehold to use IRU rates.  
 GMT 2007176122748 Slewing to desired azimuth; inertial hold.  
 GMT 2007176123418 Thrusters enabled, disable system rate checks.  
 GMT 2007176123648 Slew to 19 degree sun angle.  
 GMT 2007176123818 Slewing complete; inertial hold.  
 GMT 2007176123848 Thrusters firing. (See anomaly notes below).  
 GMT 20071761240 Thruster firing ends.  
 GMT 20071761240 Thrusters disabled.  
 GMT 20071761241 Catbed htrs off.  
 GMT 20071761242 Going to 22.5 degrees in inertial mode.  
 GMT 2007176124340 Going to observing mode.

Note: A few minutes after the burn it was noted that the thruster valves did  
 not heat up over and above the heating due to the catbed heaters. Analysis of  
 propulsion housekeeping telemetry indicated thrusters did not fired. The most  
 likely explanation is that the power service to the thrusters (SSPC#6) was

turned off (i.e., at an unknown time in the past bounded by the last usage of this service) by an SEU without indicating this state in telemetry. A similar incident occurred on 2005:048 with the power supply to reaction wheel #1. This is a known "feature" of the SSPC circuitry in the flight radiation environment.

---

End Station-keeping Maneuver #17, part 1.

---



---

Station-keeping Maneuver #17, part 2.

---

This is an attempt to make-up failed maneuver #17.  
 The revised plan is similar to the original: primarily in -Z  
 (thrusters 1&2). Commanded burn duration is 68.7 sec  
 (expected duration is 75.28 sec). Planned delta-v is  
 44.67 cm/sec using TSF = 0.984 based on previous experience.

GMT 20071772304 Send command to disable PSE FDS and turn off SSPC#6.  
 Telemetry indicates that it's off.  
 GMT 20071772305 Send command to reenable PSE FDS and to turn on SSPC#6.  
 Telemetry indicates that it's on.  
 GMT 2007177232748 ATS started.  
 GMT 2007177232748 First command - close data sets.  
 GMT 2007177233048 Catbed htrs turned on. Power on iso-valve driver.  
 GMT 2007177234348 Commence spin down.  
 GMT 2007177234848 Spin down complete; go to inertial mode.  
 Enable safehold to use IRU rates.  
 GMT 2007177234948 Slewing to desired azimuth; inertial hold.  
 GMT 2007177235618 Thrusters enabled, disable system rate checks.  
 GMT 2007177235848 Slew to 19 degree sun angle.  
 GMT 2007178000018 Slewing complete; inertial hold.  
 GMT 2007178000048 Thrusters firing.  
 GMT 2007178000203 Thruster firing ends.  
 GMT 2007178002050 Thrusters disabled.  
 GMT 2007178000305 Catbed htrs off.  
 GMT 2007178000340 Going to 22.5 degrees in inertial mode.  
 GMT 2007178000855 Going to observing mode.  
 We were out of observing mode for 25 minutes 07 seconds

---

End Station-keeping Maneuver #17, part 2.

---

GMT 2007222 End of year-six data

---

END: WMAP YEAR-SIX DATA

---



---

Shadow Avoidance Maneuver

---

---

This maneuver is designed to cause WMAP to avoid being eclipsed by the Earth. Thrusters 4-8 will be used. Commanded burn duration is 623 sec (expected duration is 659 sec). Planned delta-v is 819.97 cm/sec using TSF = 0.9523 based on P3FM. Expected fuel consumption is 3.6695 kg (starting with 55.5247 kg, ending with 51.8552 kg).

GMT 20072481341 Send command to disable PSE FDS and turn off SSPC#6.  
Telemetry indicates that it's off.

GMT 20072481341 Send command to reenable PSE FDS and to turn on SSPC#6.  
Telemetry indicates that it's on.

GMT 2007248140444 ATS started.

GMT 2007248140444 First command - close data sets.

GMT 2007248140544 Switch to Engineering T0 filter tables.  
Set DS filter table to ENG.

GMT 2007248140744 Catbed htrs turned on. Power on iso-valve driver.

GMT 2007248142044 Commence spin down.

GMT 2007248142544 Spin down complete; go to inertial mode.  
Enable safehold to use IRU rates.

GMT 2007248142644 Slewing to desired azimuth; inertial hold.

GMT 2007248143314 Thrusters enabled, disable system rate checks.

GMT 2007248143544 Slew to 19 degree sun angle.

GMT 2007248143714 Slewing complete; inertial hold.

GMT 2007248143744 Thrusters firing.

GMT 2007248144845 Thruster firing ends.

GMT 2007248145020 Thrusters disabled.

GMT 2007248145048 Catbed htrs off.

GMT 2007248145125 Going to 22.5 degrees in inertial mode.

GMT 2007248145520 Enabling rate check.

GMT 2007248145620 Going to observing mode.  
We were out of observing mode for 35 minutes 36 seconds

---

End Shadow Avoidance Maneuver

---



---

Shadow Avoidance Correction Maneuver

---

This maneuver is designed to cause WMAP to correct the orbit after the SAM. Thrusters 1 & 2 will be used. Commanded burn duration is 24.825 sec (expected duration is 26.96 sec). Planned delta-v is 15.69 cm/sec. Expected fuel consumption is 0.0726 kg (starting with 51.978 kg, ending with 51.9054 kg).

GMT 2007269131030 Send command to disable PSE FDS and turn off SSPC#6.  
Telemetry indicates that it's off.

GMT 2007269131130 Send command to reenable PSE FDS and to turn on SSPC#6.  
Telemetry indicates that it's on.

GMT 2007269132635 ATS started.

GMT 2007269132635 First command - close data sets.

GMT 2007269132735 Switch to Engineering T0 filter tables.

Set DS filter table to ENG.  
 GMT 2007269132935 Catbed htrs turned on. Power on iso-valve driver.  
 GMT 2007269134235 Commence spin down.  
 GMT 2007269134735 Spin down complete; go to inertial mode.  
 Enable safehold to use IRU rates.  
 GMT 2007269134835 Slewing to desired azimuth; inertial hold.  
 GMT 2007269135505 Thrusters enabled, disable system rate checks.  
 GMT 2007269135735 Slew to 19 degree sun angle.  
 GMT 2007269135905 Slewing complete; inertial hold.  
 GMT 2007269135935 Thrusters firing.  
 GMT 2007269140016 Thruster firing ends.  
 GMT 2007269140050 Thrusters disabled.  
 GMT 2007269140111 Catbed htrs off.  
 GMT 2007269140140 Going to 22.5 degrees in inertial mode.  
 GMT 20072691402 Enabling rate check.  
 GMT 2007269140255 Going to observing mode.  
 We were out of observing mode for 36 minutes 20 seconds

---

End Shadow Avoidance Correction Maneuver

---



---

Transponder B Anomaly

---

GMT 2007315 Transponder B has been experiencing intermittent drops in output power (by 20-30dB) over the past several days:

Day	Time	Duration	Pass time	During pass?
	GMT	minutes	GMT	
2007				
301	20:15	~5	13:10	N
307	12:15	~5	11:30	end
311	12:45	~10	11:45	end
312	12:40	~10	11:45	end
313	23:50	~10	11:30	N

Each of these events lasted less than 10 minutes before correcting itself. 3 of the 5 appear to have coincided with the end of a pass, when we drop lock with the transmitter.

Today (day 315) the power dropped by a similar amount for several hours, then, during the pass on this day, the power level picked up again for several short intervals, but remained low at the end of the day.

On day 316 there were repeated attempts to establish lock with the transponder again but no reliable contact could be established. At this point the spacecraft was commanded to switch over to the backup transponder A.

---

---

End Transponder B Anomaly

---



---

Station-keeping Maneuver #18

---

This is a typical stationkeeping maneuver.  
Thrusters 3 & 4 will be used. Commanded burn duration is  
35.9 sec (expected duration is 35.9 sec).

GMT 2008023133540 Send command to disable PSE FDS and turn off SSPC#6.  
Telemetry indicates that it's off.

GMT 2008023133718 Send command to reenable PSE FDS and to turn on SSPC#6.  
Telemetry indicates that it's on.

GMT 2008023135138 ATS started.

GMT 2008023135138 First command - close data sets.

GMT 2008023135238 Switch to Engineering TO filter tables.  
Set DS filter table to ENG.

GMT 2008023135438 Catbed htrs turned on. Power on iso-valve driver.

GMT 2008023140738 Commence spin down.

GMT 2008023141238 Spin down complete; go to inertial mode.  
Enable safehold to use IRU rates.

GMT 2008023141338 Slew to desired azimuth; inertial hold.

GMT 2008023142008 Thrusters enabled, disable system rate checks.

GMT 2008023142238 Slew to 19 degree sun angle.

GMT 2008023142408 Slewing complete; inertial hold.

GMT 2008023142438 Thrusters firing.

GMT 2008023142528 Thruster firing ends.

GMT 2008023142610 Thrusters disabled.

GMT 2008023142625 Catbed htrs off.

GMT 2008023142652 Going to 22.5 degrees in inertial mode.

GMT 2008023142823 Enabling rate check.

GMT 2008023143215 Going to observing mode.

GMT 2008023145500 Uploaded a new solar ephemeris.  
We were out of observing mode for 40 minutes 37 seconds

Note: SA switched segment 3 transitioned from 'off' to 'on'  
as a result of this event (as it does for some station keeping  
maneuvers). Minor thermal disturbance is observed.

---

End Station-keeping Maneuver #18

---



---

Station-keeping Maneuver #19

---

This is a typical stationkeeping maneuver.  
Thrusters 1 & 2 will be used. Commanded burn duration is  
91.3 sec (expected duration is 99.7sec). Planned delta-v  
is 58.78 cm/sec. Expected fuel consumption is 0.27 kg  
(starting with 51.8 kg, ending with 51.5 kg).

---

GMT 2008156154206 Send command to disable PSE FDS and turn off SSPC#6.  
                                 Telemetry indicates that it's off.  
 GMT 2008156154325 Send command to reenable PSE FDS and to turn on SSPC#6.  
                                 Telemetry indicates that it's on.  
 GMT 2008156160220 ATS started.  
 GMT 2008156160220 First command - close data sets.  
 GMT 2008156160320 Switch to Engineering TO filter tables.  
                                 Set DS filter table to ENG.  
 GMT 2008156160520 Catbed htrs turned on. Power on iso-valve driver.  
 GMT 2008156161820 Commence spin down.  
 GMT 2008156162320 Spin down complete; go to inertial mode.  
                                 Enable safehold to use IRU rates.  
 GMT 2008156162420 Slewing to desired azimuth; inertial hold.  
 GMT 2008156163050 Thrusters enabled, disable system rate checks.  
 GMT 2008156163320 Slew to 19 degree sun angle.  
 GMT 2008156163450 Slewing complete; inertial hold.  
 GMT 2008156163520 Thrusters firing.  
 GMT 2008156163703 Thruster firing ends.  
 GMT 2008156163756 Thrusters disabled.  
 GMT 2008156163818 Catbed htrs off.  
 GMT 2008156163839 Going to 22.5 degrees in inertial mode.  
 GMT 2008156163950 Going to observing mode.  
 GMT 2008156163950 Enabling rate check.  
 GMT 2008156164417 RTS Reconfiguration  
                                 We were out of observing mode for 37 minutes 20 seconds

---

End Station-keeping Maneuver #19

---

Lunar shadow transit

---

WMAP will transit the lunar shadow at L2 for approximately 6 hours. The initial shadow starts at GMT 18:07:42 and achieves a maximum depth of 4.0% shortly after 19:15:00. The maximum shadow lasts until roughly 22:45:00, and ends at about 23:50:00. After much discussion, the plan is to fly through the shadow in observing mode and to monitor the transit during the pass. The first half of the event will be monitored from the Canberra station (17:00-20:00) while the second half will be monitored by Madrid (21:40-02:25).

GMT 20082141700 Canberra acquires track and ~5 minutes of telemetry is obtained.  
 GMT 20082141705 The station goes red due to a loss of both commercial and backup power. Attempts to restore power are unsuccessful. We fly through the first half of the shadow in the dark.  
 GMT 20082142020 Madrid established voice contact to initiate pre-pass activities.  
 GMT 20082142110 Data is acquired and things appear to be about as expected. The array damper temperatures dropped by ~3C with other systems responding accordingly.

---

End of lunar shadow transit

---

GMT 2008222 End of year-seven data

---

END: WMAP YEAR-SEVEN DATA

---

---

Station-keeping Maneuver #20

---

This is a typical stationkeeping maneuver.  
Thrusters 1 & 2 will be used.  
Commanded burn duration is 79.40 sec  
(expected duration is 86.84 sec).  
Planned delta-v is 50.92 cm/sec using TSF = TBD.  
Expected fuel consumption is 0.2 kg  
(starting with 51.5 kg, ending with 51.3 kg).

GMT 2008282130921 Send command to disable PSE FDS and turn off SSPC#6.

Telemetry indicates that it's off.

GMT 2008282131016 Send command to reenable PSE FDS and to turn on SSPC#6.

Telemetry indicates that it's on.

GMT 2008282131510 ATS started.

GMT 2008282132910 First command - close data sets.

GMT 2008282133010 Switch to Engineering T0 filter tables.

Set DS filter table to ENG.

GMT 2008282133210 Catbed heaters turned on. Power on iso-valve driver.

GMT 2008282134510 Commence spin down.

GMT 2008282135010 Spin down complete; go to inertial mode.

Enable safehold to use IRU rates.

GMT 2008282135110 Slewing to desired azimuth; inertial hold.

GMT 2008282135740 Thrusters enabled, disable system rate checks.

GMT 2008282140010 Slew to 19 degree sun angle.

GMT 2008282140140 Slewing complete; inertial hold.

GMT 2008282140210 Thrusters firing.

GMT 2008282140319 Thruster firing ends.

GMT 2008282140340 Thrusters disabled.

GMT 2008282140350 Catbed heaters off.

GMT 2008282140530 Going to 22.5 degrees in inertial mode.

GMT 2008282141033 Going to observing mode.

GMT 2008282141033 Enabling rate check.

GMT 2008282141540 RTS Reconfiguration

Out of observing mode for 25 minutes 25 seconds

---

End Station-keeping Maneuver #20

---

---

---

ACE-A SSPC Event

---

At approximately 2009008113000, ACE-A powered down.  
Evaluation of data and discussion led to the  
opinion that a SSPC reset event occurred.

GMT 20090081923 Disable FDC  
GMT 20090081924 FDC noted off  
GMT 20090081924 SSPC opened, noted open.  
GMT 20090081925 SSPC closed. OM1 current is back up where it belongs.  
GMT 20090081926 Re-enable FDC. FDC noted on.  
GMT 20090081930 Error counters reset.

---

---

---

End ACE-A SSPC Event

---

---

---

Station-keeping Maneuver #21

---

This is a typical stationkeeping maneuver.  
Thrusters 3 & 4 will be used.  
Commanded burn duration is 66.12 sec  
(expected duration is 66.88 sec).  
Planned delta-v is 35.7 cm/sec using TSF = 0.942.  
Expected fuel consumption is 0.163 kg  
(starting with 51.318 kg, ending with 51.155 kg).

GMT 2009042204200 Send command to disable PSE FDS and turn off SSPC#6.  
Telemetry indicates that it's off.  
GMT 2009042204300 Send command to reenable PSE FDS and to turn on SSPC#6.  
Telemetry indicates that it's on.  
GMT 2009042204500 ATS started.  
GMT 2009042205355 First command - close data sets.  
GMT 2009042205455 Switch to Engineering TO filter tables.  
Set DS filter table to ENG.  
GMT 2009042205655 Catbed heaters turned on. Power on iso-valve driver.  
GMT 2009042210955 Commence spin down.  
GMT 2009042211510 Spin down complete; go to inertial mode.  
Enable safehold to use IRU rates.  
GMT 2009042211555 Slewing to desired azimuth; inertial hold.  
GMT 2009042212225 Thrusters enabled, disable system rate checks.  
GMT 2009042212455 Slew to 19 degree sun angle.  
GMT 2009042212625 Slewing complete; inertial hold.  
GMT 2009042212655 Thrusters firing.  
GMT 2009042212811 Thruster firing ends.  
GMT 2009042212857 Thrusters disabled.  
GMT 2009042212923 Catbed heaters off.

---

GMT 2009042213007 Going to 22.5 degrees in inertial mode.  
GMT 2009042213120 Going to observing mode.  
GMT 2009042213412 Enabling rate check.  
GMT 2009042213523 RTS Reconfiguration  
GMT 2009042220223 Uploaded a new solar ephemeris.  
Out of observing mode for 25 minutes 14 seconds

---

-----  
End Station-keeping Maneuver #21  
-----

---

-----  
Station-keeping Maneuver #22  
-----

This is a typical stationkeeping maneuver.  
Thrusters 1 & 2 will be used.  
Commanded burn duration is 77.04 sec  
(expected duration is 84.24 sec).  
Planned delta-v is 48.8 cm/sec using TSF = 0.981.  
Expected fuel consumption is 0.224 kg  
(starting with 51.154 kg, ending with 50.930 kg).

GMT 2009197152438 Send command to disable PSE FDS and turn off SSPC#6.  
Telemetry indicates that it's off.  
GMT 2009197152534 Send command to reenable PSE FDS and to turn on SSPC#6.  
GMT 2009197152634 Telemetry indicates that it's on.  
GMT 2009197152730 ATS started.  
GMT 2009197153508 First command - close data sets.  
GMT 2009197153608 Switch to Engineering T0 filter tables.  
Set DS filter table to ENG.  
GMT 2009197153808 Catbed heaters turned on. Power on iso-valve driver.  
GMT 2009197155108 Commence spin down.  
GMT 2009197155608 Spin down complete; go to inertial mode.  
Enable safehold to use IRU rates.  
GMT 2009197155708 Slewing to desired azimuth; inertial hold.  
GMT 2009197160338 Thrusters enabled, disable system rate checks.  
GMT 2009197160608 Slew to 19 degree sun angle.  
GMT 2009197160738 Slewing complete; inertial hold.  
GMT 2009197160808 Thrusters firing.  
GMT 2009197161004 Thruster firing ends.  
GMT 2009197161030 Thrusters disabled.  
GMT 2009197161054 Catbed heaters off.  
GMT 2009197161120 Going to 22.5 degrees in inertial mode.  
GMT 2009197161230 Going to observing mode.  
GMT 2009197161623 Enabling rate check.  
GMT 2009197161630 RTS Reconfiguration  
GMT 2009197161646 Uploaded a new solar ephemeris.  
Out of observing mode for 25 minutes 18 seconds

---

-----  
End Station-keeping Maneuver #22

---

-----  
GMT 2009222      End of year-eight data

---

-----  
END: WMAP YEAR-EIGHT DATA

---

-----  
Station-keeping Maneuver #23

These notes were recreated from the ATS at a later date.  
This is a typical stationkeeping maneuver.  
Thrusters 1 & 2 will be used.  
Commanded burn duration is 113.45 sec  
(expected duration is 124.16 sec).  
Planned delta-v is 72.3 cm/sec using TSF = 0.981.  
Expected fuel consumption is 0.224 kg  
(starting with 50.932 kg, ending with 50.601 kg).

GMT 2010020141916 Send command to disable PSE FDS and turn off SSPC#6.  
Telemetry indicates that it's off.  
GMT 2010020142016 Send command to reenable PSE FDS and to turn on SSPC#6.  
GMT 2010020142116 Telemetry indicates that it's on.  
GMT 2010020142216 ATS started.  
GMT 2010020142216 First command - close data sets.  
GMT 2010020142316 Switch to Engineering T0 filter tables.  
Set DS filter table to ENG.  
GMT 2010020142516 Catbed htrs turned on. Power on iso-valve driver.  
GMT 2010020143816 Commence spin down.  
GMT 2010020144316 Spin down complete; go to inertial mode.  
Enable safehold to use IRU rates.  
GMT 2010020145046 Slewing to desired azimuth; inertial hold.  
GMT 2010020145046 Thrusters enabled, disable system rate checks.  
GMT 2010020145316 Slew to 19 degree sun angle.  
GMT 2010020145446 Slewing complete; inertial hold.  
GMT 2010020145516 Thrusters firing.  
GMT 2010020145710 Thruster firing ends.  
GMT 2010020145736 Thrusters disabled.  
GMT 2010020145800 Catbed heaters off.  
GMT 2010020145826 Going to 22.5 degrees in inertial mode.  
GMT 2010020145936 Going to observing mode.  
GMT 2010020150329 Enabling rate check.  
GMT 2010020150339 RTS Reconfiguration  
GMT 2010020150354 Uploaded a new solar ephemeris.  
Out of observing mode for 26 minutes 28 seconds

---

-----  
End Station-keeping Maneuver #23

---

Station-keeping Maneuver #24

---

Started by putting a 9% charge into the battery  
before the start of ATS.

This is a typical stationkeeping maneuver.  
Thrusters 3 & 4 will be used.  
Commanded burn duration is 120.785 sec  
(expected duration is 122.280 sec).  
Planned delta-v is 64.2 cm/sec using TSF = 0.948.  
Expected fuel consumption is 0.293 kg  
(starting with 50.605 kg, ending with 50.312 kg).

GMT 2010133165000 Send command to disable PSE FDS and turn off SSPC#6.  
Telemetry indicates that it's off.  
GMT 2010133165200 Send command to reenable PSE FDS and to turn on SSPC#6.  
GMT 2010133165300 Telemetry indicates that it's on.  
GMT 2010133170501 ATS started.  
GMT 2010133170501 First command - close data sets.  
GMT 2010133170601 Switch to Engineering T0 filter tables.  
Set DS filter table to ENG.  
GMT 2010133170801 Catbed heaters turned on. Power on iso-valve driver.  
GMT 2010133172101 Commence spin down.  
GMT 2010133172601 Spin down complete; go to inertial mode.  
Enable safehold to use IRU rates.  
GMT 2010133172701 Slewing to desired azimuth; inertial hold.  
GMT 2010133173331 Thrusters enabled, disable system rate checks.  
GMT 2010133173601 Slew to 19 degree sun angle.  
GMT 2010133173731 Slewing complete; inertial hold.  
GMT 2010133173801 Thrusters firing.  
GMT 2010133174002 Thruster firing ends.  
GMT 2010133174100 Thrusters disabled.  
GMT 2010133174118 Catbed htrs off.  
GMT 2010133174132 Going to 22.5 degrees in inertial mode.  
GMT 2010133174328 Going to observing mode.  
GMT 2010133174621 Enabling rate check.  
GMT 2010133174628 RTS Reconfiguration  
GMT 2010133181816 Uploaded a new solar ephemeris.  
Out of observing mode for 41 minutes 27 seconds

---

End Station-keeping Maneuver #24

---



---

Tip Back Tests

---

Nominal science operations have terminated.  
Prior to releasing the spacecraft to the flight operations

group for disposition, a number of tests changing the precession angle will be performed over the next ten days.

Transition to a 24 deg. precession angle.

GMT 2010223184300 Disable TSM 78  
GMT 2010223184500 Load table 56 update  
GMT 2010223184600 Check-sum is correct  
GMT 2010223184800 Switch to 24 deg...  
GMT 2010223184800 Poke memory (actual switch)  
GMT 2010223185000 Memory dwell value is updated and correct  
This transition was very fast.

---

END: WMAP YEAR-NINE DATA

---

---

END: WMAP SPACECRAFT PLACED IN PARKING ORBIT AND COMMANDED OFF

---

# Appendix C

## Mnemonics Lists

Signals in the *WMAP* telemetry are uniquely identified by a set of mnemonics. Identifying a specific signal using its mnemonic allows the user to extract it from a more complex data structure using software routines which are provided (see Chapter 5). The main signals of interest in the *WMAP* time-ordered data are described by the science and the housekeeping mnemonics, these are all listed in this appendix grouped by their functionalities. For the mnemonics associated with a temperature sensor the description field indicates the approximate position of that sensor on the observatory.

## C.1 Science Mnemonics

Raw Data	Major Frame First Point	Major Frame Average	Major Frame RMS
DK113	QDK113	ADK113	RDK113
DK114	QDK114	ADK114	RDK114
DK123	QDK123	ADK123	RDK123
DK124	QDK124	ADK124	RDK124
DKA113	QDKA113	ADKA113	RDKR113
DKA114	QDKA114	ADKA114	RDKR114
DKA123	QDKA123	ADKA123	RDKR123
DKA124	QDKA124	ADKA124	RDKR124
DQ113	QDQ113	ADQ113	RDQ113
DQ114	QDQ114	ADQ114	RDQ114
DQ123	QDQ123	ADQ123	RDQ123
DQ124	QDQ124	ADQ124	RDQ124
DQ213	QDQ213	ADQ213	RDQ213
DQ214	QDQ214	ADQ214	RDQ214
DQ223	QDQ223	ADQ223	RDQ223
DQ224	QDQ224	ADQ224	RDQ224
DV113	QDV113	ADV113	RDV113
DV114	QDV114	ADV114	RDV114
DV123	QDV123	ADV123	RDV123
DV124	QDV124	ADV124	RDV124
DV213	QDV213	ADV213	RDV213
DV214	QDV214	ADV214	RDV214
DV223	QDV223	ADV223	RDV223
DV224	QDV224	ADV224	RDV224
DW113	QDW113	ADW113	RDW113
DW114	QDW114	ADW114	RDW114
DW123	QDW123	ADW123	RDW123
DW124	QDW124	ADW124	RDW124
DW213	QDW213	ADW213	RDW213
DW214	QDW214	ADW214	RDW214
DW223	QDW223	ADW223	RDW223
DW224	QDW224	ADW224	RDW224
DW313	QDW313	ADW313	RDW313
DW314	QDW314	ADW314	RDW314
DW323	QDW323	ADW323	RDW323
DW324	QDW324	ADW324	RDW324
DW413	QDW413	ADW413	RDW413
DW414	QDW414	ADW414	RDW414
DW423	QDW423	ADW423	RDW423
DW424	QDW424	ADW424	RDW424

## C.2 Instrument Housekeeping Mnemonics

### C.2.1 Amplifier Drain Currents

Mnemonic	Description	Mnemonic	Description
DFK111B8DNI	K111 FPA	DFV211B9DNI	V211 FPA
DFK112B8DNI	K112 FPA	DFV212B9DNI	V212 FPA
DFK121B8DNI	K121 FPA	DFV221B9DNI	V221 FPA
DFK122B8DNI	K122 FPA	DFV222B9DNI	V222 FPA
DRK111B8DNI	K111 RXB	DRV211B9DNI	V211 RXB
DRK112B8DNI	K112 RXB	DRV212B9DNI	V212 RXB
DRK121B8DNI	K121 RXB	DRV221B9DNI	V221 RXB
DRK122B8DNI	K122 RXB	DRV222B9DNI	V222 RXB
DFKA111B3DNI	Ka111 FPA	DFW111B4DNI	W111 FPA
DFKA112B3DNI	Ka112 FPA	DFW112B4DNI	W112 FPA
DFKA121B3DNI	Ka121 FPA	DFW121B4DNI	W121 FPA
DFKA122B3DNI	Ka122 FPA	DFW122B4DNI	W122 FPA
DRKA111B3DNI	Ka111 RXB	DRW111B4DNI	W111 RXB
DRKA112B3DNI	Ka112 RXB	DRW112B4DNI	W112 RXB
DRKA121B3DNI	Ka121 RXB	DRW121B4DNI	W121 RXB
DRKA122B3DNI	Ka122 RXB	DRW122B4DNI	W122 RXB
DFQ111B1DNI	Q111 FPA	DFW211B5DNI	W211 FPA
DFQ112B1DNI	Q112 FPA	DFW212B5DNI	W212 FPA
DFQ121B1DNI	Q121 FPA	DFW221B5DNI	W221 FPA
DFQ122B1DNI	Q122 FPA	DFW222B5DNI	W222 FPA
DRQ111B1DNI	Q111 RXB	DRW211B5DNI	W211 RXB
DRQ112B1DNI	Q112 RXB	DRW212B5DNI	W212 RXB
DRQ121B1DNI	Q121 RXB	DRW221B5DNI	W221 RXB
DRQ122B1DNI	Q122 RXB	DRW222B5DNI	W222 RXB
DFQ211B10DNI	Q211 FPA	DFW311B6DNI	W311 FPA
DFQ212B10DNI	Q212 FPA	DFW312B6DNI	W312 FPA
DFQ221B10DNI	Q221 FPA	DFW321B6DNI	W321 FPA
DFQ222B10DNI	Q222 FPA	DFW322B6DNI	W322 FPA
DRQ211B10DNI	Q211 RXB	DRW311B6DNI	W311 RXB
DRQ212B10DNI	Q212 RXB	DRW312B6DNI	W312 RXB
DRQ221B10DNI	Q221 RXB	DRW321B6DNI	W321 RXB
DRQ222B10DNI	Q222 RXB	DRW322B6DNI	W322 RXB
DFV111B2DNI	V111 FPA	DFW411B7DNI	W411 FPA
DFV112B2DNI	V112 FPA	DFW412B7DNI	W412 FPA
DFV121B2DNI	V121 FPA	DFW421B7DNI	W421 FPA
DFV122B2DNI	V122 FPA	DFW422B7DNI	W422 FPA
DRV111B2DNI	V111 RXB	DRW411B7DNI	W411 RXB
DRV112B2DNI	V112 RXB	DRW412B7DNI	W412 RXB
DRV121B2DNI	V121 RXB	DRW421B7DNI	W421 RXB
DRV122B2DNI	V122 RXB	DRW422B7DNI	W422 RXB

### C.2.2 Radiometer RF Bias (Total Power)

Mnemonic	Description
DRK113RFB10	K113 RF bias
DRK114RFB11	K114 RF bias
DRK123RFB12	K123 RF bias
DRK124RFB13	K124 RF bias
DRKA113RFB136	Ka113 RF bias
DRKA114RFB137	Ka114 RF bias
DRKA123RFB138	Ka123 RF bias
DRKA124RFB139	Ka124 RF bias
DRQ113RFB120	Q113 RF bias
DRQ114RFB121	Q114 RF bias
DRQ123RFB122	Q123 RF bias
DRQ124RFB123	Q124 RF bias
DRQ213RFB128	Q213 RF bias
DRQ214RFB129	Q214 RF bias
DRQ223RFB130	Q223 RF bias
DRQ224RFB131	Q224 RF bias
DRV113RFB132	V113 RF bias
DRV114RFB133	V114 RF bias
DRV123RFB134	V123 RF bias
DRV124RFB135	V124 RF bias
DRV213RFB112	V213 RF bias
DRV214RFB113	V214 RF bias
DRV223RFB114	V223 RF bias
DRV224RFB115	V224 RF bias
DRW113RFB14	W113 RF bias
DRW114RFB15	W114 RF bias
DRW123RFB12	W123 RF bias
DRW124RFB13	W124 RF bias
DRW213RFB124	W213 RF bias
DRW214RFB125	W214 RF bias
DRW223RFB126	W223 RF bias
DRW224RFB127	W224 RF bias
DRW313RFB116	W313 RF bias
DRW314RFB117	W314 RF bias
DRW323RFB118	W323 RF bias
DRW324RFB119	W324 RF bias
DRW413RFB18	W413 RF bias
DRW414RFB19	W414 RF bias
DRW423RFB110	W423 RF bias
DRW424RFB111	W424 RF bias

### C.2.3 TRS Temperatures

Mnemonic	Description
DTATOPPRIT	A side primary temp (top)
DTAMIDPRIT	A side primary temp (middle)
DTATOPSECT	A side secondary temp (top)
DTAMIDSECT	A side secondary temp (middle)
DTABOTSECT	A side secondary temp (bottom)
DTBTOPPRIT	B side primary temp (top)
DTBMIDPRIT	B side primary temp (middle)
DTBTOPSECT	B side secondary temp (top)
DTBMIDSECT	B side secondary temp (middle)
DTAPXIMIDRADT	+X radiator, A side temp (middle)
DTBPXIMIDRADT	+X radiator, B side temp (middle)
DTAMXTOPRADT	-X radiator, A side temp (top)
DTBMBOTRADT	-X radiator, B side temp (bottom)

### C.2.4 FPA Temperatures

Mnemonic	Description
DFK1AFEEDT	K1 A side feed temp (upper)
DFW3BFEEDT	W3 B side feed temp (middle)
DFQ1AFEEDT	Q1 A side feed temp (lower)
DFKA1BFEEDT	Ka1 B side feed temp (upper)
DFW3AFEEDT	W3 A side feed temp (middle)
DFQ2BFEEDT	Q2 B side feed temp (lower)
DFK1BOMTT	K1 B side OMT temp (upper)
DFW3AOMTT	W3 A side OMT temp (middle)
DFQ1BOMTT	Q1 B side OMT temp (lower)
DFKA1AOMTT	Ka1 A side OMT temp (upper)
DFW3BOMTT	W3 B side OMT temp (middle)
DFQ2AOMTT	Q2 A side OMT temp (lower)
DFV11FPATEET	V11 FPA magic tee temp
DFV22FPATEET	V22 FPA magic tee temp
DFW11FPATEET	W11 FPA magic tee temp
DFW22FPATEET	W22 FPA magic tee temp
DFW32FPATEET	W32 FPA magic tee temp

### C.2.5 RXB Temperatures

Mnemonic	Description
DRV111RXBAMPT	V111 RXB amplifier temp
DRV222RXBAMPT	V222 RXB amplifier temp
DRW111RXBAMPT	W111 RXB amplifier temp
DRW221RXBAMPT	W221 RXB amplifier temp
DRW321RXBAMPT	W321 RXB amplifier temp
DRK12RXBRIBT	K12 RXB rib temp
DRKA12RXBRIBT	Ka12 RXB rib temp
DRQ1RXBRIBT	Q1 RXB rib temp
DRQ2RXBRIBT	Q2 RXB rib temp
DRW3RXBRIBT	W3 RXB rib temp
DRPYPSHPRTKT	+Y phase switch driver board temp
DRMYPSHPRTKT	-Y phase switch driver board temp

### C.2.6 AEU Temperatures

Mnemonic	Description
DAW323_4AMPt	W3 board temp between 23/24 amps
DAW2_14_23AMP_ADT	W2 board temp between 14/23 amps & a/d
DAV113_4ADT	V1 board temp between 13/14 a/d's
WDAW113_4ADT	W1 board temp between 13/14 a/d's
DAV223_4AMPt	V2 board temp between 23/24 amps
DAQ113_4ADT	Q1 board temp between 13/14 a/d's
DAIHK1BDT	Housekeeping board 1 temp
DAIHK2BDT	Housekeeping board 2 temp
DACONVBDT	Power converter board temp

### C.2.7 PDU Temperatures

Mnemonic	Description
DPPINTT1	PDU internal temperature #1
DPPINTT2	PDU internal temperature #2
DPPINTT3	PDU internal temperature #3
DPV111_2FPAT	V111/2 FPA regulator board temp
DPW221_2FPAT	W221/2 FPA regulator board temp
DPW321_2FPAT	W321/2 FPA regulator board temp
DPV221_2RXBT	V221/2 RXB regulator board temp
DPW111_2RXBT	W111/2 RXB regulator board temp
DPW321_2RXBT	W321/2 RXB regulator board temp

### C.2.8 AEU Voltages and Reference Roads

Mnemonic	Description
DAP15VBD1	Housekeeping board 1 +15V converter
DAM15VBD1	Housekeeping board 1 -15V converter
DAP12VBD1	Housekeeping board 1 +12V converter
DAM12VBD1	Housekeeping board 1 -12V converter
DAP5VBD1	Housekeeping board 1 +5V converter
DAP15VBD2	Housekeeping board 2 +15V converter
DAM15VBD2	Housekeeping board 2 -15V converter
DAP12VBD2	Housekeeping board 2 +12V converter
DAM12VBD2	Housekeeping board 2 -12V converter
DAP5VBD2	Housekeeping board 2 +5V converter
DABD1V	Housekeeping board 1 ref. voltage
DARREF1BD1	Housekeeping board 1 ref. resistance #1
DARREF2BD1	Housekeeping board 1 ref. resistance #2
DABD2V	Housekeeping board 2 ref. voltage
DARREF1BD2	Housekeeping board 2 ref. resistance #1
DARREF2BD2	Housekeeping board 2 ref. resistance #2
DASPARE1	Spare

### C.2.9 PDU Voltages

Mnemonic	Description
DPFP7_2V	FPA HEMT regulator +7.2V converter
DPFM7_2V	FPA HEMT regulator -7.2V converter
DPRP7_2V	RXB HEMT regulator +7.2V converter
DPRM7_2V	RXB HEMT regulator -7.2V converter
DPFLED10V	LED +10V converter voltage
DPPHSWCONVP9V	Phase switch driver +9V converter
DPPHSWCONVM9V	Phase switch driver -9V converter
DPFLDAP6_2V	Line driver A, DAs 1-5 +6.2V converter
DPFLDAM6_2V	Line driver A, DAs 1-5 -6.2V converter
DPFLDBP6_2V	Line driver B, DAs 6-10 +6.2V converter
DPFLDBM6_2V	Line driver B, DAs 6-10 -6.2V converter
DPHKP15V	Housekeeping +15 V converter
DPHKP5V	Housekeeping +5 V converter
DPHKM15V	Housekeeping -15 V converter

## Appendix D

### Acronym List

°C	[degree centigrade]
A	[amp]
A-hr	[amp hour]
A/D	Analog to Digital
A/C	Air Conditioning
AC	Alternating Current
ACE	Attitude Control Electronics
ACS	Attitude Control System
AEU	Analog Electronics Unit
ANSI	American National Standards Institute
AO	Announcement of Opportunity
AOS	Acquisition of Signal
APID	Application Process Identification
ASIC	Application Specific Integrated Circuit
ASIST	Advanced System for Integration and Spacecraft Testing
ASQC	American Society for Quality Control
AST	Autonomous Star Tracker
ATC	Active Thermal Control
ATS	Applications Technology Satellite
	Absolute Time Sequence
AWG	American Wire Gauge
AWS	Associate Work Station
BB	Breadboard
BER	Bit Error Rate
BIB	Bus Interface Box
BOA	Beginning of Activity
BOL	Beginning of Life
BOT	Beginning of Track
bps	[bits per sec]
BPT	Business Product Team
BSOC	Battery State of Charge
BTE	Bench Test Equipment
BWG	Beam Wave Guide
BW	Bandwidth
C&DH	Command & Data Handling

---

CADU	Channel Access Data Unit
CCAS	Cape Canaveral Air Station
CCB	Configuration Control Board
CCD	Charge Coupled Device
CCR	Configuration Change Request
CCSDS	Consultative Committee for Space Data & Systems
CCT	Close Circuit Television
CDR	Critical Design Review
CG	Center of Gravity
CGS	Combined Ground System
CIRS	Composite Infrared Spectrometer
CLA	Coupled Loads Analysis
CLK	Clock
CMB	Cosmic Microwave Background
CMD	Command
CM	Configuration Management
CMS	Command Management System
CNT	Count
COBE	Cosmic Background Explorer
COI	'Composite Optics, Inc.'
COP-1	Command Operations Procedure #1
COTS	Commercial Off-the-Shelf
CPT	Comprehensive Performance Test
CPV	Common Pressure Vessel
CQ	Command Quaternion Target
CQT	Command Quaternion Table
CRC	Cyclic Redundancy Check
CSLP	Cooperative Satellite Learning Project
CSS	Coarse Sun Sensor
CT1	Cold Test #1 (of CVC Test)
CT2	Cold Test #2 (of CVC Test)
CTE	Coefficient of Thermal Expansion
CTT	Compatibility Test Trailer
CUC	CCSDC Unsegmented Time Code
CVC	Cold-Vibe-Cold
CVCDU	Coded Virtual Channel Data Unit
CVCM	Collected Volatile Condensable Material
CVT	Current Value Table
CY	Calendar Year
D/A	Digital to Analog
D/NAR	Design/Non-Advocate Review
DA	Differencing Assembly
DAC	Digital/Analog Converter
DADRA	Diffraction Analysis of a Dual Reflector Antenna
dB	[decibel]
dBi	[decibel relative to an isotropic distribution]
DBS	'DBS Microwave, Inc.'
dBw	[decibel relative to one watt]
DC	Direct Current
DDD	DSN Data Delivery
DDTE	Design, Development, Test, and Evaluation
DEU	Digital Electronics Unit

---

DHDS	Digital History Data Storage
DMR	Differential Microwave Radiometer
	Detailed Mission Requirements
DoD	Depth of Discharge
DSCC	Deep Space Communications Complex
DSOC	DSN Space Operations Center
DSN	Deep Space Network
DSPT	Data Systems Product Team
DSSE	Digital Sun Sensor Electronics
DSS	Digital Sun Sensor
DFT-21	Development and Test Facility - 21
DTO	Detailed Test Objective
EDAC	Error Detection and Correction
EEE	Electrical, Electronics and Electromechanical
EEPROM	Electrically Erasable Programmable Read Only Memory
EIRP	Equivalent Isotropically Radiated Power
EMC	Electromagnetic Compatibility
EMI	Electromagnetic Interference
EOL	End Of Life
EOM	End of Mission
EO	Engineering Order
EO-1	Earth Observer-1
EOP	End of Pass
EOT	End of Track
EPT	Electrical Product Team
EPV	Extended Precision Vector
ESD	Electrostatic Discharge
ESN	Essential Services Node
ER	Established Reliability
ETF	Environmental Test Facility
ETR	Eastern Test Range
ET	Established Time
ETU	Engineering Test Unit
EU	Engineering Unit
EVD	Engine Valve Driver
FAM	Flight Assurance Manager
FAR	Federal Acquisition Regulations
FAST	Fast Auroral Snapshot Explorer
FDC	Fault Detection and Correction
FDF	Flight Dynamics Facility
FEDS	Front-End Data System
FEM	Finite Element Model
FET	Field Effect Transistor
FIRS	Far Infrared Survey
FlatSat	WMAP Spacecraft Simulator Facility (GSFC)
FMEA	Failure Modes and Effects Analysis
FORTRAN	FORmula TRANslator
FOT	Flight Operations Team
FPA	Focal Plane Assembly
FSDF	Flight Software Development Facility
FSW	Flight Software
FSWM	Flight Software Maintenance Team

---

FRR	Flight Readiness Review
FTP	File Transfer Protocol
FWHM	Full Width at Half Maximum
FY	Fiscal Year
G&A	General & Administrative
G/O	Gain Offset
GaAs	Gallium Arsenide
GAC	Gamma-Alumina Cylinder
Gbit	[gigabit]
GCI	Geocentric Inertial
GEMAC	GSFC ElectroMagnetic Anechoic Chamber
GEO	Geosynchronous Earth Orbit
GHe	Gaseous Helium
GHz	[gigahertz]
GMT	Greenwich Mean Time
GN	Ground Network
GN2	Gaseous Nitrogen
GND	Ground
GOS	Geomagnetic Observing System
GSE	Ground Support Equipment
GSFC	Goddard Space Flight Center
GTDS	Goddard Trajectory Determination System
GUI	Generic User Interface
H&S	Health and Safety
H/W	Hardware
HDF	Hierarchical Data Format
HEALPix	Hierarchical Equal Area isoLatitude Pixelisation
HEMT	High Electron Mobility Transistor
HFSS	High Frequency Structure Simulator
Hg	Mercury
HiFi	High Fidelity Simulation
HK	Housekeeping
HPBW	Half Power Beam Width
hr	[hour]
HVAC	Heating, Ventilating and Air Conditioning
Hz	[hertz]
I&T	Integration & Test
I&V	Integration & Verification
I/F	Interface
I/O	Input/Output
IC	Integrated Circuit
ICD	Interface Control Document
IDEAS	'Information Development and Applications, Inc.'
ID	Identification
IDL	Interactive Data Language
IDR	Instrument Design Review
IGSE	Instrument Ground Support Equipment
IHK	Instrument Housekeeping
IITA	Information Infrastructure Technology and Applications
IMAGE	Imager for Magnetopause-to-Aurora Global Exploration
IMAPS	Interstellar Medium Absorption Profile Spectrograph
in <sup>3</sup>	[cubic inch]

---

in	[inch]
InP	Indium Phosphide
IOC	Initial Operational Capability
	Initial Orbiting Configuration
	In-Orbit Checkout
IPM	Instrument Project Manager
IP	Internet Protocol
IR	InfraRed
IRU	IVA Replacement Unit
	Inertial Reference Unit
ISE	Instrument Systems Engineer
Isp	Specific Impulse [s]
ITO	Indium-Tin-Oxide
IUE	International Ultraviolet Explorer
JPL	Jet Propulsion Laboratory
JURAP	Joint User Resource Allocation Panel (DSN)
kbps	[kilobits per second]
kg	[kilogram]
kHz	[kilohertz]
K	[kelvin]
KF	Kalman Filter
km	[kilometer]
KSC	Kennedy Space Center
kw	[kilowatt]
L&IOC	Launch & In-Orbit Checkout
L1	First Sun-Earth Libration (Lagrange) Point
L2	Second Sun-Earth Libration (Lagrange) Point
LAN	Local Area Network
lbf	[pounds, force]
lbm	[pounds, mass]
LED	Light-Emitting Diode
LEE	Lightweight Electronics Enclosure
LEISA	Linear Etalon Imaging Spectrometer Array
LEO	Low Earth Orbit
LET	Linear Energy Transfer
LF	Launch Facility
LHe	Liquid Helium
LLV	Lockheed Launch Vehicle
LMAC	Little MIDEX Attitude Control Electronics
LOS	Loss of Signal
	Line of Sight
LN2	Liquid Nitrogen
LOX	Liquid Oxygen
LRR	Launch Readiness Review
LVPC	Low Voltage Power Controller
LV	Launch Vehicle
LZ	Level Zero
LZP	Level Zero Processing
m	[meter]
M_PDU	Multiplexing Protocol Data Unit
MAC	Maximum Allowable Concentration
	MIDEX Attitude Control (Electronics)

---

MATLAB®	Matrix Laboratory
MAP	Microwave Anisotropy Probe
MAR	MIDEX Assurance Requirements
MAX	Microwave Anisotropy Experiment
Mbps	[megabits per second]
MCC	Mid-Course Correction
MCM	Multi Chip Module
MCMC	Markov Chain Monte Carlo
MDM	Multiplexer/Demultiplexer
Mdot	Mass Flow Rate
MECO	Main Engine Cut Off
MEOP	Maximum Expected Operating Pressure
MET	Mission Elapsed Time
MGA	Medium Gain Antenna
MHz	[megahertz]
MICM	Multi-variable Instrument Cost Model
MIDEX	Medium-Class Explorer
MIL-71	DSN Merritt Island Testing Facility
MILA	Merritt Island Station (GN)
MITOC	MAP Integration and Test Operations Center
MLI	Multi Layer Insulation
MMFD	Multi-Mission Flight Dynamics
MPPF	Multi-Payload Processing Facility
MO&DA	Mission Operations & Data Analysis
MOC	Mission Operations Center
MPI	Message Passing Interface
MPS	Multi-Program Support
MPT	Microwave Product Team
MRR	Mission Requirements Review
	Mission Readiness Review
MRT	Mission Readiness Test
MS	Microwave System
ms	[millisecond]
MSAM	Medium Scale Anisotropy Measurement
MSX	Mid-Course Space Experiment
MV	Mongoose 5; [megavolt]
N	[newton]
N2H4	Hydrazine
NASA	National Aeronautics and Space Administration
NASCAP	NASA Surface Charging Analysis Program
NAVGSE	Navigational Ground Support Equipment
Nch	Number of Channels
ND	Network Director
NHB	NASA Handbook
NISN	NASA Integrated Services Network
Nms	Newton Meter Seconds
NOCC	Network Operations Control Center (DSN)
NRAO	National Radio Astronomy Observatory
NRZ-L	Non-Return to Zero-Level
NSF	National Science Foundation
NSPAR	Non-Standard Parts Approval Request
NSSDC	National Space Science Data Center

---

OC	Operations Center
OD	Orbit Determination
OMEGA	Office of the MAP Experiment General Archive
OMNI	Omni-directional Antenna
OMT	Orthomode Transducer
OPM	Orbital Parameter Message
OS	Operating System
PAF	Payload Adapter Fitting
PB	Playback
Pc	Thrust Chamber Pressure
PC	Printed Circuit; Personal Computer
PCA	Proportional Counter Array
PCB	Printer Circuit Board
PCI	'Programmed Composites, Inc.'
PD	Proportional and Derivative
PDR	Preliminary Design Review
PDT	Product Development Team
PDU	Power Distribution Unit
PEB	Parts Evaluation Board
PER	Pre-Environmental Review
PERT	Program Evaluation and Review Technique
PFR	Problem/Failure Report
PFU	Proto-flight Unit
PHSF	Payload Hazardous Servicing Facility
PI	Principal Investigator
PIND	Particle Impact Noise Detection
pixel	picture-element
PM	Project Manager, Phase Modulation
PN	Pseudo-Random Noise Coding
POC	Point of Contact
POP	Program Operating Plan
PROM	Programmable Read Only Memory
PR	Problem Report
PRT	Platinum Resistance Thermometer
PSE	Power Supply Electronics
psia	[pounds per square inch, absolute]
psig	[pounds per square inch, gauge]
PSK	Phase Shift Keying
PSLA	Project Service Level Agreement
PSR	Pre-Ship Review
PS	Phase Switch
PTF	Pressure Transducer and Filter
PU	Portable Telemetry Formatter
PWM	Princeton University
PWS	Pulse Width Modulator
QA	Primary Work Station
QTM	Quality Assurance
R/D	Qualification Test Model
RAAN	Reed-Solomon
RAM	Right Ascension of the Ascending Node
RAO	Random Access Memory
	Resources Analysis Office

---

RCS	Reaction Control System
RCVR	Receiver
RDL	Record Definition Language
RE	Earth Radius
REU	Reflector Evaluation Unit
RF	Radio Frequency
RFI	Radio Frequency Interference
RFP	Request for Proposal
RFSOC	Radio Frequency Simulations Operations Center
RID	Review Item Discrepancy
RISC	Reduced Instruction Set Computing
RM	Resources Manager
RMS	Root Mean Square
ROM	Read Only Memory
REV	Revolutions
ROSAT	Roentgen Satellite
rpm	[revolutions per minute]
RR	Requirements Review
RSI	'Research Systems, Inc.'
RSN	Remote Services Node
RS	Solar Radii
	Radiated Susceptibility
RSS	Root-Sum-Square
RTS	Relative Time Sequence
	Range Tracking Station
RT	Real Time
RWE	Reaction Wheel Electronics
RW	Reaction Wheel
RWA	Reaction Wheel Assembly
RXB	Receiver Box
s	[second]
S&MA	Safety & Mission Assurance
S/C	Spacecraft
SA	Solar Array
SAA	South Atlantic Anomaly
SADEB	Solar Array Deployment Electronics Box
SAEF-2	Spacecraft Assembly and Encapsulation Facility #2
SAM	Solar Array Module
SAMPEX	Solar Anomalous and Magnetospheric Particle Explorer
SAS	Solar Array Simulator
SCAPE	Self Contained Atmospheric Personnel Ensemble
SCC	Standard Cubic Centimeter
SCOPR	Systems Concept & Operating Plan Review
SCR	Spacecraft Concepts Review
	System Concept Review
SCT	Spacecraft Controller Team
SDSS	Sloan Digital Sky Survey
SDT	Spacecraft Development Team
SECO	Second-Stage Engine Cutoff
SEE	Single Event Effect
SEIT	Systems Engineering & Integration Team
SERS	Spacecraft Emergency Response System

---

SERTS	Solar Extreme-UV Rocket Telescope Spectrograph
SEU	Single Event Upset
SFDU	Standard Formatted Data Unit
SGI	Silicon Graphics, Inc.
SGSE	Spacecraft GSE
SH	Safe Hold
SHOOT	Superfluid Helium On-Orbit Transfer
SICM	Scientific Instrument Cost Model
SiO	Silicon Oxide
SK	Station Keeping
SLC	Space Launch Complex
SMEX	Small Explorer Program
SMM	Solar Maximum Mission
SMOC	Science and Mission Operations Center
SN	Space Network
SOH	State of Health
SOHO	Solar and Heliospheric Observatory
SPS	Small Purchase System
SPSS	Science Planning and Scheduling System
SRM	Solid Rocket Motor
SSR	Solid State Recorder
SS	Subsystem; Steady States; Stainless Steel
SSPC	Solid State Power Controller
SSTI	Small Spacecraft Technology Initiative
STK	Satellite Tool Kit
STM	Structural/Thermal Model
STOL	Spacecraft Test and Operations Language
STOP	Structural/Thermal Optical
STPT	Structural/Thermal Product Team
STScI	Space Telescope Science Institute
ST	Star Tracker
SWAS	Submillimeter Wave Astronomy Satellite
SWG	Science Working Group
TARA	Two Axis Rate Assembly
TBD	To Be Determined
TBR	To Be Resolved; To Be Required; To Be Refined
TBS	To Be Specified; To Be Supplied
TCP/IP	Transmission Control Protocol/Internet Protocol
TCS	Thermal Control System
TDI	Time Delay Integration
TDRS	Tracking and Data Relay Satellite
TEC	Thermo-Electric Cooler
Ti	Titanium
TID	Total Ionizing Dose
TIF	Timing & Interference
TLM	Telemetry
TML	Total Mass Loss
TOD	Time of Day; True of Date
TOMS-EP	Total Ozone Mapping Spectrometer-Earth Probe
TOTS	Transportable Orbital Tracking Station
TOT	Table of Tables
Transistor	TRAnsfer-reSISTOR

---

TRMM	Tropical Rainfall Measuring Mission
TRS	Thermal Reflector System
TSM	Telemetry and Statistics Monitor
Tsys	System Noise Temperature
TTI	Transfer Trajectory Insertion
TURFTS	TDRS User RF Test Set
UBC	University of British Columbia
UCLA	University of California Los Angeles
UPR	User Problem Report
UTMC	United Technologies Microprocessor Chip
V	Velocity; [volt]
V/F	Voltage-to-Frequency
V/T	Voltage/Temperature
VC	Voltage/Taper
VCDU	Virtual Channel
VDA	Virtual Channel Data Unit
VDC	Vapor-Deposited Aluminum
VDS	[volt, direct current]
VLSI	Voice Distribution System
VPF	Very Large Scale Integration
VRAIL	Vertical Processing Facility
VRAIL	Voltage Regulator and In-Rush Limiter
VR	Virtual Recorder
W	[watt]
WBS	Work Breakdown Structure
WIND	Solar Wind Mission
WMAP	Wilkinson Microwave Anisotropy Probe
WSC	White Sands Complex
WS	Workstation
WTR	Western Test Range
XCAL	External Calibrator
XDS	XRS Detector System
XPDR	Transponder
XRSN	Transponder RSN
XRS	X-ray Spectrometer
XTE	X-ray Timing Explorer
YRS	[year]
$\Delta H$	Change in Angular Momentum [Nms]
$\Delta V$	Delta-V, Change in Velocity [m/s]
$\Omega$	[ohm]